UNIVERSITÀ DEGLI STUDI DI PALERMO

UNIVERSITÀ degli STUDI di CATANIA

Dottorato di ricerca in ' Scienza dei materiali e nanotecnologie' XXXI ciclo

Electrochemical sensors for environmental and clinical analyses

Dottorando:

Bernardo Patella

Tutor:

Carmelo Sunseri

Anno 2015/2018

Index

List of acronyms

AA	*Ascorbic Acid*
A	*Working electrode area*
AP	*Acetomiophen*
BDD	*Boro Doped Diamond*
BSA	*Bovine Serum Albumine*
BV	*Buttler-Volmer*
C_b	*Bulk Concentration*
C_d	*Capacitance of Double Layer*
CA	*Citric Acid*
CHFH	*copper hexacyanoferrate*
CNTs	*Carbon Nanotubes*
CRGO	*Chemical Reduced Graphene Oxide*
CV	*Ciclic Voltammetry*
D	*Diffusion Coefficient*
DA	*Dopamine*
DI	*Distillated Water*
DPV	*Differential Pulse Voltammetry*
E^o	*Standard Potential*
EDC	*1-ethyl-3 (3-(dimethylamino)-propyl) carbodiimide*
EDL	*Electrical Double Layer*
EDS	*Energy Dispersive Spectroscopy*
ELISA	*Enzyme Linked ImmunoSorbent Assay*
EPA	*Enviromental Protection Agency*
ETA	*Etanolammine*
EToH	*Ethanol*
F	*Faradic Constant*
f	*Frecuency of Square Wave*
GAT	*Gold Aggregation Test*
GCE	*Glassy Carbon Electrode*
GFAAS	*Graphite Fournace Atomic Absorpiton Spectroscopy*
Glu	*Glucose*
GO	*Graphene Oxide*
HER	*Hydrogen Evolution Reaction*
HIgG	*Human Immunoglobulin G*
HRP	*Horseradish Oxidaxe*
i_f	*Forward Current of Square Wave*
i_p	*Peak Current*
i_r	*Reverse Current of Square Wave*
ICP-MS	*Inductecly Coupled Plasma Mass Spectroscopy*
ITO	*Indium Tin Oxide*

LOD	*Limit Of Detection*
LR	*Linear Range*
LSGO	*Laser Scribed Graphene Oxide*
LSV	*Linear Sweep Voltammetry*
MAE	*Microband Array Electrode*
n	*Number of electrons*
NHS	*N-Hydroxysuccinimide*
NiO@Ni	*Nickel oxide/ Nickel core/shell*
NPs	*Nanoparticles*
NTs	*Nanotubes*
NWs	*Nanowires*
PB	*Prussian Blue*
PBS	*Phosphate Buffer Solution*
PTHLH	*Parathyroid Hormon Like Hormon*
PTWI	*Provisional Tolerable Weekly Intake*
Pox	*Potassium Oxalate*
R	*Gas Constant*
R_{ct}	*Resistance of solution*
R_{Ω}	*Resistance of charge transfer*
r.d.s	*Rate Determining Step*
rGO	*reduced Graphene Oxide*
S	*Sensitivity*
SEM	*Scanning Electron Microscopy*
SO	*Sodium Oxalate*
SPCE	*Screen Printed Carbon Electrode*
SPE	*Screen Printed Electrode*
t_d	*Deposition time*
T	*Temperature*
TEM	*Transmission Electron Microscopy*
UA	*Uric Acid*
ULR	*Upper Limit of Linear Range*
UPD	*Under Potential Deposition*
V_d	*Deposition potential*
WHO	*World Health Organization*
WSR	*Water Splitting Reaction*
XRD	*X-Ray Driffraction*
ε	*Accuracy*
υ	*Scan Rate*
δeff	*Thickness of diffusion layer*
ΔE_p	*Step Potential*
ΔE_s	*Step Amplitude*

Motivation and aim of the research

The main aim of my Ph.D research was the development of novel sensors for clinical and environmental analyses. Nowadays, the concepts of smart cities, smart houses and Homo Deus (potential next stage in human evolution) are taking more and more attention [1-2-3-4]. Sensors have a key role in this context: recording different parameters, such as pollution, traffic jam, blood pressure, blood composition, brain activities or the functioning of organs, it will be possible to design cities able to manage efficiently all the resources or to warn people if a particular kind of disease, such as cancer or diabetes, is taking place. Current way of detecting these parameters or molecules are often laborious and expensive and cannot be used as in situ and real time [5]. In this scenario, the development of new kind of sensors, able to fit to these new necessities is of great importance. Electrochemical sensors, especially nano-sized sensors, are perfect candidates to address these challenges. Indeed, these sensors do not require special instrumentations to work but just an usual battery, so that this technology is really cheap and suitable for in situ action. Furthermore, the signal, which is an electrical signal (current, potential or resistance), can be recorded over time and can be acquired and managed in remote [6]. The main challenge of this technology is to achieve a Limit Of Detection (LOD) low enough to make the use of these sensors competitive with other analytical techniques, such as Inductively Coupled Plasma Mass Spectrometry (ICP-MS) or Enzyme Linked ImmunoSorbent Assay (ELISA) and, at the same time, to achieve a good reproducibility and stability when used with real samples like blood, urine or sea/river water [7]. These goals can be achieved by nano-sized materials because they enhance mass transport and electron transfer rate. In addition, to once found the right sensing material, it is

possible to select the electrochemical detection technique giving the best performances in dependence on the analyte that has to be detected [8].

During my 3 years of Ph.D I studied different electrodes to detect, electrochemically, 3 different analytes: i) heavy metals, ii) proteins, and iii) hydrogen peroxide. Heavy metals are the main source of water pollution. They have been extensively used in various applications due to their specific properties. The main problem using these chemicals is that they are non-biodegradable and thus they can accumulate in the human body through either the food chain or respiratory function. Among heavy metals, one of the most dangerous is mercury because just the exposure to some ppb (μg/l) can cause several problems to human body. Lead, cadmium, zinc, arsenic and copper are considered toxic and dangerous as well, therefore, their monitoring is really important [9-10-11]. H_2O_2 is a widely used chemical, employed as bleaching agent in textile and paper industry, for medical and pharmaceutical applications and to remove organic compounds from waste water and contaminated soil. Furthermore, H_2O_2 has a key role in the human body as well. For instance, its detection can be useful because can give indications about the glucose concentration and so it could be useful for diabetic patients. Furthermore, it is a biomarker of oxidative stress that is a pathological condition due to breakdown of the antioxidant defense system. [12-13-14]. Detection of proteins was also investigated during my Ph.D. In order to detect these bio-compounds it is mandatory to use some bio recognition elements (such as antibodies, DNA or aptamers) so that the sensors are usually named *biosensors.* During my studies, I developed a biosensors towards Human ImmunoGlobulin G (*H-IgG*) and ParaThyroid Hormone Like Hormone (*PTHLH*). H-IgG is a protein always present in the human fluids (blood, urine, sweat) and its detection has not any particular relevance. It can be used as a model because is a cheap protein that has the bio-chemical properties of many other proteins. Instead, PTHLH is

overproduced owing to different kind of cancer, consequently it can be used as a biomarker. This kind of application is really of great value because PTHLH starts to be produced at the beginning of the disease, so that its detection is useful for early diagnosis. [15-16-17].

Summarizing, the main goals of this Ph.D work are:

1. To develop new and innovative ways to fabricate electrodes with high surface area such as nanowires, nanotubes, thin film, microbands and porous substrates;
2. To find new and cheap electrochemical sensors featured by fast response in real time, high selectivity, low LOD, and able to work in situ, for detecting hydrogen peroxide, heavy metals, and proteins was the challenge of the research. It has been addressed with the proper development of nanostructured materials easy to be prepared. ;
3. Validate these sensors using real sample such as real water sample, cell cultures or body fluids.

References

1 L. Berntzen, M. R. Johannessen, A. Florea, Sensors and the Smart City, SMART conference, 2016,

2 R. M. Alarm, M. B. I. Reaz, M. A. M. Ali, A review of smart homes - Past, present, and future, IEEE Transaction on system, man and cybernetics C, 2012, 42, 1190-1203

3 H. Alemdar, C. Ersoy, Wireless sensor networks for healthcare: A survey, Computers Networks, 2010, 54, 2688-2710

4 O. Tane, J. Polonetsky, A.R. Sadeghi, Five Freedoms for theHomo Deus, IEEE Security and privacy, 2018, 16, 15-17

5 A. Turner, Biosensors: then and now, Trends. Biotechnol., 2013, 31, 119- 120

6A. J. Bandodkar, J. Wang, Non-invasive wearable electrochemical sensors: a review, Trend. Biotechn., 2014, 32, 363-371

7 K. Stulik, Challenges and Promises of Electrochemical Detection and Sensing, Electroanal., 1999, 11, 1001-1004

8 P. R. Bueno, C. Gabrielli, Electrochemistry, Nanomaterials, and Nanostructures, Nanostr. Mat. Electrochem. En. Prod. Stor.,2009, 81-149

9 Järup L., 2003, Hazards of heavy metal contamination, Br. Med. Bull.68, 167-182.

10 W. Hao, Screen-Printed gold electrode with gold nanopartilcles modification for simultaneous electrochemical determination of lead and copper, Sensors and Actuators B:Chemical, 2015, 209, 336-342

11 N. Ratner, D. Mandler, Electrochemical Detection of Low Concentrations of Mercury in Water Using Gold Nanoparticles, Analytical Chemistry, 2015, 87, 5148-5155

12 B. Thirumalraj, D.H. Zhao, S. M. Chen, S. Palanisamy, Non-enzymatic amperometric detection of hydrogen peroxide in human blood serum samples using a modified silver nanowire electrode, J. Colloid Interface Sci., 2016, 470, 117-122.

13 F. Tamay-Cach, J. C. Quintana-Pérez, J. G. Trujillo-Ferrara, R. I. Cuevas-Hernánde, L. Del Valle-Mondragón, E. M. García-Trejo, M. G. Arellano-Mendoza, A review of the impact of oxidative stress and some antioxidant therapies on renal damage, Ren Fail., 2016, 38, 171.

14 M. Han, S. Liu, J. Bao, Z. Dai, Pd nanoparticle assemblies--as the substitute of HRP, in their biosensing applications for H2O2 and glucose, Biosens. Bioelectron., 2012, 31, 151-156

15 C. Fenzl, P. Nayak, T. Hirsch, O. S. Wolfbeis, H. N. Alshareef, A. J. Baeumner, Laser-Scribed Graphene Electrodes for Aptamer-Based Biosensing, ACS Sens.,2017, 2, 616–620

16 H. B. Noh, M. A. Rahman, J. E. Yang, Y. B. Shim, Ag(I)-cysteamine complex based electrochemical stripping immunoassay: ultrasensitive human IgG detection, Biosens Bioelectron., 2011, 26, 4429-4435

17 A. Chamorro-Garcia, A. de la Escosura-Muniz, M. Espinosa-Castaneda, C. J. Rodriguez-Hernandez, C. de Torres, A. Merkoci, Detection of parathyroid hormone-like hormone in cancer cell cultures by gold nanoparticle-based lateral flow immunoassays, Nanomedicine., 2016, 12, 53-61

2. General Introduction

2.1 A monitored world

A sensor is a device able to detect a change in its environment and convert this change into a readable signal that can be electrical, optical, thermal, mechanical and so on. A sensor is formed by two separate parts, namely a *sensing element* able to detect the parameter of interest and a *transducer* to get a reliable reading of the signal. This signal can have different forms: it could be binary (yes/no) or a numeric value (for example temperature, light, wind, humidity, precipitation, position, composition) and it provides us the desired information. We actually live surrounded by sensors, often without even noticing. Just to make an example, a car from 2013 has installed at least 70 sensors, while, a luxury car of the same period, has up to *300* [1]. These numbers are expected to grow and grow over time. Another sensor application is for the environmental monitoring: an interesting example can be found in the *Green Watch Project*. In this case, 200 sensors have been distributed among the people living in Paris. These devices were able to detect air composition and the level of noise pollution while people lived their 'normal life'. This study shown how it is possible to drastically reduce the city pollution (and so to save money) just applying a network of sensors that work in real time and in situ [2]. One of the main challenges in the field of sensors is the real time and in situ analysis. These functions will allow the personnel/citizens to trigger a corresponding action in a fast and efficient way. Let us think about a city where air, seawater, river water, drinkable water, traffic jam and so on are regularly monitored over time: this can save a lot of money and, at the same time, it can improve the citizens quality of life, over and over.

FIGURE 2.1 CONCEPT OF SMART CITY [3]

Another interesting application of sensors is in the field of healthcare. In the last 5-10 years, Apple and Google released different kind of '*Smart Watches*' able to tell you how long and how good do you sleep, what is your blood pressure over a day, your heartbeat and so on. In this scenario, electrochemical sensors can play a key role: let us think about a wearable device that, regularly over time, or once/twice in a day, make a check-up of your blood, urine or sweat and alerts the person about the plausible onset of disease. Again, this system can save a lot of people and money.

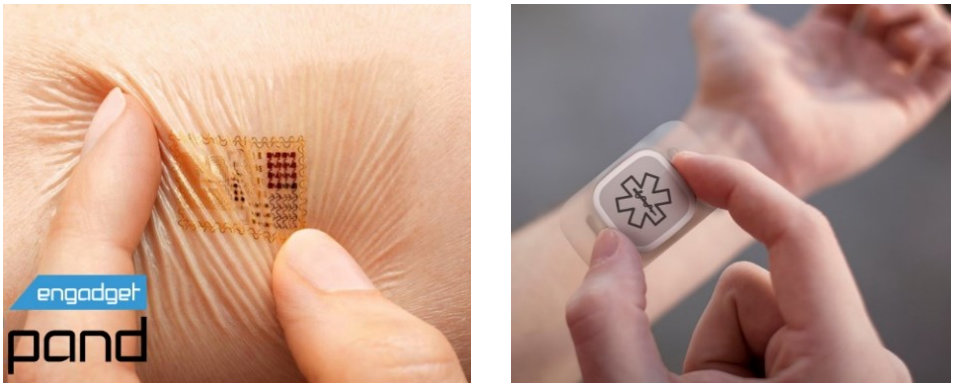

FIGURE 2.2NEW GENERATION OF WEARABLE SENSORS [4-5]

In the last year, Wang et al. developed a 1.5μm thick, gold based, e-tattoo sensor that can be directly pasted on human skin. They tested it under different mechanical stress, like compression, stretch and twist and they found a good performance under these conditions. This e-tattoo sensor is able to measure electrocardiogram, body temperature, skin hydration, heart and respiratory rate in a non-invasive way [6]. Similarly, Ameli et al. developed a graphene-based electrode, with a sub μ-meter thickness (less than 500nm thick). The aim of this work is to decrease the cost of the e-tattoo sensor replacing gold, a biocompatible and expensive material, with a cheaper material like graphene. Different graphene-based sensors have been developed but they require expensive fabrication process, such as photolithography. Here, the graphene electrodes were fabricated by a 'wet transfer, dry patterning' process, that is cheaper and minimizes the chemical contamination of the electrode, providing a more reproducible and biocompatible sensor. Furthermore, this kind of e-tattoo sensor looks totally transparent and can be applied on visible part of the body, such as face or arms [7]. In the same way, Kim et al. developed a wearable temporary electrochemical sensor, made of Bismuth/Nafion, that detects zinc cation trace in sweat, from 100 to 2000 ppb, with a constant scanning rate of 5 minutes [8]. Zinc is an important component of many biological processes and its concentration in bio fluids, such as sweat, is an indicator of many physiological states. Main problems are related with a zinc deficiency owing to a loss in resistance and muscular damage. Moreover, athletes need a continuous, non-invasive and in situ monitoring of many parameters during the training. Lactase, sodium, chloride ions, pH, can be used as markers to estimate the quality of the training or, for example, to warn the athlete of a possible muscular cramp. In 2017, Anastasova et al. developed a multi-platform system able to detect, simultaneously, Na^+, Lactase and pH during the training in human sweat, directly on-body. A continuous sampling of sweat is achieved using a flexible microfluidic system that brings sweat, with a constant flow rate, into the sensor

trough microneedles of 50 μm of diameter. [9] These examples are referred to electrochemical sensors and show how it is possible to improve human being using an appropriate, efficient and easy to use network of sensors. All the data are transferred directly, through a wireless connection, to our mobile phone that, just using an App, alerts us about a possible problem concerning our sport activity or about the water we use to drink or about our healthcare. Among the clear advantages that these new technologies may bring to the users, there is another one, maybe more hidden and less obvious: the patient care will move from the hospital to the home, drastically reducing the health care costs.

In this scenario, electrochemical (bio)sensors are perfect candidates being cost effective, small, portable, wearable, user friendly and providing an electrical output signal that can be easily controlled in remote. As a proof of that, the global market of electrochemical sensors and biosensors is expected to grow, with a Compound Annual Growth Rate (CAGR) of 9.7%, to USD 23707 million by 2022 [10]. Among all the applications of these sensors, the market of electrochemical sensors for healthcare will be by far the fastest growing, reaching USD 12689 million by 2022.

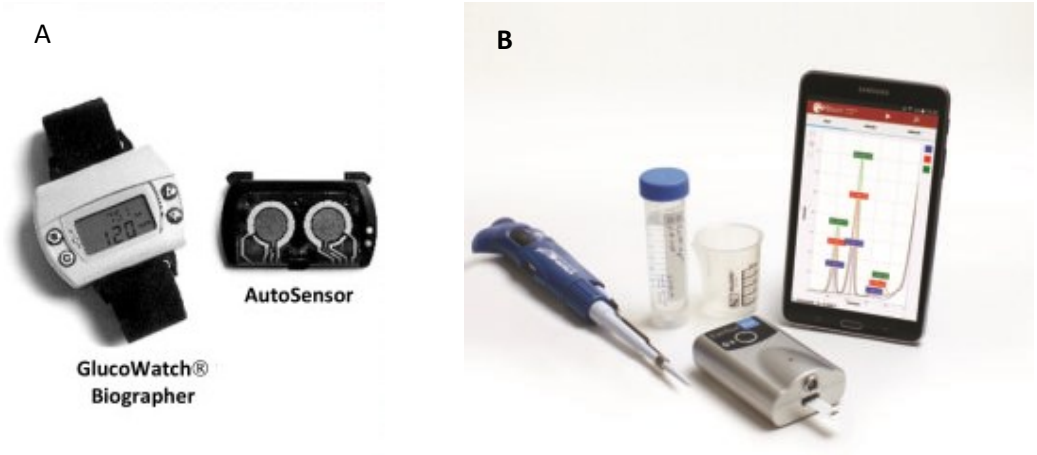

FIGURE 2.3 A) WEARABLE SENSOR FOR GLUCOSE MONITORING B) EXAMPLE OF PORTABLE POTENTIOSTAT WIRELESSLY CONNECTED WITH A MOBILE PHONE FOR HEAVY METAL DETECTION

This huge and fast-growing market is taking more and more place due to the development of nanotechnology. Indeed, sensitivity, selectivity and Limit Of Detection (LOD) of these sensors are highly affected by surface area and so, nanostructures like NanoWires (NWs), NanoTubes (NTs) and NanoParticles (NPs), can drastically enhance these features.

2.2 Electrochemical sensors and effect of nano-sized electrodes

The American National Standard Insitute defines a sensor as a device which provides a usable *output signal* (V) in response to a specific *measurand, M* (or *input*) [11]. The output signal is often an electrical signal while the input one could be every kind of quantity or property. When the input is a concentration of a chemical present in an environment, the sensor is named *'chemical sensor'*. There are different kinds of chemical sensors, depending on the chemical reaction that occurs at the sensing surface. When the reaction is a redox reaction the electrode is named *electrochemical sensor*. A typical electrochemical sensing element is composed of three parts: *working electrode*, where the redox reaction of interest occurs, *counter electrode*, where a second redox reaction occurs to close the circuit, and a *reference electrode*, necessary to polarize the working electrode by applying a known and fixed potential.

The main feature of an electrochemical sensor, and in general of every kind of a sensor, is the calibration curve. This is the mathematical function between the input and the output, V=f (M). The main feature of an electrochemical sensor, and in general of every kind of a sensor, is the calibration curve. This is the mathematical function between the input and the output, V=f (M). It is possible to find different trends of the calibration curve such as logarithm, exponential or polynomial. Besides, electrochemical sensors quiet often show a behaviour

typically evidenced by the plot of Figure 2.4 where, at low value of M (the parameter to be detected) the calibration curve has a linear trend. At higher analyte concentration, the calibration curve shows a transition region, where different linear correlation can be found. At the highest analyte concentration, the calibration curve became almost flat, reaching the '*surface saturation*'.

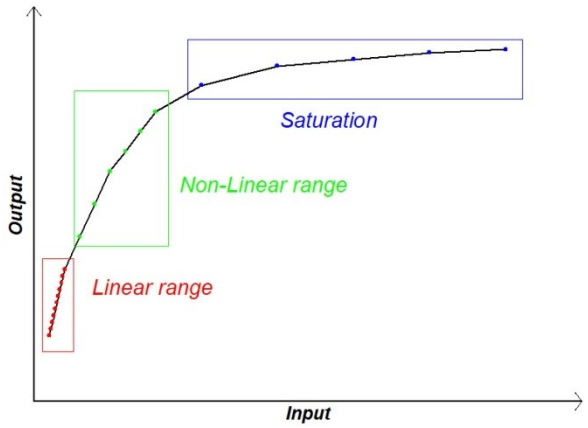

FIGURE 2.4 STANDARD CALIBRATION CURVE FOR AN ELECTROCHEMICAL SENSOR

In the case of a linear dependence, the sensor is calibrated in the linear range, where the input and the output are related by a linear equation:

$$V_m = S * M + a \tag{2.1}$$

EQ 2.1 GENERAL EQUATION TO CALIBRATE AN ELECTROCHEMICAL SENSOR

Where V_m is the output in the linear range, a the intercept at M=0, i.e. the value of the blank, and S is the slope of the linear interval, also named *sensitivity*. This is a very important feature because it is the increment in the output due to an unitary increment of the input: higher is the sensitivity, higher is the resolution of the sensor. As it is evidenced in Figure 2.4, the sensitivity is maximum in the first linear range. This is why is usual to calibrate the sensor just in this range of

concentration. Another important feature of the sensor is the *Limit Of Detection* (LOD). This is defined as the lowest concentration that, statistically, the sensor is able to detect with a reliable precision. A more precise and accurate definition of the LOD is provided by IUPAC according which, it represents the concentration that provides an output equal to the blank plus 3 times the standard error of the blank [12]. Substituting this definition into the equation (2.1):

$$a + 3\,S_d = S * LOD + a \tag{2.2}$$

$$LOD = 3\,\frac{S_d}{S} \tag{2.3}$$

EQS. 2.2-2.3: MATHEMATICAL PROCEDURE TO CALCULATE LOD

Where S is the sensitivity and S_d is the standard error of the blank.

Other important features are *accuracy* and *reproducibility*. They are often confused despite have totally different meanings. *Accuracy* involves how close you get to the correct result; instead, *reproducibility* is how consistently you can get the same result using the same method. Figure 2.5 shows how a sensor is reproducible but not accurate or vice versa. A non-accurate sensor simply needs of a new calibration, probably due to some modification of the sensing element; instead, reproducibility is often related to some random phenomena occurring during the sensing process that modify the system itself.

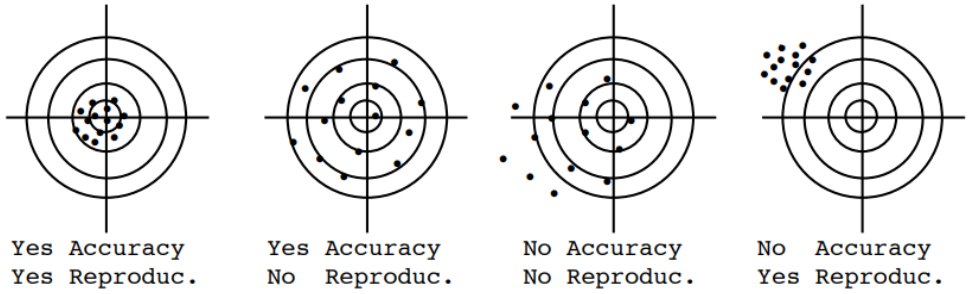

FIGURE 2.5 SCHEME OF ACCURACY AND REPRODUCIBILITY

Another important parameter is the selectivity. It involves how much the sensor can be affected by the presence of other compounds in the environment. This feature is highly important working with real sample such as blood, urine or sea water. For instance, electrochemical detection of dopamine (DA) is highly affected by the presence of ascorbic acid (AA) and uretic acid (UA) because the redox potentials of these compounds are close to the dopamine one. Unfortunately, these three compounds are present all together in the blood, where DA is normally detected, consequently, it is crucial to check the effect of these compounds on DA detection.
Briefly, other important features are:

- *Drift*: it represents the life time of the sensor. The electrode surface can change over time, so that a new calibration could be necessary. The *drift time* is the average time during which a calibration is reliable;
- *Reversibility*: it depends on how a sensor responds to the same stimulus over time. It is possible to distinguish, *reversible*, *semi-reversible* and *disposable* sensors.

All these features can be drastically enhanced using nanostructured based electrodes. The properties of nanostructures, such as NWs, NTs or NPs, are widely known and studied. Briefly, several novel properties appear as a dimension goes down, in addition to the surface enhancement. For instance, materials with a dimension less than 100 nm show also dramatic change of the chemical reactivity due to change in density and distribution of electrons in the outermost energy level. These changes lead to novel optical, electrical, magnetic thermal properties. A nanoparticle of about 10 nm contains about 100 atoms and 1–5% of them are on the surface [13]. Thus, compared to a massive material, the surface area and the number of ‘edge atoms’ are drastically enhanced.

Electrochemical (bio)sensors at nano-scale benefit arising from enhanced mass to volume ratio, electron transfer rate, reduced capacitive charging, and lower signal to noise ratio [14-15]. For instance, when the critical dimension of the electrode goes down to 10 nm, standard Butler-Volmer (BV) equation is not valid anymore, or not totally. Indeed, the effective thickness of diffusion layer, δ_{eff}, linearly depends on the nominal electrode radius, as shown in Figure 2.6.

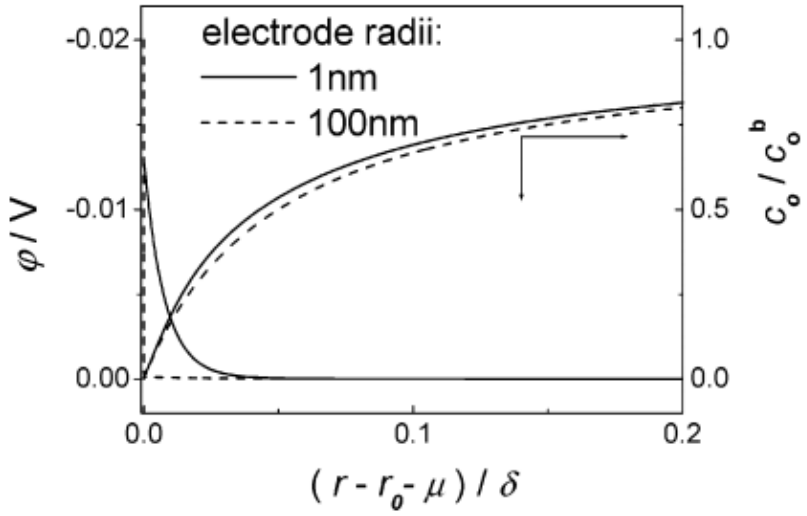

FIGURE 2.6 CONCENTRATION PROFILE AND DIFFUSION LAYER OVER 1NM AND 100 NM SCALE

When the radius is higher than 10^{-7} m, the diffusion layer and the Electrical Double Layer (EDL) are completely separate (dotted line of Figure 2.6). When δ_{eff} decreases up to 5nm the EDL and the diffusion layer start to overlap, enhancing mass transfer at nano-sized electrodes (continuous line of Figure 2.6) [16]. Such an effect explains the faster electron transfer kinetics at nano-sized electrodes. Formally, the BV equation cannot be used anymore and it has to be replaced by the Marcus-Hush or Marcus-Hush-Chidsey model [17].

Furthermore, nano-scale can improve performances of (bio)sensors owing to steric hindrance: indeed, most of biomolecules, like proteins and nucleic acids,

have dimensions of about 1-100 nm, and so the interaction and/or reaction between them is much easier.

All these issues characterize a lot of applications, not only in the field of sensors and biosensors [18-19], but also in the field of energy storage [20] and energy conversion[21], catalysis [22], ultra-capacitors [23] , and so on.

2.3 Main electrochemical techniques

The major advantage of the electrochemical sensors consists also in the opportunity to select the most suitable detecting technique in dependence on the type of analyte. Indeed, it is possible to polarize the sensing electrode by applying different potential and/or current waveforms for controlling molecules/ions reactions.

In this chapter, the main electrochemical techniques are briefly described. Primarily, it has to be highlighted the effect of the presence of water in the media. 90% of the solutions of practical interest in sensing field use water as a solvent. Water can interfere with electrode reactions through the Water Splitting Reaction (WSR):

$$2\,H_2O = O_2 + 2H_2 \qquad (2.4)$$

REACTION 2.1. WATER SPLITTING REACTION

This reaction is the resultant of two semi-reactions:

$$4H^+ + 4e^- = 2H_2 \qquad E^0 = 0 - 0.059\,pH\ (V)$$

$$2\,H_2O = O_2 + 4H^+ + 4e^- \qquad E^0 = 1.23 - 0.059\,pH\ (V)$$

REACTIONS 2.2-3. CATHODIC AND ANODIC REACTIONS OF WSR

For example, at physiological pH, hydrogen evolution occurs at potentials more cathodic than -0.413 V, while molecular oxygen is produced at potentials more anodic than 0.817 V. These two reactions have to be always considered to properly study an electrochemical cell.

Cyclic voltammetry is one of the most used electrochemical technique to investigate the electrochemical behaviour of a materials acting as a working electrode. The electrode is polarized through a triangular potential waveform applied between reference and working electrode. The slope of the triangular waveform gives the polarization rate of the working electrode, which can be selected in dependence of the application. The current response under potential polarization is recorded and usually plotted vs. potential. Figure 2.7 shows a plot of reactant concentration vs. distance from the electrode (Figure 2.7 A) and typical CV curves at different scan rates (Figure 2.7 B).

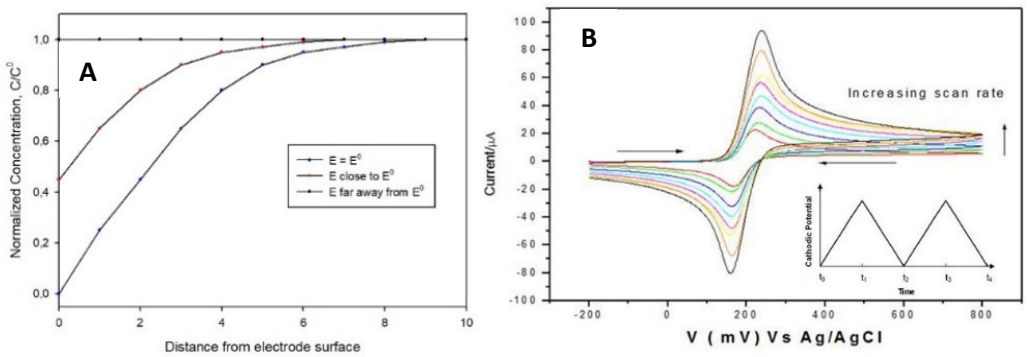

FIGURE 2.7 CONCENTRATION PROFILE DURING A CV (A) AND TYPICAL CV IN PRESENCE OF $Fe^{2+}/^{3+}$ IONS AND POTENTIAL WAVEFORM (INSET) (B)

When the potential is far away from the formal redox potential of the couple, E^0, the current flowing through the cell is a non-faradic current. When the potential is close to E^0, a faradic current starts with a consequent increase in the total current, i. This faradic current leads to a consumption of reactant and when the reactant concentration at the electrode/solution interface is depleted, owing to higher reaction rate than mass transport one, the electrode process goes under

diffusion control and a peak appears in the CV curves. For a diffusion controlled electrode process, the peak current is related to the scan rate by the Randles-Sevick equation:

$$i_p = 0{,}446 * n * F * A * C_b * (\frac{n*F*v*D}{R*T})^{0.5} \quad (2.6)$$

EQ 2.4. RANDLES-SEVICK EQUATION

Where i_p is the peak current, n is the number of electrons that take place in the redox reaction, F is the faradic constant, A the area of the working electrode, C the concentration of the redox couple, R the gas constant, T the temperature, D the diffusion coefficient of the reactant in the media, and ν the scan rate.

Since A is referred to the total working electrode area, CV can be used also for determining the real electrode surface when either porous or nanostructured electrodes are used. In addition, the linearity of the i_p vs. $\nu^{0.5}$ is revealing of diffusive control of the electrode process. The reversibility of the electrode reaction can be estimated by the anodic and cathodic peak separation which has to be constant with the scan rate, and equal to 0.059 V/n. Therefore, CV analysis is a valuable technique, because can provide many useful information, but it is not reliable for electrochemical sensing because gives a LOD in the μM-mM range. [24-25-26-27-28]

A more precise and useful electrochemical technique in sensing is the *chronoamperometry*. A general compound Ox is present in the media and the following redox reaction can occur, with a general formal potential, E^0:

$$Ox + ne^- = Red \quad (2.7)$$

REACTION 2.4 GENERAL REDOX REACTION

A fixed potential is applied and, at electrode potential more anodic than E^0, reduction of Ox occurs, therefore, its concentration at the electrode/solution interface decreases up to depletion. The thickness of the depletion layer

increases over time up to a limit value of current density. As the depletion layer is established under the potential scan, the current density decreases because the depletion layer increase. Of course, the current density depends on the bulk concentration of the oxidized species in otherwise identical condition.

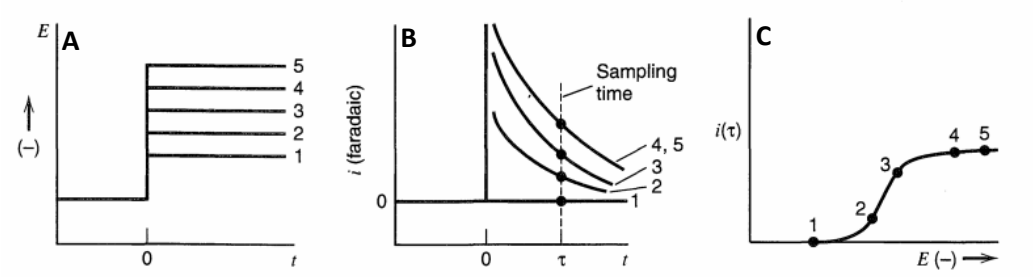

FIGURE 2.8 (A): APPLIED POTENTIAL VS. TIME PLOT; (B): FARADIC CURRENT VS. TIME PLOT FOR DIFFERENT APPLIED POTENTIAL; C: CURRENT DENSITY SAMPLED AT THE TIME τ OF FIG. 2.8 B VS. POTENTIAL

Figure 2.8 well schematizes this behaviour. Figure 2.8A shows different values of applied potential for a generic reduction process. In particular, level 1 represents a potential value more anodic than the thermodynamic one of the reduction process. Consequently, the faradic current at this potential is zero (Figures. 2.8B and C). Level 2, and 3 of Figure 2.8A represents two potential values at which the oxidised species concentration at the electrode surface is lower than the bulk one but higher than zero. Level 4 and 5 correspond at potential values at which the oxidized species is depleted at the electrode/solution interface. The current density at a time τ shows a sigmoidal trend as a function of the applied potential (Figure 2.8C). This last figure clearly evidences how is needles to apply a potential more cathodic than the level 4 for detecting the species Ox, because the current density does not increase as the limiting value is attained at a less cathodic level. Furthermore, a potential higher than level 4 can just decrease the selectivity of the sensor because, if other species are present in the media, they can start to react at more cathodic potentials. A theoretical explanation of this behaviour can be found by second

Fick's law, with the appropriate boundary conditions. By this way, Cottrel's equation is obtained:

$$i_t = \frac{n\,F\,A\,D^{0.5}C_b}{(\pi\,t)^{0.5}} \qquad (2.8)$$

EQ 2.5. COTTREL'S EQUATION

Cottrel equation shows how it is possible to use chronoamperometry as a sensing technique due to the linear dependence of i from C_b. With this technique lower LOD can be achieved, in the nM-µM range, as shown in the literature. [29-30-31-32]

Chronoamperometry can be used in many cases but is not suitable for some analytes, such as heavy metals. In this case, a more effective and precise technique is the *Square Wave Voltammetry* (SWV), discovered by Ramaley and Krause and further developed by Osteryoungs and their co-workers. The strength of this technique is based on the application of the square waves. A typical sequence of potential waveforms to be applied to the sensing electrode is shown in Figure 2.9.

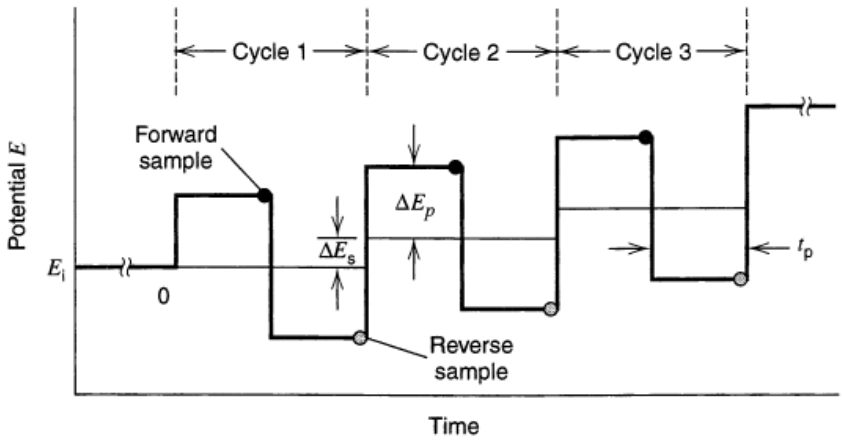

FIGURE 2.9 WAVEFORM OF POTENTIAL IN SQUARE WAVE VOLTAMMETRY (SWV) [35]

During the scan, the potential is swept from cathodic to anodic potential but not linearly, like in the CV. The main parameters of this technique are:

- ΔE_p: Step Potential;
- ΔE_s: Step Amplitude;
- frequency: number of cycle per second.

As a consequence, the scan rate is not a parameter of the process but is automatically calculated by these 3 parameters. During the process, two current density values are recorded: a forward current (i_f, at the beginning of the pulse) and a reverse current (i_r, at the end of the pulse). At the end, the difference between i_f and i_r (Δi) is plotted vs. potential, as shown in Figure 2.10.

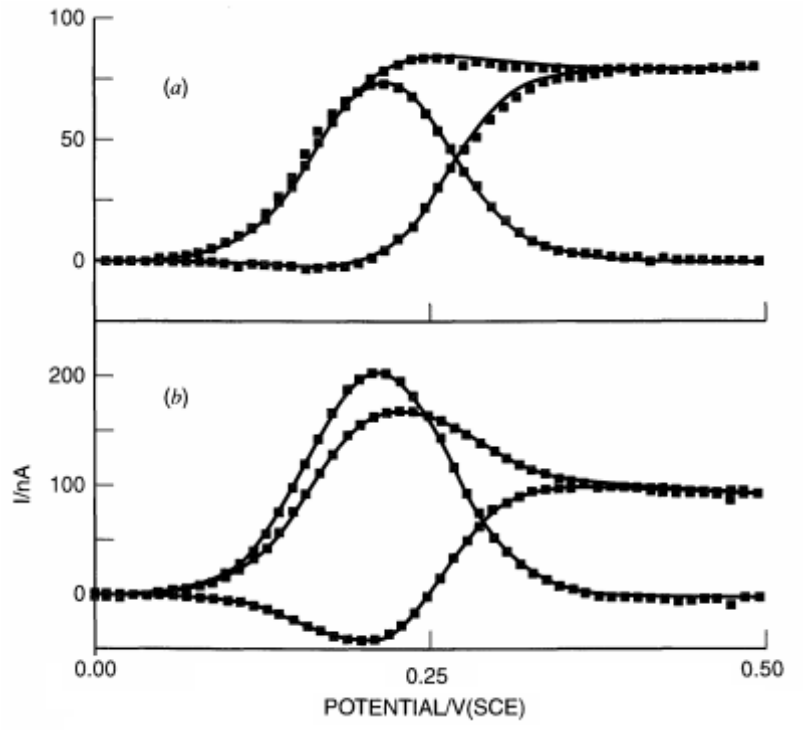

FIGURE 2.10 TWO EXAMPLES OF PEAK ENHANCEMENT AND BACKGROUND DEPRESSION USING SWV [35]

Let's consider a general reversible redox reaction like 2.7, where Ox is reduced to Red. When the potential is more anodic than the thermodynamic one E^0, both the reverse and forward current will be non faradic so that Δi will be close to zero. This is the first advantage of SWV: the background current is depressed almost to zero, because non faradic current are very low. When the potential goes next to E°, Ox reduction starts with formation of Red, close to the electrode surface. A faradic current is circulating giving a peak. During the 'reverse step', Red is oxidized back to Ox producing a current peak opposite at the previous one. The net current will be so the difference between an oxidation and a reduction peak. This is the second advantage of SWV: the peak current in the Δi-E plot is enhanced compared to the one coming from the forward or reverse current. Peaks in the differential current vs. applied potential plot are indicative of redox processes, and the magnitudes of the peaks in this plot are proportional to the concentrations of the various redox active species according to:

$$\Delta i_p = \frac{n\,F\,\Delta\Psi_p\,D^{0.5}C_b}{(\pi\,t)^{0.5}} \qquad (2.9)$$

EQ 2.6. SWV EQUATION [24]

where Δi_p is the differential current peak value, A is the surface area of the electrode, C_b is the concentration of the species, D is the diffusivity of the species, t_p is the pulse width, and $\Delta\Psi_p$ is a dimensionless parameter which gauges the peak height in SWV relative to the limiting response in normal pulse voltammetry.

The main application of this technique is for heavy metals detection. Here, an heavy metal cation is dissolved in the media and the following reaction can occur:

$$M_n^{z+} + ze^- = M_n \qquad (2.10)$$

REACTION 2.5. METAL DEPOSITION REACTION

For heavy metals detection, SWV is slightly modified and takes the name of *Square Wave Anodic Stripping Voltammetry* (SWASV). Here, before to apply SWV, a fixed cathodic potential is applied for a certain time t. During this time, heavy metal is deposited on the electrode surface, according to the Reaction 2.10. Then, SWV is applied, starting from a cathodic potential higher than E^0 to an anodic one. The deposited metal will be stripped off from the electrode surface, giving a current peak that is related to the metal concentration. By this technique, it is possible to detect heavy metals also in trace, up to pM-nM range as shown in the literature. [33-34-35-36-37]

Another valuable and useful technique is the Electrochemical Impedance Spectroscopy (EIS). An electrochemical cell can be seen as an electrical circuit, including resistances (resistance of the electrolyte, the electrode, charge transfer and so on) and capacitances (first of all, the double layer capacitance).

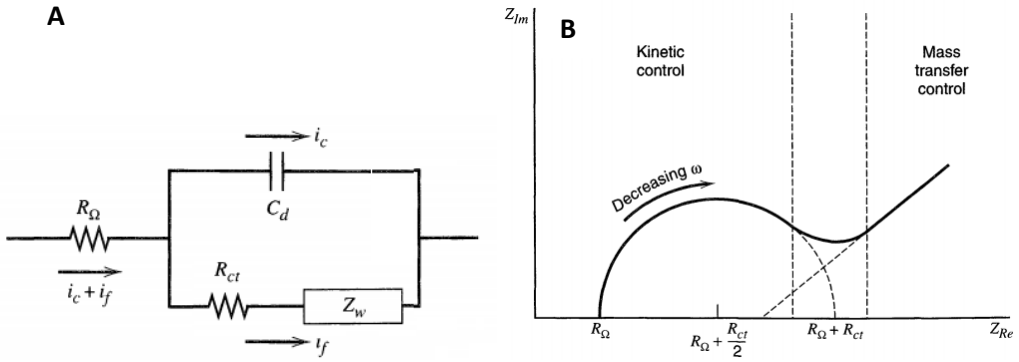

FIGURE 2.1 A): TYPICAL EQUIVALENT CIRCUIT OF AN ELECTROCHEMICAL CELL; B) :TYPICAL ELECTROCHEMICAL IMPEDANCE SPECTROSCOPY (EIS) DIAGRAM

Figure 2.11A shows a typical equivalent circuit where R_Ω, R_{ct}, C_d and Z_w are the resistance of the solution, the charge transfer resistance, the capacitance of double layer and the Warburg impedance, respectively. The last one is kind of a resistance related to the diffusive mass transport. In a typical EIS measurement,

the total impedance of the cell/electrode is calculated over a frequency range and by this way, it is possible to check the interfacial properties of an electrode in terms of resistance and capacitance with high precision. The most common EIS plots show the real part of the impedance vs the imaginary one (Figure 2.11B). This curve is made of a semicircle and a straight line. By the semicircles, it is possible to calculate the resistances of the circuit, because it is possible to demonstrate that the radius is equal to $R_{tot}/2$. The intersect of the straight line with the x-axes represents the double layer capacitance. EIS is an hard and difficult method, highly affected by many parameters but, if properly used, can be really useful. For example, if the detection method requires physical interaction of the analyte with the electrode surface (for instance, for protein detection, where the protein has to bond with its antibody), it is possible to detect also a single molecule by this method, reaching low LOD, in the order of fM-pM. [38-39-40-41]

References

1 S. Abdelhamid, H. S. Hassanein, and G. Takahara, Vehicle as a Mobile Sensor, Procedia Computer Science, 2014,. 34, 286–295.

2 *C. Ratti , A. Townsend, Smarter Cities - The Social Nexus, Scientific American, 2011,. 305, 42–48,.*

[3] http://motori.ilgiornale.it/smart-cities-globali-un-mercato-da-2-trilioni-di-dollari/

[4] https://www.engadget.com/2014/11/09/engadget-expand-mc10-wearables/

[5] https://www.dezeen.com/2014/03/14/epilepsy-aid-uses-wearable-technology-to-predict-seizures/

6 Y. Wang, Y. Qiu, S. K. Ameri, H. Jang, Z. Dai, Y. A. Huang, N. Lu, Low-cost, μm-thick, tape-free electronic tattoo sensors with minimized motion and sweat artifacts, npj Flexible Electronics, 2018, 2, 1-7

7 *S. K. Amerit, R. Ho, H. Jang, L- Tao, Y. Wang, L. Wang, D. M. Schnyer, D. Akinwande, N. Lu, Graphene Electronic Tattoo Sensors, ACS Nano, 2017, 11, 7634-7641*

8 J. Kim, W. R.de Araujo, I. A.Samek, A. J.Bandodkar, W. Jia, B. Brunetti, T.R.L.C.Paixão, J. Wang, Wearable temporary tattoo sensor for real-time trace metal monitoring in human sweat, Electrochem. Comunic., 2015, 51, 41-45

9 S. Anastasova,B. Crewther,P. Bembnowicz,V. Curto, H. M. Ip, B. Rosa, G.Z. Yang, A wearable multisensing patch for continuous sweat monitoring, Biosens Bioelectron., 2017, 93, 139-145

10 https://www.prnewswire.com/news-releases/global-electrochemical-biosensors-market-research-report---forecast-to-2022-300643898.html

11 https://www.ansi.org/

12 A. D. McNaught, A. Wilkinson , IUPAC. Compendium of Chemical Terminology, 2nd ed. (the "Gold Book"), Blackwell Scientific Publications, 1997

13 Bueno P.R., Gabrielli C. (2009) Electrochemistry, Nanomaterials, and Nanostructures. In: Leite E.R. (eds) Nanostructured Materials for Electrochemical Energy Production and Storage. Nanostructure Science and Technology. Springer, Boston, MA

14 P. H. Robbs, N, V. Rees, Nanoparticle electrochemistry, Phys. Chem. Chem. Phys., 2016,18, 24812-24819

15 Y. Liu, R. He,Q. Zhang, S. Chen, Theory of Electrochemistry for Nanometer-Sized Disk Electrodes, Phys. Chem. C,2010,114, 10812–10822

16 R. He, S. Chen, F. Yang, B. Wu Dynamic Diffuse Double-Layer Model for the Electrochemistry of Nanometer-Sized Electrodes, J. Phys. Chem. B, 2006,110, 3262–3270

17 R. A. Marcus, On the theory of oxidation-reduction reactions involving electron transfer, Int. J. Chem .Phys., 1956, 24, 966–978

18K. J. Kim, J. H. Choi, S. H. Pyo, K.S. Yun, J. Y. Lee, J. W. Choi, B. K. Oh, Nanostructure Modified Microelectrode for Electrochemical Detection of Dopamine with Ascorbic Acid and Uric Acid, J Nanosci Nanotechnol. 2016;16, 3058-61.

19 C. Zhu, G. Yang, H. Li, D. Du, Y. Lin, Electrochemical Sensors and Biosensors Based on Nanomaterials and Nanostructures, Anal. Chem., 2015, 87, 230–249

20 J. Park, J. Li,W. Lu, A. M. Sastry, Geometric consideration of nanostructures for energy storage systems, Journal of Applied Physics, 2016, 119

21 S. Buller, J. Strunk, Nanostructure in energy conversion, Journ. Energ. Chem., 2016, 25, 171-190

22 Y. J. Pagàn-Torres, J. Lu, E. Nikolla, A. C. Alba-Rubio, Chapter 17-Well-Defined Nanostructures for Catalysis by Atomic Layer Deposition, Studies Surf. Scien. Catal., 2017, 177, 643-676

23 P. Xiong, J. Zhu, X. Wang, Recent advances on multi-component hybrid nanostructures for electrochemical capacitors, Journ. Power Sour., 2015, 294, 31-50
24 A. Scozzari, V. Evangelista, L. Barsanti, A.M. Frassanito, V. Passarelli, P. Gualtieri, Electrochemical Sensing Methods: A Brief Review, Algal Toxins: Nature, Occurrence, Effect and Detection,2008
25 A. J. Bard, L. R. Faulkner, Electrochemical Methods: Foundamentals and applications, 2nd Edition, 2011
26 R. S. Nicholson, Theory and Application of Cyclic Voltammetry for Measurement of Electrode Reaction Kinetics, Anal. Chem., 1765, 37, 1351-1355
27 http://shodhganga.inflibnet.ac.in/bitstream/10603/88264/10/10_chapter%201.pdf
28 J. D. Wiedemann, K. T. Kawagoe, R. T. Kennedy,E. L. Ciolkowski, R. M. Wightman, Strategies for Low Detection Limit Measurements with Cyclic Voltammetry, Anal. Chem.,1991, 63, 2965–2970
29 R. G. Compton, M. E. Laing, D. Mason, R. J. Northing, P. R. Unwin , Rotating Disc Electrodes: The Theory of Chronoamperometry and Its Use in Mechanistic Investigations, Proceedings of the royal society A, 1988, 418
30 M.Sluyters-Rehbach, J.H.O.J.Wijenberg, E.Bosco, J.H.Sluyters, The theory of chronoamperometry for the investigation of electrocrystallization mathematical description and analysis in te case of diffusion controlled growth, Journ. Electroanal. Chem. Intef. Electrochem., 1987, 236, 1-20
31 B. Patella. R. Inguanta, S. Piazza, C. Sunseri, A nanostructured sensor of hydrogen peroxide, Sens. Act. B., 2017, 245, 44-54
32J. C. Vidal, M. A. Yague, J. R. Castillo, A chronoamperometric sensor for hydrogen peroxide based on electron transfer between immobilized horseradish peroxidase on a glassy carbon electrode and a diffusing ferrocene mediator, Sens. Act. B, 1994, 21, 165-141
33 J. G. Osteryoung, R. A. Osteryoung, Square wave voltammetry: Anal. Chem., 1985, 57, 101-110 •
34L. Ramaley, M.S. Krause, Theory of square wave voltammetry, Anal. Chem., 1969, 41, 1362-1365
35V. Mirceski, S. Komorsky-Lovric, M. Lovric, Square-Wave Voltammetry Theory and Application
36 B. Patella, S. Piazza, C. Sunseri, R. Inguanta, NiO thin film for mercury detection in water by square wave anodic stripping voltammetry, CET, 2017, 60, 1-6
37 S. H. Wu, Z. Y. Zheng, J. F. Zhang, Z. W. Song, F. Fang, J. J. Sun, Subppt Level Detection of Mercury(II) Based on Anodic Stripping, Electroanal., 2015, 27, 1610-1615
38 E- Barsoukov, J. R. Macdonald, Impedance Spectroscopy: Theory, Experiment, and Applications, 2005
39 W. Reitz, A Review of: "Impedance Spectroscopy, Theory, Experiment, and Applications, Mat. Manuf. Processes, 2007, 22, 294-
40 B. Zhu, O. A. Alsager, S. Kumar, J. M. Hodgkiss, J. Travas-Sejdic, Label-free electrochemical aptasensor for femtomolar detection of 17β-estradiol, Biosens. Bioelectr., 2015, 398-403
41 R. Salimian, L. Kèkedi-Nagy, E. E. Ferapontova, Specific Picomolar Detection of a Breast Cancer Biomarker HER- 2/neu Protein in Serum: Electrocatalytically Amplified Electroanalysis by the Aptamer/PEG Modified Electrode, Chem. Electro. Chem., 2017, 4, 872-879

Preface

Part of the experimental activity of this work has been conducted in the Tyndall National Institue at Nanotechnology Lab, Ireland (chapter 4.3) and at Catalan Institute of Nanoscience and Nanotechnology, ICN2 , – Spain (chapter 5). As it is usual in these cases, the experimental procedure and results are shared with the host Lab, therefore every detail cannot be disclosed. Despite such constraints, I will present and discuss almost completely the results and expose the experimental procedure. Here, I regret for some minor but unavoidable omission, and simultaneously I acknowledge Prof. Alan O'Riordan, Dott. Pierre Lovera and Prof. Arben Merkoci for their kind hosting and scientific assistance during my stay in Cork, and Barcelona, respectively. In addition, I would like to acknowledge the many friends and colleagues who supported and cooperate with me for the lab activity.

3. *Sensors for hydrogen peroxide*

Abstract

In this chapter, the development of two nanostructured sensors to detect H2O2 are described. This has relevance for both environmental and clinical applications. Indeed, its concentration in human body fluids (mainly in blood) is related to glucose concentration and can be used to evaluate the oxidative stress of our body. Today, there is not any device able to detect this compound in a easy, portable and cheap way. Currently, the sample has to be collected, moved into a laboratory, tested and, often after several days, the result is sent to the patient. The possibility to make this process shorter and easier, using electrochemistry, has been studied in this chapter. The high surface area of the electrode allowed to reach low limit of detection, in the μM range (less than 1 mg per liter). We also found that the electrode material plays an important role because a noble metal, such as palladium, has high selectivity, high stability and reproducibility, while a less noble metal, like copper, has good features but is less performing. On the other side, the copper based electrode is 10 times cheaper than the palladium one so the applicability of these sensors are different: the copper one can be used for a qualitative analysis, when minor precision is accepted, while palladium has to be used for a more precise and reliable analysis. In order to check its technological applicability, we used it to evaluate the oxidative stress by detecting hydrogen peroxide produced by different cellular culture under stressing conditions. The good results support the conclusion that just stimulated macrophages release hydrogen peroxide, whose amount can be easily detected by these sensors.

3.1 Introduction

Hydrogen peroxide is the simplest peroxide, with a chemical formula H_2O_2. A covalent bond links the hydrogen atoms while a polar covalent bond links the oxygen and hydrogen atoms. It is a non planar molecule, with a bond angle of 111°. At room temperature, it is an uncoloured liquid and is diluted in aqueous solutions. Due to the low activation energy (49 kcal/mol), it spontaneously reacts, producing water and molecular oxygen:

$$H_2O_2 = H_2O + O_2 \quad (3.1)$$

REACTION 3.1. HYDROGEN PEROXIDE DECOMPOSITION REACTION

It is an exothermal reaction (-98.3 kJ/mol). The main peculiarity of hydrogen peroxide concerns the oxidation state of oxygen, equal to -1. It makes hydrogen peroxide both a reducing and an oxidant agent:

$$H_2O_2 = O_2 + 2H^+ + 2e^- \quad (3.2.1)$$

$$H_2O_2 + 2\,H^+ + 2e^- = 2H_2O \quad (3.2.2)$$

REACTIONS 3.2. HYDROGEN PEROXIDE AS REDUCING (3.2.1) AND OXIDIZING AGENT (3.2.2)

Both these reactions produce 'green compounds', such as either oxygen or water, therefore, hydrogen peroxide can be used as a 'green oxidising/reducing agent'. This is why, in the last years, many chemical plants started to use hydrogen peroxide to minimize the environmental impact of the factory.

H_2O_2 was discovered in 1818 by Louise Jacques Thènard, by the reaction between nitric acid and barium di-oxide [1]. Today, the main process to produce hydrogen peroxide is the oxidation of 2-etil-antrachinone to 2-alchilantrachinol producing a quiet concentrated solution (close to 40% in volume). In order to

obtain more concentrated solutions, a vacuum distillation is required, drastically increasing the price [2]. Actually, hydrogen peroxide concentration unit is the 'volume'. It represents the volume of oxygen that can be produced by 1 L of a solution of hydrogen peroxide, at room temperature. It is possible to convert the 'volume concentration' to molarity by the following equation [3]:

$$M_{H2O2} = 0.08931 * V_{H2O2} \quad (3.1)$$

EQ. 3.1 CORRELATION BETWEEN MOLAR AND VOLUME CONCENTRATION

At low concentration, H_2O_2 is a non toxic and dangerous compound, but it became really aggressive at concentration higher than 40%.

The world production of this compound is about 2.2 Mton/year and is mainly employed as bleaching agent in textile and paper industry [4], but also in pharmaceutical and medical applications and for chemical syntheses [5]. Another important application concerns treatment of waste water and contaminated soils [6-7] to remove organic impurities by Fenton's reaction, in which hydrogen peroxide is used to generate highly reactive hydroxyl radicals, able to destroy aromatic and halogenated compounds which are difficult to remove by other methods. For many of these applications (e.g., the use as anti-pathogen agent), it is important to detect the exact concentration of hydrogen peroxide in the given environment either before or after its reaction. For instance, during Fenton's reaction, it is fundamental to maintain suitable concentration of hydrogen peroxide for ensuring efficient degradation of the organic compounds.

In the field of health, hydrogen peroxide is a marker of oxidative stress, a pathological condition due to breakdown of the antioxidant defense system with consequent imbalance between production and elimination of oxidizing chemicals. During the course of this disease, hydrogen peroxide is released so it

can be used as a biomarker for a rapid and noninvasive detection of the disease [8]. Furthermore, hydrogen peroxide sensors can be used to detect glucose, for diabetic patients. When glucose reacts with its enzyme, glucose oxidase, hydrogen peroxide is produced:

$$Glucose + O_2 = Gluconic\ Acid + H_2O_2 \quad (3.3)$$

REACTION 3.3. REACTION BETWEEN GLUCOSE AND GLUCOSE OXIDASE

Hydrogen peroxide detection is faster and more efficient than glucose one, therefore, a more reliable, rapid and sensitive detection can be achieved [9-10], as demonstrated by different commercial devices already in the market [11]. Hydrogen peroxide is also a secondary product of many other enzymes (alcohol oxidase, lactate oxidase, urate oxidase, cholesterol oxidase, and so on), therefore, its detection is of value in many other fields [12]. Besides its well-known cytotoxic effects, H_2O_2 plays an important role in living organisms, because it acts as an 'alert' of many biological processes, such as immune cell activation, vascular remodeling, apoptosis, stomatal closure and root growth. [13-14]

Therefore, real-time and reliable monitoring of H_2O_2 concentration is important. The most used methods for detection of hydrogen peroxide are IR spectroscopy, spectrophotometry, citometry and redox titration. These methods are often expensive or require very high detection time. Besides, are just qualitative methods and cannot be used for in situ and real time analyses [15]. Instead, electrochemical sensors are cheap with detection time lower than 3s. Besides, it is highly reliable and easy to produce. Among electrochemical sensors, the amperometric ones are the most used because are easier to use. Another great advantage of the amperometric sensors is that the managing costs are very low because they can work under an applied potential close to 0 V (The standard potential of hydrogen peroxide is E^0 = 1.8 – 0.066 pH V (NHE)) [16-17-18].

Electrochemical sensors detect the presence of hydrogen peroxide owing to a redox reaction occurring at the electrode/solution interface. Consequently, performance of the sensor will be improved by increasing the surface area. For this reason, the use of nanostructures, such as nanowires, nanotubes or nanoparticles, is of advantage owing to the high surface to volume ratio which considerably improves the performance of the sensor.

Electrochemical sensors for hydrogen peroxide can be classified as bio-labeled and non-enzymatic sensors.

Bio-labeled electrochemical sensors are often more selective owing to the bio-recognition of the hydrogen peroxide by peroxidase (HRP). The high selectivity is due to the structure of the HRP (and in general to the enzyme structure): enzymes have an active site with a stereospecific interaction that allows just to the right substrate to penetrate and react. When the active site and the substrate react, the products will leave the site and regenerate the active site, therefore, the enzyme is not consumed over time.

On the other hand, the immobilization of these compounds into the electrode surface is often unreproducible and unstable [19]. For these reasons, these electrodes generally have a shelf life often lower than 7 days. The other severe drawback is the electron transfer between the enzyme and the electrode. This kind of transfer generally occurs by tunneling effect. In many proteins, the active site is shielded by a thick layer of polypeptides that make this transfer hard owing to the long distance [19].

In this field, Jönsson et al. [20] developed a graphite electrode with absorbed peroxidase for hydrogen peroxide detection. They obtained a LOD of 0.5 μM with a wide linear range but they confirmed the scarce stability. They found that just after 10 sample injections (10 measurements) the electrode loses about 10 to 15% of its initial response and more than 40% after 300 measurements. In order

to decrease this effect, Zhang et al. [21] modified an Indium Tin Oxide (ITO) electrode with magnetic NPs of Fe_3O_4, the main compound of peroxidase enzyme. They found a longer stability but the features are not so good, having a LOD of 200 μM and a linear range up to 2mM. In 2013, Xin et al. [22] slightly modified this process, by modifying a Screen Printed Carbon Electrode (SPCE) with Fe_3O_4-Au nanoparticles coated with horseradish peroxidase and graphene. In their work, they obtained an excellent stability over time (decrease of 10% of the current density after 28 days of storage) with a 10 times lower LOD (12 μM). Ferric hexacyanoferrate or Prussian blu (PB) is a compound morphologically similar to HRP so that has been named '*artificial peroxidase*'. Its polycrystalline structure allows small molecules to reach the active side, increasing the selectivity in comparison with Fe_3O_4. Big molecules, such as Ascorbic Acid (AA), Uretic Acid (UA), Potassium Oxalate (POX), glucose (GLU) cannot react with the electrode. Du. et al. [23] used electro co-deposited Prussian Blu and carbon nanotubes (CNTs) on the surface of a planar gold electrode. Due to the presence of both the CNTs and PB a LOD of 23 nM has been achieved with high sensitivity (almost 1 μA/nM). Cao et al. [24] developed a graphene based electrode with a PB layer chemically deposited via wet process. The results are really interesting, reaching a LOD of 45 nM with an extremely high stability over time. After 100 consecutive cycles, the signal remained highly stable (the current density decrease was less than 5%) while the current decrease was of about 9% over 2 weeks of storage. The main drawback of this material is its stability in neutral and alkaline media. The reduced form of PB, named 'Prussian white', is soluble in these solutions. In order to overcome this problem, other kinds of metal hexacyanoferrates (copper, lead, nickel) have been investigated. This aspect has been confirmed by Garjonite et al. [25] that developed a copper hexacyanoferrate (CHFH) based electrode. They compared the electro-catalytic stability of PB electrodes with CHFH electrodes and found interesting results. Operating at pH5, PB based electrodes are stable for H_2O_2

detection, but when the pH arises to 7 (physiological pH), the PB based electrode loses 45% of its sensitivity from the 1th to 3th cycle. This drop diminishes a little bit by working at anodic potential (0.6V instead of - 0.2V) but it is still present and deep. Using CHFH electrode, the sensitivity at low pH (=5) is lower than PB electrode, but it drastically increases (+25% working at cathodic potentials and +100% at anodic potential) working at pH 7. Ali Eftekhari [26], developed an aluminum electrode covered with cobalt hexacyanoferrate film and they demonstrated how it is possible to work at neutral pH, achieving a LOD of 200 nM.

In the case of *non-enzymatic sensors*, metals, metallic oxides, and carbonaceous materials has been investigated, each with different morphologies such as NWs, NTs and NPs. The reduction of hydrogen peroxide to water occurs on these materials through an adsorption mechanism where the Rate Determining Step (R.D.S.) is the formation of adsorbed OH (OH_{ads}) [27].

$$H_2O_{2\,(bulk)} = H_2O_{2\,(surface)} \quad (3.4.1)$$

$$H_2O_{2\,(surface)} + e^- = OH^- + OH_{ads} \quad (3.4.2)$$

$$OH_{ads} + e^- = OH^- \quad (3.4.3)$$

$$2OH^- + 2H^+ = 2H_2O \quad (3.4.4)$$

REACTIONS 3.4. MECHANISM OF ELECTRO REDUCTION OF HYDROGEN PEROXIDE

Metallic atoms such Ag, Pd, Cu, and their alloys can act as active sites for OH adsorption, suggesting that the use of nano-structured sensors based on these metals should imply an increase of the reaction kinetics, with consequent better performance of the sensor. Since performances of the sensor can be improved considerably by enhancing active area, the use of different shaped nanostructures, such as nanowires, nanotubes or nanoparticles is of great advantage. Nasirizadeh et al. [28] have shown that multiwall carbon nanotubes

on glassy carbon electrode have excellent catalytic activity and reproducibility for detecting hydrogen peroxide, reaching a LOD of 0.27 μM and an excellent stability. They were also able to detect H_2O_2 in orange juice. About metal-based electrode, Nie et al. [29], developed a Pd nanocube modified electrode to detect H_2O_2. They found good features, with a LOD of 7.4 μM and a wide linear range up to 24mM. Furthermore, the interference from other compound was negligible and the standard deviation was lower than 9%. Nevertheless the good features of this enzyme-free sensor, palladium is an expensive material. Selvaraju et al. [30] fabricated a Cu-NPs modified glassy carbon electrode and they found a LOD of 0.5 μM. Anyway, the good result in term of LOD was not supported by stability and linear range. In fact, the linear range was really narrow, from 0.5 to 8 μM. In addition, the electrode properly worked just for 1 week. Furthermore, they did not test the nanostructured electrode against any interference compound, that is mandatory for an enzyme-free electrochemical sensor. In recent years, bimetallic nanomaterials have attracted great attention for application in many fields, including detection of hydrogen peroxide. Xiao et al. [31] modified in 2008 a chitosan film with AuPt-NPs, using an electrodeposition method. Chitosan has the property to adsorb different material so that has been used to trap the metal ions that were cathodically electrodeposited. A really low LOD of 0.5 nM has been reached. They tested the electrode with real samples, as well (honey, milk, urine and plasma) obtaining excellent results as confirmed by a standard photometric method. The good features of this electrode should come from the combination of Au and Pt: Pt is an excellent electroactive material but OH groups hardly desorb from it. The authors suggest that gold decrease this effect, increasing the electro activity of the electrode. Table 3.1 summarizes most of the example reported.

TABLE 3.1. EXAMPLES OF ELECTROCHEMICAL SENSORS AND BIOSENSORS FOR HYDROGEN PEROXIDE

N.S. NOT STUDIED, BL BIO LABELLED, MEA MIMIC ENZYMATIC ACTIVITY, NL NOT LABELLED

	LOD-ULR (μM)	***Stab. Days***	***Select.***	***Real sample***	***Type of sensor***	
HRP/graphite	*0.5-500*	*300 cycles*	*N.S.*	*N.S.*	*BL*	*20*
Fe3O4/Au/ HRP	*12-2500*	*28*	*UA,AA,GLU*	*Lenscare sol.*	*BL*	*22*
Fe3O4-NPs	*10-2000*	*30*	*UA, AA*	*N.S.*	*MEA*	*21*
Graphene/PB	*0.045-120*	*100 cycles*	*N.S.*	*N.S.*	*MEA*	*24*
PB/CNTs	*0.023-5000*	*N.S.*	*N.S.*	*N.S.*	*MEA*	*23*
Co-HCF	*0.2-1700*	*120*	*K, Cl, Br, I, Na*	*Seawater*	*MEA*	*26*
CNTs	*0.27-28*	*N.S*	*UA,AA,OXA,DA*	*Orange Juice*	*NL*	*28*
Cu-NPs	*0.5-8*	*7*	*N.S.*	*N.S.*	*NL*	*30*
Cu-NWs	*13.8-3700*	*7*	*AA, AU, GLU*	*N.S.*	*NL*	*This work*
Pd-NPs	*7.4-24000*	*N.S*	*N.S.*	*N.S.*	*NL*	*29*
Pd-NWs	*13.3-4400*	*30*	*AA, UA, GLU, POX*	*N.S.*	*NL*	*This work*
AuPt NPs	*0.003-0.35*	*30*	*Metals, cysteine, etoh*	*Milk, honey, urine, plasma*	*NL*	*31*

AMT Analysenmesstechnik GmbH and *Dulcostest* [32-33], already developed two prototypes of electrochemical sensors for hydrogen peroxide, that are available in the market (Figure 3.1 A-C). The AMT sensor has a wide linear range (8mM-4200 mM) but with a quiet high LOD (8 mM). It is able to make a measurement each 2 seconds and is stable in a wide range of pH (0-11). If

properly used, it has a shelf life of about 5-9 months. The Dulcostest sensor has similar features in terms of stability and pH range but its linear range is shifted towards µM range (15-1500 µM) and it can work also with high temperature (up to 50°C). Furthermore, they developed three different systems, able to detect H_2O_2 in different concentrations ranges (µM range the *PER 1-mA-50 ppm*, mM range the *PER 1-mA-200 ppm* and molar the *PER 1-mA-2000 ppm*). On the other hand, it has a longer response time, close to 7 minutes.

FIGURE 3.1 A) DULCOTEST H_2O_2 SENSOR; B,C) ATM PROTOTYPE

In my Ph.D work, I developed two nanostructured electrodes for sensing hydrogen peroxide. This part of my Ph.D work has been carried out in the ***Applied Physical Chemisry Lab at University of Palermo, under the supervision of Prof. Carmelo Sunseri, Prof. Rosalinda Inguanta and Prof. Salvatore Piazza***. Both electrodes, made of copper and palladium NWs, were

fabricated through galvanic deposition into the pores a nano-sized polycarbonate membrane acting as a template. Galvanic deposition does not require any external power supply, because the electromotive force for the deposition reaction arises from the galvanic coupling of a noble metal sputtered on the pore bottom of the template and a less noble one acting as a sacrificial anode. By this technique, which is novel for this application, structure, composition, and morphology of the deposit can be adjusted through a strict control of the operative parameters such as solution composition, pH, anodic to cathodic area ratio and so on.

The aims of this research were:

1. Asses the effect of the surface area, by comparing massive Cu and Pd electrodes and nanostructured ones with different nanowires length;
2. Asses the wettability of the nanostructures. Despite the high surface area of the NWs, the wettability of these electrodes can be a limiting factor, hindering the permeation of the porous structure of the nanowires by the aqueous solution containing the analyte;
3. To compare the features of a copper electrode made of a cheap material with a Pd one, made by a noble and expensive material.

Briefly, we found that the LOD does not depend strongly on the surface area, likely because, at low analyte concentration, the number of active sites is not the limiting factor. On the contrary, the upper limit of the linear range strongly depends on the surface area, for both copper and palladium based electrodes. Comparing the two materials, we found that Pd-based electrodes are more performing and more stable than Cu ones. Furthermore, Pd based are more selective towards potassium oxalate, whereas Cu electrodes are slightly influenced. On the other hand, we estimate that Pd sensor is more than 10 times more expensive than a copper one (about 70 €cents/sensor). We also found that

these nanostructures are highly hydrophobic and the use of a wetting agent, like ethanol, improves the performances of the sensor

3.2 Experimental

Electrode Synthesis

Commercial polycarbonate membranes (PoreticsTM PCTETM Filter Membranes) having a nominal mean pore diameter of about 200 nm, a pore density of 3×10^8 pores m^{-2} and a thickness of 6 μm, were used as a template for the galvanic deposition of the nanostructures. The Poretics membrane consists of interconnected cylindrical pore as shown in Figure 3.2, where SEM micrograph of the cross-sectional and top views are shown.

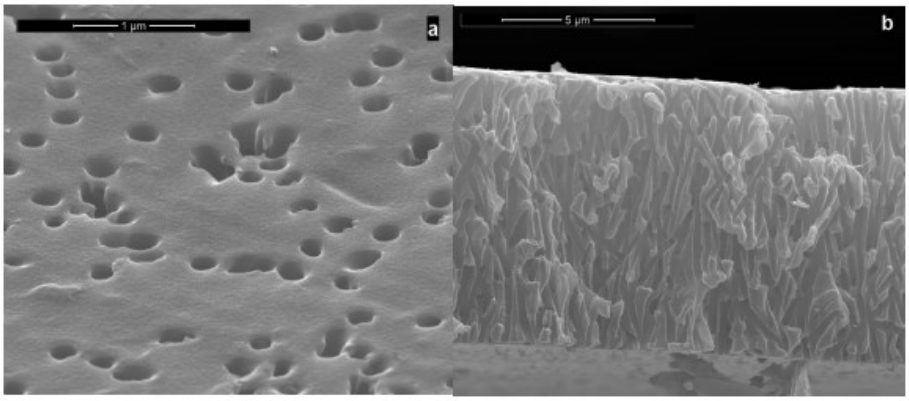

FIGURE 3.2 A) TOP VIEW AND B) CROSS-SECTION OF POLYCARBONATE MEMBRANE USED AS A TEMPLATE FOR GALVANIC DEPOSITION OF METAL NANOSTRUCTURES

By SEM analysis, we found that real mean pore diameter is close to 210 nm, pore density is 4.8 × 108 pores m−2, while thickness is about 8 μm. This morphology has been found for all membranes SEM examined. Nanowire growth was performed according to previous work [34]. Briefly, one surface of

the membrane was sputtered for 3 minutes with gold in order to make it conductive; then a thin copper layer (about 12 μm thick), acting as a current collector, was deposited on this surface. Copper deposition was performed in a two-electrode cell using a Pt mesh as a counter electrode, at room temperature from an aqueous solution of 0.1 M $CuSO_4 \cdot 5H_2O$ + 0.2 M H_3BO_3 having pH=3.9. Deposition was carried out at the constant cathodic current of 8 mA/cm^2 for 1 h, using a PAR potentiostat/galvanostat (PARSTAT, mod. 2273). Then, nanostructures were deposited inside the template channels by a galvanic process. Galvanic deposition is a spontaneous process where a sacrificial anode (in this case aluminium) is electrically coupled with the copper current collector and the bimetallic couple was immersed in a solution of $Pd(NH_3)_4(NO_3)_2$ and boric acid (0.05 M H_3BO_3) or $CuSO_4$ $5H_2O$ and boric acid (0.05 M H_3BO_3) for Pd and Cu deposition, respectively. The pH was adjusted through either nitric or sulphuric acid addition. A scheme of the galvanic cell used for the fabrication of Pd NWs is reported in Figure 3.3.

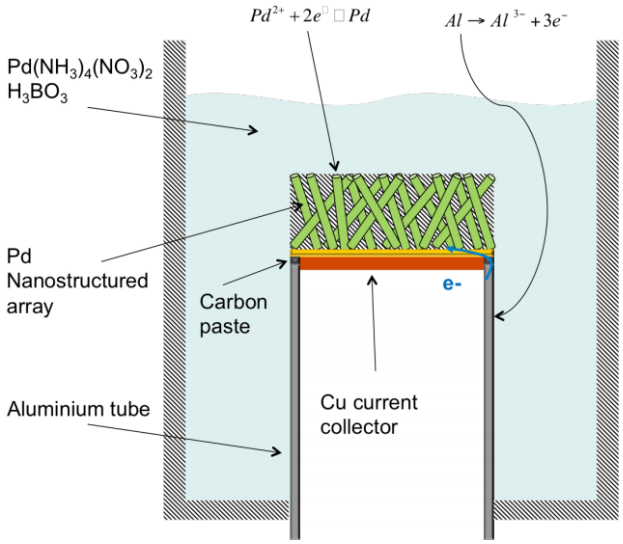

FIGURE 3.3 SCHEME OF GALVANIC CELL FOR PALLADIUM DEPOSITION INSIDE THE CHANNELS OF THE POLYCARBONATE MEMBRANE OF FIG. 3.1. SIMILAR SCHEME FOR COPPER DEPOSITION

The sacrificial aluminium anode works as a reducing agent that, dissolving into the solution, produce electrons that are consumed by the metallic ions that spontaneously deposit into the pores of the membrane. The energetic thermodynamic scale is schematized in Figure 3.4.

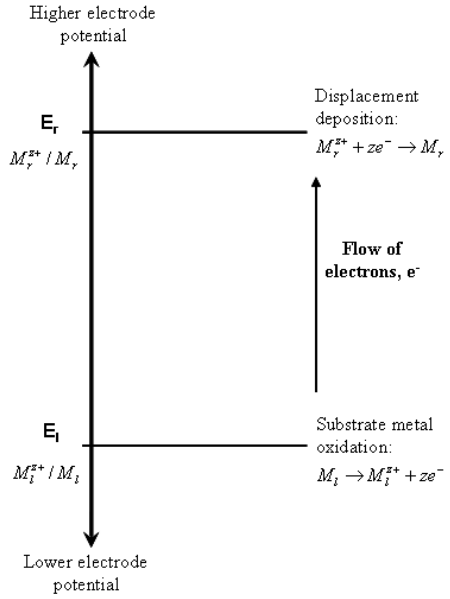

FIGURE 3.4 ENERGETIC SCALE OF THE GALVANIC COUPLING OF TWO DIFFERENT METALS WITH DIFFERENT NOBILITY

The Gibbs energy of this process is:

$$\Delta G^0 = -n\,F\,\varepsilon^0 \tag{3.2}$$

EQ. 3.2 FREE ENERGY OF AN ELECTROCHEMICAL PROCESS

Where n is the number of electrons exchanged in the reaction, F is Faraday's constant and ε^0 is the electromotive force (e.m.f), equal to $E_r^0 - E_l^0$. Using Al as an anode and Cu as a cathode, the electromotive force is positive (negative Gibbs energy), therefore, a spontaneous reaction occurs. Table 3.2 shows the standard electrochemical potential of different metals

TABLE 3.2 STANDARD POTENTIAL OF DIFFERENT METAL/METAL IONS COUPLE

Metal /metal-Ion	*Electrode Reaction*	*Standard Value (V vs NHE)*
Au/Au^{+}	$Au^{+} + e^{-} = Au$	1.69
Cu/Cu^{2+}	$Cu^{2+} + 2e^{-} = Cu$	0.35
Pd/Pd^{4+}	$Pd^{4+} + 4e^{-} = Pd$	0
Fe/Fe^{3+}	$Fe^{3+} + 3e^{-} = Fe$	-0.037
Pb/Pb^{2+}	$Pb^{2+} + 2e^{-} = Pb$	-0.126
Ni/Ni^{2+}	$Ni^{2+} + 2e^{-} = Ni$	-0.26
Co/Co^{2+}	$Co^{2+} + 2e^{-} = Co$	-0.28
Zn/Zn^{2+}	$Zn^{2+} + 2e^{-} = Zn$	-0.762
Al/Al^{3+}	$Al^{3+} + 3e^{-} = Al$	-1.66

In order to grow either Pd or Cu nanostructures by galvanic deposition, an aluminum tube was previously polished with 320, 800 and 1200 grade emery paper, washed with distilled water and rinsed ultrasonically in pure acetone. The gold film sputtered on one side of the template was electrically coupled with the aluminum tube through carbon conductive paste. Prior to starting the deposition, the assembled galvanic couple was immersed in pure ethanol for 5 min in order to favor template wettability. The galvanic coupling of two metals with different nobility leads to deposition of either Pd or Cu into the polycarbonate pores with simultaneous dissolution of aluminum. Deposition time, concentration of metal ions, and cathodic to anodic area ratio were optimized to grow an array of nanowires uniformly distributed on the surface. After NWs deposition, samples were etched in pure di-chloromethane in order to dissolve the template. Then, nanostructured electrodes were assembled with a copper tape and insulated with a lacquer (Lacomit - Cousins UK) to have a geometric area of about 0.05 cm^2. Morphology was characterized through scanning electron microscopy (SEM), using a FEI FEG-ESEM (mod. QUANTA 200) equipped with an Energy

Dispersive Spectroscopy (EDS) detector. Samples were also characterized by X-ray diffraction (XRD) using a RIGAKU diffractometer (model: D-MAX 25600 HK). All the diffraction spectra were obtained in the 2θ range from 10° to 100° with a step of 0.004° and a measuring time of 0.067 s for step, using the copper Kα radiation (λ= 1.54Å). Diffraction patterns were analyzed by comparison with ICDD database [35].

Electrochemical tests

Cyclic voltammetry was carried out at a scan rate of 50 mV/s in the potential range from −0.6 to +0.3V vs. Ag/AgCl in a three-electrode cell with a Pt mesh as a counter electrode. Sensor calibration curves were obtained by means of chronoamperometric tests carried out in aerated stirred solution at the constant potential of −0.2V vs. Ag/AgCl. Electrochemical tests were carried out in aqueous phosphate buffer solution (0.2 M PBS) and hydroalcoholic electrolyte prepared by mixing PBS with ethanol. In this case, a given volume of 0.4 M aqueous PBS was added to an identical volume of pure ethanol, so that 0.2 M was the final concentration of PBS in the electrolyte. The chronoamperometric curves were obtained by adding the desired amount of H_2O_2 to the solution at concentration up to 1 M. Selectivity tests were carried out using 4 different electro-active species (glucose, ascorbic acid, potassium oxalate and uric acid) at two different concentrations (1 mM and 10 mM) in the presence of hydrogen peroxide at a concentration an order of magnitude lower than that one of the interfering species (0.1 mM and 1 mM). Accuracy tests were also conducted by analyzing 4 different concentrations (0.2, 0.7, 1, and 2 mM) after different time of aging of nanostructured electrode and using the calibration line obtained previously.

3.3 Results and discussion

Electrodes fabrication

Figure 3.5 shows the complete fabrication process.

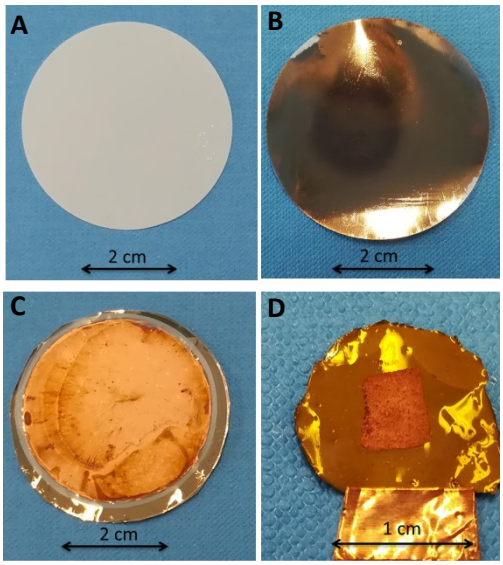

FIGURE 3.5 A) POLYCARBONATE MEMBRANE; POLYCARBONATE MEMBRANE SPUTTERED WITH GOLD (B) AND WITH ELECTRODEPOSITED CURRENT COLLECTOR (C); (D) ELECTRODE AFTER NANOSTRUCTURE DEPOSITION AND DISSOLUTION OF TEMPLATE

The polycarbonate membrane (Figure. 3.5A) has been sputtered with gold, in order to make conductive, one side of the template (Figure. 3.5B). A thin and uniform layer of gold (about 10 nm thick) is obtained after 3 min of sputtering. Due to the high aspect ratio (over 10^5), vertically aligned NWs/NTs are highly unstable if not properly attached to a base. In order to give a mechanical stability to the nanostructures, a copper current collector has been deposited on the sputtered gold film (Figure 3.5C). The current collector was deposited applying a constant current density of 8 mA/cm^2 for 1h, using a solution of boric acid (0.2M) and copper sulphate (0.1M), and a Pt mesh as a counter electrode in a

two electrode cell. A uniform layer of about 11 μm was obtained. Figure 3.6 shows the cell potential vs. time plot during the copper deposition.

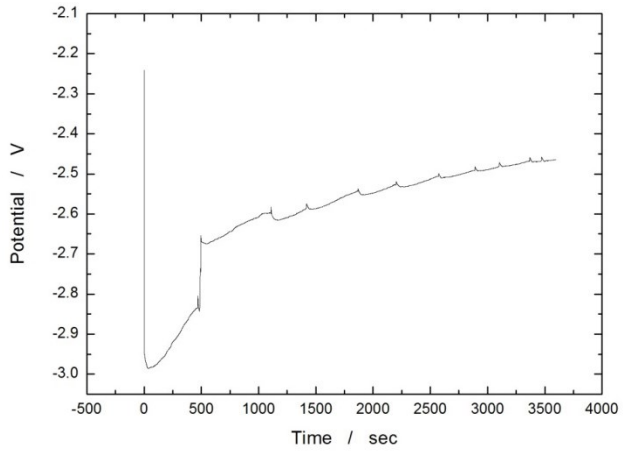

FIGURE 3.6 TYPICAL TREND OF POTENTIAL DURING COPPER CURRENT COLLECTOR DEPOSITION

The deposition of the copper current collector initially occurs on a gold film, while, it continues as a deposition of copper on copper. This explains the potential drop at the beginning of the experiment that reaches a semi-plateau after 500 s, when a uniform copper layer is already deposited. The current collector was deposited in a two electrodes cell, therefore some scattering of the results was found owing to impossible control of parameters such as electrodes distance or anodic surface, and so on.

Galvanic deposition is a spontaneous process where a sacrificial anode (in this case aluminium) is electrically coupled with the copper current collector and the bimetallic couple is immersed in a solution containing either Pd or Cu ions (Figure 3.3). During the galvanic deposition, the membrane colour moves from white to black and brown for palladium and copper respectively. The last step concerns the dissolution of the template by etching the electrode several times in a solution of pure DCM (Figure 3.5 D).

The morphology of the electrode highly depends on the deposition parameters, such as batch composition, pH, deposition time and anodic to cathodic area ratio [34, 36-37]. All these parameters were varied in order to find the best conditions to obtain an array of metal nanostructures uniformly distributed over the current collector.

Due to the change of template and type of galvanic cell in comparison to what used previously [38], here it was necessary to optimize the deposition conditions. In particular, the new cell permitted to reduce drastically the deposition time using an aluminium tube that provided a large anodic area. Initially, a cell with a cathodic/anodic area ratio equal to 0.055, and containing either 7 mM $Pd(NH_3)_4(NO_3)_2$ or 0.1 M $CuSO_4$ $5H_2O$ was used. The first investigated parameter was pH that is fundamental because it influences the process thermodynamics. Initial attempts for metal deposition were carried out at pH value of the as-prepared bath (6.8 for Pd and 4 for Cu). The deposition was slow and the membrane colour changed slightly towards black/brown after 2 days. In Figure 3.7 SEM images of the copper (A) and palladium (B) electrodes, obtained under these conditions are shown.

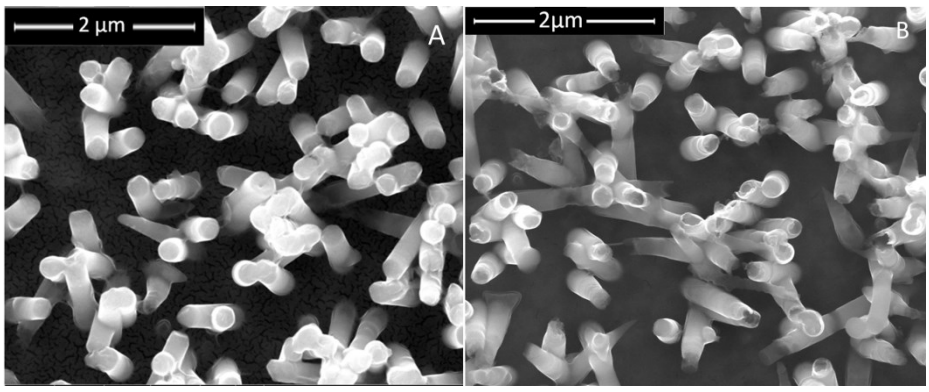

FIGURE 3.7 A) COPPER NANOWIRES (NWS) AFTER 2 DAYS OF DEPOSITION AT PH 4; B) PALLADIUM NWS AFTER 2 DAYS OF DEPOSITION AT PH 6.8

Really short Cu NWs were visualized. Surprisingly, the same NW height was observed with the electrode immersed in the Pd bath (Figure 3.7 B). This suggested us that the galvanic deposition did not occur at this pH, and the NWs shown in Fig. 3.7 came from the current collector deposition because, at the beginning of the copper current collector deposition, the copper ion solution can penetrate inside the membrane pores forming a copper deposit with a nanostructured shape. This hypothesis has been confirmed by EDAX analysis of these samples (Figure 3.8).

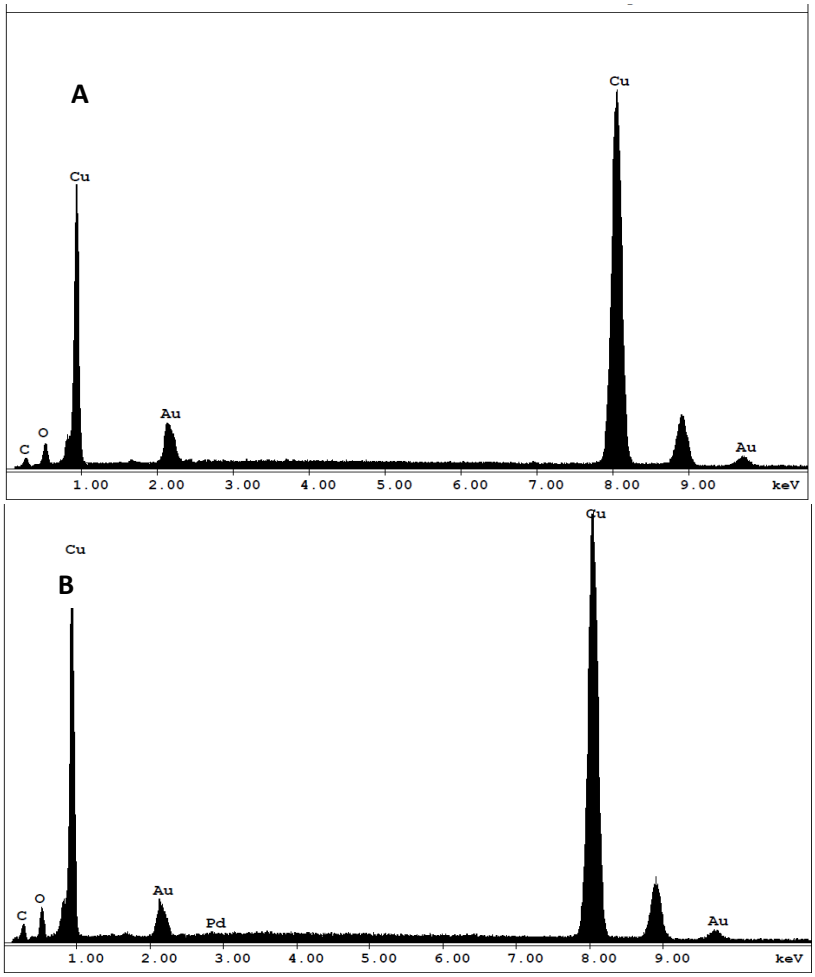

FIGURE 3.8 EDS ANALYSIS OF SAMPLE OF FIG. 3.6 A (A) AND 3.6B (B)

Carbon, oxygen, gold, and copper peaks are present in both spectra. The last one is due to the copper current collector, while C, and O come from some residual of polycarbonate. It is important to highlight that Pd is not present in the samples (Figure 3.7B), confirming that galvanic deposition did not occur. Furthermore, during the deposition in these conditions, a white gel deposit over the aluminium tube was found, probably an aluminium hydroxide. In fact, at pH>3 (Figure 3.9) the stable compound is not Al^{3+} but Al_2O_3 $3H_2O$ (white hydrargillite).

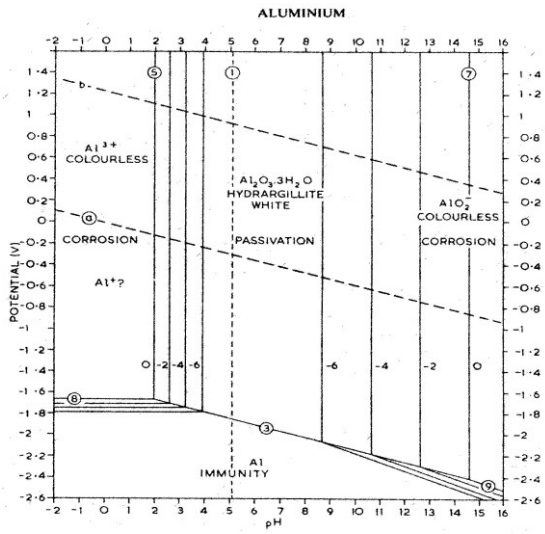

FIGURE 3.9 POURBAIX'S DIAGRAM OF ALUMINIUM

In order to favour dissolution of the Al sacrificial anode, bath pH was lowered to 2 for both types of electrodes. At this pH, upon immersion in the electrolyte containing the desired metal ions, we observed precipitation of either Pd or Cu into the pores of the membrane that changed colour just after 20 min. In the case of Pd deposition, the following reaction occurs

$$Pd(NH_3)_4^{2+} + 2e^- + 4H_2O = Pd + 4NH_4^+ + 4OH^- \qquad E^0=0.0V(NHE) \qquad (3.5)$$

REACTION 3.5 GALVANIC DEPOSITION OF TETRAMINE PALLADIUM

During galvanic deposition, pH was increasing owing to the side reaction of base electro-generation in nitrate solution, which occurs simultaneously to that of Pd NW deposition [38-39]:

$$NO_3^- + H_2O + 2e^- \rightarrow NO_2^- + 2OH^- \qquad E^0 = 0.01 \text{ V(NHE)} \qquad (3.6)$$

REACTION 3.6 BASE ELECTRO-GENERATION IN NITRATE SOLUTION

The electrons necessary to these reactions were supplied by aluminum dissolution:

$$Al \rightarrow Al^{3+} + 3e^- \qquad E^0 = -1.7 \text{ V(NHE)} \qquad (3.7)$$

REACTION 3.7 GALVANIC DISSOLUTION OF ALUMINUM

The electron transport from the anodic area (Al surface) to the cathodic one (pore bottom) occurs through the carbon conductive paste, electrically connecting the sacrificial anode with the copper current collector grown on the template surface. Similar reactions occurs for copper deposition, except reaction 3.6. In these deposition conditions, nanostructures reach the top of the membrane (length 8µm) after about 70-80 minutes but the deposition was not reproducible, as can be seen from Figure 3.10 A and B.

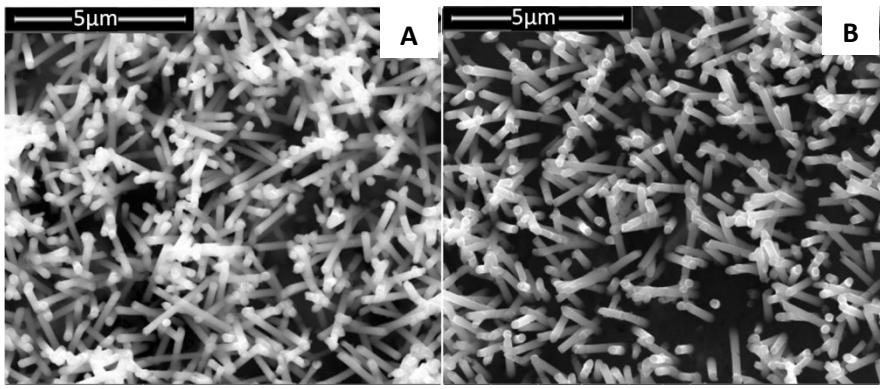

FIGURE 3.10 PD-NWS AFTER 40 MIN OF GALVANIC DEPOSITION OF TWO DIFFERENT SAMPLES

Furthermore, the deposition was not uniform over the entire membrane surface, because nanostructures with different length were measured in different areas of the same sample (Figure 3.11).

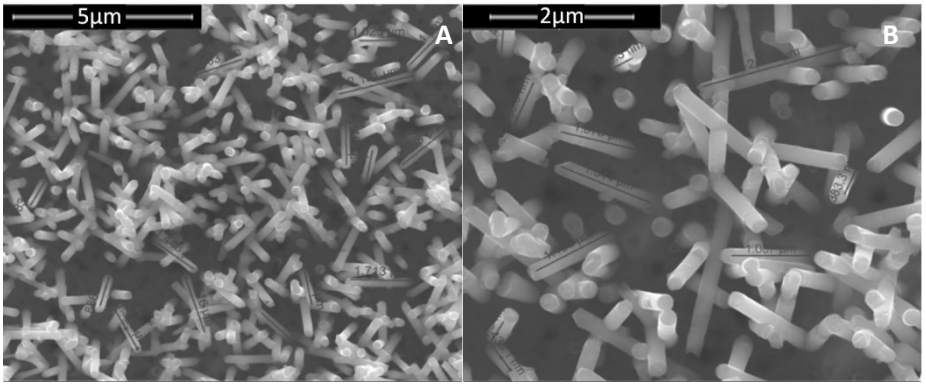

FIGURE 3.11 LENGTH OF CU NWS IN DIFFERENT REGION OF THE SAME SAMPLE

In order to eliminate these drawbacks, metal concentration in solution was halved (3.5 mM for Pd and 50 mM for Cu), and the ratio between anodic and cathodic area was set to 0.065, at the aim of decreasing the driving force for nanostructures growth. Under these new conditions, the deposition of nanostructures was uniform and reproducible and in particular, it was possible to control the length of nanowires through deposition time. SEM images of Figure 3.12 show morphology of Pd and Cu nanostructures after 20 to 40 minutes of deposition. From these micrographs, it appears that length of the nanostructures was increasing with deposition time.

TABLE 3.3 NANOSTRUCTURES HEIGHT AND MORPHOLOGY OF PD AND CU AFTER 20, 30 AND 40 MIN OF DEPOSITION

Deposition time min	***Cu-NWs height/ Morphology***	***Pd-NWs/Nts height/ Morphology***
20	*1.6 µm / NWs*	*1.7 µm /NTs*
30	*2.1 µm / NWs*	*2.1 µm / NWs-NTs*
40	*3.0 µm / NWs*	*5.1 µm / NWs*

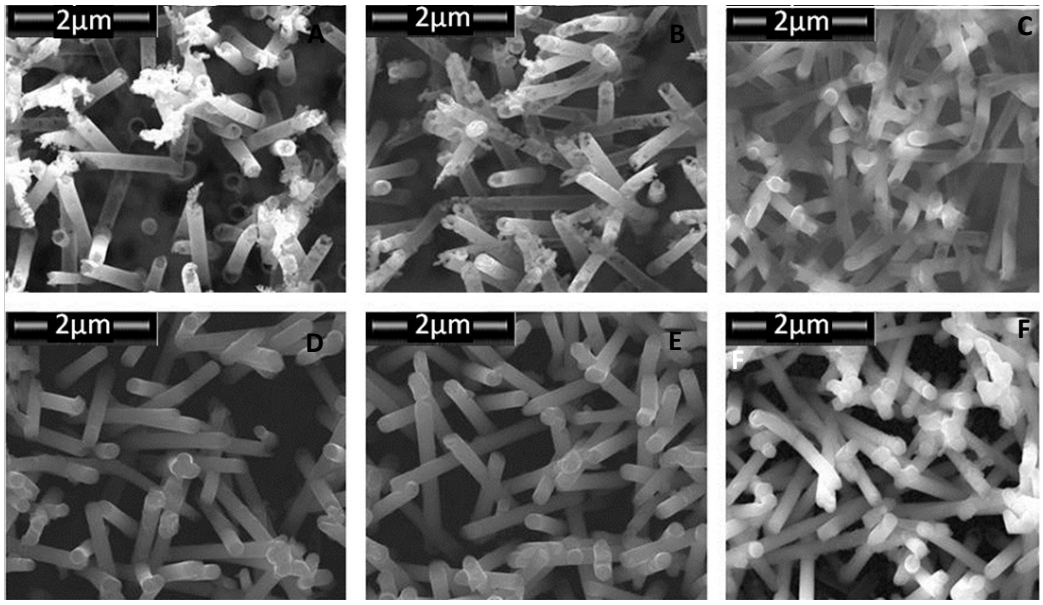

FIGURE 3.12 A),B),C): PD NWS AFTER 20-30-40 MIN OF GALVANIC DEPOSITION. D),E),F): CU NWS AFTER 20-30-40 MIN OF GALVANIC DEPOSITION

Table 3.3 summarizes the average height of the nanostructures with different deposition time and their morphology (either NWs or NTs). It is clear from Table 3.3 and from Figure 3.12 that nanostructures height increased (not linearly) with the deposition time. From Fig. 3.12 we have also calculated a mean nanowire diameter of about 220 nm, close to the mean pore diameter of polycarbonate membrane. Besides, these images show the interconnection of nanostructures with free-space between nanostructures of 1.17±0.63 µm.

Furthermore, copper nanostructures always show a NW morphology, while Pd electrodes changed their morphology from NTs to NWs over time. NTs morphology can be due to the concurrent reaction of hydrogen evolution:

$$2H^+ + 2e^- \rightarrow H_2 \qquad E^0 = 0.0\text{-}0.059\text{pH V(NHE)} \qquad (3.8)$$

REACTION 3.8 HYDROGEN EVOLUTION REACTION

Development of gas bubbles into the template channels forces Pd deposition toward the pore walls. For longer deposition times, as the local pH increases owing to the reaction 3.6, the driving force for hydrogen evolution decreases and reaction 3.8 slows down, so that morphology of the nanostructure switches from nanotubes to nanowires. These phenomena did not occur during copper deposition because the copper standard potential is more than 0.3 V nobler and so hydrogen evolution cannot happen. To fully characterize nanostructures, EDS and XRD analyses were carried out, as shown in Figure 3.13.

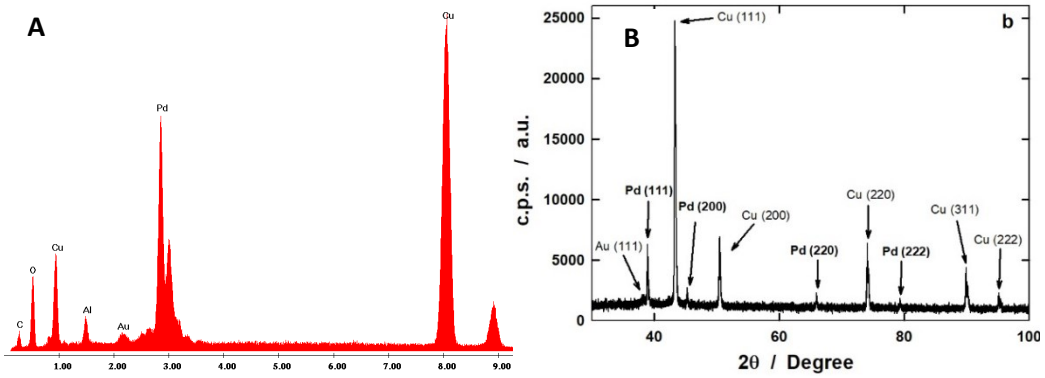

FIGURE 3.13 EDS (A) AND XRD (B) ANALYSIS OF PD NWS

EDS spectrum of Figure 3.13A shows peak of Pd arising from the galvanic deposit, while peaks of Cu is due to the current collector, peaks of Au, C and O are due to sputtered gold layer and residual trace of polycarbonate membrane, respectively. Some XRD peaks of Figure 3.13 B correspond to Pd face-centered cubic phase (card 87-637 of the ICDD database [35]), the other ones are attributable to copper (card 4-836) and Au (card 4-784) coming from the current collector and gold sputtered layer. At all deposition time, Pd nanostructures are

polycrystalline with the most intense peak along the plane (111). Using Scherrer's equation [40], an average grain size of about 34 nm was calculated. Similar results were found for Cu NWs.

For the sake of comparison, also nanostructured thin films of Pd and Cu were fabricated by galvanic deposition, in the same conditions of Pd or Cu NWs, into a commercial copper foil. SEM pictures obtained after 40 min of deposition (Figure 3.14 A-D) show the formation of a thin layer of either Cu or Pd, uniformly covering the Cu substrate (grooves due to the abrasion with abrasive paper are clearly visible) and consisting of nanoparticles with 114±2.6 nm and 260±3.8 nm size for Pd and Cu, respectively.

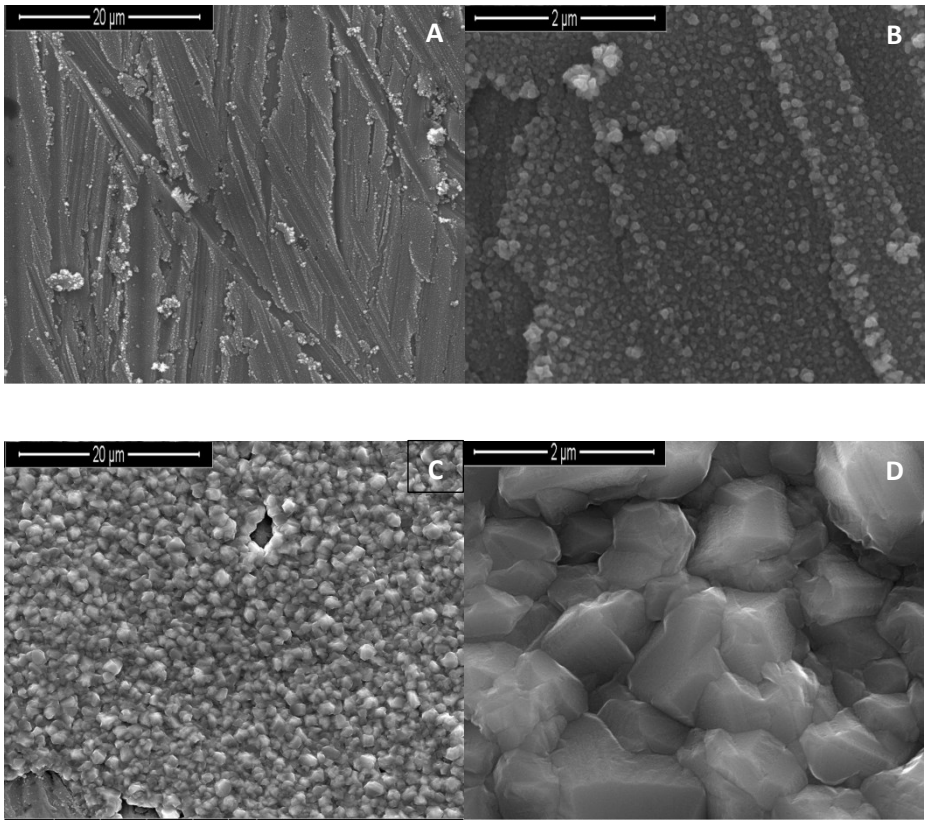

FIGURE 3.14 SEM IMAGES OF PD (A, B) AND CU NPS (C,D)

Sensor calibration

In order to analyze the sensing behavior of Pd and Cu nanostructures, CV and chronoamperometric tests were carried out. Cyclic voltammetry were conducted in the absence and presence of 0.1 mM H_2O_2 in PBS to found the potential to be applied for the subsequent chronoamperometric test. Figure 3.15 shows CV curves of Pd NWs obtained after 40 minutes of deposition.

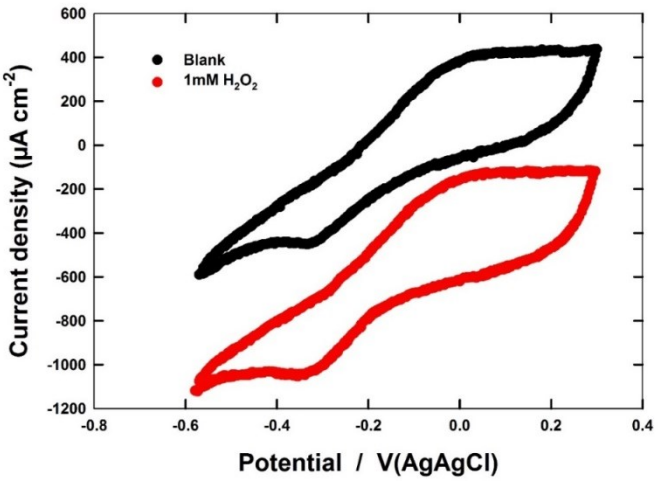

FIGURE 3.15 CV OF 40 MIN DEPOSITED PD NWS IN PURE PBS (BLACK CURVE) AND WITH 1MM HYDROGEN PEROXIDE (RED CURVE) AT 0.05 VS^{-1}

In the presence of 1 mM H_2O_2, the CV curve shifts toward higher currents confirming the electrocatalytic properties of Pd NWs. The difference between reduction current values of these two CVs increases from 0 to -0.2 V. and then, it remains constant from -0.2V to -0.4V. Greater is the difference between the blank current and that one recorded in the presence of H_2O_2, better are the electrocatalytic properties of the sensor; thus the subsequent chronoamperometric tests were performed at -0.2 V (vs Ag/AgCl). To work at this low potential is of value for guaranteeing the selectivity of the sensor, because many biological systems contain electroactive species such as ascorbic

acid, uric acid and other ones, which can interfere with the electro-reduction of H_2O_2 [17-18]. The same experiment was carried out using Cu NWs, and we found a lower signal compared to Pd NWs. Anyway, an applied potential of -0.2V vs Ag/AgCl has been selected also in this case.

Also, the sensing behaviour of a nanostructured thin film was investigated in comparison with a planar electrode. This investigation led to valuable results concerning not only the influence of the active surface area on sensor performance but also the wettability of the nanostructures.

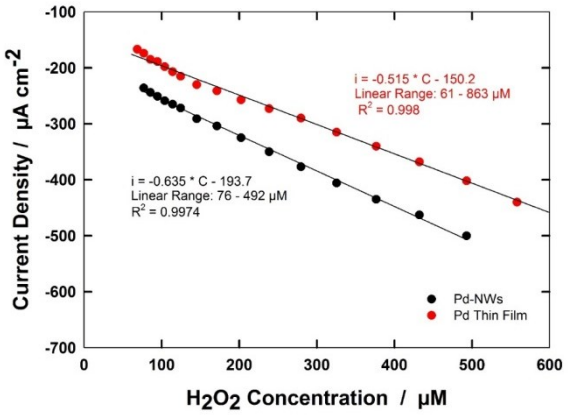

FIGURE 3.16 SENSING CALIBRATION LINE OF PD NPS (RED LINE) AND PD NWS (BLACK LINE) IN PURE PBS

Initial tests carried out with in a PBS solution showed (Figure 3.16) similar electro-catalytic behavior of nanoparticle thin film (red plot) and Pd NWs (black plot). NPs based electrode shows a wider linear range but a lower sensitivity. Furthermore, the nanostructured electrode starts to saturate faster (1mM vs 100 mM). Considering the high surface area of NWs in comparison to that of planar NPs, these results are very surprising. We think that the no-excellent performances of the nanostructured electrodes are attributable to their scarce wettability. Likely, the solution does not soak fully into the porous mass because the NWs are hydrophobic, as evidenced by contact angle analysis of Figure

3.17. Owing to the high surface tension, only the top of the NWs is wetted by the aqueous solution, therefore the working surface area is lower than the total one.

FIGURE 3.17 CONTACT ANGLE OF WATER DROP ON PD NWS

To overcome this problem, we found that electrochemical tests must be carried out in a hydro-alcoholic solution that ensures the wettability of the nanostructures. In fact, we have found a contact angle of about 100° when only PBS was used, while in the case of hydro-alcoholic solution no drop was visible on the electrode surface because the porous mass was permeated instantaneously. Ethanol (EtOH) was selected because in advance we checked that it does not interfere with the electro-reduction of H_2O_2.

In hydro-alcoholic solution, very good performances of the nanostructured electrodes (both Pd and Cu) were found.

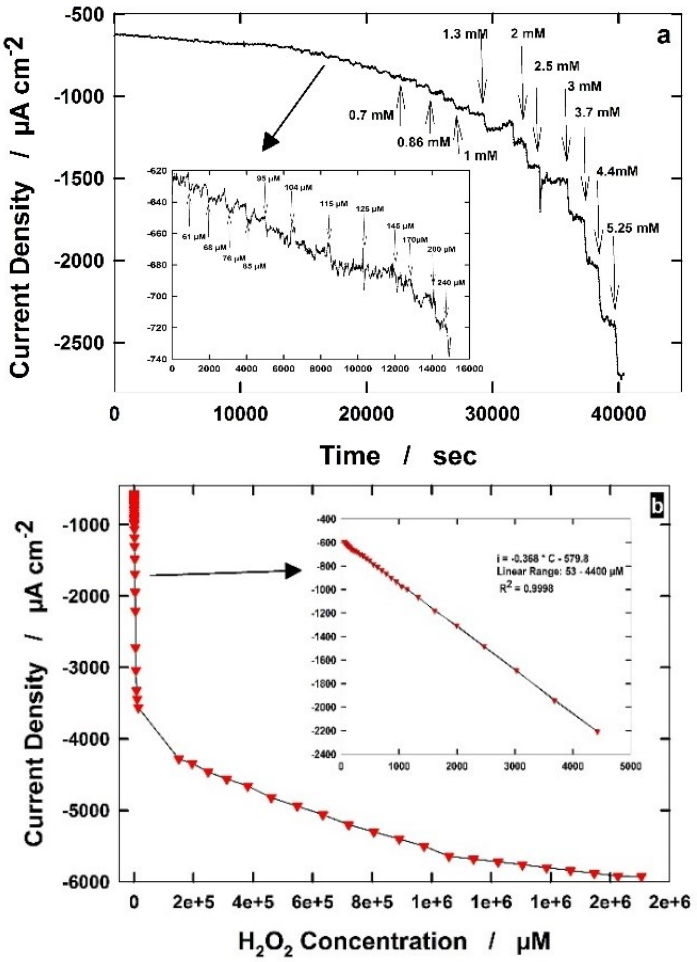

FIGURE 3.18 (A) CHRONOAMPEROMETRIC TEST OF PD NWS IN HYDROALCOHOLIC SOLUTION; (B) CALIBRATION LINE

Figure 3.18A shows the fast response of Pd NWs after injection of H_2O_2. A sudden increase of cathodic current is observed, followed by a fast (less than 4 seconds) stabilization to a new value. Figure 3.18 B shows the calibration curve obtained from the test of Figure 3.18A. A linear response from 53 µM to 4400 µM was found (inset figure 3.18 B). At higher concentration of hydrogen peroxide, there is a linear dependence but with lower and lower sensitivity (1.5 µA mM^{-1} cm^{-2} from 0.15 to 1 M and 0.5 µA mM^{-1} cm^{-2} from 1 M to 1.6 M).

Limits of the linear range were selected in order to obtain a calibration line with a R^2 greater than 0.995. The LOD of these sensors is highly limited by the current noise, as shown in Figure 3.19.

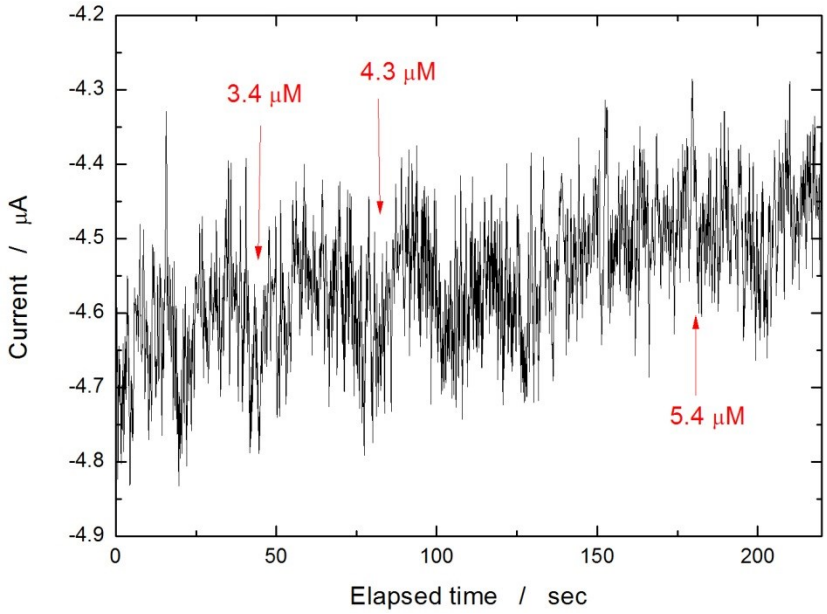

FIGURE 3.19 NOISE IN THE CHRONOAMPEROMETRIC TEST OF PD NWS IN HYDROALCOHOLIC SOLUTION FROM 3 TO 6 μM OF HYDROGEN PEROXIDE

When small amount of H_2O_2 was injected into the cell, a sudden increase of current is visualized but, when the system goes back to a steady state value, the noise is higher than the current change due to this small increase of H_2O_2 concentration. We think it is possible to decrease the LOD using a more precise reading system, such as, for example, a digital/analogical filter.

Figure 3.20 shows the effect of the active area on the sensor performance. In detail, the calibration lines of electrodes with nanostructures of different length are shown. For the sake of comparison, also the calibration lines of nanoparticle thin films and planar Pd sensors are shown. For a better comparison, in Figure

3.20 all calibration lines are referred to the y-axis intercept, that is almost coincident with the blank current density.

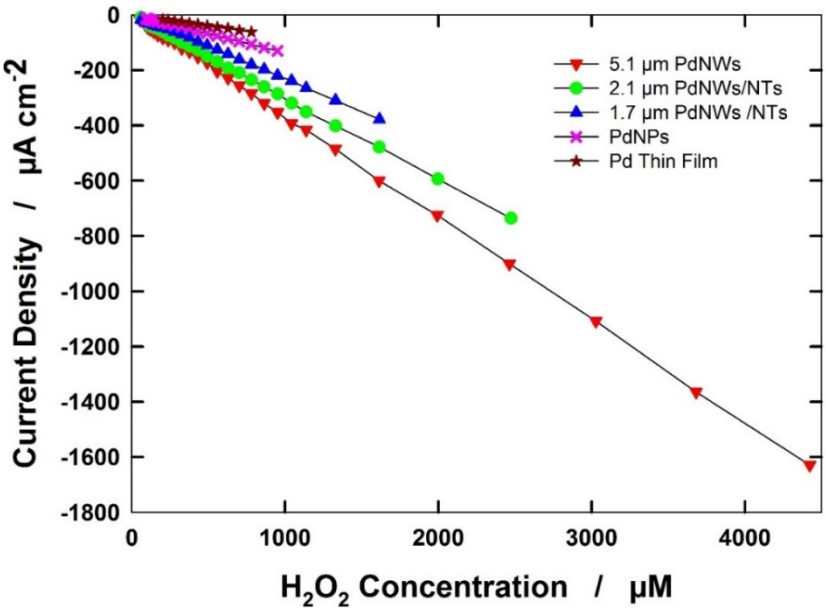

FIGURE 3.20 EFFECT OF SURFACE AREA ON CALIBRATION LINE OF PD BASED SENSING ELECTRODES

It can be observed a noticeable increase of the sensing performance when a nanostructured Pd is used in place of planar Pd surface, owing to the increase of the sensing surface. Table 3.4 shows Linear Range (LR), LOD, and Sensitivity values of Pd based sensing electrodes: a significant increase of the upper limit of the linear range is observed with increasing NWs length, while the lower limit remains almost constant. Thus, the increase of active sites number guarantees a linear sensing of H_2O_2 up to higher concentration without reaching saturation. On the contrary, the lower limit does not depend on surface area, because the number of active sites is always high enough for the electrochemical reduction of small amount of hydrogen peroxide. Table 3.4 also shows that LOD slightly

decreases and sensitivity increases with nanowires length, confirming the good electro-catalytic behavior of the nanostructured electrodes.

TABLE 3.4 LINEAR RANGE (LR), LOD AND SENSITIVITY OF PD BASED SENSING ELECTRODES

Sample	*LR* *µM*	*LOD* *µM*	*Sensitiv.* *µA mM^{-1} cm^{-2}*
Pd thin film	*202-780*	*21*	*0.078*
Pd-NPs	*104-951*	*18.8*	*0.136*
1.72µm Pd-NWs	*60-1600*	*17.7*	*0.173*
2.1µm Pd-NWs	*60-2400*	*15*	*0.299*
5.1µm Pd-NWs	*53-4400*	*13.3*	*0.368*

The standard deviation of these measurements was lower than 12%. The increase of sensitivity is not linear with nanostructures length, probably due to a nonlinear relationship between the nanostructures length and electrochemical active area, because of the interconnections between the channels visible in the SEM images of Figure 3.2. Furthermore, ethanol improves the wettability of the NWs but there is no certainty that the NWs are totally wetted, especially when are longer. Similar conclusion was reached by Li et al [41] in the case of Pt nanowires grown electrochemically in anodic alumina template. According to these results, we can conclude that 5 µm long nanowires exhibit the better performances, therefore, the selectivity, accuracy and stability tests were carried out by employing these sensing electrodes. Similar results were obtained using Cu electrodes. In this case, the best results were found with 3µm long NWs (Figure 3.21A-C and Table 3.5).

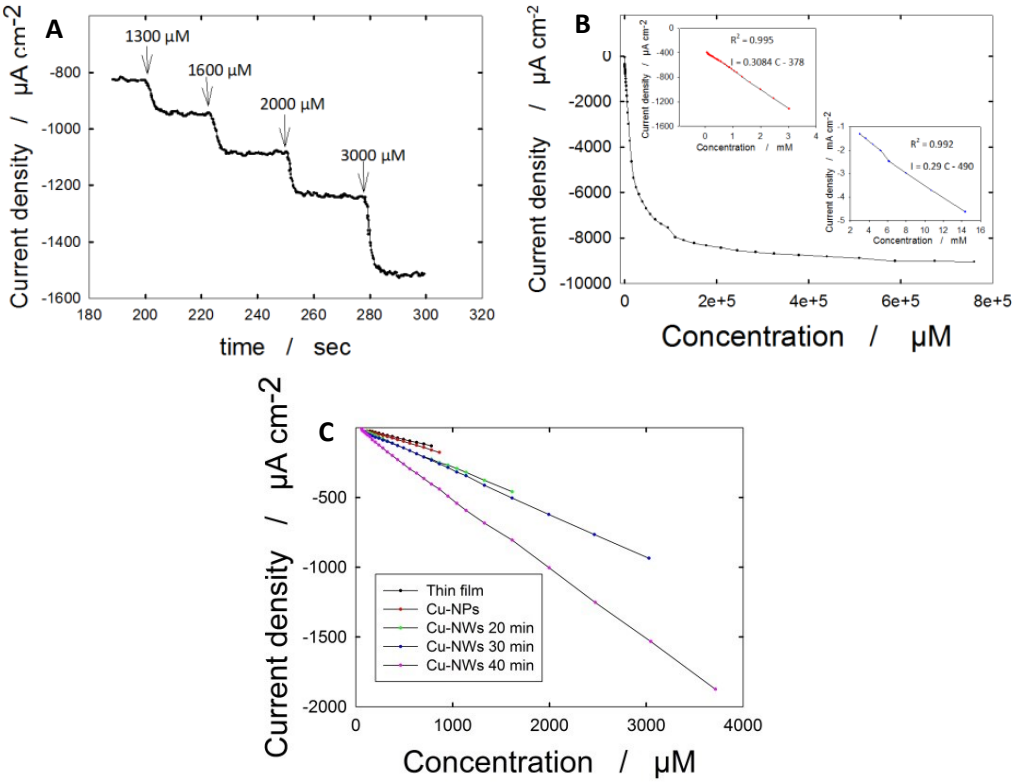

FIGURE 3.21 PERFORMANCES OF CU NWS ACTING AS SENSING ELECTRODES IN HIDROALCHOLIC SOLUTION: A) CHRONOAMPEROMETRIC CURVES; B) CALIBRATION CURVES; C) INFLUENCE OF THE SURFACE ARE ON CALIBRATION LINE

TABLE 3.5 LINEAR RANGE, LOD AND SENSITIVITY OF CU BASED SENSING ELECTRODES

Sample	*LR / µM*	*LOD / µM*	*Sensitivity / µA uM^{-1} cm^{-2}*
Cu thin film	*145-780*	*19.4*	*0.168*
Cu-NPs	*114-863*	*16.6*	*0.202*
1.6µm Cu-NWs	*104-1600*	*15.4*	*0.285*
2.1µm Cu-NWs	*61-3000*	*14.8*	*0.308*
3µmCu-NWs	*61-3700*	*13.8*	*0.507*

We found that the sensing stability highly improves if the electrode is stored in PBS. In detail, when the electrodes are stored in air, the open circuit potential

changes over time almost randomly, while, when stored in PBS, it is almost constant (0.08 V vs Ag/AgCl for the copper sensing electrodes and 0.27 V vs Ag/AgCl for the palladium ones). Furthermore, we found that when the electrodes (both Cu and Pd) are in contact with H_2O_2 higher concentration than 0.5M, the open circuit potential slightly modifies. The origin is due to the mechanism of hydrogen peroxide detection which is based on an adsorption step, which, likely, is the rate determining step (r.d.s.): as the H_2O_2 concentration is high, some OH groups remain adsorbed on the electrode with consequent alteration of the electrode surface state, leading to open circuit potential change. It is important to highlight that this is an invertible phenomenon, because it disappears after 24h of storage in PBS. Furthermore, such a high level of hydrogen peroxide is not usual in the practice and anyway, is far away from the linear range of both Pd or Cu sensing electrodes.

Selectivity, Accuracy and stability

In order to investigate selectivity of the nanostructured sensors, some chronoamperometric tests were carried out in the presence of four relevant electroactive species (glucose, ascorbic acid, potassium oxalate and uric acid) at two different concentrations (1 mM and 10 mM) in PBS/EtOH solution containing H_2O_2 at concentration an order of magnitude lower than that of the interference species. In particular, the contaminants were introduced after stabilization of the current following the addition of 0.1 mM (first step) and 1 mM (second step) of H_2O_2. Figure 3.22 shows the results using a nanostructured Pd electrode.

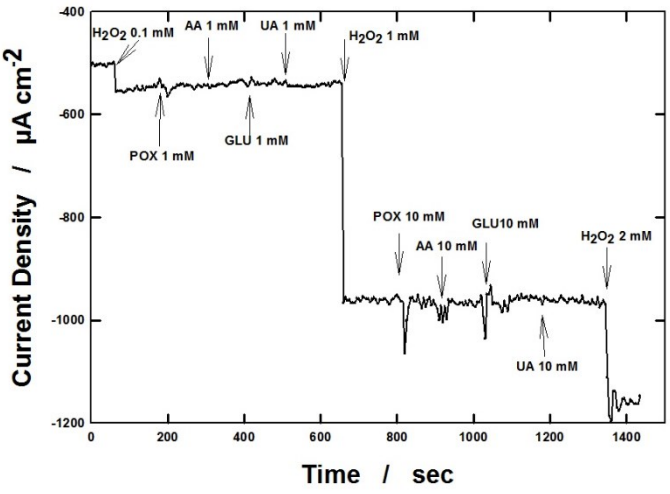

FIGURE 3.22 SELECTIVITY OF PD NWS BASED SENSING ELECTRODE AGAINST ASCORBIC ACID (AA), POTASSIUM OXALATE (POX), URETIC ACID (UA), AND GLUCOSE (GLU)

Negligible response to the injection of 1mM of these species is evident. When 10 mM of electroactive species were added, an instantaneous variation of sensor response was observed for glucose, ascorbic acid and potassium oxalate, after which the current got back to the original value. This transient is probably related to the instantaneous change of the composition at the electrode/solution interface following the addition of the electroactive species close to the sensing electrode. On this basis, it is possible to conclude that the sensing electrode is selective toward hydrogen peroxide. Such a significant selective behavior is due to the low applied polarization potential hindering the reaction of other species at the sensing surface. It is interesting to note that a further injection of H_2O_2 to the solution containing electroactive species produces a stepwise increase of current, suggesting that the presence of interferent species does not affect detection of hydrogen peroxide. Figure 3.23 shows the same experiments carried out using a 40 min long deposited Cu NW based sensing electrode.

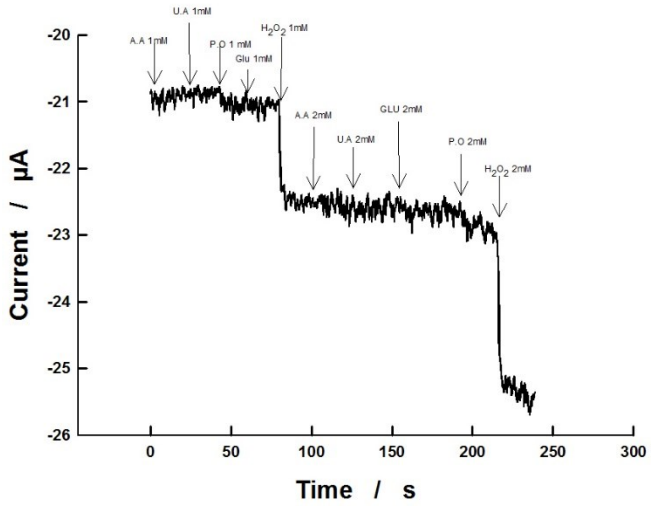

FIGURE 3.23 SELECTIVITY OF CU NW BASED SENSING ELECTRODE AGAINST ASCORBIC ACID (AA), POTASSIUM OXALATE (POX), URETIC ACID (UA) AND GLUCOSE (GLU)

It is possible to observe that the copper based sensing electrode is still selective towards glucose, ascorbic acid and uric acid, but it is not towards potassium oxalate. When 1mM and 2mM POX was injected into the solution, a fast and stable increase of the current signal occurred. Anyway, it is important to highlight that also in the presence of high concentration of POX, the electrode is still able to detect hydrogen peroxide (see last injection of Figure 3.23).

In addition, accuracy was evaluated by testing the nanostructured sensors after about 1 month of storage in PBS solution. Four different concentrations of hydrogen peroxide (0.2, 0.7, 1, and 2 mM) were tested with 3 different electrodes and accuracy was calculated by the following equation:

$$\varepsilon = \frac{Cm - Cv}{Cv} * 100 \qquad (3.3)$$

EQUATION 3.3 EQUATION USED TO EVALUATE SENSOR ACCURACY

where ε is the accuracy percent, c_m is the detected concentration and c_v the real one. Figure 3.24 shows the results of these tests with 40 min long growth of Pd NWs.

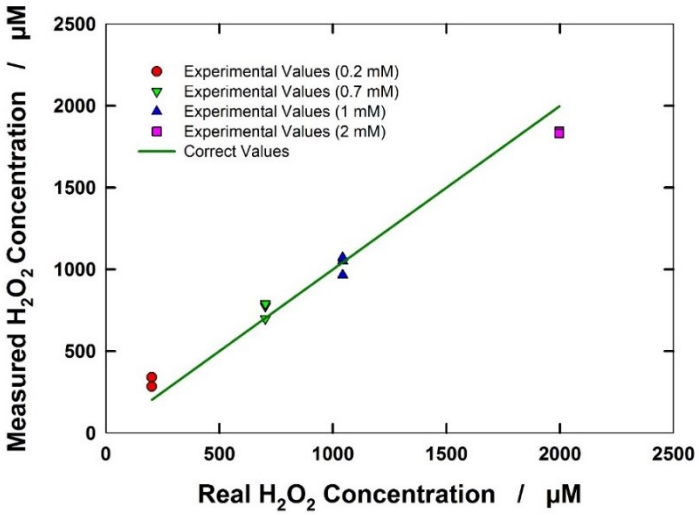

FIGURE 3.24 ACCURACY OF 40 MIN LONG DEPOSITED PD NWS IN HYDROALCHOLIC SOLUTION

At concentration close to both upper and lower limits of the linear range, accuracy decreases. In particular, an error of about 15% was calculated at low and high concentration, respectively. A good agreement between measured and real values was found for intermediate concentration inside the limit values, with a calculated error of about 5%. After 1 month long storage, the nanostructured sensing electrode is less precise when the concentration to be detected approaches the limits of the range of linearity. This result suggests that after 1 month, a new calibration of the electrode is necessary. After recalibration, accuracy tests revealed errors less than 5%, that means a very good precision of the Pd nanostructured sensing.

The same experiment was carried out with Cu NWs based sensing electrode stored for 7 days in PBS. Table 3.6 shows the results of this experiment.

TABLE 3.6 ACCURACY OF CU NWS AFTER 7 DAYS OF STORAGE IN PBS

Real concentration µM	*Average Experimental Value µM*	*Accuracy*
198.5	*98.6*	*50 %*
695	*144.3*	*80%*
1042.6	*180.1*	*82%*
1996.8	*253*	*87%*

Here, the accuracy of the sensing electrode is really scarce. After these tests, the sensing electrodes have been calibrated again and the tests were carried out after 1 day of storage in PBS. The results are shown in Table 3.7 and evidence that the accuracy is now highly improved.

TABLE 3.7 ACCURACY OF CU NWS AFTER RICALIBRATION AND 1 DAY OF STORAGE IN PBS

Real concentration µM	*Average Experimental Value µM*	*Accuracy*
198.5	*112*	*41 %*
695	*495*	*28%*
1042.6	*706*	*28%*
1996.8	*1150*	*41%*

Therefore, it is possible to conclude that the drift time of a nanostructured Cu electrode is less than 1 week.

Economic Analysis

The results of these experiments clearly indicate that the performances of Pd based sensing electrodes are much better compared to the Cu ones. Indeed, the LOD is slightly lower, the linear range is wider, the stability is longer and the selectivity is higher. On the other hand, the cost of these electrodes is much higher. We carried out an easy and fast economic analysis taking into account all the steps to develop the electrode. All the costs are summarized in Table 3.8.

TABLE 3.8 COST OF DIFFERENT STEPS FOR CU AND PD NWS DEPOSITION

	Price (cents/electrode)	***Cu***	***Pd***
Polycarbonate template	*10*	*Yes*	*Yes*
Sputtering	*22*	*Yes*	*Yes*
Current collector	*13*	*Yes*	*Yes*
DCM	*10*	*Yes*	*Yes*
Assembly	*10*	*Yes*	*Yes*
Copper for NWs deposition	*10*	*Yes*	*No*
Palladium for NWs deposition	*651*	*No*	*Yes*
Total Price per electrode		*0.75*	*7.4*

In this analysis, we did not consider the cost of the power energy, aluminum tube, and reagents, and those to assembly the cell for the galvanic deposition (Lacomit, carbon conductive paste). These costs are small compared to the other ones and so the total cost should not change a lot. The result of this analysis is

clear: 85% of the cost of a Pd based sensing electrode is due to the purchase of the Pd precursor. Therefore, the copper based sensing electrode, nevertheless the less performances, can be useful for a qualitative analysis as an accurate and precise quantification is not mandatory, being 10 times cheaper.

In order to emphasize the low price of these prototypes, we asked for a price quotation of the *Dulcotest* and *Analysenmesstechnik [32-33]* but they did not answer so this comparison was not possible.

Real samples

In the last part of the Ph.D. activity, a collaboration with Ri.Med Foundation (Ricerca Mediterranea) started for a research project aimed to detect hydrogen peroxide in biological medium to safely diagnose the oxidative stress. In Ri.Med laboratories, different cellular cultures simulating oxidative conditions (both anti oxidant and pro-oxidant) were prepared. They studied the release of H_2O_2 in two different cellular media: in epithelial and macrophages cells. The main differences is the amount of hydrogen peroxide released by these cells: epithelial cells release less hydrogen peroxide compared to macrophages. The project started recently, so that just preliminary results can be shown.

The concentration range of hydrogen peroxide in these media was unknown, because from the literature study it can vary from nM to mM. Furthermore, in the cellular medium many different compounds are present (such as Glucose, Glycine, Aspartic Acid, Glutamic Acid), which can interfere with detection of hydrogen peroxide.

As widely known, Pt is an excellent material for hydrogen peroxide detection [41], therefore, we tested a Pt wire as a sensing electrode (with Pt mesh as a

counter and Ag/AgCl as a reference), just to have a fast response about the possibility to use electrochemical techniques with this particular and heterogeneous medium. The first attempt has been carried out using the cellular culture of macrophages cells. The calibration line of the sensing electrode (Pt wire) in this medium is shown in Figure 3.25 A-B.

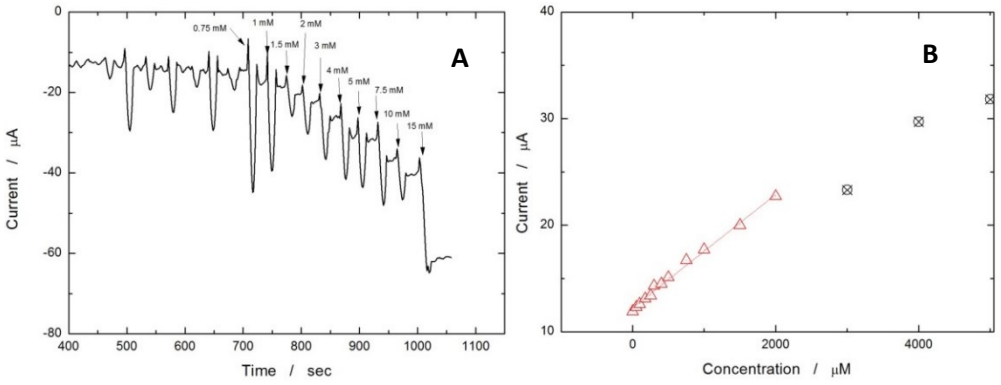

FIGURE 3.25 TEST OF A PT WIRE AS A SENSING ELECTRODE IN MACROPHAGES MEDIUM: A) CHRONOAMPEROMETRIC CURVE; B) CALIBRATION LINE

It shows that the electrode is able to quickly detect hydrogen peroxide. We found a linear range from 50 to 2000 µM, confirming that Pt is much more effective in comparison with Pd or Cu thin film (200 and 100 µM respectively). Four different samples were tested: (1) normal macrophages 'healthy' grown (NT, not treated), (2) macrophages grown with LPS, (3) macrophages grown with LPS and Nigicerin and (4) macrophages grown with LPS, Nigicerin and Epox. Ri.Med laboratories tested these samples (Figure 3.26) with flow citometry, a qualitative technique, and they found that the amount of H_2O_2 increase from sample (1) to sample (3) and then it drops when sample (4) was tested, accordingly with the biochemistry of the process.

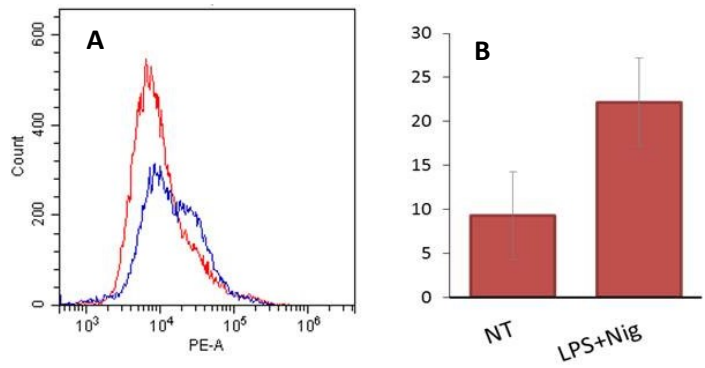

FIGURE 3.26 FLOW CYTOMETRY TEST OF MACROPHAGES NOT STIMULATED AND STIMULATED WITH LPS AND NIG

The results of our experiments are shown in Fig 3.27 A-D.

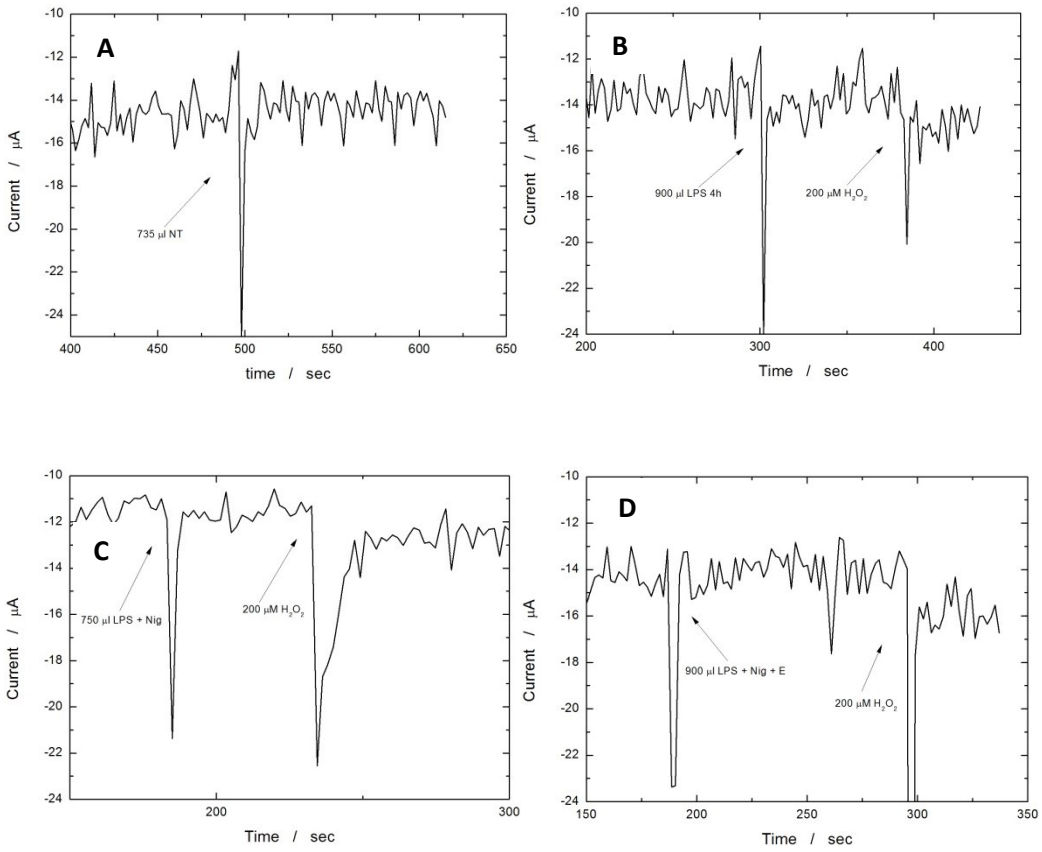

FIGURE 3.27 CHRONOAMPEROMETRIC TEST OF MACROPHAGES: A) NOT TREATED; B) TREATED WITH LPS; C) TREATED WITH LPS AND NIGICERIN; D) TREATED WITH LPS, NIGICERIN, AND EPOX

Figure 3.27 A shows that when 750 µl of NT sample were added to 3 ml of solution current density did not change. When 900 µl of sample (2) were added, a slightly increase of signal is visualized (Figure 3.27 B). In order to confirm that the sensing electrode is able to detect hydrogen peroxide, 200 µM of H_2O_2 has been injected successively. Figure 3.27 C shows that addition of 750 µl of the sample (3) determined a significant increase in current density, in comparison with Figure 3.27 B. When sample (4) was tested, a really small increase, almost comparable with the noise, is visualized (Figure 3.27 D). This trend agrees with the results of Fig 3.26. A quantification analysis is shown in Fig 3.28.

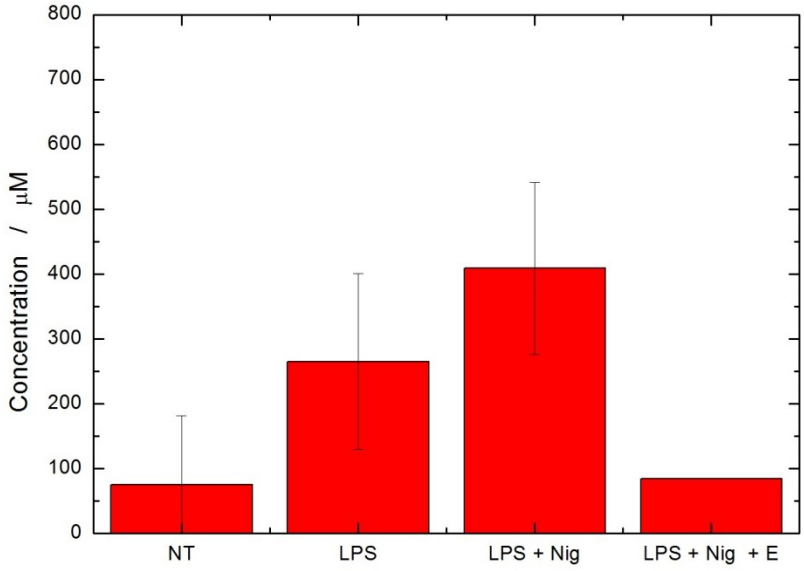

FIGURE 3.28 CONCENTRATION OF HYDROGEN PEROXIDE OF MACROPHAGES SAMPLE DIFFERENTLY TREATED

Being just preliminary study, just 3 experiments for each type of sample were conducted. Details on macrophages are not available because owned by the Ri.Med Lab.. These are highly satisfying preliminary results because show that the Pt sensing electrode is able to detect hydrogen peroxide also in this heterogeneous medium and can be used to quantify the oxidative stress in human beings.

Comparison with the literature

From the above results, it can be concluded that it is possible to fabricate Pd and/or Cu nanostructured electrodes for sensing of hydrogen peroxide through galvanic deposition. Their performances are highly satisfying if compared either with those of other materials having the same nanostructured morphology or with those of identical materials (Pd or Cu) with other morphologies (Table 3.9).

TABLE 3.9 COMPARISON BETWEEN DIFFERENT NON LABELLED NANOSTRUCTURED BASED ELECTROCHEMICAL SENSORS FOR HYDROGEN PEROXIDE DETECTION

Sensor type	Detection potential V	Linear Range µM	Sensitivity µA μM^{-1} cm^{-2}	Stability Days	Interf.	Ref.
Pd nanoparticles	-0.45 VSCE	1-820	n.a.	60	GLU, AA, AP, UA	[42]
Pd hollow nanocubes	-0.4 V vs SCE	100-24000	0.2877	n.a.	n.a.	[29]
PdCu nanoporous	08 V vs NHE	500-8000	n.a.	30	n.a.	[43]
Pd nanoparticles / graphene nanosheets	-0.25 V vs SCE	0.1-1000	n.a.	7	AA, GLU, DA	[44]
Pd NWs array (5 µm long)	**-0.2 V vs Ag/AgCl**	**53-4400**	**0.368**	**30**	**GLU, AA, UA, POX, EtOH**	**This Work**
Cu NWs array (3 µm long)	**-0.2 V vs Ag/AgCl**	**60-3700**	**0.509**	**7**	**GLU, AA, UA, POX, EtOH**	**This Work**
Pt-Cu NPs	+0.2 V vs Ag/AgCl	0.5-1280	0.051	n.a	DA, UA, AA	**[45]**
MoS2-Cu NWs	-0.3V vs Ag/AgCl	85-38000	n.a.	12	DA, UA, AA	[46]
AuCu-NWs	0.484 vs SCE	0.002-0.36	2.71	14	DA, UA, AA	[47]
$CuFe_2O_4$ NTs	0 V vs Hg/HgO	500-2500	0.219	14	DA, UA, AA	[48]
Ag NWs array (300 nm long)	-0.2 V vs SCE	100-3100	0.0329	42	GLU, AA, UA, POX, EtOH, OA, SO	[17]
Pt NWs array (12 µm long)	-0.2 V vs Ag/AgCl	10-4000	0.654	n.a.	CA, GLU, AA, UA	[41]

3.3 Conclusions

Hydrogen peroxide sensor has been successfully fabricated growing regular and uniform array of metallic Pd and Cu nanostructures. In particular, the array was fabricated through metal displacement deposition in template. The galvanic method is advantageous because external power supply is not required, and, in addition, it is easy to be conducted, and quite fast. Results obtained here showed that

1. an accurate control of the nanostructure length can be achieved by adjusting pH, solution composition, deposition time, and anodic to cathodic area ratio;
2. sensing performances depend on the electrochemical active surface area. Electrochemical tests were carried out in a hydro-alcoholic solution that allows to overcome the hydrophobicity of the nanostructured electrodes;
3. Both Pd and Cu sensing nanowires exhibit good features for detecting hydrogen peroxide, with a wide linear range, low LOD, and high selectivity. The best performance was obtained with array of Pd nanowires about 5 μm long. This sensor has a sensitivity of 0.368 μA μM-1 cm-2 in a linear range from 53 to 4400 μM, with a limit of detection of 13.3 μM.
4. Pd NWs are highly selective for H2O2 detection as evidenced by the negligible response after injection of potassium oxalate, glucose, ascorbic acid, and uric acid. Cu NWs are also selective towards hydrogen peroxide showing a negligible response towards glucose, ascorbic acid and uric acid but there is a slight change in the response after addition of potassium oxalate.

5. After 1 month of storage in phosphate solution, the palladium nanostructured sensor is less precise when the concentration of H2O2 approaches either upper or lower limit of the range of linearity, while it holds a good precision for intermediate concentrations. After recalibration, accuracy tests revealed errors less than 5%, suggesting that operational stability of the nanostructured sensors is about 1 month. Copper based sensing electrode is less stable, having a shelf life of about 7 days, because more than 40% of its original accuracy is lost after this time.
6. Copper based sensing electrodes are ten times cheaper than palladium one, therefore, they can be useful for qualitative measurements, when high precision and accuracy are not mandatory.
7. Hydrogen peroxide released by macrophages has been detected using a Pt wire as a sensing electrode showing that it can be used to monitor oxidative stress in humans.

References

1 E. Wernimont, M. Ventura, G. Garboden, P. Mullens General Kinetics, Past and Present Uses of Rocket Grade Hydrogen Peroxide, Conference Proceedings, 2005,

2 M. Park, Hydrogen Peroxide Process Economics Program Report 68B, Process Economic Program, 1992, 1-36

3 https://www.solvay.us/en/binaries/HH-2323-236798.pdf

4 R. Hage, A. Lienke, Applications of transition-metal catalysts to textile and wood-pulp bleaching, Angw. Chem. Int. Ed. 45 (2006) 206-222.

5 M.E. Falagas, P.C. Thomaidis, I.K. Kotsantis, K. Sgouros, G. Samonis, D.E. Karageorgopoulos, Airborne hydrogen peroxide for disinfection of the hospital environment and infection control: a systematic review, J. Hosp. Infect. 78 (2011) 171-177.

6 D. R. V. Guelfi, F. Gozzi, I. Sirés, E. Brillas, A. Machulek Jr, S. C. de Oliveira, Degradation of the insecticide propoxur by electrochemical advanced oxidation processes using a boron-doped diamond/air-diffusion cell, Environ. Sci. Pollut. Res. 23 (2016) 1-13

7 J.J. Pignatello, E. Oliveros, A. MacKay, Advanced Oxidation Processes for Organic Contaminant Destruction Based on the Fenton Reaction and Related Chemistry, Crit. Rev. Env. Sci. Tec. 36 (2006) 1-84

8 F. Tamay-Cach, J. C. Quintana-Pérez, J. G. Trujillo-Ferrara, R. I.Cuevas-Hernánde, L. Del Valle-Mondragón, E. M. García-Trejo, M. G. Arellano-Mendoza, A review of the impact of oxidative stress and some antioxidant therapies on renal damage, Ren Fail. 38, 171 (2016).

9 W.L. Baker, Glucose oxidase reaction for estimation of glucose without horseradish peroxidase. Some microbiological and fermentation applications, Inst. Brew., 1991, 97, 457-462

10 G. Palleschi, F.H. Faridnia, G. J. Lubrano, G.G Guilbault, Ideal Hydrogen Peroxide-Based Glucose Sensor, Appl. Biochem. Biotechn., 1991, 31, 21-35

11 Mascini, M. and Palleschi, G. (1989), Design and application of enzyme electrode probes, Selective Electrode Rev. 11(2), 191-264.

12 K. Hernandez, A. B. Murcia, R. C. Rodrigues, R. F. Lafuente, Hydrogen Peroxide in Biocatalysis. A Dangerous Liaison, Current Organic Chemistry, 2012, 16,

13 W. J. Zhang, L. Bai, L. M. Lu, and Z. Chen, A novel and simple approach for synthesis of palladium nanoparticles on carbon nanotubes for sensitive hydrogen peroxide detection., Colloids Surf. B, 2012, 97, 145-149

14 M. Geiszt and T. L. Leto, The Nox Family of NAD(P)H Oxidases: Host Defense and Beyond, J. Biol. Chem., 2004, 279, 51715–51718

15 E. A. Veal, A. M. Day, B. A. Morgan, Hydrogen Peroxide Sensing and Signaling, Mol. Cell, 2007, 26, 1-14

16 X. Li, L. Wang, Q. Wu, Z. Chen, X. Lin, A nonenzymatic hydrogen peroxide sensor based on Au–Ag nanotubes and chitosan film, J. Electroanal. Chem., 2014, 735, 19-23.

17 E. Kurowska, A. Brzozka, M. Jarosz, G.D. Sulka, M. Jaskuła, Silver nanowire array sensor for sensitive and rapid detection of H2O2, Electrochim. , 2013, 104, 439-447.

18 M. Garcia, P. Batalla, A. Escarpa, Metallic and polymeric nanowires for electrochemical sensing and biosensing, Trends Anal. Chem., 2014, 57, 6-22.

19 S. Abdellaoui, K. L. Knoche, K. Lim, D. P. Hickey, S. D. Minteer, TEMPO as a Promising electrocatalyst for the electrochemical oxidation of hydrogen peroxide in bioelectronics application, J. Electrochem. Soc., 2016, 163, H3001-H3005

20 G. Jönsson, L. Gorton, An Electrochemical Sensor for Hydrogen Peroxide Based on Peroxidase Adsorbed on a Spectrographic Graphite Electrode, Electroanal., 1989, 1, 465-468

21 Z. Zhang, H. Zhu, X. Wang, X. Yang, Sensitive electrochemical sensor for hydrogen peroxide using Fe3O4 magnetic nanoparticles as a mimic for peroxidase, Microchimica Acta, 2011, 174, 183-189
22 Y. Xin, X.F. Bing, L.H. Wei, W.F. Chen, D. Zhao, W. Zhao, A novel H2O2 biosensor based on Fe3O4–Au magnetic nanoparticles coated horseradish peroxidase and graphene sheets–Nafion film modified screen-printed carbon electrode, Electrochimica Acta, 2013, 109, 750-755
23 D. Du, M. Wang, Y. Qin, Y. Lin, One-step electrochemical deposition of Prussian Blue–multiwalled carbon nanotube nanocomposite thin-film: preparation, characterization and evaluation for H2O2 sensing, Journ. Mat. Chemic., 2010, 20, 1532-1537
24 L. Cao, Y. Liu, B. Zhang, L. Lu, In situ Controllable Growth of Prussian Blue Nanocubes on Reduced Graphene Oxide: Facile Synthesis and Their Application as Enhanced Nanoelectrocatalyst for H2O2 Reduction, Appl. Mat. Interf., 2010, 2, 2339-2346
25 R. Garjonyte, A. Malinauskas, Operational stability of amperometric hydrogen peroxide sensors, based on ferrous and copper hexacyanoferrates, Sens. Act. B, 1999, 56, 93-97
26 A. Eftekhari, Electrocatalysis and Amperometric Detection of Hydrogen Peroxide at an Aluminum Microelectrode Modified with Cobalt Hexacyanoferrate Film, Microchim. Acta, 2003, 141, 15-21
27 D. Jiang, Y. Zhang, M. Huang, J. Liu, J. Wan, H. Chu, M. Chen, Carbon nanodots as reductant and stabilizer for one-pot sonochemical synthesis of amorphous carbon-supported silver nanoparticles for electrochemical non enzymatic H2O2 sensing, J. Electroanal. Chem., 2014, 728, 26-33
28 N. Nasirizadeh, Z. Shekari, A. Nazari, M. Tabatabaee, Fabrication of a novel electrochemical sensor for determination of hydrogen peroxide in different fruit juice samples, Journ. Food Drug Anal., 2016, 24, 72-82
29G. Nie, X. Lu, J. Lei, L. Yang, X. Bian, Y. Tong, C. Wang, Sacrificial template-assisted fabrication of palladium hollow nanocubes and their application in electrochemical detection toward hydrogen peroxide, Microchim. Acta, 2013, 99. 145-151
30 T. Selvaraju, R. Ramaraj, Electrocatalytic reduction of hydrogen peroxide at nanostructured copper modified electrode, Journ. Appl. Electrochem., 2009, 39, 321-327
31 F. Xiao, F. Zhao, Y. Zhang, G. Guo, B. Zeng, Ultrasonic Electrodeposition of Gold-Platinum Alloy Nanoparticles on Ionic Liquid-Chitosan Composite Film and Their Application in Fabricating Nonenzyme Hydrogen Peroxide Sensors, Journ. Appl. Phys. Chem. C, 2009, 113, 849-855
32 Amperometric Hydrogen Peroxide micro-sensor, *http://www.amt-gmbh.com/pdf/Microsensor%20H2O2.pdf*
33 DULCOTEST® Sensors for Hydrogen Peroxide, https://www.prominent.com/en/Products/Products/Measuring-Control-and-Sensor-Technology/Sensors/p-sensors-hydrogen-peroxyde.html
34 M. Battaglia, S. Piazza, C. Sunseri, R. Inguanta, Amorphous Silicon Nanotubes via Galvanic Displacement Deposition, Electrochem. Commun., 2013, 34, 134-137
35 International Centre for Diffraction Data, Power Diffraction File (2007), Pennsylvania USA, card number: Pd 87-367; Cu 4-836, Au 4-784.
36 R. Inguanta, G. Ferrara, S. Piazza, C. Sunseri, Fabrication and characterization of metal and metal oxide nanostructures grown by metal displacement deposition into anodic alumina membranes, CET., 2011, 24, 199-204.
37M. Battaglia, R. Inguanta, S. Piazza, C. Sunseri, Fabrication and characterization of nanostructured Ni - IrO2 electrodes for water electrolysis, Int. J. Hydrogen Energy, 2014, 39, 16797-16805.
38 R. Inguanta , S. Piazza, C. Sunseri, Synthesis of Self-Standing Pd Nanowires via Galvanic Displacement Deposition, Electrochem. Commun. 2009, 11, 1385-1388.

39 R. Inguanta, G. Ferrara, S. Piazza, C. Sunseri, A new route to grow oxide nanostructures based on metal displacement deposition. Lanthanides oxyhydroxides growth, Electrochim. Acta, 2012, 76, 77-87.
40 A.R. West, Solid State Chemistry and its Applications, Wiley, Chichester, (1985) Ch. 5, 173
41 Z. Li, C. Leung, F. gao, Z. Gu, Effects of nanowires lenght and surface roughness on the electrochemical sensor properties of nafion-free, vertically aligned Pt nanowire array electrodes, Sensors, 2015, 15, 22473-22489.
42 M. Han, S. Liu, J. Bao, Z. Dai, Pd nanoparticle assemblies-As the substitute of HRP, in their biosensing applications for H2O2 and glucose, Biosens. Biolectron., 2012, 31, 151-156.
43 A. Liu, H. Geng, C. Xu, H. Qin, A three-dimensional hierarchical nanoporous PdCu alloy for enhanced electrocatalysis and biosensing, Anal. Chim. Acta, 2011, 703, 172-178.
44 X-M. Chen, Z-X. Cai, Z-Y. Huang, M. Oyama, Y-Q. Jiang, X. Chen, Ultrafine palladium nanoparticles grown on graphene nanosheets for enhanced electrochemical sensing of hydrogen peroxide, Electrochim. Acta, 2013, 97, 398-403.
45 A. A. Ensafi, M. M. Abarghoui,B. Rezaei, Facile synthesis of Pt-Cu@silicon nanostructure as a new electrocatalyst supported matrix, electrochemical detection of hydrazine and hydrogen peroxide, Electrochim. Acta, 2016, 190, 199-207
46 D. Li, X. Liu, R. Yi, J. Zhang, Z. Su, G. Wei, Electrochemical sensor based on novel twodimensional nanohybrids: MoS2 nanosheets conjugated with organic copper nanowires for simultaneous detection of hydrogen peroxide and ascorbic acid, Inorg. Chem. Front., 5, 2018, 112-119
47 N. Wang, Y. Han, Y. Xu, C. Gao, X. Cao, Detection of H2O2 at the Nanomolar Level by Electrode Modified with Ultrathin AuCu Nanowires, Anal. Chem., 2015, 87, 457-463
48 H. Xia, J. Li, L. Ma, Q. Liu, J. Wang, Electrospun porous CuFe2O4 nanotubes on nickel foam for nonenzymatic voltammetric determination of glucose and hydrogen peroxide, Journ. Alloys Comp., 2018, 739, 764-770

4. Sensors for heavy metals

Abstract

In this chapter, the development of two nanostructured sensors to detect heavy metals are described. Heavy metals pollution is highly dangerous for human life because these compounds are highly toxic and carcinogenic. Nowadays, the only way to detect them is to use ICP-MS. This technique is expensive, hard to use and needs of skilled personnel to carry out an analysis. Moreover, due to the big dimension of the analytical apparatus, it is just a laboratory technique. It means that the heavy metal pollution can be detected just after many days that occurred. The possibility to develop an easy, cheap and portable device to detect heavy metals has been studied in this chapter. Using a thin film of Nickel Oxide, 500 ppt (less than 1 millionth of gram per liter) of mercury were detected after less than 15 min of analysis. The main problem of this technique is the acidification of the sample for reliable results, so that its pre-treatment is mandatory. This drawback makes the in situ and real time detection harder (but not impossible). To overcome this issue, I developed an electrochemical procedure for modifying the local pH just in proximity of the electrode surface. By this way, even if the original pH is about the same (6-7 for either river or sea water), locally it is made more acidic and the analysis can be carried out. This is a huge improvement and allowed us to detect, simultaneously, copper, mercury and lead in real sample (river water) avoiding any sample pre-treatment. This work clearly shows that it is possible to conduct a real time and in situ water analysis allowing to alert people promptly about a heavy metal contamination prior to reaching them.

4.1 Introduction

Heavy metals are described as metals with density higher than 5g/cm^3 and include lead, copper, arsenic, cadmium, mercury, nickel and many others [1]. Heavy metals contamination has become a theme of primary importance in the last two/three decades: the rapid technological progress has led to a sharp increase of the emission of these metals. Heavy metals are natural constituents of earth's crust and therefore, they can pass into the food chain through natural phenomena such as erosion, wind, and rain. However, today heavy metal emission by natural processes is almost negligible compared to those due to anthropological activities: for instance, in the 80s and 90s, when the peak of heavy metal emission by human activities occurred, the emission of lead from production processes exceeded the natural ones by a factor 28, while for mercury this factor was 1.4 [2]. Due to the toxicity of these metals, European legislators have tried to reduce the emission of chemical contamination by setting the limits of metal concentration in food and water: in particular, the European Commission, in 2000, released the '*White paper on Food Safety*', which confirmed the high priority of the matter in the light of the dangers concerning heavy metals in food and water [3].

Metals can have different effects on the organism depending on the taken amount and how long it is taken. An high quantity intake in a short time is called *acute poisoning*, while if absorption takes place over long time and it concerns small quantities, that individually would not give any problem, we talk about *chronic intoxication*. In particular, in this last case, there is bioaccumulation: it is due to the progressive accumulation over time in our organism of heavy metals, because it is able to eliminate only modest quantity or nothing at all [4]. The metals do not all have the same degree of toxicity (Table 4.1 classify the metal toxicity depending on the *Provisional Tolerable Weekly Intake, PTWI*):

the tolerability level by the human body depends on the amount necessary for a proper metabolic activity. Therefore, the massive ingestion of some heavy metal leads to the above mentioned bioaccumulation. Metals that are not part of the metabolism, or required in modest amount, are the most dangerous, because they easily cause bioaccumulation.

TABLE 4.1 LIST OF HEAVY METALS CLASSIFIED ACCORDING TO THEIR TOXICITY LEVEL

Heavy metal	***Toxicity***
Nickel, Arsenic, Mercury, Lead, Antimony, Cadmium, Chromium,	*High*
Manganes, Copper, Zinc	*Medium*
Alluminium, Silver, Gold, Tin	*Low*

Also trace (parts per billion, ppb) of heavy metals can cause serious problems, depending on the amount and on the heavy metal. Table 4.2 shows some effects of different heavy metals on the organism, in dependence of the *PTWI*

TABLE 4.2 PTWI AND EFFECTS OF DIFFERENT HEAVY METALS [5]

	PTWI (mg/kg)	***Acute Poisoning***	***Chronic Intoxication***
Cu	*3.5*	*- Kidney and liver damages*	*- Dementia*
Pb	*0.025*	*- Renal and brain failure* *- irreversible aplastic anemia* *- intestinal cramps*	*-block in the synthesis of the heme group* *- cognitive deficits in children* *-accumulation in the bones*
Hg	*0.004*	*-changes in brain development of the fetus* *-destruction of the nervous system* *- abortion*	*-neurological changes* *- impotence* *-DNA damage*
Sn	*14*	*- irritations to the skin and eyes* *- general malaise and dizziness* *- urination and breathing problems* *- strong sweating*	*-depression* *-damage to the chromosomes, liver, central nervous system, immune system* *-anemia*
Zn	*2.1-7*	*- damage to the pancreas* *-protein metabolism disorder* *- arteriosclerosis*	*-stomach spasm* *-skin irritations*

Food contamination can occur throughout the food chain, from production to the end users. The contamination occurring during the production is called *primary*

contamination, while the contamination in the subsequent phases (transformation, distribution, conservation) is called *secondary*.

The primary contaminations are those that occur directly in the field or breeding and also due to the natural high content of metals in the environment in which the agricultural or breeding takes place. The main source of contamination is represented by soil and water, or better, by the amount of metals they contain. However, the contamination can come from many other different sources, including irrigation water, use of urban or industrial biomass, manure, and so on. As above mentioned, for the humans not all the amount of metals introduced with the diet is assimilated by the animal body, because it is partially eliminated through urine, faeces, bile and sweat. However, the repeated accumulation of metals in animal tissues can reach dangerous levels to human health: this process is the *biomagnification*, i.e. bioaccumulation in living beings of toxic and harmful substances whose concentration in organisms is growing from bottom to top of the food pyramid. The biomagnification is very serious in the case of mercury accumulation in fishes: owing to many microorganisms present in the water, mercury undergoes transformation into organic compounds, such as methylmercury, and enters into the food chain through the plankton. Then it passes, through invertebrates and fish, to large predators where the higher concentrations are found and finally reaches human beings that are the last link in the food chain[6].

Secondary contaminations are those occurring during processing, distribution and conservation of foodstuffs. The technology has allowed the development of optimal systems and materials for the transformation and storage processes, which prevent contamination from metals in the food or beverage. For example, aluminum cans, widely used in the beverage sector, are internally enameled with special polymer resins in order to prevent the metal to pass into the solution. In the past, there have been numerous problems concerning secondary contamination which have led to the release of specific regulatory standards

concerning the transformation, distribution and conservation of food. Now, it is mandatory for the food industry to meet consumer expectations in terms of safety and to meet legal requirements. The food industries rely on modern quality control systems to guarantee the quality and safety of the manufactured products. The three main systems currently used are:

- *Good Manufacturing Practices*: they indicate the working conditions and procedures which, on the basis of long experience, have proven to offer high quality and safety;
- *Hazard Analysis Critical Control Points*: this is a recently proactive technique, focused on the assessment of potential problems. It provides the control during the production process instead on the final product;
- *Quality assurance standards*: compliance with the standards set by the International Standards Organization (ISO 9000) and the European Standard (ES 29000) ensures that food industries, catering companies and other companies operating in the food sector comply with established procedures. The effectiveness of these programs is regularly analyzed by external experts.

Some cases of secondary contaminations from metals are cited in the literature: at the beginning of 1900 in Britain, there was a poisoning of about 6000 people due to the use of arsenical pyrite, usually employed for the production of sulfuric acid, for the hydrolysis of starch in the beer production; while in 1955 in Japan, another arsenic poisoning occurred when about 12000 children ingested sodium phosphate-stabilized baby products obtained as a by-product from the aluminum production industry. In the 1970s, in Iraq, wheat treated with mercurial compounds to preserve them from fungal attacks were used for bread making, causing thousands of cases of intoxication, about a hundred of which turned out to be mortal. Other problems occurred in foodstuffs with acidic pH,

such as carbonated drinks: the zinc present in the galvanized containers was transformed into its soluble salts and then ingested with the drink. Similar problems were found with tin present in the welds of tin plated cans: due to the low pH, tin can be abundantly released into the food or beverage altering the organoleptic characteristics without causing problems of health origin.

Lead contamination is probably the most common and famous. As evidenced in Table 4.2, exposure to lead can cause neurological, hematological, renal, liver, and kidney diseases [4]. The use of gasoline containing tetraethyl lead, as an anti-knockdown agent, characterized the last century and led to the diffusion of lead in the atmosphere to levels never achieved before. Fortunately (but, almost always, for other reasons), the list of countries that have banned the use of tetraethyl lead in gasoline is continually lengthening: currently about 80% of the fuel circulating in the world is of the type, so called, "Green", i.e. without lead. Between the 80s and the 90s, it was calculated that the emissions of this element have been reduced by two thirds, due not only to the transition to green gasoline, but also to the optimization of incineration treatments, water purification technologies, and the progressive reduction of the use of lead in paints and batteries. Despite the significant reduction of the lead emission, it continues to be present in the environment owing to the high quantities emitted in the past.

Another very dangerous source of contamination is due to lead in water pipes: for instance, lead is added as a stabilizer to PVC. Urban environments are highly exposed to lead contamination: it has been extensively used as building material for pipes and as fitting material and as active material in the battery industry. The main lead contamination comes from the old pipes for drinkable and wastewater, made by lead: depending on different parameters, like pH, temperature or mineral content, these pipes can release lead into the water. For this reason, the Safe Water Drinking Act imposed the maximum amount of lead in the pipes system to 0.25% of all the pipes system, including pipes, pipes fitting and solders [7].

Mercury is probably the most dangerous one because a short exposure to low concentration can cause problems to brain, heart, kidney, lungs and immune system [8]. The world's health organization (WHO) recognizes mercury as one of the ten most dangerous chemical for human health [8]. Mercury pollution is due to several sources: it naturally exists in coal, so all the coal-fired power plants are a huge source for mercury pollution [9]. For the same reason, it is possible to have a mercury leakage from cement kilns. Furthermore, different chemical plants (bleach, PVC and so on) use mercury as a reagent, essentially as a catalyzer, producing huge amount of mercury waste that can pass directly into the environment if not properly treated. Last but not least, huge amount of mercury is used for gold extraction: the Environment Protection Agency (EPA) stated that more than 11.5tons per year of mercury waste are produced from gold mining [10]. Mercury is an excellent example of biomagnification: once introduced into the environment through vapors or waste liquids, it contaminates soil, passes into the groundwater where enters into the food chain. The toxicity of the mercury is greatly amplified by the bacteria that inhabit the water and the intestinal microflora of many animal species, including fishes. These microorganisms transform inorganic mercury into its organic forms, among which the most widespread and dangerous is methylmercury. The high liposolubility gives these compounds the ability to trace the food chain, accumulating mainly in the nervous tissue of smaller fishes, which in turn transmit it to their predators. Thus, in general, the greater the size of the fish and the greater its mercury content. In this context, it is worth mentioning what happened in Japan in 1952: large amounts of waste containing mercury were released in the Bay of Minimata since 1932. The accumulation in marine creatures determined the entry of mercury into the food chain of the inhabitants of the bay and in 1952, the first case of poisoning appeared. A total of 500 cases were ascertained in the 1950s, all of them fatal. Between 1971 and 1972 in Iraq, there were 6530 hospitalizations with 4599 deaths due to the consumption of

contaminated fish. Finally, again in Japan, in the city of Nijgata, at the end of the 1970s, there was another case of mercury contamination contained in fish.

Despite *copper* is an essential element for human body, high levels of copper are dangerous for humans causing hepatitis, jaundice and liver diseases [5]. The main copper pollution source is the mining of Cu containing earths. During this process, powders containing copper compounds, like sulfide, are produced. These compounds tend to oxidase in contact with air producing sulphate salts, which are highly soluble in water, so releasing copper into the environment [11]. Copper is used for fabrication of electrical equipment (60%). In the construction field, copper is used for roofs and plumbing (20%), and for heat exchangers (15%) and alloys (5%). Even in agriculture, it is widely used, because it is contained in the formulation of some plant protection products. Copper is ideal for electrical connections, because it is easily machinable, can be extruded in wires and has a high electrical conductivity. Copper production is constantly growing in the world, and consequently its diffusion in the environment is constantly increasing: there is continuous deposition of contaminated sludge in rivers owing to the discharge of wastewater containing copper. Even in the air, the presence of copper has increased due to the use of fossil fuels. Because of precipitation, copper is deposited in the soil, from which it can be absorbed by plants where it can accumulate even in large quantities. In heavily contaminated soils, only a few plants survive: this is why copper contamination of the soil poses a serious threat to agricultural land. The absorption by the plants of this element causes its intake by their consumers and therefore, enters into the food chain directly, if the primary user is the man, or indirectly, if the plant is used as fodder in animal husbandry.

The EPA settled the maximum concentration of these metals in drinking water as 2 ppb for mercury, 15ppb for lead and 1.2ppm for copper [12]. Considering all these hazards, the detection of heavy metals in water samples is of great urgency and importance. The most commonly used techniques for this purpose

are the Atomic Absorption Spectroscopy (AAS), Graphite Furnace Atomic Absorption Spectroscopy (GFAAS) and Inductively Coupled Plasma Mass Spectroscopy (ICP-MS). They are highly efficient in terms of sensitivity, selectivity, LOD and accuracy, but they have different drawbacks: first of all, they are extremely expensive due to both equipment and operational costs, require highly skilled personnel, are time consuming and, above all, these are big machines that cannot be used for in situ and real time analysis [4]. Electrochemical methods, like Cyclic Voltammetry (CV), Differential Pulse Voltammetry (DPV), Square Wave Anodic Stripping Voltammetry (SWASV), are perfect candidates for the analysis of trace heavy metals, being highly sensitive and selective. Furthermore, electrochemical sensors based on nanostructures or nanomaterial, provide brilliant performances, similar to the classical analytical methods, mostly due to the high surface area of the electrodes. In addition, electrochemical sensors based on nanostructured present the advantages of miniaturized dimensions, low power consumption, friendly use. Besides, they can also be used in situ and for in real-time analysis, so overcoming most of the drawbacks of the current detection methods [13-14]. Electrochemical sensing techniques for detection of heavy metals is suggested by US-EPA [8], confirming the big advantages of such techniques. In the last years, different materials, like polymers [15-16], metals nanostructures [17-18], DNA and enzyme-based electrodes [19-20], carbon [21-22], together with different electrochemical methods (SWV, LSV, DPV) [23-24-25] have been investigated, achieving very low LOD. Among these methods, stripping methods are preferable because of the high sensitivity due to the pre-concentration step [26].

Li et al. [18] made an extensive and excellent study on heavy metals detection by different techniques, including electrochemistry. In this study, it is easy to understand the importance of the electrode size. They cite Lee et al.[27] about the development of an electrode made of Bismuth NPs and they found that the

LOD highly depends on the NPs size, moving from 2 ppb with a bulky electrode to 0.51, 0.32 and 0.17 ppb using smaller and smaller NPs. In the same review, Li et al. focus the attention on the effect of the active material. Carbonaceous materials, such as Carbon NTs, and graphene are good materials for this goal because are able to sorb heavy metals [28]. On the other hand, carbon NTs are hydrophobic and suffers of high background current, therefore, they are often modified with different compounds, such as epoxy [29] or hiacalixarene [30]. They also focus on gold based electrode: nano-sized gold sensing electrode can improve the features of glassy carbon electrodes, eliminating the memory effect, and improving the LOD towards mercury and arsenic of one order of magnitude [31-32]. Furthermore, using gold based electrodes, Under Potential Deposition (UPD) can take place. This phenomenon is of advantage because allows to reach really low LOD. During the pre-concentration step, heavy metal ions deposit on the surface of the electrode: at the beginning of the deposition, a bond between the active material of the sensing electrode and the metal has to be created while, when the first layer of metal has been deposited, a metal-metal bond has to be formed. If the affinity of the metal is higher with the electrode than with itself, UPD occurs. In this way, two different stripping peaks will appear: one due to the stripping of the bulky deposited metal and the other one due to the stripping of the first metal layer. This second peak is highly sensitive and can be used to detect low concentration of metals. This phenomena has been extensively studied [33-34] and occurs in detecting lead [35-36], mercury [37], copper [38] and zinc [39] by gold based electrodes.

Many heavy metal ions can selectively bond with certain DNA bases and form stable base pairs that sometimes are even stronger than the Watson-Crick pair. For example, mercury can interact with two thymine (T) bases [19]. Taking advantage from this effect, it is possible to detect mercury using different techniques based on optical [40], fluorescent [41], calorimetric, [41] and electrochemical properties. Zhang et al. modified a glassy carbon electrode with

reduced graphene oxide and DNA, fabricating probes for mercury detection which reached a LOD of 1 ppb with a linear range up to 200 ppb, using $[Ru(NH_3)_6]^{3+}$ as indicator [42]. Wu et al. used the same indicator and the same electrochemical technique for reaching a LOD of about 50 ppt using gold as substrate [43]. This approach is very interesting because it provides low LOD with a good selectivity but, on the other hand, it suffers of all the drawbacks of the biosensors discussed in Chapter 2.

Microbands Arrays Electrodes (MAE) have been widely studied due to the properties of microelectrodes, such as high mass transport, high current density and low ohmic drop. The main problem in the working with microelectrodes is the low current due to the small surface area. In order to overcome this problem, a MAE contains different parallel microbands that allow to increase the current and maintain the characteristics of micro-sized electrode[44]. Zhao et al. [45] developed a gold based MAE with a 45 μm gap to detect copper, zinc, cadmium and lead. They found that the bare MAE is not able to detect zinc and cadmium. Therefore, a thin film of mercury has been deposited on the Au-MAE to increase the sensitivity of the electrode, so they were able to detect cadmium, lead and copper up to 0.3 ppb, 1 ppb, 1 ppb, respectively. Despite the good results, this technology is not suitable for in-situ analysis due to the presence of a highly toxic material such as mercury. Zaouok et al. [46] developed a new generation of MAE sensing electrodes cutting a Screen Printed Carbon slice to fabricate a single microband electrode, 20μm width and 1.2mm long, for cadmium detection. The carbon microband electrode was covered with a thin film of bismuth to increase the sensitivity of the electrode. A LOD of 1.3ppb was achieved.

Metal oxide based electrodes have attracted great attention because they have unique optical, electrical and molecular properties and can be easily functionalized [47-48]. The electrochemical performance of an electrode highly depends on the nature of the materials. Various metal oxide based electrodes

with different morphologies and sizes have been investigated as sensing materials [49]. Wu et al. modified a GCE with chitosan and copper oxide nanoparticles and they were able to detect mercury ions at almost neutral pH reaching a quiet high LOD of 0.2 ppm [50]. This high LOD is probably due to the high pH that doesn't allow a proper dissolution of the mercury salt. Nickel oxide is a cheap material, easy to obtain from a nickel substrate and is environmental friendly. Due to these properties, nickel(II) oxide electrodes have been largely investigated in the last years as catalysts [51], supercapacitors [52] and active material for electrochemical sensing [53-54]. Again Wu et al. calcinated a $Ni(OH)_2$ nano-sheet and obtained a NiO mesoporous electrode, which was used to detect mercury at neutral pH, achieving a LOD of 160 ppb [54]. A LOD of 50 ppt has been achieved by Armas et al.[53] modifying a screen printed carbon electrode with polystyrene sulfonate-NiO and carbon nanopowder, and working in a solution at pH 2.7, so demonstrating that metal oxide based electrodes, especially nickel oxide, can be used to detect selectively low concentration of mercury.

The main drawback of these techniques is the necessity to use solutions at acidic pH, between 1 and 4 (depending on the active material and analyte), so that acid has to be added to the solution. Consequently, the use of such sensing electrode for in-situ and real time analysis is questionable.

When an anodic potential higher than the thermodynamic value is applied to an electrode in contact with an aqueous electrolyte, the secondary reaction of oxygen evolution will occur according to

$$\mathbf{2\,H_2O = O_2 + 4H^+ + 4e^-}$$

REACTION 3.1 OXYGEN EVOLUTION REACTION

Due to this reaction, O_2 and H^+ are produced at the electrode/electrolyte interface and the local pH decreases. Read et al. took advantage of such reaction

to detect mercury ions in water by using a Boron Doped Diamond (BDD) ring electrode [55]. The sensing electrode was made of two concentric BDD rings with a gap of 440µm. The external electrode generated H^+, decreasing the local pH, while the internal one was used as a sensing, using a stripping method. Since pH was locally adjusted, it was possible to operate with a solution at neutral pH.

Table 4.3 summarizes most of the examples reported above.

TABLE 4.3. EXAMPLES OF ELECTROCHEMICAL SENSORS AND BIOSENSORS FOR HEAVY METALS *NOT STUDIED, **RIVER WATER

	Metal	*LOD-ULR*	*Dep. Time*	*pH*	*Real Sample*
Bi-NPs [27]	*Zn* *Cd* *Pb*	*0.6-50 ppb* *0.1-50 ppb* *0.17-50 ppb*	*10 min*	*5*	*N.S**
rGO-AgNPs[56]	*Pb* *Cd* *Cu* *Hg*	*28-500 ppb* *28-390 ppb* *11-220 ppb* *55-600 ppb*	*150 sec*	*5*	*N.S**
GCE-DNA [42]	*Hg*	*0.5-200 ppb*	*40 min*	*7.4*	*sewage samples*
Au-DNA [43]	*Hg*	*0.05-0.2 ppb*	*60 sec*	*7.2*	*N.S. **
Au-NPs [57]	*Cd* *Hg* *Pb*	*0.1–2.7 ppb* *0.1–2.7 ppb* *0.1–2.7 ppb*	*N.S. **	*N.S.**	*N.S. **
Au/Hg-MAE [45]	*Cd* *Pb* *Cu*	*0.3 ppb* *1 ppb* *1 ppb*	*120 sec*	*4*	*N.S. **
C-MAE [46]	*Cd*	*1.3-45 ppb*	*N.S. **	*4.5*	*RW ***
CuO [50]	*Hg*	*0.2-40ppm*	*N.S. **	*6*	*N.S. **
SPCE-NiO [53]	*Hg*	*0.05-2 ppb*	*300 sec*	*2.7*	*RW ***
BDD [55]	*Hg*	*N.S. **	*60 sec*	*6*	*N.S **
NiO Thin Film (this work)	*Hg*	*0.5 ppb*	*12 min*	*3*	*Tap Water*
Au Microbands (this work)	*Hg* *Pb* *Cu*	*1-75 ppb* *10-100 ppb* *1-100 ppb*	*3 min*	*6*	*RW ***

Steroglass and *Metrohm* already developed two commercial devices of electrochemical sensors for heavy metal, that are available in the market. The Steroglas device (Figure 4.1 A) is made of glassy carbon as a sensing electrode and is able to detect many metals (Zn, Al, Cd, Co, Ni, Hg, Cu, Pb, Sn) with limit of detection of about 0.1 ppb depending on the matrix, but is able to analyze many liquids, from milk to wine, from water to oil. The whole analysis requires just some minutes and the sample does not has to be pre-treated. Furthermore, it

is quiet small (20*23*35 cm) and light (less than 10 kg), therefore, it can be moved from lab to lab even if it needs an external power supply [58]. The Metrohm (Figure 4.1 B) sensor [59] is able to detect copper, mercury and arsenic with LOD of 500 pt. It can also work with different water matrixes (tap, drinkable, river, lake and sea water). It is smaller and lighter than the Steroglass device and it can work with an external battery, making possible to work in-situ. Furthermore, in the case of As, it is able to distinguish between different oxidation state (As(III) and As(V)): this is very important because As(III) is a very unstable compound and could be easily oxidized if the sample should be transported to a laboratory

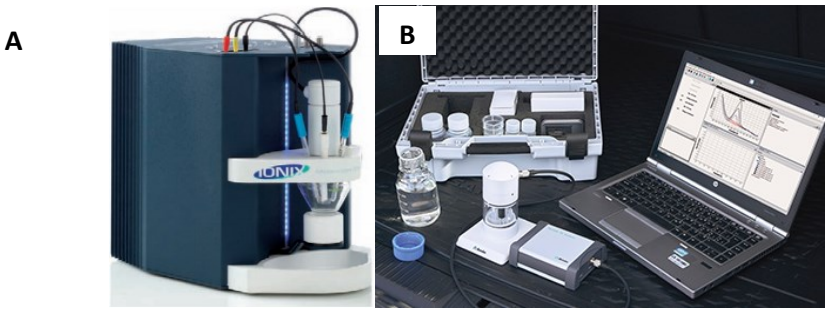

FIGURE 4.1 STEROGLASS (A) AND METROHM (B) ELECTROCHEMICAL DEVICES FOR HEAVY METAL DETECTION

During my Ph.D, I developed two different sensing electrodes for heavy metals detection: a nickel oxide based electrode (either thin film or nanostructured) for mercury detection and an interdigitated gold microband electrode for copper, lead and mercury detection. The activity on Ni oxide has been carried out at the ***Applied Physical Chemistry Lab of University of Palermo, under the supervision of Prof. Carmelo Sunseri, Prof. Rosalinda Inguanta and Prof. Salvatore Piazza***, while the other one has been carried out at ***Tyndall National Institute, Cork, Ireland, in the Lab of Nanotechnology***, supervised by ***Dott. Alan O'Riordan*** and ***Dott. Pierre Lovera***

4.2 Nickel oxide based electrode for mercury detection

4.2.1 Experimental

Sensing electrode synthesis and characterization

Fabrication of NiO thin film and synthesis of NiO@Ni NWs was performed by annealing in an air oven of either a commercial Ni foil (Alfa Aesar Product, 127μm thick, purity higher than 99%) or pre-synthesized Ni NWs, respectively. Even electrochemical oxidation of the nickel substrate was investigated using a solution of 1M KOH or borate.

In order to obtain a thin film of nickel oxide, a commercial nickel foil has been annealed as bought, without any pre-treatment.

Prior to synthesize Ni NWs, a Ni current collector was deposited on one side of a polycarbonate membrane (the same procedure like Chapter 3) at a constant potential of -1.25V (vs. SCE) using the typical Watt's solution (300 g/l of $NiSO_4 \cdot 6H_2O$, 45g/l of H_3BO_3 and 45g/l of $NiCl_2$). Then, Ni nanowires deposition was carried out applying pulsed potential between the open circuit potential and -1.5V (vs SCE) for 90 cycles [60]. Also in this case, the precursor solution was the Watt's bath. After deposition of the nanostructures, the template was dissolved in pure di-chloromethane in order to expose the nanowires, in the same way used to grow Pd and Cu nanostructures of Chapter 3.

Mohanty et al. [61] obtained 200nm of NiO NPs after 3-6 hours of annealing at 500˚C . On the other hand, Valladares et al. [62] showed that just 3 hours of oxidation at 350˚C were enough to obtain nickel (II) oxide from a

commercial nickel foil. Because of this discrepancy, in this work, Ni foil was oxidized for 120 min at three different temperatures (350˚C, 500˚C and 700˚C) and successively characterized by XRD, using a RIGAKU X-ray diffractometer (model: D-MAX 25600 HK), and SEM, using a FEI FEG-ESEM (mod. QUANTA 200) equipped with a detector for EDS (Energy Dispersive Spectroscopy). XRD patterns were obtained in the 2θ range from 10° to 100° with a sampling width of 0.004° and a scan speed of 3 deg./min, using Ni-filtered Cu Kα radiation (λ= 1.54 Å). Diffraction patterns were analyzed by comparison with ICDD database (International Centre for Diffraction Data, Power Diffraction File (2007), Pennsylvania USA).

Electrochemical measurements

The procedure for revealing Hg^{2+} ions consists of two successive steps, as described in Chapter 2. Briefly, Hg is initially potentiostatically deposited on NiO electrode, and then, it is polarized through square wave voltammetry, recording the current response, and, in particular, the current stripping peak due to Hg dissolution. Through a calibration curve, the stripping current intensity can be correlated to the Hg^{2+} concentration in solution. NiO works as a cathode during the enrichment step (first step), while, it works as an anode in the second step (SWV). The first step is very challenging because NiO is a p-type semiconductor therefore it tends to block cathodic current. For a correct working as a sensing element, it has been necessary to find a satisfying value of NiO thickness, which was sufficiently thin to avoid block effects in working as a cathode, and significant ohmic drop in working as an anode, and also, sufficiently high to avoid fast dissolution under repeated SWASV cycles, due to the low pH. In order to achieve this challenging compromise, two annealing times were investigated: 15 and 120 minutes, finding the second one as the best. After annealing, NiO@Ni was sealed

with an insulating lacquer to expose a NiO geometric area of about 0.1 cm^2 that was tested as an electrochemical sensing for mercury ions. Electrochemical experiments were conducted in a 50ml three-electrode cell, where NiO@Ni was the working electrode, a Pt mesh was the counter electrode, and Ag/AgCl worked as a reference electrode. $HgCl_2$ solution was used as an analyte (solution containing the substance to be measured), which was buffered with citric acid and Na_2HPO_4 in different ratio depending on the desired pH and was stirred at 600 rpm during deposition. Both deposition and square wave polarization parameters, such as deposition potential and time, frequency, potential step increment and duration were changed in a large range in order to find the best combination giving the highest stripping peak current. After optimization of the different parameters, a calibration curve was established, in order to find sensitivity and LOD that are the key features of a sensor. For reliability purpose, the calibration curve was repeated for 3 times, at least, and the results here presented are averaged on 3 determinations.

Selectivity tests were carried out against copper, zinc, cadmium and lead ions in a concentration at least 10 times higher than the mercury one.

Real samples analysis

Two kind of real samples were tested: tap water from a public fountain of undrinkable water in Palermo and sea water from Mondello beach, Palermo. Prior to test, the samples have been acidified to pH 3 by nitric acid.

4.2.2 Results and discussion

Electrode synthesis and characterization

Features of NiO thin film as a sensing material depend on the quality of the NiO film, in particular, on annealing time and temperature. NiO is a p-type semiconductor with a resistance of 105 MΩ [61]. For electrochemical measurements, a good electrical conductivity is mandatory; consequently, it is very important to select a configuration where pure Ni allows easy electron flow to nickel oxide that is the active material for detection of the mercury ions. Besides, NiO is quite soluble in acid medium, therefore it is important to have a thickness sufficient to evenly cover the Ni substrate during electrochemical measurements. In order to achieve this goal, it is very important to control the thickness of the NiO produced. The first attempt to obtain NiO@Ni electrodes was to electrochemically oxidize the nickel substrate in an alkaline solution. Different papers suggest to use either KOH or NaOH solution to oxidize Ni in NiO or $Ni(OH)_2$ or in the oxihydroxy form [63-64-65-66-67].

A constant potential of -0.1 V vs Ag/AgCl was applied for 2h and the i-t curve is shown in Figure 4.2 together with SEM analysis.

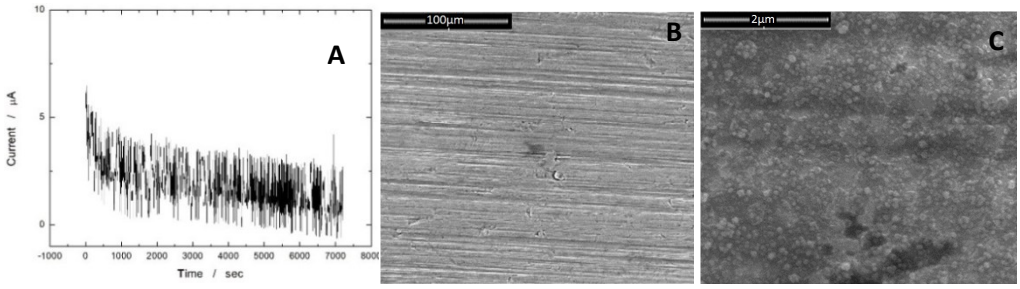

FIGURE 4.2 A): I-T CURVE DURING ELECTROCHEMICAL OXIDATION OF NI FOIL; B) AND C): SEM IMAGES OF NI FOIL AFTER ELECTROCHEMICAL OXIDATION

The current of Figure 4.2A is always positive (oxidation current) and noisy, suggesting that the process doesn't reach a steady state. Furthermore, SEM images of Figure 4.2B and C show that the oxidation did not happen, or the thickness of the oxide/hydroxide film is too thin. Indeed, the low magnification picture (Figure 4.2B) shows that the morphology of the electrode is still the same of the bare nickel foil. At higher magnification (Figure 4.2C) some small dots are visible, but the film is not uniform enough. Therefore, the electrolyte was changed from KOH to Na_2BO_4 but the results were still not satisfying (morphology not showed). We do think that electrochemical techniques were not suitable for this application, where a thick layer is mandatory, and so we gave up and we tried to obtain a NiO@Ni using a thermal process.

In this case, the NiO thickness depends mostly on temperature and time. If the temperature is not in the right range, other kinds of nickel oxides can be produced (like Ni_2O_3 of NiO_2). In addition, by adjusting the oxidation time, it is possible to control the oxide thickness that must be adequately thin in order to have an efficient transport of electrons.

Figure 4.3 shows XRD patterns of Ni foil annealed in different conditions. For comparison, the pattern of a not annealed Ni foil is also shown.

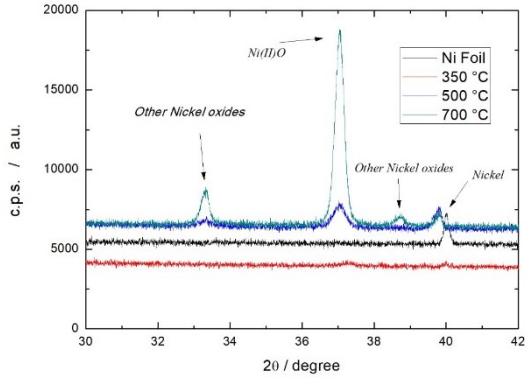

FIGURE 4.3 XRD PATTERN OF A PURE NI FOIL (BLACK CURVE) AND ANNEALED AT 350, 500 AND 700°C

Figure 4.3 shows that the lowest temperature leading to visible formation of NiO is 350˚C, but the kinetics of the process at this temperature is so slow that after a period of 120 minutes of annealing, the NiO peak was very weak. On the contrary, as annealing was conducted at 700°C, the Ni oxidation was very severe with formation of other oxidized species. The best annealing condition was found to be 120 minutes at 500°C, because the morphological analysis (see below) together with the successive tests as a sensor showed that NiO film thickness grown at 500 °C for 120 minutes is the best compromise between electrical conductivity and stability under SWASV. Only one NiO peak is shown in Figure 4.3 because the 2θ scale has been limited to a narrow interval for clarity purpose. Figure 4.4 shows three SEM images of a NiO surface after Ni oxidation (nickel foil) at 500°C for 120 minutes, and EDS analysis. For comparison, also the morphology of the nickel foil annealed at 700 °C is shown.

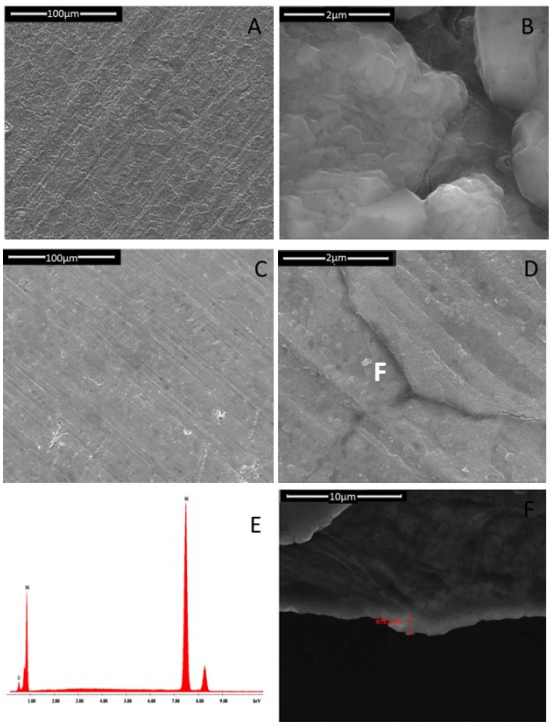

FIGURE 4.4 SEM IMAGES OF NI FOIL ANNEALED FOR 2H AT 700 °C A), B); AND 500 °C C), D); E): EDS ANALYSIS OF NI FOIL ANNEALED AT 500 °C; F): CROSS SECTION VIEW OF NI FOIL ANNEALED AT 500 °C

Figure 4.4 A, and B show the morphology of the electrode annealed at 700°C. It is clear that the electrode is not uniform, having different cracks (Figure 4.4A) and exposing Ni substrate (Figure 4.4B). On the contrary, the electrode annealed at 500°C looks much more uniform (Figure 4.4C) and, despite some cracks are still visible, these are not deep enough to show the substrate (Figure 4.4D). The ridges visible in the micrographs, likely, reproduce the initial Ni surface, so indicating that the film is thin. EDS analysis of Figure 4.4E confirms the presence of an oxide layer by the presence of the oxygen peak that is absent when the bare nickel foil has been examined (not showed) and confirms also the purity of the NiO based electrode. Figure 4.4 F shows the cross section view of NiO grown at 500 °C having a thickness of about 1µm.

Ni NWs has been fabricated using the same procedure to grow Cu and Pd nanostructures described in Chapter 3. Figure 4.5 shows SEM images of Ni NWs before and after the annealing (500 °C for 120 minutes).

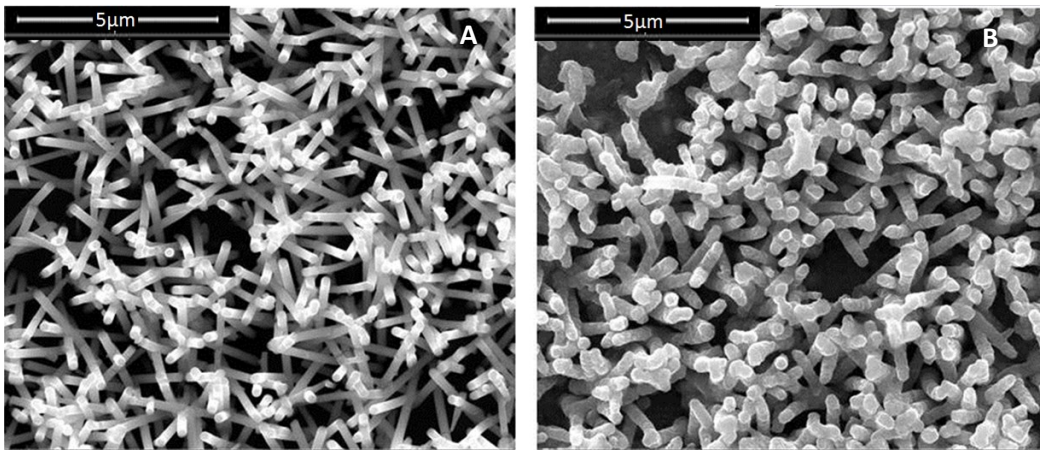

FIGURE 4.5 SEM IMAGES OF NI-NWS BEFORE (A) AND AFTER 120 MINUTES S OF ANNEALING AT 500 °C (B)

Figure 4.5 shows that as prepared Ni NWs are smooth and uniform in length while, after annealing, are rough and some heads stuck together.

XRD and EDS analysis of this electrode are similar to the NiO thin film, therefore are not shown. The conductivity of this electrode was really poor probably because the diameter of the NWs is of about 220 nm, therefore, 120 minutes of annealing might be excessively long. In order to improve electrode conductivity, Ni-NWs has been annealed for 15 min. By this way, the electrode conductivity was enhanced without variations in the morphology and XRD/EDS spectrum (see Figure 4.6)

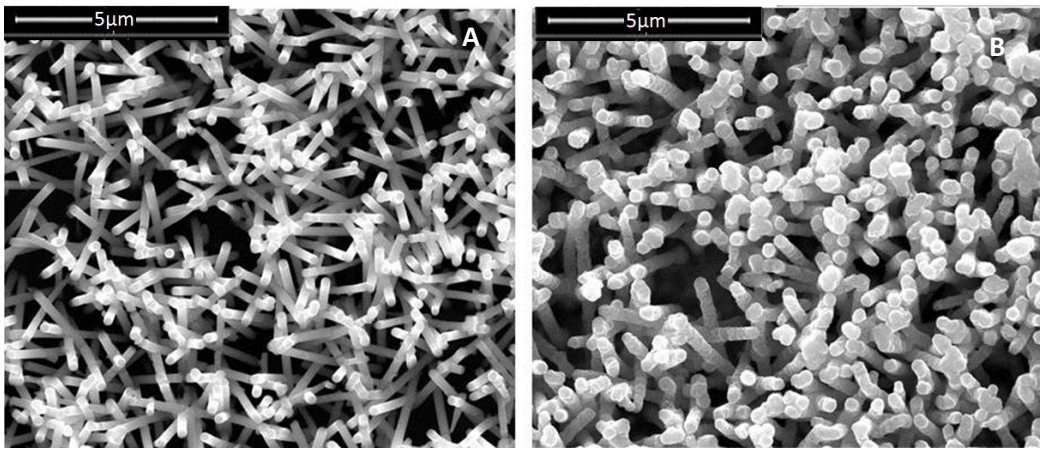

FIGURE 4.6 SEM IMAGES OF NIO@NI NWS ANNEALED AT 500 °C FOR 15 MIN

Electrochemical tests

For testing the NiO sensing performance in detecting Hg^{2+} ions through the SWASV method, different parameters were investigated according to Armas et al. [53]. Figure 4.7 shows the influence of analyte pH (A), and Hg deposition potential (B) on SWASW curves of a NiO thin film thermally grown at 500 C° for 120 minutes. The graphs show the mean value of the #3 samples.

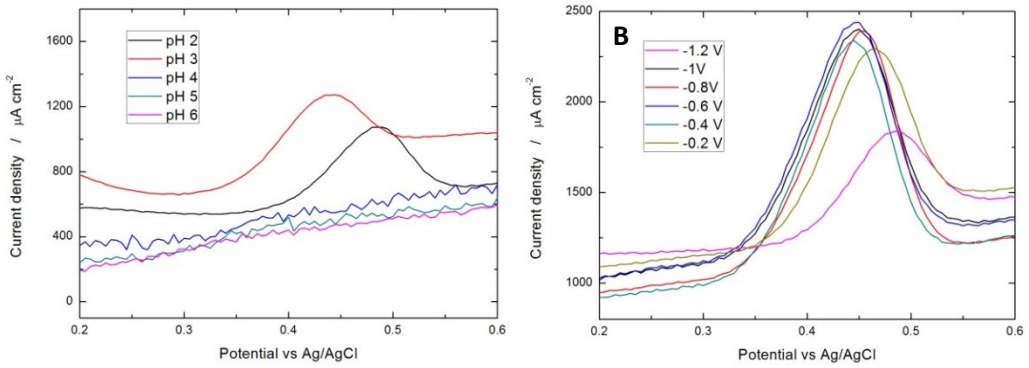

FIGURE 4.7 EFFECT OF PH (A), AND DEPOSITION POTENTIAL (B) ON STRIPPING PEAK OF 4 PPM OF MERCURY IONS

We have prepared different buffered solutions of citric acid and Na_2HPO_4. Figure 4.7A shows that the current peak at 0.45 V increases as pH diminishes according to Pourbaix's Atlas [68]. The optimum pH for detecting Hg was estimated to be 3 because NiO is unstable at lower pH and tends to dissolve.

Therefore, the deposition potential of Hg on NiO was investigated at pH 3. In detail, deposition was conducted at different potentials for 3 minutes from a solution containing 4ppm of Hg^{2+}. After deposition, the sensing element was polarized through SWASV, and the current vs. potential curves showed in Figure 4.7B were recorded. It can be observed that the stripping current peak at 0.45 V is almost constant in the interval from – 0.4 to -0.8V, while the stripping peak for deposition at -0.2 V is shifted at a few higher potential with a lower intensity. When deposition was conducted at a so high potential as -1.2 V, likely, the reduction of H^+ ions strongly interfere with Hg^{2+} ones lowering Hg mass deposited on NiO. As a consequence, the stripping peak was weaker. According to these findings, -0.4 V was selected as the best deposition potential, because the lower potential guarantees higher selectivity of deposition and higher lifetime of the NiO film.

Figure 4.8 shows the effect of the step frequency, amplitude, and potential on mercury detection.

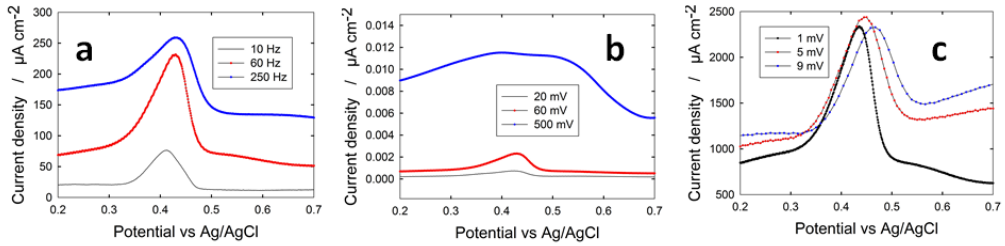

FIGURE 4.8 INFLUENCE OF FREQUENCY (A), POTENTIAL STEP (B), AND STEP AMPLITUDE (C) ON STRIPPING PEAK OF 4 PPM OF MERCURY IONS

It can be observed that the frequency and potential step have a huge effect on the stripping peak, while step amplitude does not affect. In detail, frequency higher than 60 Hz and step amplitude higher than 0.06 V start to distort the signal, making it impossible to be read.

Figure 4.9 shows the influence of deposition time on SWASV curves.

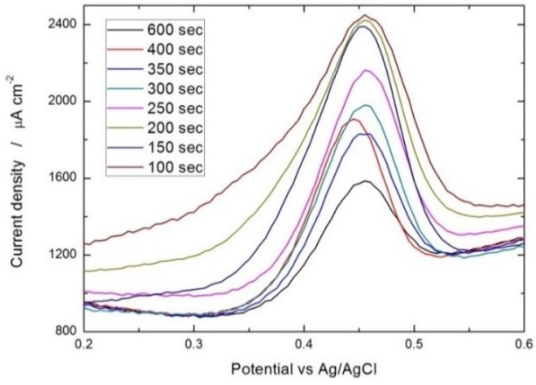

FIGURE 4.9 INFLUENCE OF DEPOSITION TIME ON STRIPPING PEAK OF 4 PPM OF MERCURY IONS

The deposition was conducted at -0.4V from a 4ppm Hg solution, at pH 3. According to the literature [69], the SWASV peak current vs. deposition time should be a sigmoid that reaches a plateau when the electrode surface is totally covered by the analyte. Figure 4.9 shows that after 350s of deposition at -0.4V, the peak current doesn't increase anymore, therefore this time was considered as

the optimum one. Table 4.4 summarizes the optimized values of operational parameters controlling the analytical determination of Hg traces in water.

TABLE 4.4 OPTIMIZED PARAMETER VALUES FOR ELECTROCHEMICAL DETECTION OF MERCURY IONS BY NIO@NI FOIL

Parameter	*Selected as an optimization*
pH	*3*
Deposition potential	*-0.4 vs Ag/AgCl*
Frequency	*50 Hz*
Step Amplitude	*60 mV*
Step Potential	*1 mV*
Deposition time	*350 sec*

Sensor calibration line was established by applying these parameters. Different $HgCl_2$ concentrations, from 6ppb to 5ppm, were investigated, and curves relative to only six concentrations are shown in Figure 4.10, for the sake of clarity.

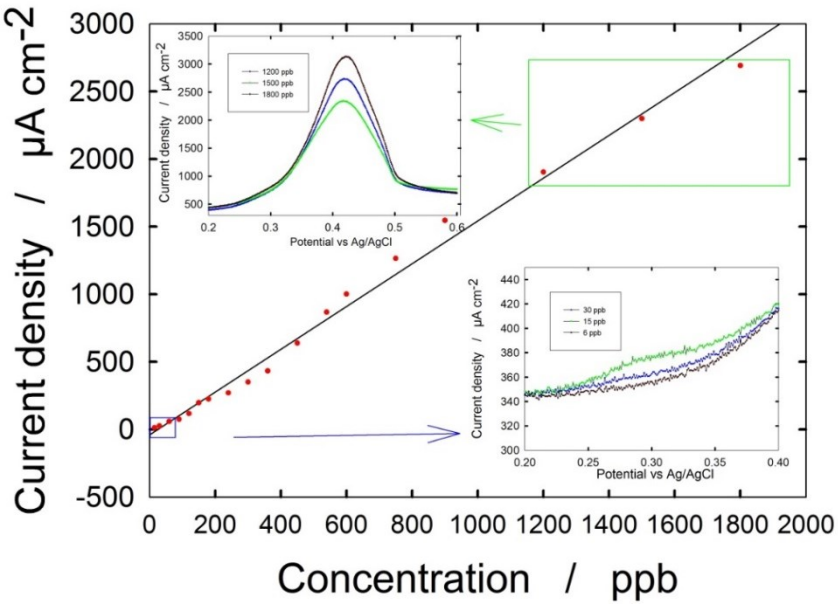

FIGURE 4.10 CALIBRATION LINE OF NIO@NI SENSING ELECTRODE FOR MERCURY IONS DETECTION, AND INFLUENCE OF MERCURY CONCENTRATION (INSETS) FROM 6 PPB TO 2 PPM

Figure 4.10 shows a linear dependence of the peak stripping current on mercury concentration in a range from 15ppb to 1.8ppm with a sensitivity of 1.1μA ppb^{-1} cm^{-2} and a limit of detection (LOD) of 4.4ppb. In order to reach a LOD lower than 2ppb (EPA limit), the deposition time was increased to 12 minutes with 0.5 to 30 ppb of Hg^{2+}. Figure 4.11 shows the stripping steps in this condition and a peak of 20μA appears for 0.5 ppb.

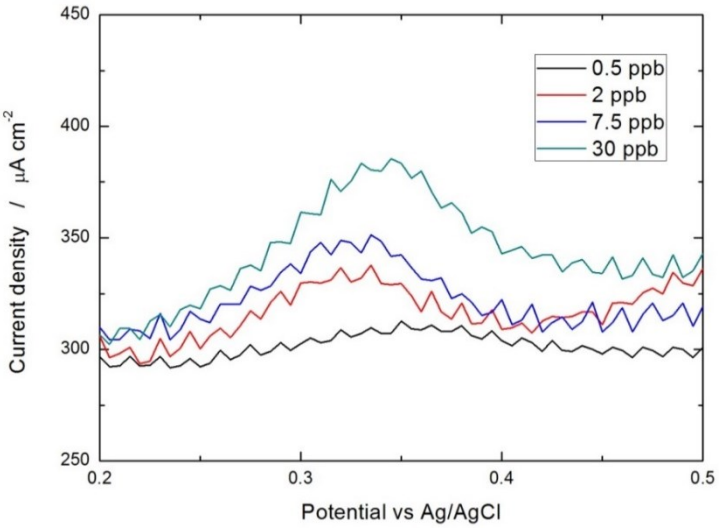

FIGURE 4.11 INFLUENCE OF DIFFERENT CONCENTRATION OF MERCURY (FROM 0.5 TO 30 PPB) AFTER 12 MINUTES OF DEPOSITION

Therefore, it is possible to use faster or slower deposition times, for higher or lower concentration of analyte, respectively. Using NiO@Ni-NWs sensing electrode annealed for 15 min, the peak current for 3ppm of mercury is smaller than that one obtained with the thin film electrode (Figure 4.12), even if the current baseline decreased from 190 to 31 μA, and the peak appears better structured. Likely, the weaker peak due to Ni@NiO NWs in comparison with flat NiO sensing electrode can be attributed to the excessive oxide thickness of the core-shell NWs.

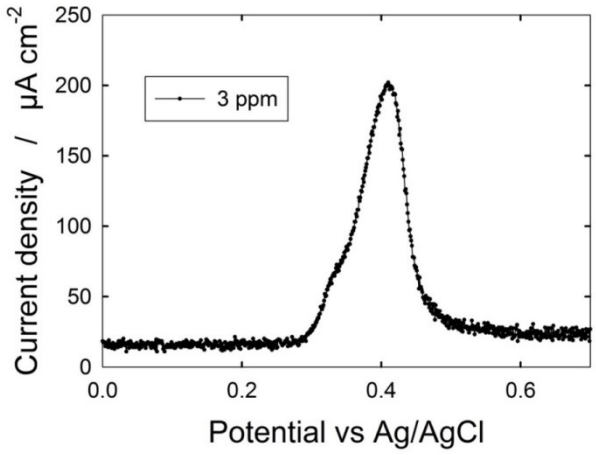

FIGURE 4.12 STRIPPING PEAK OF 3 PPM OF MERCURY ION AFTER 6 MINUTES OF ACCUMULATION ON A NIO@NI-NWS SENSING ELECTRODE ANNEALED FOR 15 MIN

This hypothesis is confirmed by Figure 4.13, which shows the stripping step of 3ppm of mercury, in the same condition of Figure 4.12, but using an electrode annealed for 120 minutes.

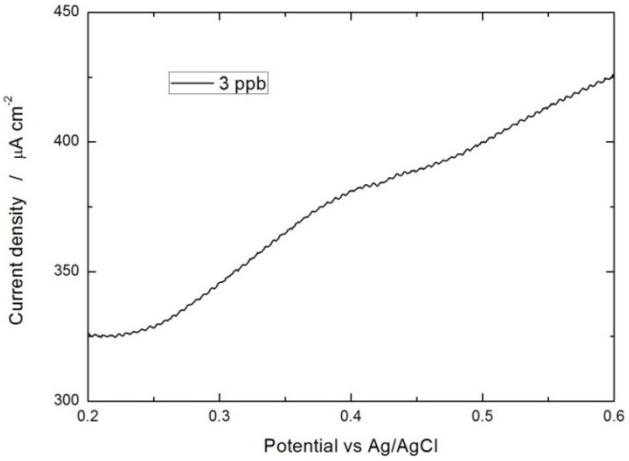

FIGURE 4.13 STRIPPING PEAK OF 3 PPM OF MERCURY AFTER 6 MIN OF ACCUMULATION ON A NIO@NI NWS ELECTRODE ANNEALED FOR 120 MINUTES

Despite the high mercury concentration (3ppm), a small peak is present, located at above 0.35 V vs Ag/AgCl. This suggests that the annealing time, and therefore the NiO thickness, has a huge effect on mercury detection.

Anyway, this behavior is still under study, but we think that it is possible to increase the peak current by a proper decrease of the oxidation time.

Selectivity tests

Selectivity tests were carried out against copper, lead, cadmium and zinc. Figure 4.14A shows the stripping step of 50 ppb of mercury deposited for 6 minutes in the presence of 50 ppb of the other heavy metals. Figure 4.14B shows the result of the same test conducted with 500 ppb of the interfering ions.

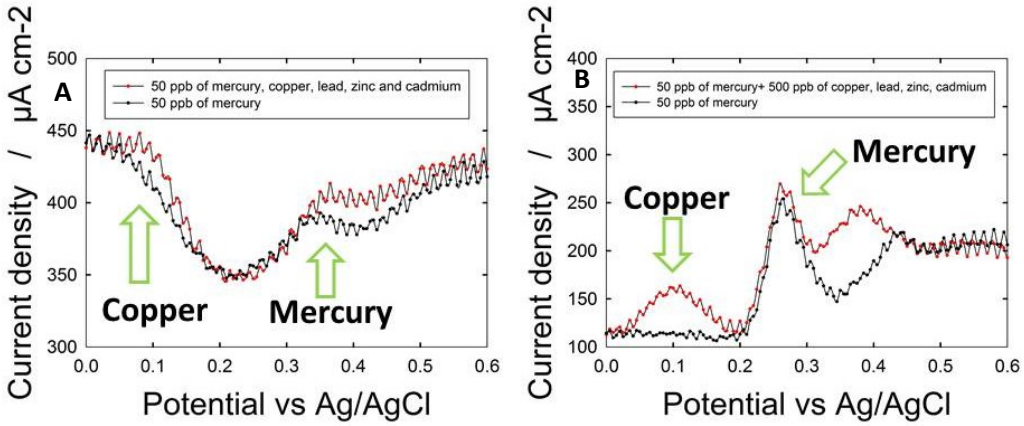

FIGURE 4.14 INTERFERENCE OF 50 PPB (A) AND 500 PPB (B) OF COPPER, LEAD, CADMIUM AND LEAD ON THE DETECTION OF 50 PPB OF MERCURY

Figure 4.14 shows a slight increase in the mercury peak current (12%) demonstrating that the electrode is quite selective towards these chemicals. Furthermore, the peak of copper is clearly present, suggesting that it is possible to use this sensing electrode for copper detection as well.

Real samples analysis

In order to evaluate the ability of the sensor to work with real samples, two different water samples were collected and tested after acidification to pH 3 with nitric acid. Sea water from Mondello beach, Palermo, Italy, was collected. Using this sample, mercury detection was not possible because the NiO layer, after polarization, immediately dissolve and a huge peak at 0.25V vs Ag/AgCl appears, probably due to the uncovered Ni exposed to the solution, even in the absence of externally added mercury (Figure 4.15). We think that this phenomena could come from the high content of chlorine of the sea water.

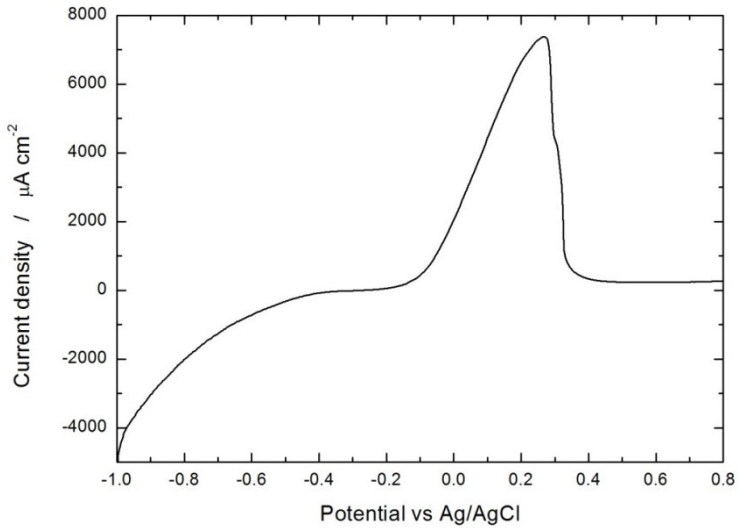

FIGURE 4.15 ANALYSIS OF SEA WATER FROM A MONDELLO BEACH, PALERMO, ITALY

Undrinkable water from a public fountain of Palermo, Italy, has been collected and tested, after acidification. In this case, mercury detection worked properly as shown in Figure 4.16, confirming that the failure with the sea water was due to the high chlorine content.

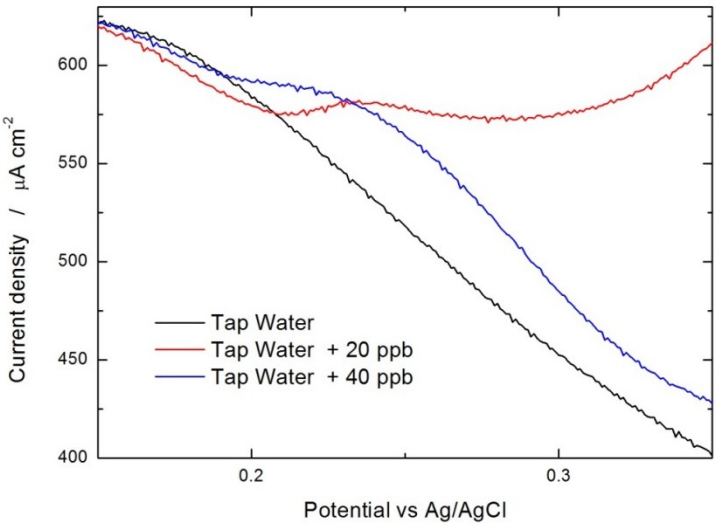

FIGURE 4.16 ANALYSIS OF UNDRINKABLE WATER FROM A PUBLIC FOUNTAIN OF PALERMO

When the sample was tested, after 6 min of deposition, a flat CV curve has been obtained (black curve of Figure 4.16), suggesting that mercury was absent or below the LOD of the sensing electrode. We tried to deposit for 12 min as well, but the curve was still flat (not shown). When 20 and 40 ppb of copper were added, a peak appears proportional to mercury concentration. The results in terms of recovery are shown in Table 4.5.

TABLE 4.5 RECOVERY ANALYSIS OF FIGURE 4.16

Mercury Added (C_a)	*Mercury Found (C_f)*	*Recovery (C_a/C_d *100)*
0	*0*	-
20 ppb	*18 ppb*	*90%*
40 ppb	*44.7 ppb*	*111%*

The results show that the sensing electrode is able to work with this kind of water sample even if an error of about 10% is obtained using the calibration line of Figure 4.10. This error could be due to a matrix interference therefore, a new calibration should be done in order to eliminate the error, using the sample instead of the buffer solution.

Comparison with the literature

According to these findings, it can be concluded that NiO based sensing electrode can be efficiently used for mercury detection. Its performance is excellent in comparison with other nickel oxide based electrodes as shown in Table 4.6. Since few researches have concerned nickel oxide as working sensing electrodes, other types of electrodes with similar morphology (metallic thin film) are shown in Table 4.6.

TABLE 4.6 COMPARISON OF SENSING BEHAVIOR OF DIFFERENT THIN FILM ELECTRODES FOR MERCURY DETECTION

Electrode material and morphology	***Deposition time (sec)***	***Linear Range (ppb)***	***Ref***
Ir microdisck	*360*	*1-9*	*[70]*
SPCE-Au thin film	*60*	*1-1000*	*[71]*
GCE-Bi thin film	*300*	*0.001-0.01*	*[72]*
NiO-Carbon Nanopowder	*300*	*2-75*	*[53]*
Mesoporous NiO	*N.S.*	*160-10* ^{5}	*[54]*
$NiCo_2O_4$	*180*	*160-560*	*[73]*
NiO thin film	*360* *720*	*6-1800* *0.5-30*	*This work*

4.2.3 Conclusions

For the first time, it has been shown that NiO film thermally grown on Ni can be used as a sensing element for detecting Hg^{2+} in water by square wave anodic stripping voltammetry [60]. Ni was oxidized in air at 500°C for 120 minutes leading to a NiO film thickness of about 990nm suitable for the desired purpose. The optimization of the sensing process parameters using a 4ppm analyte concentration gives a straight calibration line from 15ppb to 1800 ppm with a LOD of 4.4 ppb. The possibility to decrease the LOD by increasing deposition time was confirmed by a deposition time of 12 minutes, so detecting as less as 500 ppt. The NiO based sensing electrode is also selective for mercury detection, having a deviation of about 15% when 500 ppb of copper, zinc, lead and cadmium are present all together. Additionally, the sensing electrode can also detect mercury in a real undrinkable water sample without any issue. In addition, 1-D nanostructured NiO@Ni NWs were synthesized and tested showing a more sharped peak with a lower baseline. Anyway, the optimization of this sensing electrode is still under study but we think that, due to the higher surface area, it should be possible to drastically decrease the LOD of the sensor.

4.3 Gold microband array for mercury, copper and lead detection

4.3.1 Experimental

Electrode Fabrication

On-chip device formed by i) an interdigitated gold nanowire electrode array, ii) a gold counter, and iii) a platinum pseudo-reference electrode was fabricated using a combination of electron-beam and photolithography processes on Si/SiO_2 substrates as described in detail previously [74]. In brief, interdigitated gold microbands were patterned in resist by direct beam writing and metal evaporation (Ti/Au 5/50 nm) followed by standard lift-off techniques. Alignment marks were patterned along with this first metal layer to facilitate accurate positioning of subsequent optical lithography masks. Similarly, photolithography, metal evaporation (Ti/Au 10/90), and lift-off procedures were then employed to overlay electrical interconnection tracks including peripheral probe pads. Two macroscale gold electrodes were also deposited during this process. A further metal deposition step (Ti/Pt 10/90 nm) onto one of these macroscale electrodes was conducted to create an on-chip pseudo-reference electrode. Finally, a silicon nitride passivation layer (500 nm thick) was deposited to passivate the entire chip and windows selectively opened to allow exclusive contact between the gold nanowires, the gold counter and platinum pseudo-reference electrodes and the solution of interest. Openings were also patterned above peripheral contact pads to permit electrical connection. Each chip contains 6 interdigitated electrodes. Each electrode consisting of interdigitated gold microbands can be separately polarized. In order to

distinguish between these two electrodes, they have been named ‘protonator’ and ‘collector’.

Electrochemical measurements

Nitric andic (35%), Sodium Chloride, Ferrocyanide, Phosphate Buffer Solution (PBS), lead stock solution for ICP analysis (1000ppm), mercury chloride and copper chloride powder were purchased from Sigma Aldrich and used as received. All solution were prepared with DI water with resistivity of 18MΩ cm^{-1}. Heavy metals solutions were prepared by adding different amount of the stock solutions in deionized (DI) water with 10mM of NaCl. All the electrochemical measurements were carried out using a CHI920 bi-potentiostat in a three electrodes cell comprising of a Ag/AgCl as external reference electrode and a on chip gold counter electrode, at room temperature. Prior to stripping experiments, the chip was washed with pure isopropanol and DI water in order to remove any contaminants from the electrode surface. After that, a CV (scan rate 100mV/s) was carried out in a solution containing 1mM of ferrocyanide in 10mM of PBS pH 7.4 in order to characterize the electrochemical behavior of the electrode. Collector electrodes typically exhibit a peak current of 13nA, as shown in Figure 4.17.

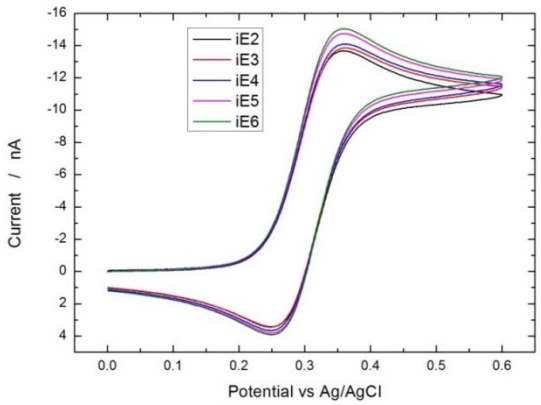

FIGURE 4.17 TYPICAL CV OF A THE COLLECTOR ELECTRODE WITH 2μM GAP IN THE PRESENCE OF 10 MM $Fe^{2/3+}$

Stock solutions were prepared by adding different amount of heavy metal stock solutions to a solution of 10mM NaCl in DI. Nitric acid was added to change the pH from 2 to 6. Different pH and deposition potentials were tested. To be sure that the metal was totally stripped out from the surface, multiple SWVs were carried out sequentially in DI with 10mM NaCl after each stripping step, until a flat CV curve was obtained. When high concentration of heavy metals were tested (in the ppm range), a cleaning step was necessary in order to regenerate the sensing electrode. The cleaning has been carried out by applying a fixed potential of 0.5V vs Ag/AgCl, in 0.1M H_2SO_4.

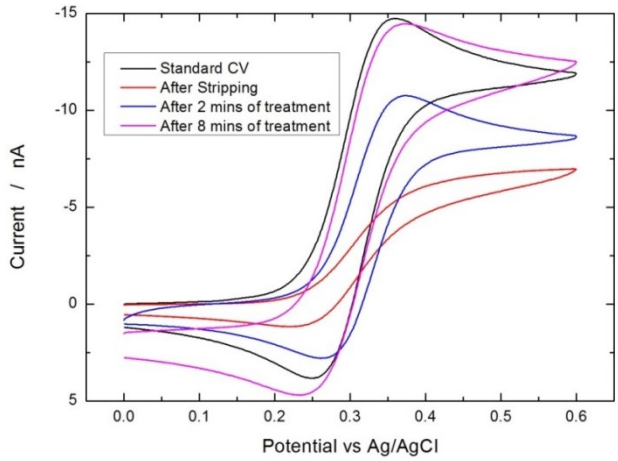

FIGURE 4.18 INFLUENCE OF CLEANING WITH SULFURIC ACID ON CV IN THE PRESENCE OF 10 MM FE^2/FE^{3+}

Figure 4.18 shows the influence of the cleaning step: the electrode after the SWV is definitely poisoned and not able to generate a good peak in the presence of ferrocyanide, while the CV is almost regenerated after 8 min of treatment. The calibration curve was obtained by 3 triplicates, starting from the lowest concentration to the highest. In order to understand the influence of the polarization of 'protonator' on the CV curve recorded on the 'collector', the protonator has been polarized at a fixed potential and a CV on the collector has been carried out simultaneously.

Chip holder fabrication

A custom built chip holder was fabricated to permit electrical contact between the electrodes and the potentiostat without the requirement for PCB packaging and wire bonding. The lower part of the holder was fabricated from a polytetrafluoroethylene (PTFE) base fixed to an aluminum tray onto which the chip was mounted. The tray into which the chip was placed was designed in order to be only 0.1mm larger than the chip edge dimensions to guarantee that the chip would remain firmly placed during measurement. The PTFE cap comprised apertures to mount spring loaded probes to contact the on chip peripheral bond pads and also a central low volume sample reservoir, sealed from beneath with an O-Ring (James Walker Ltd.), to accommodate the sample volume. The inner diameter (4.5 mm) of the O-ring was large enough to ensure that all electrodes on the chip had equivalent access to the analyte without impeding diffusion processes. Spring-loaded probes with rounded tips (Connector Solutions Ltd., U.K) were selected with a typical tip diameter 0.51 mm, (Series S Duraseal: S-00-J-1.3-G-DS-36-1), guaranteeing a good electrical contact to the contact electrodes (1.5 mm in diameter). When completed with microband electrode chip, the cell was fully water-tight with a sample volume of 300 µL, (see Figure 4.19).

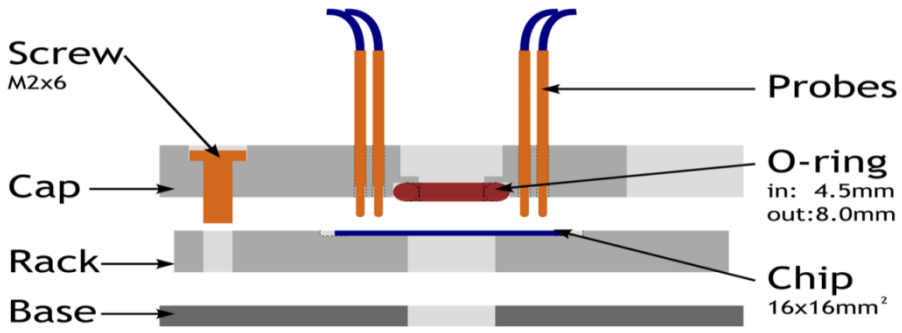

FIGURE 4.19 SCHEME OF CHIP HOLDER

Real Sample Analysis

Three river water samples, from Lee River, Cork, Ireland, named A, B, and C were collected in three different days and acidified with nitric acid to pH 3.5 after a sedimentation process to eliminate any particulate. The standard addition method was carried out for the quantification of copper, lead and mercury. A minimum of five repetitive scans were carried out.

4.3.2 Results and discussion

Electrode Characterization

Gold microband array electrodes were fabricated using photolithography process at silicon wafer substrates bearing a 300 nm layer of thermally grown silicon dioxide, (see experimental section). Standard optical lithography was employed to overlay electrical contacts and interconnection tracks onto microband arrays, followed by metal deposition and liftoff. Electrical contact to all on-chip electrodes was established by contact pads located at the chip periphery and connected to the microband using interconnection tracks traced by photolithography. Unwanted electrochemical reactions occurring between metal interconnection tracks and electrochemically active species were prevented by the deposition of a silicon nitride layer. A lithographically patterned trench (~30 x 30 μm) was selectively opened in the insulating silicon nitride layer directly above the microband array to allow exclusive exposure of the microband array to the electrochemically active species. By this way, selective openings over the on-chip counter and reference electrodes were employed to achieve a fully functional nano-electrochemical device on-chip. Therefore, 6 interdigitated gold

based electrodes, a gold counter and a silver reference were present in one chip. Each interdigitated electrode was made of two distinct interdigitated microband electrodes with a gap of 1, 2 or 10 µm. Microband electrodes were characterized using optical microscopy. Figure 4.20 shows the final electrode and optical micrograph of an interdigitated microband array device after silicon nitride passivation.

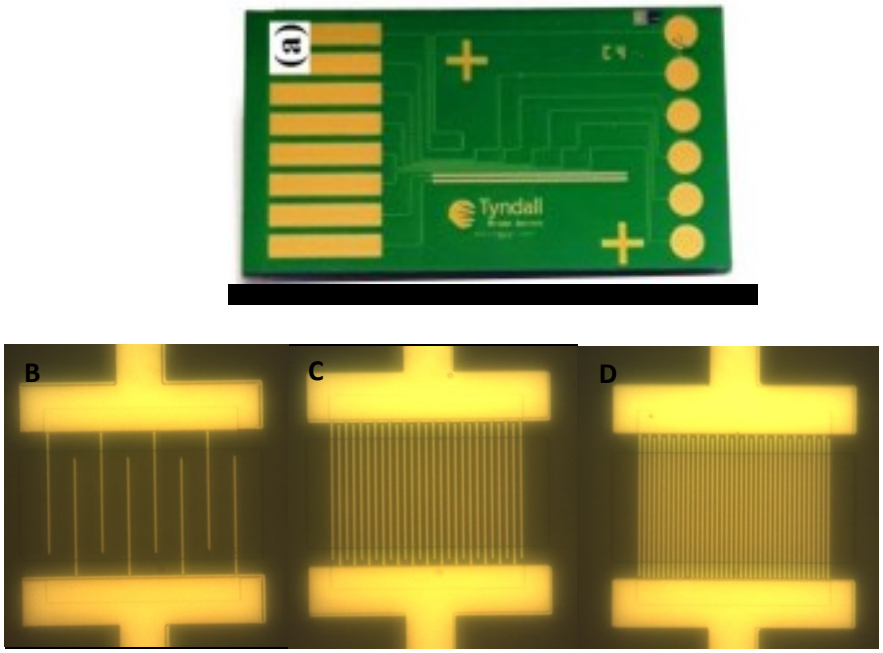

FIGURE 4.20 A) DEVICE AFTER FABRICATION, AND OPTICAL IMAGES OF 10 (B), 2(C) AND 1(D) µM GAP INTERDIGITATED MAE

Optical characterization performed on fabricated devices showed selective removal of the silicon nitride, exposing the underlying interdigitated microband electrodes. The length of the electrochemically active microband was typically 45 µm with a width of 2 µm.

Mechanism of detection

To demonstrate the mechanism of detection, 100 µl of a solution containing 10 ppm of copper has been dropped into the electrode and a portable potentiostat was used to carry out the experiment, as shown in Figure 4.21. The electrode has been isolated using a piece of silicon with a thickness of 2 mm.

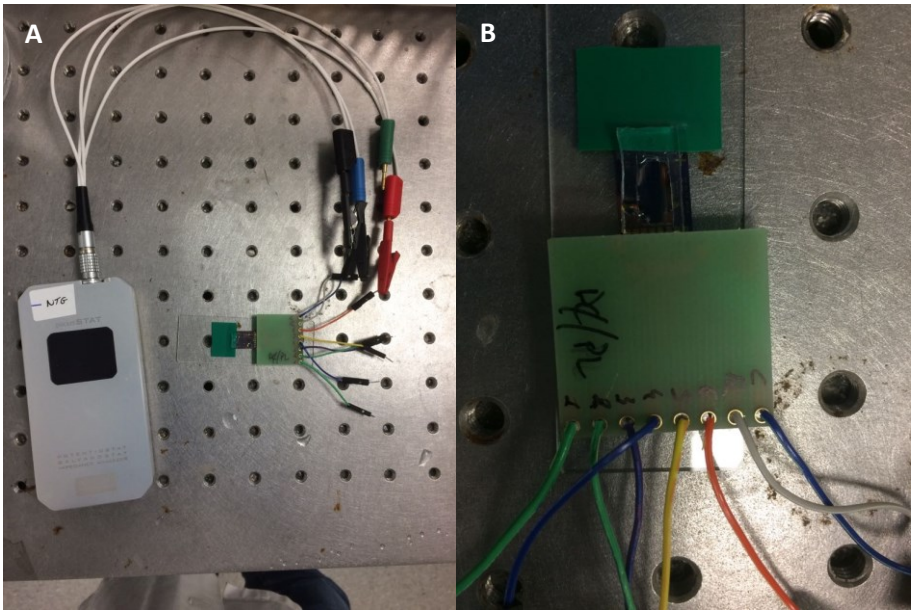

FIGURE 4.21 CONNECTION OF THE ELECTRODE WITH A PORTABLE POTENTIOSTAT

The as prepared electrode was put under an optical microscope, and the SWASV was carried out. During the experiment, a video was recorded and five frames of the video are shown in Figure 4.22.

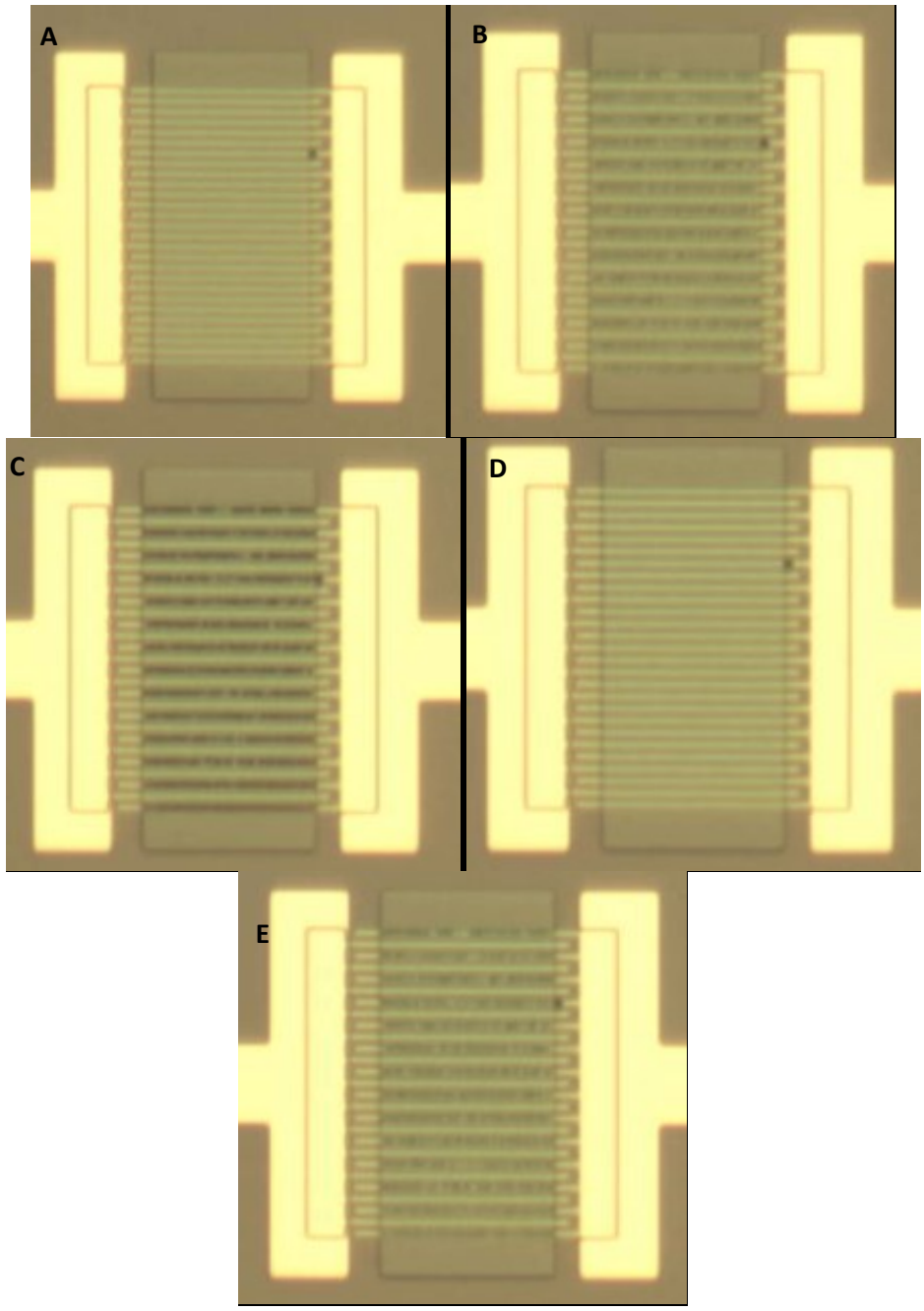

FIGURE 4.22 A) ELECTRODE BEFORE COPPER DEPOSITION, B) AFTER 10 SEC OF DEPOSITION, C) AFTER 20 SEC OF DEPOSITION, D) DURING STRIPPING STEP AT $E<E^0$ E) AFTER STRIPPING STEP

In Figure 4.22A, the experiment is not started yet, showing that the electrode is clean with a yellowish color typical of gold. When the deposition starts (Figure 4.22B) the electrode starts to become black, due to the copper deposition until, after 20 sec of deposition, the yellow color is definitely disappeared (Figure 4.22C). When the stripping step starts, the black color starts to disappear (Figure 4.22D) due to the stripping of copper and when the E^0 of copper is reached the electrode become yellow again with the same morphology of Figure 4.22A (Figure 4.22E).

Optimization of deposition time, deposition potential, and pH

To optimize sensing performance, some parameters such as pH, deposition time (dt), and deposition potential (dV) were investigated for each metal, employing gold microbands separated by 1μm gap. The metal concentration was fixed to 100 ppb for copper and lead while 10 ppb was selected for mercury, due to its higher toxicity. The optimization of more than five experiments were averaged and the resulting values are plotted. An error of about ± 10% has been found. pH significantly affects the process, as confirmed by the literature [75]. A pH range from 1 to 5 was investigated for copper deposition while a range from 2 to 5 for mercury and lead. After 3 minutes of deposition at -0.4V vs Ag/AgCl, the current peak increased in more acidic media and reached a maximum at pH 3.5 for mercury and lead, and pH 2 for copper (Figure 4.23).

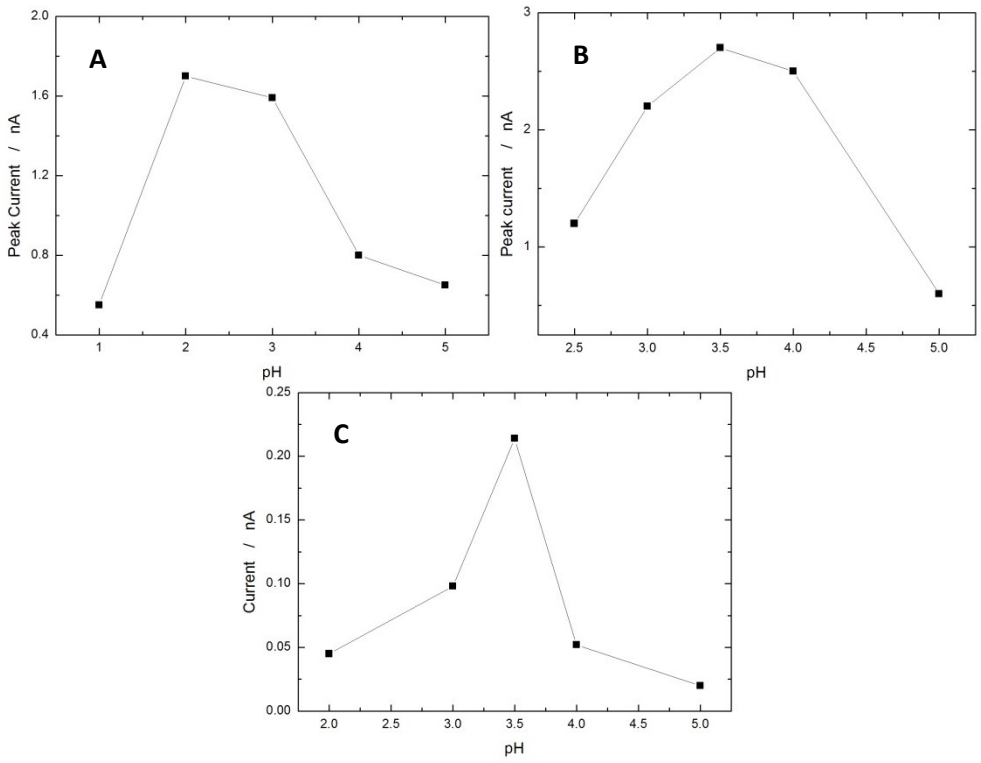

FIGURE 4.23 INFLUENCE OF PH ON THE DETECTION OF 100 PPB OF A) CU, B) PB, AND C) 10 PPB OF HG

The influence of the deposition potential was investigated in a range from -0.8V to 0 V (vs. Ag/AgCl) in a solution with the optimized pH in dependence on the metal. Moving from anodic to more cathodic potential, the output signal increased to a maximum at -0.4V for copper and lead and -0.5V for mercury (Figure 4.24). The current peak starts to decrease more cathodic potentials, likely due to the start of hydrogen evolution [76]

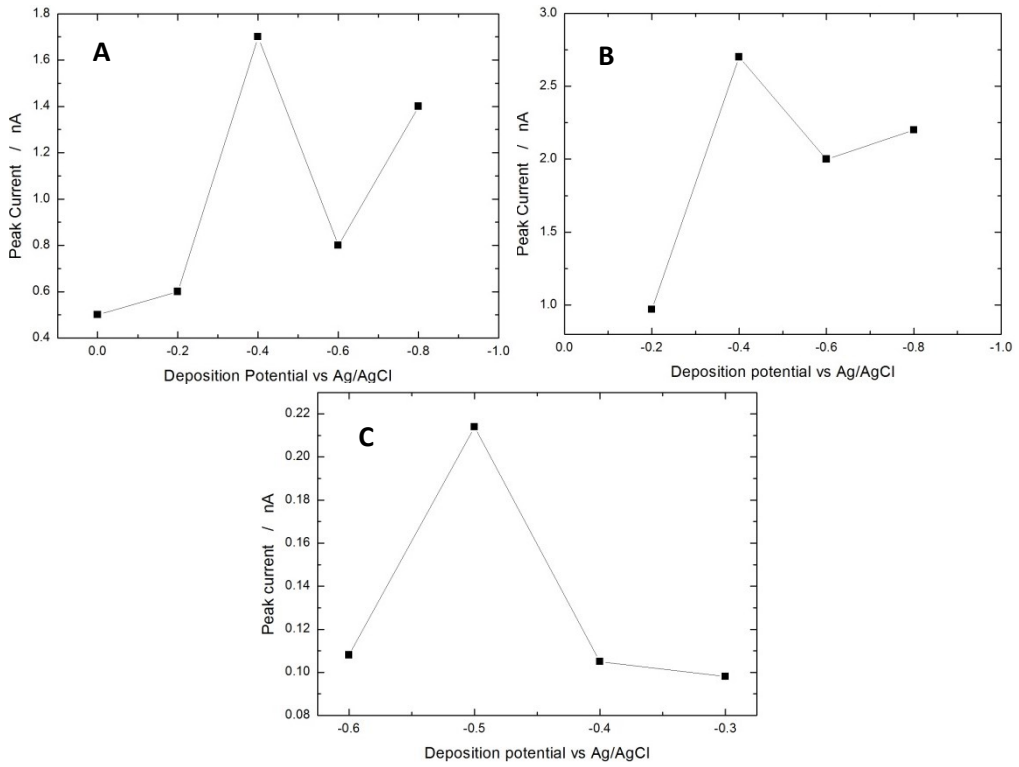

FIGURE 4.24 EFFECT OF DEPOSITION POTENTIAL (VD) ON THE DETECTION OF 100 PPB OF A) CU, B) PB AND C) 10 PPB OF HG

Figure 4.25A shows the effect of the deposition time, in a range from 1 to 300 s, at the optimal pH and Vd with 100 ppb of copper. Increasing the deposition time, the current peak increases because the coverage on the electrode surface increases. However, after 180 s of deposition, the current peak reaches a plateau, probably due to the surface saturation [53]. A similar behavior was found for lead and mercury (Figure 4.25B, C).

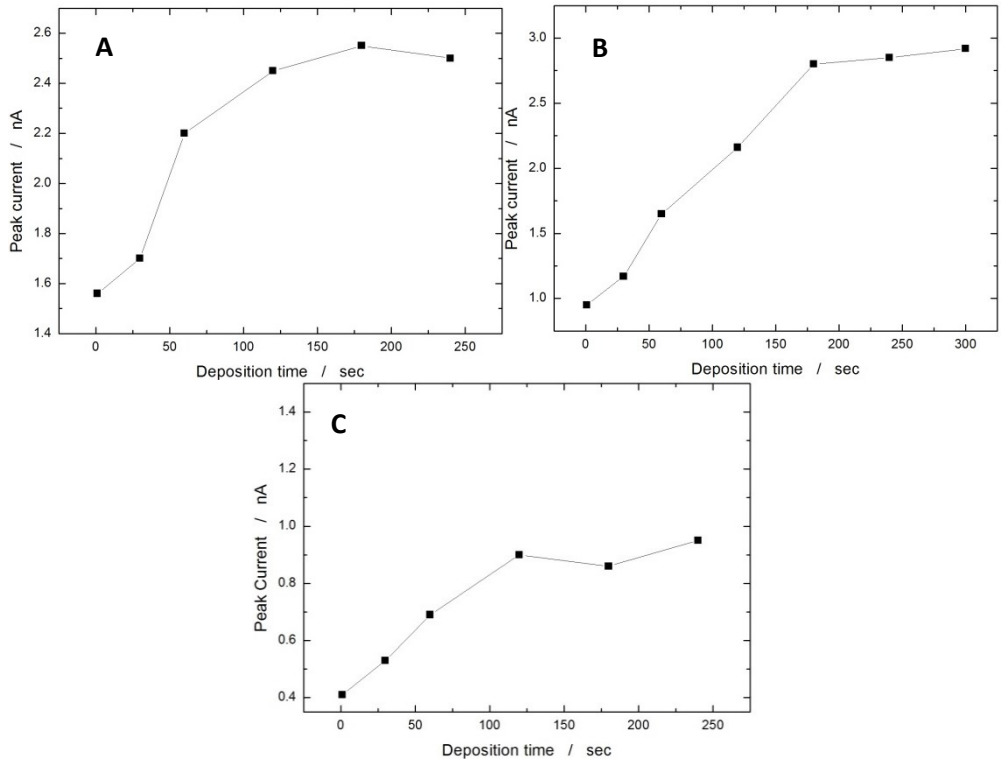

FIGURE 4.25 INFLUENCE OF THE DEPOSITION TIME (TD) ON THE DETECTION OF 100 PPB OF A) CU, B) PB AND C) 10 PPB OF HG

Table 4.7 summarizes the optimal parameters for each metal. In the perspective of simultaneous detection, when only one deposition time can be used, the calibration line of copper and mercury were carried out with 180 s of deposition as well.

TABLE 4.7 PARAMETERS SELECTED AS OPTIMIZED FOR LEAD, COPPER AND MERCURY DEPOSITION/STRIPPING

	Lead	Copper	Mercury
pH	*3.5*	*2.0*	*3.5*
t_d	*180 s*	*120 s*	*120 s*
V_d	*-0.4 V vs Ag/AgCl*	*-0.4 V vs Ag/AgCl*	*-0.5 V vs Ag/AgCl*

SWASV analysis of Lead, Copper and Mercury

In order to check the presence of some peaks due to the blank solution, SWASV was carried out in a solution containing 10mM NaCl and nitric acid. As it is possible to see in Figure 4.26, a peak at -0.4V vs. Ag/AgCl, due to the dissolved oxygen, is present.[77-78-79]

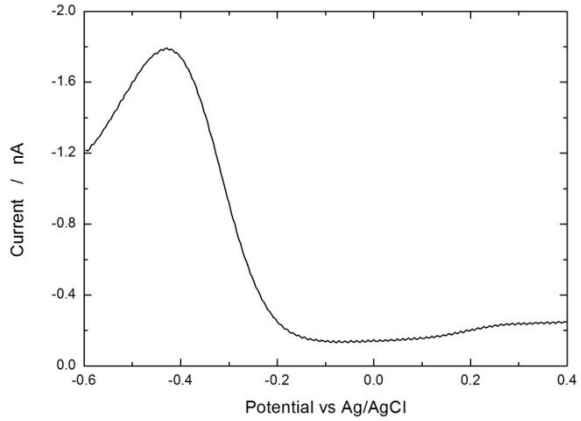

FIGURE 4.26 SWASV OVER GOLD MICROBAND ELECTRODE WITH 1µM GAP IN 10MM NACL

Using the optimized conditions, SWASV analysis was conducted with increasing concentrations of each metal. Figure 4.27 shows a CV in the presence of 10 ppm of lead.

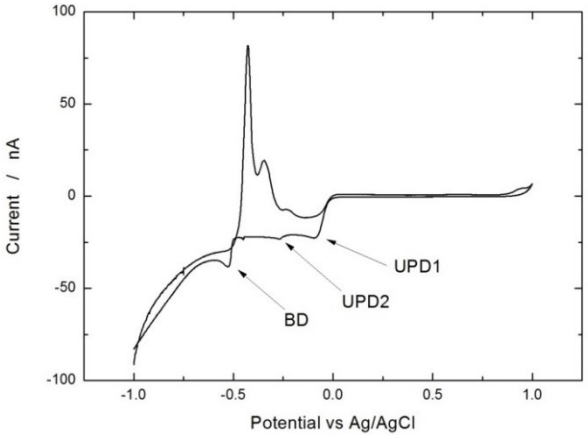

FIG 4.27 CV OVER GOLD MAE WITH 1µM GAP IN 10MM NACL AND 10 PPM OF LEAD

Three different anodic peaks at -0.6V, -0.3V, and -0.17V vs. Ag/AgCl were observed, due to the bulk deposition (-0.6V), and under potential deposition peaks (-0.3V, and -0.17V). This behavior is consistent with previous papers published about lead stripping from gold electrodes and corresponds to the formation, and consequent stripping of a monolayer of lead at potentials more positive than the Nernst one [80-81-82-83] Indeed, at low concentration of lead only the peak at -0.17V vs. Ag/AgCl was observed, confirming that it is related to an under potential deposition.

Figures 4.28 A, B show the experiments at increasing lead concentration from 10 to 1000 ppb and the related calibration line. Each concentration was tested at least 3 times and the mean value is plotted in the calibration line with the corresponding standard deviation.

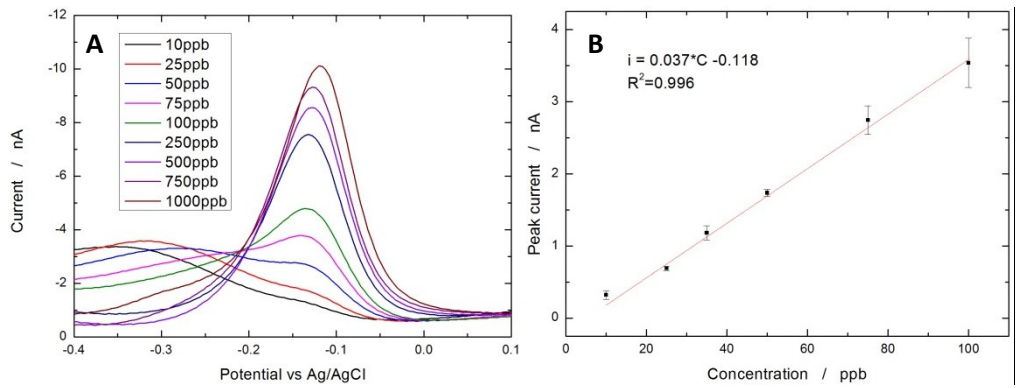

FIG 4.28 SWASV WITH INCREASING CONCENTRATION OF LEAD (A) AND CORRESPONDING CALIBRATION LINE (B)

It is clear that, the oxygen peak overlaps with the lead stripping peak from 10 to 50 ppb of lead, drastically decreasing the sensitivity of the electrode. This is confirmed by Figure 4.29 where a solution with 10 ppb of lead has been degassed for 30 min with N_2.

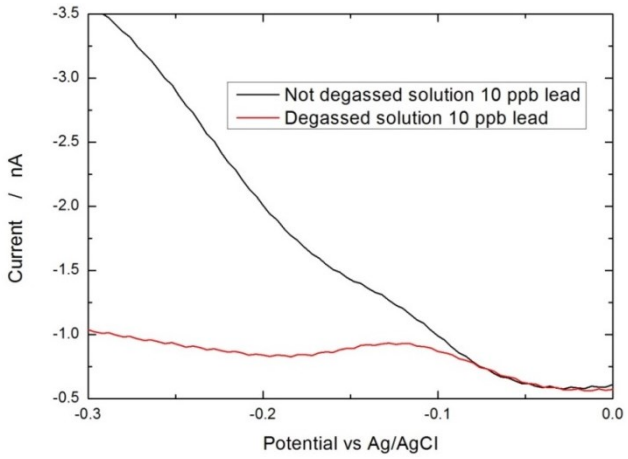

FIG 4.29 SWASV WITH 10 PPB OF LEAD IN AERATED (BLACK) AND DEGASSED (RED) SOLUTION

After 300s of deposition in a degassed solution, the current peak is more than twice, increasing from 80 pA to 210 pA, so confirming that it is possible to achieve a lower limit of detection. Figure 4.30 shows the stripping step at increasing concentration of mercury and the calibration line. Each concentration was tested at least 3 times and the mean value is plotted in the calibration line with the corresponding standard deviation. As it is possible to see, the mercury UPD is at 0.55V vs. Ag/AgCl and, increasing the concentration up to 500 ppb the bulk deposition appears at 0.45V vs. Ag/AgCl.

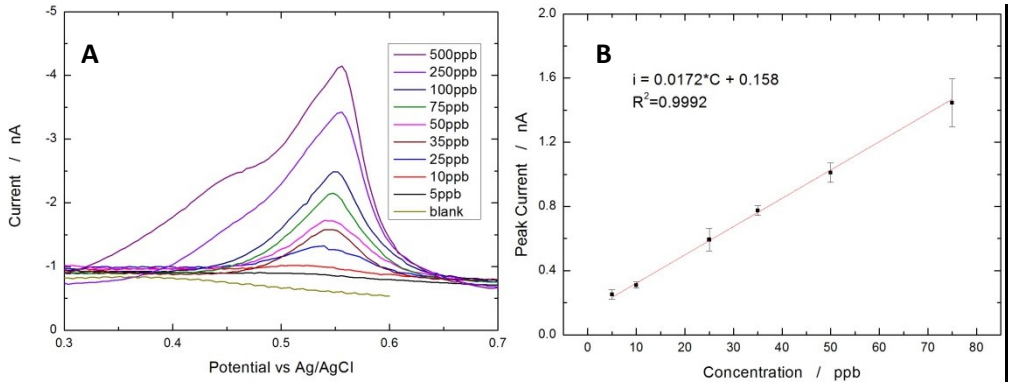

FIG 4.30 SWASV WITH INCREASING CONCENTRATION OF MERCURY (A) AND CORRESPONDING CALIBRATION LINE (B)

Similar results were found increasing copper concentration, as shown in Figure 4.31. In this case, the bulk deposition starts at 0.5 ppm at almost 0V vs Ag/AgCl (not shown). Here again, each concentration was tested at least 3 times and the mean value is plotted in the calibration line with the corresponding standard deviation.

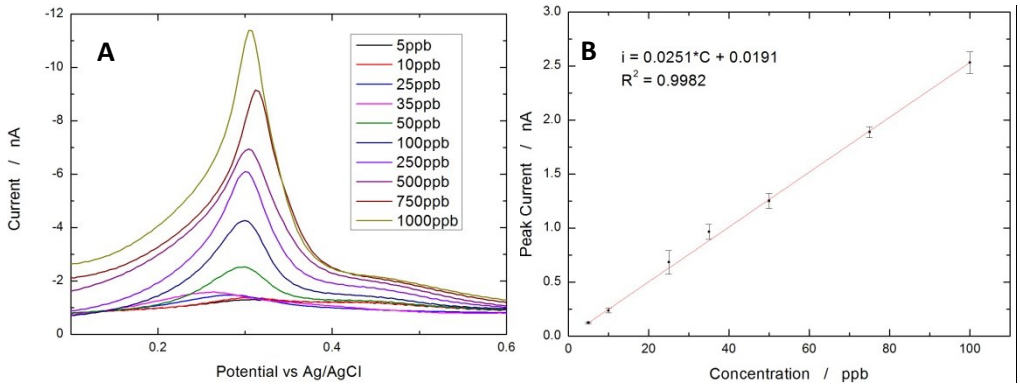

FIG 4.31 SWASV WITH INCREASING CONCENTRATION OF CU (A) AND CORRESPONDING CALIBRATION LINE (B)

In this context, it is important to highlight that for lead and copper the LOD is lower than the concentration limit settled by EPA, while for mercury, an improvement is necessary. For this reason, the concentration range from 1 to 5 ppb has been investigated by increasing the deposition time from 3 to 6 minutes. Figure 4.32 shows the stripping step from 1 to 5 ppb of mercury evidencing that it is possible to reach lower concentration increasing the deposition time. Table 4.8 summarizes all the features of the electrode in terms of linear range, sensitivity and LOD.

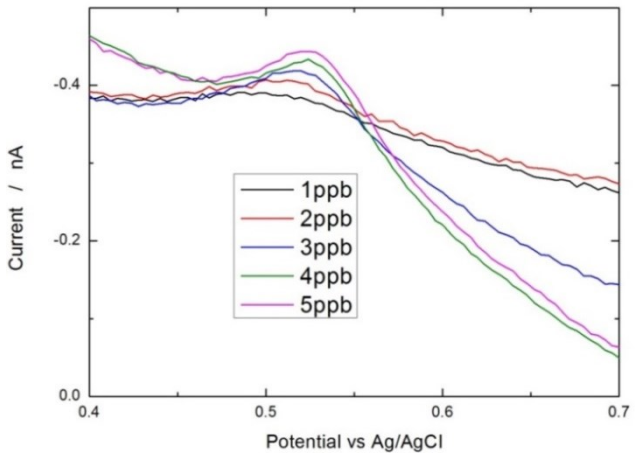

FIGURE 4.32 STRIPPING STEP WITH INCREASING CONCENTRATION OF MERCURY, FROM 1 TO 5 PPB, FOR 6 MIN OF DEPOSITION

TABLE 4.8 FEATURES OF THE GOLD MICROBANDS WITH 1UM GAP FOR PB, CU AND HG DETECTION

*NOT DEGASSING, ** 6 MIN DEPOSITION

	Sensitivity (pA/ppb)	**Linear Range (ppb)**	**R^2**	**LOD (ppb)**
Lead	37.0	10*-100	0.996	1.3
Copper	25.1	5-100	0.998	0.9
Mercury	17.2	5-75 1-75**	0.999	2 <1

According to the above results, it can be concluded that gold based MAE can be efficiently used for heavy metal detection. Their performance is excellent in comparison with other Au based sensing electrodes with similar morphologies as shown in Table 4.9.

TABLE 4.9 COMPARISON OF SENSING BEHAVIOUR OF DIFFERENT GOLD BASED ELECTRODES (NOT LABELLED)

Electrode	Heavy metal	Td (s)	Linear Range (ppb)	Reference
Au-Microband	Hg	1000	1-10	[84]
SPCE/gold film	Hg	60	1-1000	[71]
256 Au Microbands	Hg	30	10-200	[85]
Rotating Disc Au	Cu	90	0.025-0.25	[86]
Gold Electrode Modified with Penicillamine	Cu	30	50-6.3 10^3	[87]
Bi-Au Electrode	Pb	120	160-10^5	[88]
SPCE/Au-NPs	Pb	240	2.5-250	[89]
Au microband	Cu, Pb, Hg	120 180 120	5-100 10-100 1-75	This work

Metal interferences

The possibility to detect simultaneously these three metals (copper, lead, and mercury) was investigated by carrying out different stripping analysis in solutions containing them. The results showed that the presence of each heavy metal affects the detection of the others differently.

Table 4.10 summarizes the detection of copper in the presence of mercury and lead.

TABLE 4.10 EFFECT OF MERCURY AND LEAD ON COPPER DETECTION

Pb concentration (ppb)	Hg concentration (ppb)	Real Cu concentration (ppb)	Output Cu concentration (ppb)	Deviation %
10	5	5	7	40%
30	5	5	9.2	84%
50	5	5	11	120%
20	20	5	9.5	90%
20	50	5	7.1	42%

The effect of these two metals is to enhance the copper peak. This effect is probably due to the formation of an alloy between these metals [90]. In the mentioned work, Agra Gutierrez et al. showed that there is a huge interference on the detection of copper when lead is present but they found a different behavior, with a decreasing of copper peak height when lead concentration increases. A similar issue has been found by Sayen et al. when tried to detect copper in the presence of mercury [91]. In the range investigated here, the highest deviation is +120% on the output concentration.

Mercury peak is affected from the presence of copper and lead as well, but in a lesser way, as is possible to see in Table 4.11.

TABLE 4.11 EFFECT OF LEAD AND COPPER ON MERCURY DETECTION

Pb concentration (ppb)	Cu concentration (ppb)	Real Hg concentration (ppb)	Output Hg concentration (ppb)	Deviation %
20	5	5	3.3	-34%
30	5	5	2.7	-46%
50	5	5	2.4	-52%
20	10	5	3	-40%
20	50	5	2.3	-54%

In this case the effect is opposite: the presence of different amount of copper and lead slightly decreases the current peak of mercury with a maximum error of

54% in the presence of high concentration of copper. Also in this case, the problem could be due to either the deposition of an alloy on the surface of the sensing electrode or competition for the binding sites [92].

In any case, a correct approach to take into consideration these effects could be to calculate different calibration lines, not only in the presence of the target metal but also with the 'interference' ones.

The biggest interference effect is on lead peak, as shown in Figure 4.33A, B.

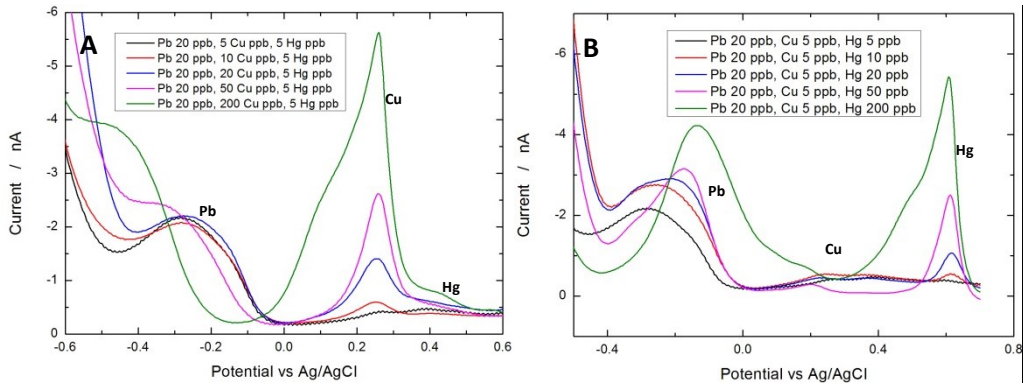

FIGURE 4.33 EFFECT OF INCREASING CONCENTRATION OF COPPER (A) AND MERCURY (B) ON LEAD CURRENT PEAK

When the copper and/or mercury concentration increase the lead's peak either disappears or starts to shift towards more anodic. Figure 4.33A shows that, nevertheless lead concentration is constant, the peak disappears when 50 ppb of copper are present. Figure 4.33B clearly evidences that, the lead current peak increases when mercury concentration increases despite lead concentration is constant. El Tall et al. found a similar result when tried to detect lead in the presence of copper, due to the deposition of a Cu/Pb alloy [93]. This behaviour was also found by other authors [94-95].

About the effect of mercury, we think that this effect is related to an enhancement of the oxygen current peak due to the presence of mercury on the

surface of the sensing electrode. When mercury is deposited on the electrode, the oxygen peak is highly enhanced and shifted towards more anodic potential, as shown in Figure 4.34.

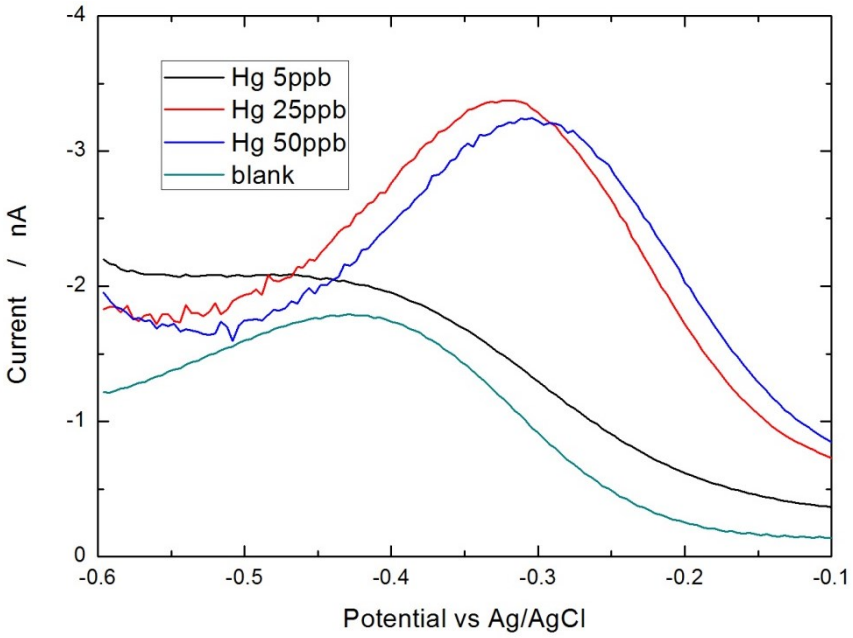

FIGURE 4.34 EFFECT OF MERCURY CONCENTRATION ON OXYGEN CURRENT PEAK

While in absence of mercury the oxygen peak potential is -0.45V vs Ag/AgCl, when mercury is deposited, the peak potential shifts to i) -0.4V with 5ppb of mercury, ii) -0.35V with 25ppb, and iii) -0.3V with 50ppb. Therefore, we infers that this enhanced oxygen peak overlaps the lead's peak, making impossible the lead's detection. However, a strange behavior was found when a second consecutive stripping step was performed, without any further deposition. In fact, performing a second consecutive stripping, the oxygen peak come back in the right position (above -0.35V vs. Ag/AgCl) decreasing in amplitude as well; as shown in Figure 4.35.

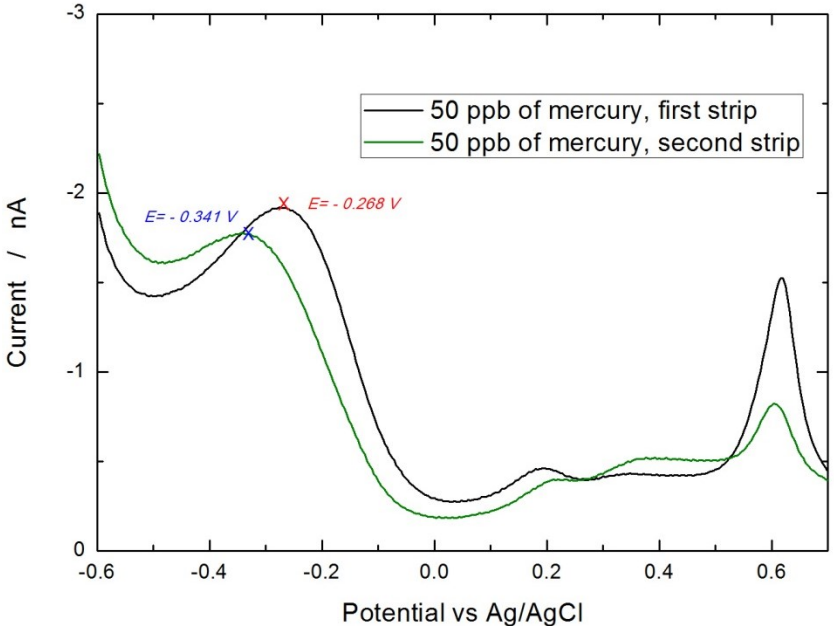

FIGURE 4.35 POTENTIAL OF OXYGEN CURRENT PEAK DURING FIRST (BLACK CURVE) AND SECOND CONSECUTIVE STRIPPING (GREEN CURVE)

On the basis of this result, we tried to detect lead performing two consecutive stripping steps in the presence of copper and mercury (Figure 4.36).

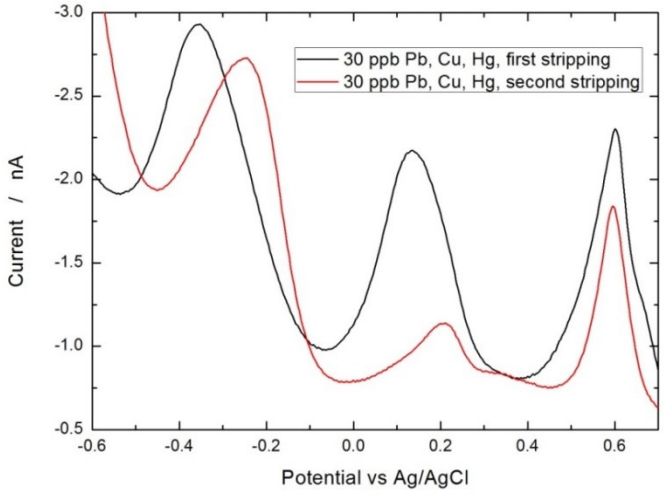

FIGURE 4.36 FIRST AND SECOND CONSECUTIVE STRIPPING OF 30 PPB OF COPPER, MERCURY AND LEAD

As before, we found that, lead peak is not present at the first stripping but, when the second stripping is performed, it comes back in the right position (of about -0.2V) with a reasonable height, as shown in Table 4.12.

TABLE 4.12 EFFECT OF MERCURY AND COPPER ON LEAD DETECTION

Hg concentration (ppb)	Cu concentration (ppb)	Real Pb concentration (ppb)	Output Pb concentration (ppb)	Error
20	20	20	27	35%
30	30	30	36	20%
50	40	40	40.5	-19%

Anyway, this behavior have to be still studied and confirmed but we think that, if these three metals are simultaneously present, it is possible to determine copper and mercury concentration by the first stripping step and then, performing a second one, to determine lead concentration.

pH control

All the previous experiments were carried out with an interdigitated gold microband electrode of 1μm gap, by adding different amount of HNO_3, depending on the metal, to the blank solution of DI and NaCl without polarizing the protonator electrode. For the sake of using this sensor for in-situ and real time analysis, we investigated the possibility to polarize the 'protonator' in a potential range where the water splitting occurs. The drawback in using this technique is the interaction between the electric fields generated by the two polarized differently interdigitated electrodes. In our previous work, we calculated that, a gap of 15μm is necessary to totally eliminate the interference between these 2 electrodes [96]. However, the higher is the gap the lower the number of interdigitated electrodes, that means a lower overall surface area. As

a good compromise between sensitivity and interaction between the electrodes, a 2µm gap electrode was used to carry out all these experiments.

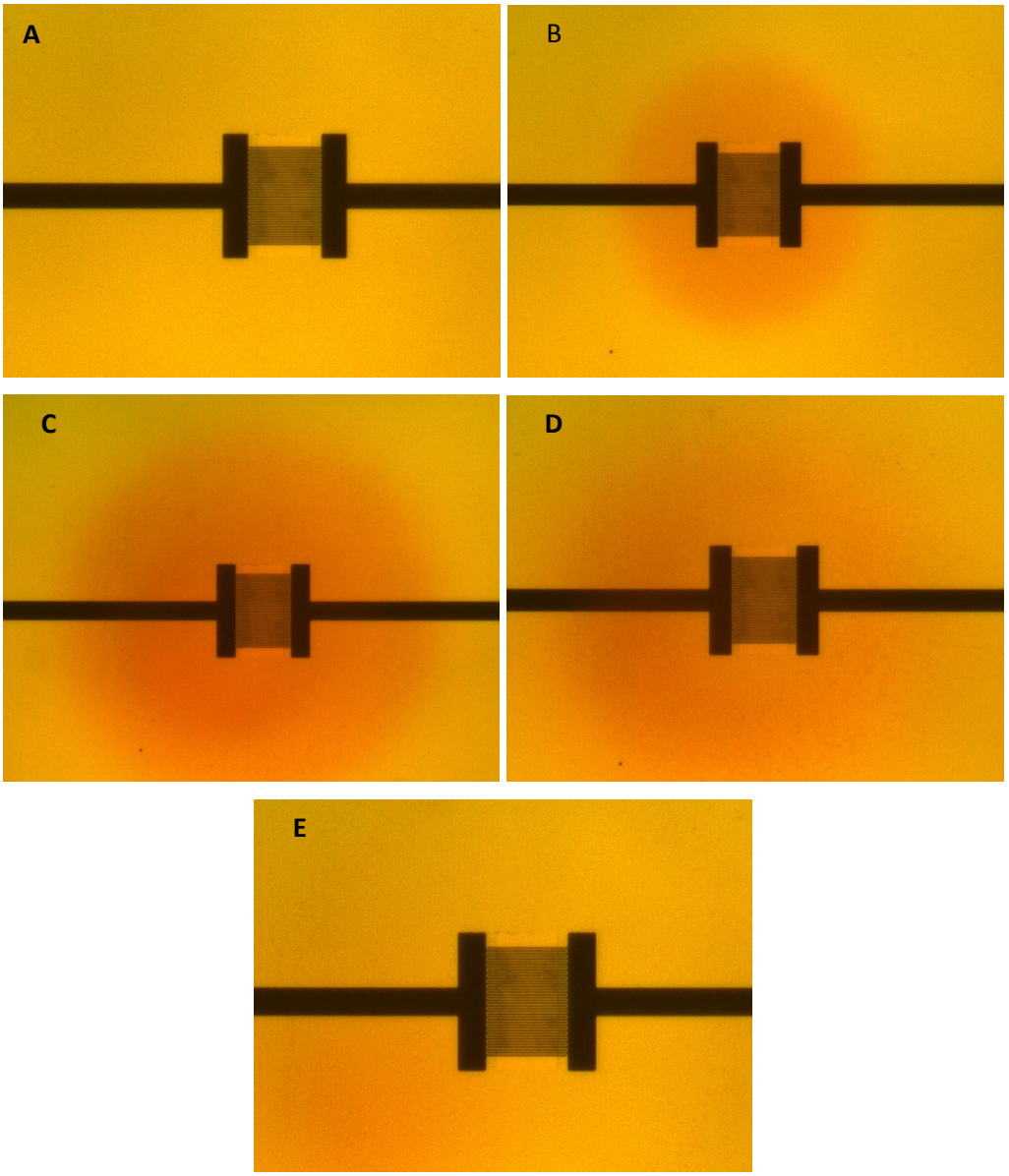

FIGURE 4.37 FRAMES OF THE VIDEO RECORD USING METHYL RED AS AN ELECTROLYTE. A) BEFORE OXYGEN EVOLUTION, B) AT THE BEGINNING OF OXYGEN EVOLUTION, C) AFTER 10 SEC OF OXYGEN EVOLUTION, D) AT THE BEGINNING OF HYDROGEN EVOLUTION, E) AFTER 10 SEC OF HYDROGEN EVOLUTION

As a proof of concept, we used the same setup of Figure 4.21 putting into the electrode a drop of methyl red. This is a particular chemical that changes color depending on the pH. In details, it has a yellowish color when the pH is higher than 6 while the color shifts toward red when the pH is more acidic than 5. We applied, constantly, a cathodic current for 10 sec and, suddenly, an anodic current for other 10 sec. Recording a video during the experiment, we were able to visualize the pH gradient close to the electrode. In Figure 4.37, five frames of the video are shown. Figure 4.37A shows the electrode when it is not polarized and a yellowish color is evident due to the neutral pH. When the protonator is polarized positively (applying a constant current of 500 nA) a reddish circle instantaneously appears (Figure 4.37B) that grows over time (Figure 4.37C). After 10 sec, a negative potential is applied (fixing the current at -200nA) and hydrogen starts to be produced, lowering the local pH. As visualized in Figure 4.37D, the reddish color starts to disappear until, after 10 seconds, the same coloration of Figure 4.37A is attained. This experiment shows that the application of a positive/negative potential really modifies the local pH of the electrode.

While the WSR occurs, H^+ and O_2 are simultaneously produced at the anode determining a local decrease of pH. To check this effect, we carried out different CVs in a blank solution, in the potential range from 0 to 1.2 V vs Ag/AgCl (scan rate 100mV/s) using the 'collector electrode' as a working electrode and simultaneously applying a constant potential to the protonator. Figure 4.38 shows the effect of the applied potential on the protonator electrode, on CVs recorded with the collector electrode.

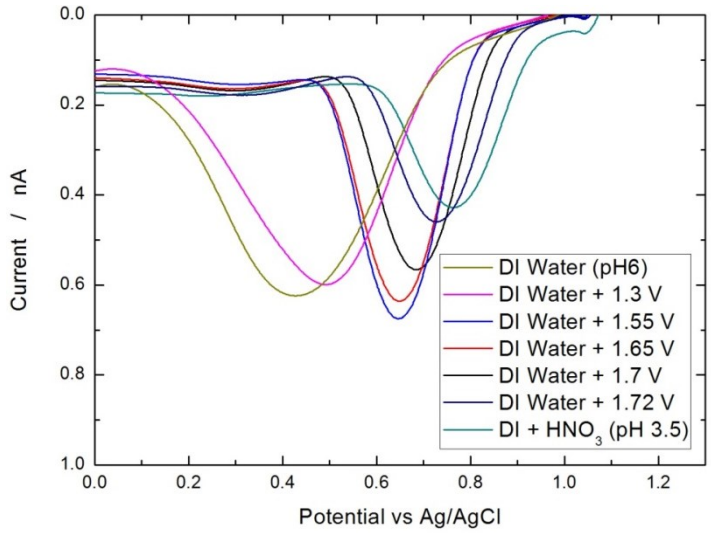

FIGURE 4.38 EFFECT OF APPLIED POTENTIAL ON THE PROTONATOR ELECTRODE

Without applying an external potential, the peak potential of the Au/AuO reaction, with a solution of pH 6 (DI water and NaCl), is 0.41V vs. Ag/AgCl while, after adjusting pH to 3.5, the peak position shifts to 0.72V vs. Ag/AgCl. When the applied potential to the protonator electrode is lower than 1.2V vs. Ag/AgCl the water splitting reaction doesn't happen and the peak potential doesn't move. Applying a potential higher than 1.3V vs. Ag/AgCl the Au/AuO peak potential starts to move towards more anodic potential and reaches 0.72V vs. Ag/AgCl when the applied potential is 1.74V.

Moving from this result, we carried out SWASVs experiments with different concentrations of copper, mercury and lead separately in a solution containing only NaCl 10mM in DI (pH 6) and applying to the protonator electrode a constant potential of 1.74V vs. Ag/AgCl. Figure 4.39A shows the SWASV of 50ppb of mercury in three different conditions: i) solution at pH 7 (black line), ii) solution at pH 3.5 (red line), and iii) solution at pH 7 with the protonator electrode polarized at +1.74V (blue line). According to Figure 4.39A, it can be concluded that the metals deposition/stripping doesn't occur without polarizing

the protonator, while using it the current peak appears, demonstrating again the modification of the pH. Anyway, polarizing the protonator, the peak is slightly lower, and slightly shifted with respect to the curve obtained with a chemical modified solution of pH 3.5. Figures 4.39 B, C show the effect of increasing concentration of mercury and a calibration line, applying 1.74 V vs Ag/AgCl on the protonator (pH of the solution 6).

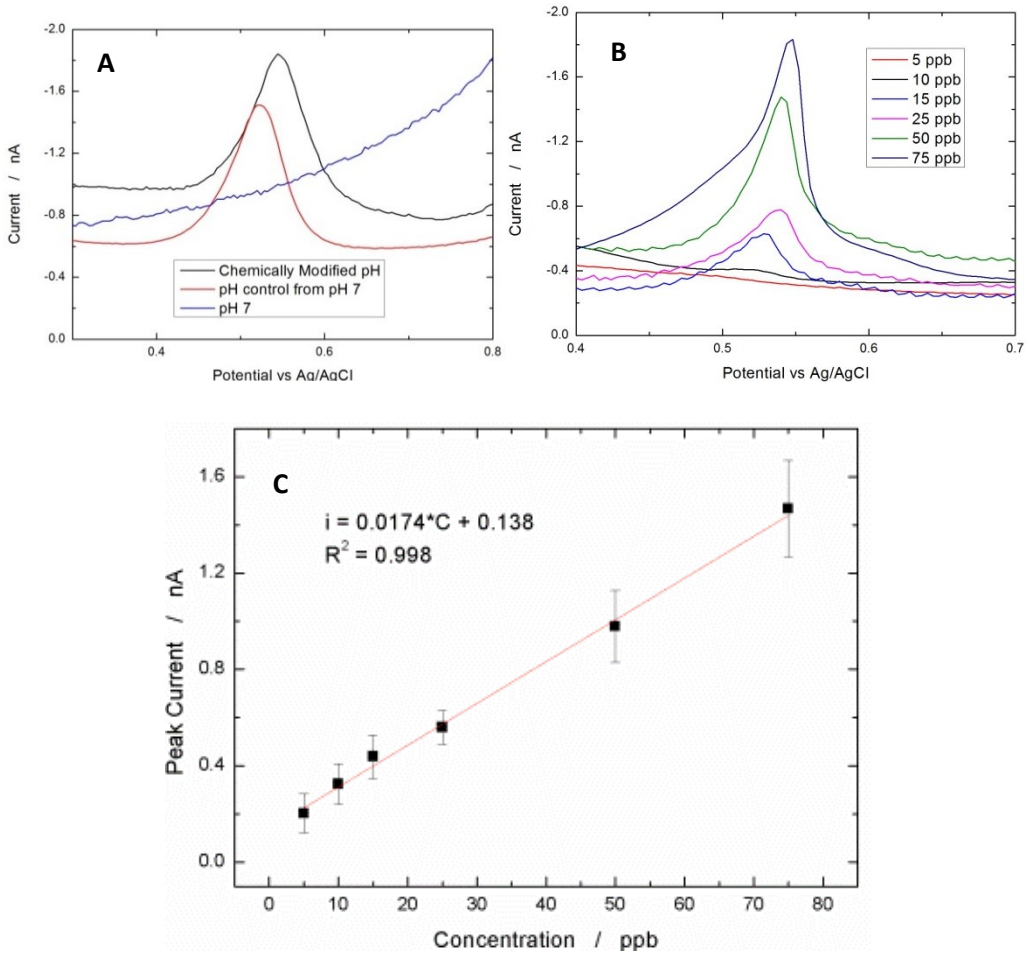

FIGURE 4.39 A) 50 PPB OF MERCURY AT DIFFERENT PH AND POLARIZATION OF THE PROTONATOR, B) INCREASING CONCENTRATION OF MERCURY WHEN 1.74 V WERE APPLIED TO THE PROTONATOR, AND C) CALIBRATION LINE

Similar results were obtained with copper (Figure 4.40A, B) and the same LOD for mercury and copper has been obtained while the copper sensitivity is 30% less.

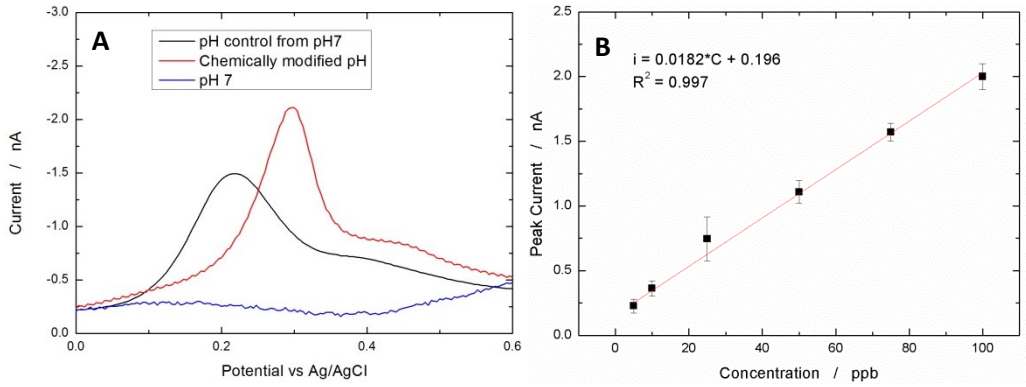

FIGURE 4.40 A) STRIPPING PEAKS OF 50PPB OF CU IN DI WATER (BLU LINE), IN DI WATER AND HNO3 (RED LINE), AND IN DI WATER WITH PH CONTROL (BLACK LINE); B) CALIBRATION LINE

During the WSR, molecular oxygen is produced determining the decreasing of the local pH. This secondary effect poses a problem for lead detection: the peak height of oxygen is more than twice, compared with the blank solution at pH3.5 (Figure 4.41). This enhancement drastically decreases the LOD for lead with the pH control. In order to see the lead peak in these condition the minimum concentration is 100ppb.

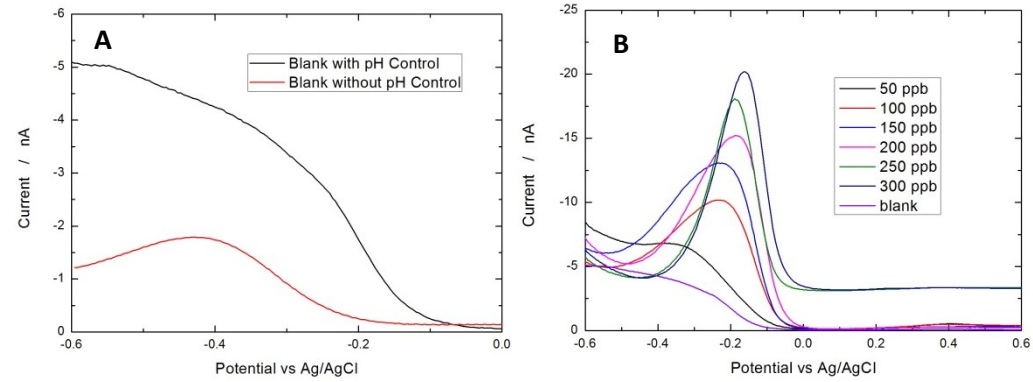

FIGURE 4.41 A) OXYGEN PEAK WITH AND WITHOUT PH CONTROL; B) LEAD DETECTION WITH PH CONTROL

Figure 4.42 shows the protonator electrode after 5 SWASVs experiments applying 1.74V.

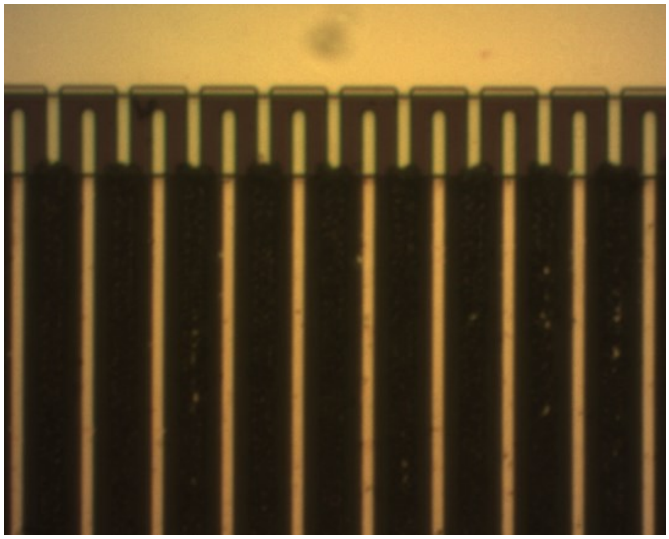

FIGURE 4.42 PROTONATOR ELECTRODE AFTER 10 MIN OF OXYGEN EVOLUTION

It is clearly visible that the electrode, after the experiments, is covered with a black film which suggests that this high applied potential definitively modifies the gold microband. Probably, this effect is due to the mechanism of oxygen evolution: this reaction involves the adsorption of OH^- and OOH on the surface of the electrode that have to be desorbed for producing O_2. The desorption step on gold electrode is not fast, therefore these species remain adsorbed on the electrode, creating the black film of Figure 4.42, as suggested by Diaz Moralez et al. [97]. They used polycrystalline gold to produce oxygen and found that different gold oxide/hydroxide are formed at 1.3 V vs. RHE. In order to overcome this problem, the gold was substituted with platinum that is a more stable material for oxygen evolution. Using this material as protonator, the applied potential necessary to reach a pH of 3.5 was about 0.2V less, as shown in Figure 4.43.

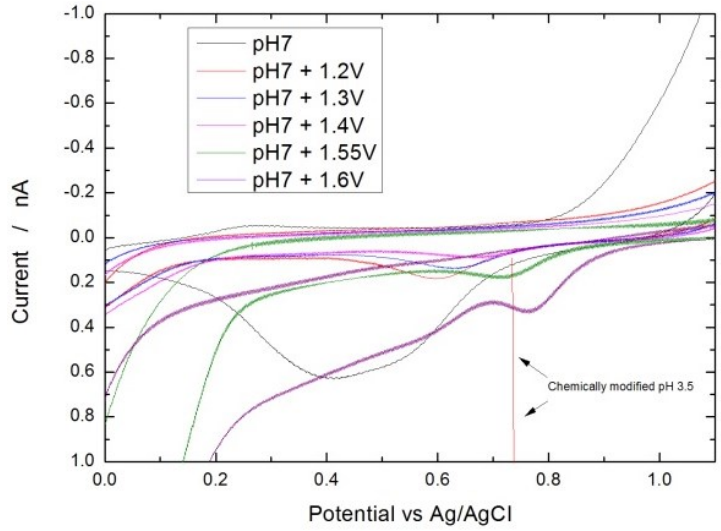

FIGURE 4.43 EFFECT OF APPLIED POTENTIAL ON THE PT PROTONATOR

The better performance of the Pt electrode was confirmed by repeating more SWASV experiments with the same electrode. Figure 4.44 shows the stripping peak of 50 ppb of copper, using a solution with pH 6, after 3, 12, and 30 min of oxygen evolution using Pt as a protonator electrode.

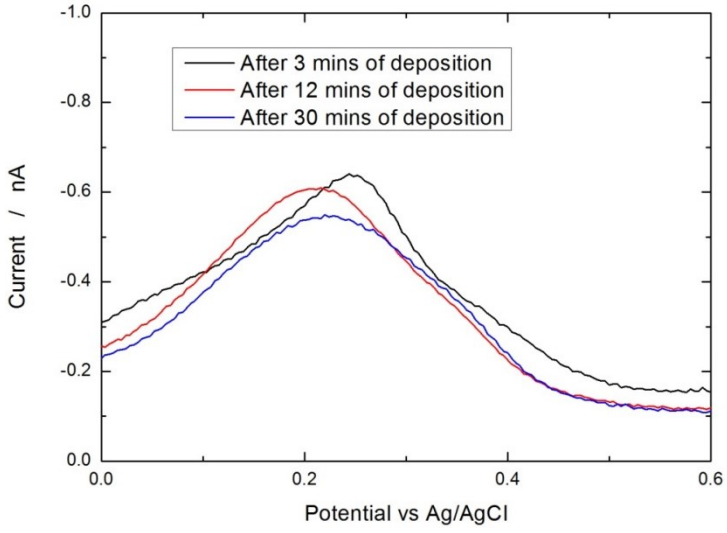

FIGURE 4.44 PEAK OF 50 PPB OF COPPER AT PH 6 USING PT AS A PROTONATOR ELECTRODE POLAERISED AT 1.55V FOR 3 (BLACK), 12 (RED) AND 30 (BLU) MINUTES

Using gold in place of platinum, the protonator electrode is completely covered by a black film after about 5 scans (≈ 10 min) and the SWASVs do not give any results (not shown). On the contrary, when Pt is used as a protonator electrode, the stripping peak is almost constant after 12 min and decrease of about 15% after 30 min (≈ 15 experiments), as shown in Figure 4.44. This result clearly demonstrates that Pt can be used as protonator achieving excellent results.

River Water Analysis

In order to evaluate the possibility to use this heavy metals sensor with real samples, three different river water samples (named A, B and C) were collected and the standard addition method was carried out. The river water was collected from Lee River, Cork, Ireland. 10mM sodium Chloride and 1mM nitric acid were added to the samples A and B while the C sample was used for detecting the heavy metals with the pH control, and adding only NaCl. The standard addition method have to be used when the matrix of a complex sample, like the river water, can change the analytical features of the sensor, including sensitivity and LOD. Every experiment was repeated at least three times and the results are showed in Table 4.13.

TABLE 4.13 MERCURY, LEAD AND COPPER CONTENT OF RIVER LEE WATER

Sample	Copper Found / ppb	Mercury Found / ppb	Lead Found / ppb
A	34.3 ppb	Lower than LOD (1ppb)	Lower than LOD (10ppb)
B	9.7 ppb	Lower than LOD (1ppb)	Lower than LOD (10ppb)
C	10.8 ppb	Lower than LOD (1ppb)	Lower than LOD (100ppb)

Mercury and lead were not found, because either absent or below the LOD, while a peak due to copper has been found at 0.22V vs. Ag/AgCl. After addition of different amount of lead and mercury, they were detected by the sensor under development, confirming its ability to detect these metals also in the river water (Figure 4.45A, B, C).

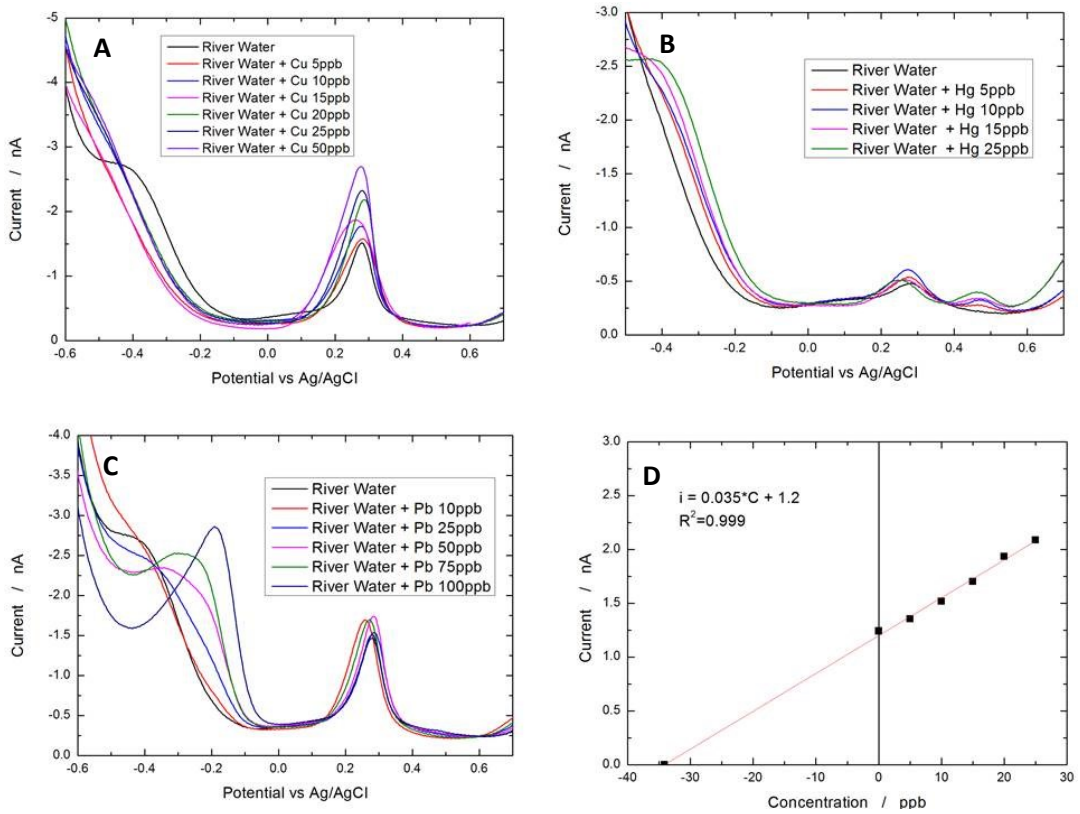

FIGURE 4.45 A) A RIVER WATER SAMPLE WITH INCREASING CONCENTRATION OF CU; B) B RIVER WATER SAMPLE WITH INCREASING CONCENTRATION OF HG; C) A RIVER WATER SAMPLE WITH INCREASING CONCENTRATION OF PB; D) CALIBRATION LINE FOR THE A RIVER WATER SAMPLE AND STANDARD ADDITION METHOD

The standard addition method is a type of quantitative analysis approach whereby the analyte is added directly to the analyzed sample. This method is used in situations where sample matrix can also contributes to the analytical

signal. Briefly, the sample has to be tested and then, different amount of analyte were added and tested. In this way, the calibration line will start from a point higher than 0, as shown in Figure 4.45D. The standard addition method says that the concentration of the sample is the intercept of this line with the X-Axes.

The standard addition method for copper with sample A is showed in Figure 4.45D, finding 34 ppb. The results show that the proposed method for copper, mercury and lead determination in river water is efficient and applicable. Furthermore, it is important to highlight that for each sample, the predicted copper concentration with the standard addition method (34ppb) is really close to the concentration obtained using the calibration line in DI+NaCl+HNO3 (43ppb). This result suggests that the matrix of the river water has slight influence on the performance of the sensor. As mentioned before, the river water sample C has been used to detect copper using the pH control procedure. The results are shown in Figure 4.46.

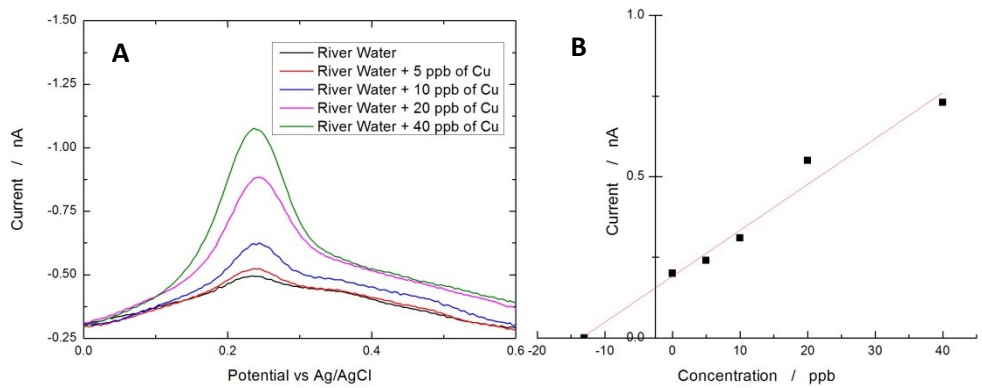

FIGURE 4.46 A) C RIVER WATER SAMPLE WITH INCREASING CONCENTRATION OF CU AT PH 6 WITH PH CONTROL; B) STANDARD ADDITION METHOD

Also in this case, the sensing electrode detected copper, finding a content of 13 ppb using the standard addition method.

4.3.3 Conclusions

A multi heavy metals sensing electroide has been successfully fabricated depositing an array of interdigitated gold microband on SiO_2 substrate. In particular, the gold microbands electrode was obtained through photolitography. The electrochemical measurements were carried out in DI water adding NaCl to increase the conductibility and nitric acid to control the pH. The LOD for all the tested metals was lower than the limit established by EPA, evidencing that this technique is applicable and powerful. When copper, lead and mercury are simultaneously present in the solution some interference is seen, especially for detecting lead. However, we found a good way to overcome this problem, making the analysis possible even in that case. Furthermore, an innovative method to control the pH close to the electrode was found. H^+ generation through water electrolysis under constant potential of the protonator electrode allowed local pH control at the surface of the collector electrode. The metal stripping response at a controlled was very similar to that when the pH was externally modified. With this technique, the sensor was able to work at a neutral pH, avoiding any sample pretreatment. We showed that the electrode is also able to detect these metals in a real matrix water such as river water, from Lee River in Cork, Ireland. This work demonstrates how electrochemical sensors can solve the problems of analytical techniques, like costs, portability and simplicity, opening new opportunities in the field of sensors for environmental analysis.

References

1 Järup L., Hazards of heavy metal contamination, Br. Med. Bull., 2003, 68, 167-182.

2 Metalli pesanti, impatto pesante Edizioni Ambiente, Cap 4, pag. 132

3 Commission of the European Communities, White paper on food safety, 2000

4 H.Wan, Q. Sun H. Li, F. Sun, N. Hu, P. Wang., Screen-Printed gold electrode with gold nanopartilcles modification for simultaneous electrochemical determination of lead and copper, Sensors and Actuators B:Chemical, 2005, 209, 336-342

[5] *Evaluation of the Joint FAO/WHO Expert Committee on Food Additivies (JECFA),* http://apps.who.int/food-additives-contaminants-jecfa-database/search.aspx?fcc=2

6 L. Severino, R. Russo, La contaminazione da metalli pesanti nei prodotti della pesca, University of Naples, 2009

*7 U. S. Environmental Protection Agency Office of Water, Lead and copper rule revision white paper,2009,*https://www.epa.gov/sites/production/files/201610/documents/508_lcr_revisions_white_paper_final_10.26.16.pdf*)*

8 N. Ratner, D. Mandler, Electrochemical Detection of Low Concentrations of Mercury in Water Using Gold Nanoparticles, Analytical Chemistry, 2015, 5148-5155

9 T.M. Sullivan, B. Bowerman, J. Adams, L. Milian, L. Lipfert, S. Subramaniam, R. Blake, Local impacts of mercury emissions from coal fired power plants, Brookhaven Science Associates, Air Quality V, 2005, https://www.bnl.gov/isd/documents/31077.pdf

10 Apple P., L. Na-Oy, Mercury-Free Gold Extraction Using Borax for Small-Scale Gold Miners, Journal of Environmental Protection, 2014, 5, 493-499

11 Shrivastava A.K., A review on copper pollution and its removal from water bodies by pollution control technologies, International Journal of Environment and Pollution, 2009, 29, 552-560

*12 National Primary Drinking Water Regulation, US-EPA,m*https://www.epa.gov/ground-water-and-drinking-water/national-primary-drinking-water-regulations

13 B. Patella, R. Inguanta, S. Piazza, C. Sunseri, A nanostructured sensor of hydrogen peroxide, Sensors and Actuators B, 2017, 245, 44-54

14 R. Ramachandran, S. Chen, G. Kumar, P. Gajendran, N. Devi, An Overview of Fabricating Nanostructured Electrode Materials for Biosensor Applications , Int. J. Electrochem. Sci., 2015, 10, 8607 – 8629

15 C. Zhang, Y. Zhou, L. Tang, G. Zeng, J. Zhang, B. Peng, X. Xie, C. Lai, B. Long, J. Zhu, Determination of Cd2+ and Pb2+ Based on Mesoporous Carbon Nitride/Self-Doped Polyaniline Nanofibers and Square Wave Anodic Stripping Voltammetry, Nanomaterials, 2016, 6, 1-11

16 S. Anandhakumar, J. Mathiyarasu, K. Phani, V. Vegnaraman, Simultaneous Determination of Cadmium and Lead Using PEDOT/PSS Modified Glassy Carbon Electrode, American Journal of Analytical Chemistry, 2011, 2, 470-474

17 Z. Zhang, K. Yu, D. Bai, Z. Zhu, Synthesis and Electrochemical Sensing Toward Heavy Metals of Bunch-like Bismuth Nanostructures, Nanoscale Res Lett. 2010; 5, 398–402.

18 M. Li, H. Gou, I. Al-Ogaidi, N. Wu, Nanostructured Sensors for Detection of Heavy Metals: A Review, ACS Sustainable Chem. Eng., 2013, 713–723

19 M.R. Saidur, A.R. Adbul Aziz, W. J. Basirun, Recent advances in DNA-based electrochemical biosensors for heavy metal ion detection: A review, Biosens Bioelectron., 2017, 90, 125-139

20 A. Q. Mugheri, T. Aneela, S. Sherazi, S. T. Hussain, A. M. Ishaque, W. Mangus, I. Z. Hussain, An Amperometric Indirect Determination of Heavy Metal Ions Through Inhibition of Glucose Oxidase Immobilized on Cobalt Oxide Nanostructures, Sensor Letters, 2016, 14, 1178-1186

21 T. Wang, W. Yue, Carbon Nanotubes Heavy Metal Detection with Stripping Voltammetry: A Review Paper, Electroanal., 2017, 29, 2178-2189

22 J. Chang, G. Zhou, E. R. Christensen, R. Heideman, J. Chen, Graphene-based sensors for detection of heavy metals in water: A review, Analytical and Bioanalytical Chemistry, 2014, 406, 3957- 3975
23 O.A. Farghaly, M.A. Ghadour, Square-wave stripping voltammetry for direct determination of eight heavy metals in soil and indoor-airborne particulate matter, Envirom. Res., 2005, 97, 229-235
24 N.W. Khun, E. Liu, Linear sweep anodic stripping voltammetry of heavy metals from nitrogen doped tetrahedral amorphous carbon thin films, Electrochim. Acta, 2009, 54, 2890-2898
25 P. Manisankar, C. Vedhi, G. Selvanathan, P. Arugugam, Differential pulse stripping voltammetric determination of heavy metals simultaneously using new polymer modified glassy carbon electrodes, Microchimica Acta, 2008, 163, 289–295
26 G. March, T. D. Nguyen, B. Piro, Modified Electrodes Used for Electrochemical Detection of Metal Ions in Environmental Analysis, Biosensors (Basel)., 2015, 5, 241–275.
27 G. Lee, C. Kim, M. Lee, C.K. Rhee, Simultaneous voltammetric determination of Zn, Cd and Pb at Bismuth Nanopowder Electrodes with Various Particle Size Distributions, Electroanalysis, 2010, 22, 530–535
28 M. M. Musameh, M. Hickey, I. Kyratzis, Carbon nanotubebased extraction and electrochemical detection of heavy metals, Res. Chem. Intermed., 2011, 37, 675−689
29 G. Liu, Y. Lin, Y. Tu, Z. Ren, Ultrasensitive voltammetric detection of trace heavy metal ions using carbon nanotube nanoelectrode array, Analyst, 2005, 130, 1098−1101
30 L. Wang, X. Wang, G. Shi, C. Peng, Y. Ding, Thiacalixarene covalently functionalized multiwalled carbon nanotubes as chemically modified electrode material for detection of ultratrace Pb2+ ions, Anal. Chem., 2012, 84, 10560−10567
31 X. Dai, R. G. Compton, Gold nanoparticle modified electrodes show a reduced interference by Cu(II) in the detection of As(III) using anodic stripping voltammetry. Electroanalysis 2005, 17, 1325− 1330
32 O. Abollino, A. Giacomino, M. Malandrino, G, Piscionieri, E. Mentasti, Determination of mercury by anodic stripping voltammetry with a gold nanoparticle-modified glassy carbon electrode, Electroanalysis, 2008, 20, 75−83
33 V. Sudha, M. V. Sangaranarayanan, Underpotential Deposition of Metals: Structural and Thermodynamic Considerations, Journ. Phy. Chem. B., 2002, 106, 2699-2707
34 O. A. Oviedo, P. Velez, V.A. Macagno, E. P. M. Leiva, Underpotential deposition: From planar surfaces to nanoparticles, Surf. Science, 2015, 631, 22-34
35 X. Zeng, S. Bruckenstein, Underpotential Deposition and Adsorption of Lead on Gold Polycrystalline Electrodes: I. XPS and TOF-SIMS Investigations in 0.1 M NaCl Electrolytes, Journ. Electrochem. Soc., 1999, 146, 2549-2554
36 Underpotential Deposition and Adsorption of Lead on Gold Polycrystalline Electrodes: II. EQCM Investigation in Acidic 0.1 M NaClO4 and 0.1 M NaCl Electrolytes, Journ. Electrochem. Soc., 1999, 146, 2549-2554
37 E. Herrero, H. D. Abruna, Underpotential Deposition of Mercury on Au(111): Electrochemical Studies and Comparison with Structural Investigations, Langmuir, 1997, 13, 4446-4453
38 T. Hachiya, H. Honbo, K. Itaya, Detailed underpotential deposition of copper on gold(III) in aqueous solutions, Journ. Electroanal. Chem. Interf. Electrochem., 1991, 315, 275-291
39 L. Guo, G. Hu, L. Wenpo, S. Zhang, Underpotential Deposition of Zinc on Au Electrode, Acta agronomico sinica, 2013, 214-219

40 Rapid on-site/in-situ detection of heavy metal ions in environmental water using a structure-switching DNA optical biosensor, Sci. Rep., 2013, 3, 2308-2314
41 X.B. Zhang, R.M. Kong, Y. Lu, Metal Ion Sensors Based on DNAzymes and Related DNA Molecules, Annu. Rev. Anal. Chem., 2011, 4, 105-128
42 J. Zhuang, L. Fu, D. Tang, M. Xu, G. Chen, H. Yang, Target-induced structureswitching DNA hairpins for sensitive electrochemical monitoring of mercury (II), Biosens. Bioelectron., 2013, 39, 315–319
43 J. Wu, L. Li, B. Shen, G. Cheng, P. He, Y. Fang, Polythymine oligonucleotidemodified gold electrode for voltammetric determination of mercury(II) in aqueous solution, Electroanalysis, 2010, 22, 479–482.
44 I. Streeter, N. Fietkau, J. del Campo, R. Mas, F. X. Munoz, G. R. Compton, Voltammetry at Regular Microband Electrode Arrays: Theory and Experiment, J. Phys. Chem. C, 2007, 111, 12058-12066
45 H. X. Zhao, W. Cai, D. Ha, H. Wan, P. Wang, The study on novel microelectrode array chips for the detection of heavy metals in water pollution, Journal of Innovative Optical Health Sciences, 2012, 5, 1150002-1150007
46 O. Zaouak, L. Authier, C. Cugnet, A. Castetbon, M. P. Gautier, Bismhut-coated Screen Printed Microband electrodes for On-Field Labile Cadmium Detection, Electroanalysis, 2009, 21, 689-695
47 G.R. Patzke, Y. Zhou, R. Kontic, F. Conrad, Oxide nanomaterials: synthetic developments, mechanistic studies, and technological innovations., Angew. Chem. Int. Ed., 2011, 50, 826.
48 N. Pinna, M. Niederberger, Surfactant-free nonaqueous synthesis of metal oxide nanostructures, Angew. Chem. Int., 2008, 47, 5292-5304
49 X. Y. Yu, Z. G. Liu, X. J. Huan, Nanostructured metal oxides/hydroxides-based electrochemical sensor for monitoring environmental micropollutants, Trends Envirom. Anal. Chem., 2014, 3, 28-35
50 Z. Wu, L. Jiang, H. Chen, C. Xu, X. Wang, Synthesis of folding flake-like CuO sub-microstructure and its application on mercury (II) sensor, Journ. Mat. Science: Material Electron., 2012, 23, 858-864
51 Y. Wang, J. Zhu, X. Yang , L. Lu, X. Wang, Preparation of NiO Nanoparticles and Their Catalytic Activity in the Thermal Decomposition of Ammonium Perchlorate, Thermochim Acta, 2005, 437, 106–109
52 C. Z. Yuan, X.G. Zhang, L.H. Su, B. Gao, L.F. Shen, Facile synthesis and self-assembly of hierarchical porous NiO nano/micro spherical superstructures for high performance supercapacitors, Journ. Mater. Chem. 2009, 19, 5772–5777
53 M. A. Armas, R. M. Hormigos, A. Cantalapiedra, M. J. Gismera, M. T. Sevilla, J. R. Procopio, Multiparametric optimization of a new high-sensitive and disposable mercury (II) electrochemical sensor, Anal. Chim. Acta, 2016, 904, 76-82
54 Z. Wu, L. Jiang, Y. Zhu, C. Xu, Y. Ye, X. Wang, Synthesis of mesoporous NiO nanosheet and its application on mercury (II) sensor, Journ. Solid State Electrochem., 2012, 16, 3171-3177
55 T. L. Read, E. Bitziou, B. Maxim, J. Macpherson, V. Macpherson , In Situ Control of Local pH Using a Boron Doped Diamond Ring Disk Electrode: Optimizing Heavy Metal (Mercury) Detection, Anal. Chem., 2014, 86, 367–371
56 S. Sang, D. Li, H. Zhang, Y. Sun, A. Jian, Q. Zhang, W. Zhang, Facile synthesis of AgNPs on reduced graphene oxide for highly sensitive simultaneous detection of heavy metal ions, RSC Advances, 2017, 35
57 S. H. Choi, J. P. Choi, Gold Nanoparticle-Based Electrochemical Sensor for the Detection of Toxic Metal Ions in Water, Joun. Research Environm. Earth Science, 2017, 3, 47-54
*58*http://www.steroglass.it/doc_area_download/ita/labware/ANALIZZATORE_METALLI_PESANTI_IONIX.pdf

59 https://www.metrohm.com/en/applications/WP-021EN
60 B. Patella, C. Sunseri, R. Inguanta, Nanostructured Based Electrochemical Sensors, Journ. Nanoscien. Nanotech., 2018, 18, 1-12
61 P. Mohanty, C. Rath, P. Mallick,R. Biswal,N. C. Mishra, UV–visible studies of nickel oxide thin film grown by thermal oxidation of nickel, Physica B, 2010, 405, 2711-2714
62 L. D. I. S. Valladares, A. Ionescu, S. Holmes,C.H.W. Barnes, Characterization of Ni thin films following thermal oxidation in air, J. Vac. Sci. Technol. B, 2014, 32, 051808_1-0518081_8.
63 K. Joudkazis, J. Joudkazyte, R. Vilkauskaite, J. Jasulaitiene, Nickel surface anodic oxidation and electrocatalysis of oxygen evolution, Journ. Solid State Electrochem., 2008, 12, 1469-1479
64 C. K. D'Alkaine, M.A. Santanna, Passivating films on nickel in alkaline solutions II. Ni(II) anodic film growth: quantitative treatment and the influence of the OH- concentration, Journ. Electroanal. Chem., 1998, 457, 13-21

65 B. Zhang, J. Wu, X. Li, H. Liu, B. Yadiant, R. V. Ramanujant, K. Zhou, R. Wu, S. Hao, Y. Hiang, Passivation of Nickel Nanoneedles in Aqueous Solutions, Journ. Phy. Chem. C, 2014, 118, 9073-9077
66 C. K. D'Alkaine, M.A. Santanna, The passivating films on nickel in alkaline solutions I. General aspects of the Ni (II) region, Journ. Electroanal. Chem., 1998, 457, 5-12
67 A. Seghiouer, J. Chevalet, A. Barhoun, F. Lantelme, Electrochemical oxidation of nickel in alkaline solutions: a voltammetric study and modelling, Journ. Electroanal. Chem., 1998, 442, 113-123
68 Pourbaix M., Atlas of Electrochemical Equilibria in Aqueous Solutions, Pergamon Press, Oxford, 1966
69 A. Afkhami, S. Sayari, F. Soltani-Felehgari, T. Madrakian, Ni0.5Zn0.5Fe2O4 nanocomposite modified carbon paste electrode for highly sensitive and selective simultaneous electrochemical determination of trace amounts of mercury (II) and cadmium (II), Journ. Iranian Chem. Soc., 2015, 12, 257-265.
70 A. M. Nolan, S. P. Kounaves, Microfabricated Array of Iridium Microdisks as a Substrate for Direct Determination of Cu2+ or Hg2+ Using Square-Wave Anodic Stripping Voltammetry, Anal. Chem., 1999, 71, 3567-3573
71 V. Meucci, S. Laschi, M. Minunni, C. Pretti, L. Intorre, G. Soldani, M. Mascini, An optimized digestion method coupled to electrochemical sensor for the determination of Cd, Cu, Pb and Hg in fish by square wave anodic stripping voltammetry, Talanta, 2009, 77, 1143-1148
72 S. H. Wu, Z. Y. Zheng, J. Fang- Zhang, Z. Song, L. Fang, J. J. Sun, Sub-ppt Level Detection of Mercury(II) Based on Anodic Stripping Voltammetry with Prestripping Step at an In Situ Formed Bismuth Film Modified Glassy Carbon Electrode, Electroanal., 2015, 27, 1610-1615
73 S. Yao, L. Zhi, J. Guo, S. Yan, M. Zhang, Hierarchical Porous NiCo2O4 array grown on Ni foam for the Simultaneous Electrochemical Detection of Copper(II) and Mercury(II), Int. J. Electrochem. Sci, 2018, 13, 542-550
74 K. Dawson,A. Wahl, S. Barry, C. Barrett, N. Sassiat, A. J. Quinn, A. O'Riordan, Fully integrated on-chip nano-electrochemical devices for electroanalytical applications, Electrochimica Acta, 2014, 115, 239-246
75 X. We, C. Wang, P. Dou, J. Zheng, Z. Cao, X. Xu, Synthesis of NiCo2O4 nanoneedle@polypirrole arrays supported on 3D graphene electrode for high-performance detection of trace Pb2+, J. Mater. Sci, 2017, 52, 3893-3905

76 M. Eduardo, J. J. Pedrotti, L. Angnes, Square Wave Quantification of lead in rainwater with disposable gold electrode without removal of dissolved oxygen, Electroanal, 2003, 15, 1871-1877
77 S. A. Trammel, D. Zabetakis, M. Moore, J. Verbarg, D. A. Stenger, Square Wave Voltammetry of TNT at Gold Electrodes Modified with Self-Assembled Monolayers Containing Aromatic Structures, Plos One, 2014, 9, 1-12
78 D. Zhang, Y. Fang, Z. Miao, M. Ma, Q. Chen, Electrochemical determination of dissolved oxygen based on three dimensional electrosynthesis of silver nanodendrites electrode, Journal of Applied Electrochemistry, 2014, 44, 419–425
79 O. Berkh, H. Ragones, D. Schreiber, L. Burstein, Y. Shachman-Diamand, Surface-modified reusable gold electrode for detection of dissolved oxygen, Journal of Applied Electrochemistry, 2012, 42, 491–499
80 G. Martinez-Paredes, M. B. Gonzalez-Garcia, A. Costa-Garcia, In situ electrochemical generation of gold nanostructured screen-printed carbon electrodes. Application to the detection of lead underpotential deposition, Electrochimica Acta, 2009, 54, 4801-4808
81 E. Kirowa-Eisner, Y. Bonfil, D. Tzur, E. Gileadi,Thermodynamics and kinetics of upd of lead on plycristallyne silver and gold, Journal of Electroanalytical Chemistry, 2003, 552, 171-183
82 A. Hamelin, J. Lipkowski, Underpotential deposition of lead on gold single crystal faces: Part II. General discussion, J.Electroanal. Chem, 1984, 171, 317
83 M.F. Noh, F. Tothill, Development and characterization of disposable gold electrodes, and their use for lead(II) analysis, Anal Bioanal Chem, 2006, 386, 2095-2106
84 A. Uhlig, U. Schnakemberg, R. Hintsche, Highly Sensitive Heavy Metal Analysis on Platinum- and Gold-Ultramicroelectrode Arrays, Electroanal., 1997, 9, 125-129
85 O. Ordeig, C.E. Banks, J. del Campo, F. X.Munoz, R. G. Compton, Trace Detection of Mercury(II) Using Gold Ultra - Microelectrode Arrays, Electroanal., 2006, 18, 573-578
86 Y. Bonfil, M. Brand, E. Kirowa-Eisner, Determination of sub-mg l -1 concentrations of copper by anodic stripping voltammetry at the gold electrode, Anal. Chim. Acta, 1999, 387, 85-95
87 L. M. Niu, H. Q. Luo, N.B. Li, L. Song,Electrochemical detection of copper(II) at a gold electrode modified with a self-assembled monolayer of penicillamine, Journ. Anal. Chem., 2007, 62, 470-474
88 Y. Dai, C.C. Liu, A Simple, W.R. Seitz, Cost-Effective Sensor for Detecting Lead Ions in Water Using Under-Potential Deposited Bismuth Sub-Layer with Differential Pulse Voltammetry (DPV), Sensors (basel), 2017, 17, 950
89 G. Martinez-Paredes, M. B. Gonzalez-Garcia, A. Costa-Garcia, Lead Sensor Using Gold Nanostructured Screen-Printed Carbon Electrodes as Transducers, Electroanal., 2009, 21, 925-930
90 C. Agra-Gutierrez, J. L. Hardcastle, J. C. Ball, R. G. Compton, Anodic stripping voltammetry of copper at insonated glassy carbon-based electrodes: application to the determination of copper in beer, Analyst, 1999, 124, 1053-1057
91 S. Sayen, C. Gerardin, L. Rodehuser, A. Walcarius, Electrochemical Detection of Copper(II) at an Electrode Modified by a Carnosine–Silica Hybrid Material, Electroanal., 2003, 15, 442-430
92 S. Goubert-Renaudin, M. Moreau, C. Despas, M. Meyer, F. Denant, B Lebeau, A. WAlcarius, Voltammetric Detection of Lead(II) Using Amide-CyclamFunctionalized Silica-Modified Carbon Paste Electrodes, Electroanal., 2009, 21, 1731-1742
93 O. El Tall, N. Jaffrezic-Renault, M. Sigaud, O. Vittori, Anodic Stripping Voltammetry of Heavy Metals at Nanocrystalline Boron-Doped Diamond Electrode, Electroanal., 2007, 19, 1152-1159

94 C. Babyak, R. B. Smart, Electrochemical Detection of Trace Concentrations of Cadmium and Lead with a Boron- Doped Diamond Electrode: Effect of KCl and KNO3 Electrolytes, Interferences and Measurement in River Water, Electroanal.,2004, 16, 175-182

95 D. Dragoe, N. Spataru, R. Kawasaki, A. Manivannan, T. Spataru, D. A. Tryk, A. Fujishima, Detection of trace levels of Pb2+ in tap water at boron-doped diamond electrodes with anodic stripping voltammetry, Electrochim. Acta, 2006, 51, 2437-2441

96 A. Wahl, K. Dawson, J. MacHale, S. Barry, A. J. Quinn, A. O' Riordan, Gold nanowire electrodes in array: simulation study and experiments, Faraday Discussion, 2013, 164, 377

97 O. Diaz-Moralez, F. Calle-Vallejo, C. De Munck, M.T.M. Koper, Electrochemical water splitting by gold: Evidence for an oxide decomposition mechanism, Chem. Sci., 2013, 4, 2334-2343

5. *Sensors for proteins: proof of concept and application towards cancer biomarkers*

Abstract

In this chapter, a paper based electrode for proteins electrochemical detection has been developed. Proteins are important biological compounds of human body and can act as biomarkers for many different goals. Indeed, proteins concentration can be used to monitor i) the effect of a drug, ii) a pathogenic process or iii) the healthy state of individuals. I focused on the detection of PTHLH: it is a hormone (protein) than can be used as a biomarker for cancer, especially for breast cancer. Therefore, the possibility to detect PTHLH in an easy, fast, and portable way is of big relevance. Indeed, early diagnosis of cancer is fundamental for successfully therapy against cancer. Nowadays, this analysis is carried out using ELISA assay. This analytical technique is good in terms of sensitivity and selectivity but, it must be carried out in a laboratory. Therefore, patients' liquors (urine, or blood) have to be collected, sent to the lab, consequently, several days pass prior to having the result. The mean idea of the research was to develop a paper based electrode that was user friendly and that can be used at home in a fast and easy way (like the pregnancy test). This is a very important goal because it will increase the possibility to defeat diseases such as a cancer and, at the same time, could decrease the health care costs, avoiding to move the patient from the hospital to home and vice-versa.

5.1 Introduction

Nucleic acids, antigens, DNA fragments are important compounds of the human body because they contain genetic information and can provide useful indications about the health state of the individuals. For this reason, researchers all over the world worked, and are still working, to understand and unravelling their secrets. Proteins are the molecular expression of the genetic information and so are the keystone of our biological function. Besides, proteins can be used as *biomarkers* of many diseases: a biomarker is a biological compound that can be measured in different human samples (urine, blood, sweat) to evaluate normal biological processes or pathogenic processes as well as the pharmacological response to some drugs. For instance, *MUC-1* and *Carcinoembryonic antigen* can be used as biomarkers for breast cancer [1], *β-chain of human HP* (haptoglobin) is a protein biomarker for lung cancer [2] and *cathepsin D* for insulin resistance (a precursor of type 2 diabetes) [3]. In the light of these findings, it is evident that the detection of biomarkers can improve the living condition, preventing the spreading of diseases, infections and pathologies. This detection has to be cheap, rapid, sensitive, selective, portable and easy to use. *Enzyme Linked Immunosorbent Assay* (ELISA) has been discovered more than 30 year ago and, since then, has become the most used technique for these purposes [4]. The reasons of this success are different. First of all, ELISA works by trapping the antigen into a sandwich with the corresponding antibodies (primary and secondary): there are almost infinite antibodies that can tag almost any antigens. Secondary, this technique is highly performing in terms of sensitivity and LOD and can be improved by using an enzymatic amplification step. In the last decades, many different ELISA plates have been developed, obtaining the possibility to simultaneously carry out 96 experiments. For these reasons, ELISA is currently used to detect many diseases

such as *HIV* [5] or *West Nile Virus* [6]. In recent years, many efforts have been spent to improve the efficiency of ELISA assay because it is based on an optical approach therefore, it suffers of the different drawbacks related with i) the light sources (bulky and power-intense), ii) the detectors, iii) and the interference from coloured samples that can lead to false positive results. Furthermore, sensitivity of the optical techniques is regulated by the Lambert-Beer law, therefore, a big enough volume of the sample is required [7]. In this scenario, the development of new kinds of analytical devices, able to overcome these issues, is of great value. Radioimmunoassay [8], mass spectrometry assay [9] and electrochemical biosensors [10] have been studied as alternatives for ELISA assay. Among these techniques, electrochemical biosensors have superior advantages over the other ones, because can provide rapid, simple, low-cost, and sometimes on-field detection. Furthermore, the sensing materials are grown on the surface of different either unmodified or modified electrodes that are also suitable for extensive fabrication. As a proof, self-testing glucose strips, based on screen printed enzyme electrodes, fabricated in a pocket size, dominates the market of glucose sensors [11].

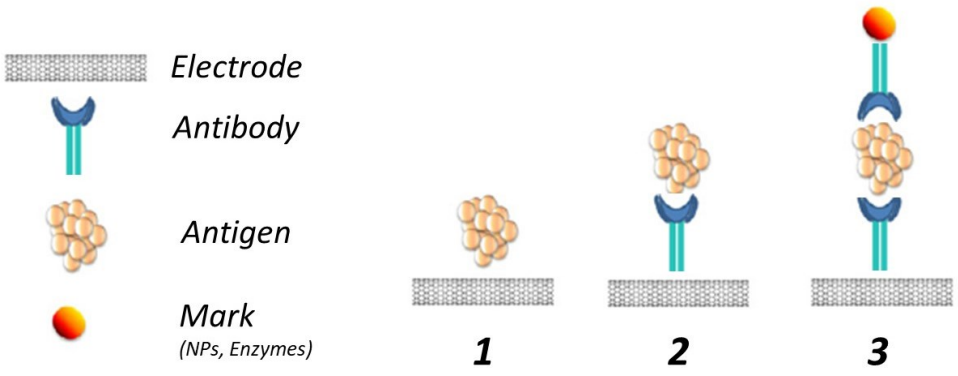

FIGURE 5.1 DIFFERENT STRATEGIES FOR ELECTROCHEMICAL DETECTION OF PROTEINS, DNA OR NUCLEIC ACIDS

Talking about immunosensors for the protein detection, there are 3 different ways, showed in Figure 5.1, to use electrochemistry for this purpose:

1. direct detection of the protein, if it is electroactive;
2. trapping the antigen in the surface of the electrode using just a primary antibody (*half-sandwich*);
3. trapping the antigen using a primary antibody and a secondary marked antibody (*sandwich configuration*).

Each technique has advantages and drawbacks. In the configuration 1 (Figure 5.1), the protocol for the detection is simple and easy but the selectivity is poor because there is not any biological recognition. Furthermore, not all the proteins are electro active. An example can be found in the work by Vestergaard et al. [12], where they showed for the first time the possibility to directly detect Amyloid beta (biomarker for Alzheimer disease) using a Glassy Carbon Electrode. Moving to configuration 2, the protocol is longer and a good way to immobilize the antibodies into the surface with a reproducible and stable protocol has to be adopted. On the other hand, the selectivity is highly improved because the antibodies bio-recognize just the target antigen. In this case, the main electrochemical technique is the electrochemical impedance spectroscopy, because it can detect the bond between antibodies and antigens by the increase in resistance displayed by the Nyquist Plot [13]. The last configuration concerns a *sandwich configuration* where the secondary antibody is marked with some marks, such as NPs [14-15] or enzymes [16-17]. In this case, there is an indirect detection of the antigen. Indeed, the mark is electrochemically detected using different techniques: NPs can be used to catalyze the hydrogen evolution reaction or HRP enzyme can be used to detect hydrogen peroxide. The point is that the mark concentration is related to the antigen concentration: the marked antibody will link the primary antibody (and so the electrode) only if the target antigen is present. The higher is the antigen concentration, the higher will be the

amount of marks stuck in the electrode and so it is possible to use this signal to quantify the antigen. This procedure allows to reach lower LOD, especially when nano-sized materials are used as sensing electrode, with extremely high selectivity, but the protocol starts to be laborious and an accurate optimization of the different incubation steps is mandatory. Almost all the ELISA kits work with the configuration 3 of Figure 5.1. When used with electrochemical techniques, all these configurations work with cheap, small and low-power consumption devices. Several investigations in this field used Indium Tin Oxide (ITO) [18], Glassy Carbon Electrode (GCE) [19], metals [20], and metal oxides [21] to develop different electrochemical sensors, for both clinical and environmental applications.

In this context, it is very important to find a good electrode material because it determines significantly the LOD. In the last decades, *graphene* attracted gradually more attention. This is a two-dimensional material composed of single sheet of sp2 hybridized carbon linked with hydrogen atoms [22]. This structure yields to high surface area, high aspect ratio, a mechanical stability comparable to the diamond, high flexibility similar to the plastics, and excellent electrical and thermal properties. For these reasons, researchers all over the world are working with graphene for several applications such as energy storage [23], sensors and biosensors [24-25], transistors [26], as absorbent material [27]. In the clinical field, graphene-based electrodes have been used for sensing proteins [28], DNA [29], neurotransmitters [30], and bacteria [31]. In fact, the high electron transfer rates, the high peak current response, the porosity and the flexibility are key features for electrochemical detection of biomolecules.

There are different methods to produce graphene electrodes such as the exfoliation of highly ordered pyrolytic graphite [22], the epitaxial growth [32], and chemical vapor deposition [33-34]. These techniques produce uniform, homogeneous and reproducible graphene, but they have different disadvantages such as cost, use of highly toxic and/or dangerous chemicals, and are

incompatible with a mass production. *Graphene Oxide* (GO) is a cheap and water soluble material and, nowadays, the most common way to obtain graphene starts from a GO solution to subsequently reduce it to obtain graphene. GO can be reduced by annealing graphene at high temperature [35], or through a chemical reduction, using alcohols [36], dimethylhydizine [37], hydrazine [38], or ascorbic acid [39] for obtaining the *Chemically Reduced Graphene Oxide* (CRGO). Electrochemistry can be used as well to reduce GO [40], but the reduction grade is often not high enough. In this context, a new and innovative way to reduce GO is the use of laser light, obtaining the *Laser Scribed Graphene Oxide* (LSGO). This technique is based on heating up a GO substrate in a very precise and localized area which breaks the C=O bond producing graphene [41-42]. Furthermore, LSGO has a highly porous surface that increases both surface area and the conductivity of the sheet, making it very suitable for electrochemical applications. This porosity is very important for immunoassay sensors because it creates many spots where the primary antibodies can attach. Additionally, it is possible to program the laser to scribe the surface with a predefined shape avoiding the use of patterned mask, so that the process is cost-effective, scalable and waste-free. Due to these advantages, this technology could fill the gap that divides the labs-research and the market of graphene-based electrodes. At the best of my knowledge, this technology has been studied and developed in the last years basically using plastics or ITO as substrates to build sensors and capacitors [43-44-45-46]. There are no works employing paper as a substrate to grow LSGO electrodes.

Paper is one of the most used and common material: it is made of randomly interconnected cellulose fibers, depending on the kind of paper. Paper based electrodes are highly interesting because they are environmentally friendly, cheap, abundant, recyclable, flexible, wearable, and portable [47]. Furthermore, the adhesion of the active material to a porous substrate, like paper, is much higher compared with plastics, GCE or ITO, increasing the electrode shelf-life.

Especially when a full sandwich immunoassay has to be grown, the electrode reproducibility is very important because all the incubation steps are highly affected by many parameters and it is important to maintain always the same conditions in order to have a good reproducibility. In this scenario, Screen Printing is a new and promising technique to produce electrodes with high reproducibility, low cost and speed of mass production [48-49]. Furthermore, these electrodes have a geometric area in the order of mm^2, which allows to reduce the sample volume to less than 10 microliters. Screen printing is a layer-by-layer technique where different inks are deposited upon a solid substrate (polycarbon, polymide, PEEK, paper, ceramic). Typically, SPEs (Screen Printing Electrodes) consist of a three electrodes integrated system (Counter, Working and Reference Electrodes) that make it smaller and easier to use [50]. There are different works where un-modified SPEs are used as electrochemical sensors [51-52] but generally SPEs are modified with different compounds to increase the sensitivity and selectivity. Jarocka et al. [53] developed an immunosensor to detect influenza A virus H5N1 in hens serum using a SPCE and they obtained a 4 order of magnitude LOD lower than the ELISA one. In a similar study, Parkash et al. [54] developed an immunosensor for Dengue NS1 Antigen detection using a SPCE as a substrate, with a linear response between 0.5 and 2 μg/ml.

In Table 5.1 some examples of electrochemical immunoassay for the detection of different proteins and the comparison with a commercial ELISA kit are shown.

TABLE 5.1 EXAMPLES OF ELECTROCHEMICAL IMMUNOASSAY AND COMPARISON WITH ELISA KIT

Electrode	*Protein*	*LOD*	*LOD ELISA*	*Ref*
SPCE – Pt NPs	*human chorionic gonadotropin hormone*	*0.1 ng/ml*	*0.25 ng/ml [55]*	*[14]*
PANI-AuNP-PNT	*prostate specific antigen*	*0.68 ng/ml*	*0.98 ng/ml [56]*	*[57]*
Gold electrode	*β-amyloid*	*22 ng/ml*	*0.1 ng/ml [58]*	*[59]*
SPCE-CdS	*Human IgG*	*10 pg/ml*	*0.03 pg/ml [60]*	*[61]*
Gold CDs	*prostate specific antigen*	*6 pg/ml*	*0.98 pg/ml*	*[62]*
Gold SAMs	*aflatoxin B1*	*10 pg/ml*	*0.65 pg/ml[63]*	*[64]*
SPCE-AP	*atrazine*	*1.47 µg/ml*	*1 ng/ml[65]*	*[66]*
Pt disk - NADH oxidase	*thyrotropin*	*0.2 µUI/ml*	*0.2 µUI/ml [67]*	*[68]*

From this table, it is clear that electrochemical sensors based on immunoassay are able to reach LOD really close to the ELISA, sometimes even lower, but overcoming all the limits of this technique. It is important to highlight that many ELISA Kits can be found in the market, with different LOD. Here, the average LOD of the ELISA Kit are reported.

In this work, a new graphene-based electrode, using photographic paper as a substrate, has been fabricated with the same shape of SPEs by reduction of GO with a desktop laser. This electrode was firstly used to detect *Human Immunoglobulin G* (H-IgG) through an immunoassay with configuration 3. There are 5 types of Human Immunoglobulin, the A, M, E, G, and D. Among them, the G has the higher concentration in human serum because it has the properties of all the other immunoglobulins [69]. H-IgG can be used for disease diagnosis and therapeutic uses. In the first case, many studies showed that this protein can be used as a potential biomarker for different diseases such as Alzheimer [70], cancer [71], inflammatory bowel disease [72], and autoimmune disease [73]. Anyway, many researchers are skeptical about it and this property

must be investigated, still. In any case, H-IgG is a protein that can be used as a cheap model to show how the electrode can be used for detecting any kind of proteins. Indeed, Human Immunoglobulin G has the same chemical, physical and biological properties of many proteins and so it can be used as a cheap model. ELISA kits for Human IgG detection have LOD in the range from 0.1 to 10 ng/ml, with just some prototypes able to detect 30 pg/ml []74. In 2010, Qui et al. modified a gold film with a thin film of polythionine and Au-NPs and they obtained a linear range from 10 to 40 ng/ml using the configuration 2 of Figure 5.1 [75]. Later, in 2016, Jumpathong et al. modified a SPCE with graphene oxide and they used it to detect Human IgG without using a secondary antibody achieving a LOD of 2 ng/ml and a linear range up to 100 ng/ml [76]. We think that this result, decreasing the LOD of about 1 order of magnitude, is due to the presence of a highly porous substrate such as graphene oxide. A good result has been obtained by Wang et al. [77]. They were able to decrease the LOD down to 0.1 pg/ml using a nanostructured electrode made of ultralong CuS-NWs, showing the huge effect of the surface area. Anyway, this extremely low LOD has been hardly reached by other investigated devices. Most of the latest papers have LOD in the range from 0.005 to 10 ng/ml. In 2017. Chen et al. achieved a linear range from 10 pg/ml to 100 ng/ml using CdS as bonded tags in the secondary antibody [61]. At once, Tang et al. [78] used the same procedure with CdS and CuS tags and they obtained the same LOD, confirming the limit of this technique. One of the latest papers on this field, has been published by Prado et al., in 2018 [79]. They used a SPCE where the primary antibody and the antigen were immobilized. A secondary antibody with *alkaline phosphatase* tag has been immobilized to 'close' the sandwich and they obtained a LOD of 10 ng/ml using human serum as a matrix.

The sensing electrode here presented has been developed at the ***Catalan Institute of Nanoscience and Nanotechnology, Barcelona, Spain,*** under the supervision of ***Prof. Arben Merkoci***. It uses *Gold NanoParticles* (Au NPs) to

tag sandwiches between Human IgG and its related capture antibody immobilized on the electrode surface, made of a LSGO deposited on photographic paper. Au NPs can catalyze the *Hydrogen Evolution Reaction* (HER) and can be detected using chronoamperometry in an acidic media. It was obtained a wide linear range with an excellent sensitivity.

The same electrode has been tested to detect *ParaThyroid Hormone Like Hormon* (PTHLH). This protein regulates cell differentiation and proliferation and it is present in many tissues during their development, such as tooth, bone, and mammary gland [80-81]. Furthermore, PTHLH is a hormone that regulates the homeostasis of calcium in blood. It is a widely known biomarker for different cancers, especially breast cancer [82-83-84-85-86], but there still is some uncertainty about it [87]. ELISA kit is able to detect this compound down to 16 pg/ml [88]. Truong et al. [89] studied the PTHLH level in serum of healthy people and people with hypercalcemia. They found that people who suffer from these diseases have a high PTHLH level in the blood, up to 3.45 pg/ml. Fraser et al. [90] showed that 46% of people who have hypercalcemia associated with malignancy had PTHLH concentration in serum higher than 10 pg/ml. Similar results has been obtained by Pandian et al. [91]. They tested volunteers and patients with various disorders of calcium metabolism and PTHLH concentrations were above than normal (greater than 5 pg/mL) in 91% of the patients (42 of 46) with hypercalcemia associated with nonhematological malignancy. So, it is possible to say that over concentration of PTHLH, ***above 1-10 pg/ml***, could be an indicator of the presence of cancer. Up to day, not many works have been done on the electrochemical detection of PTHLH. Table 5.2 summarizes some of them.

TABLE 5.2 EXAMPLES OF ELECTROCHEMICAL IMMUNOASSAY FOR PTHLH DETECTION

Electrode	*Configuration*	*LOD*	*Ref*
MoS2-Graphene-HRP	3	1 pg/ml	[92]
Nanoporous membrane	1	55 ng/ml	[93]
PAMAM dendrimers	2	10 fg/ml	[94]
Nylon Membrane-Biotin	3	5 ng/ml	[95]
Au-SAMs mercaptohexanol-silane	2	10 pg/ml	[96]

There is a huge discrepancy in the LOD of these sensors, going from fg/ml to ng/ml. The aim of the present study was i) to fabricate and to characterize a cheap, flexible, wearable electrode made of reduced graphene oxide reduced by laser and grown onto photographic paper, ii) to use it to detect a cheap model protein such as Human IgG, (iii) to detect a cancer biomarker, such as PTHLH, using the same optimized parameters for H-IgG detection, but avoiding the optimization process with an expensive material such as PTHLH (both antibodies and antigen), and to reach a lower LOD, compared to the previous one obtained by our group using nano-porous membrane (55 ng/ml) [46].

5.2 Experimental

Reagents and apparatus

Polycarbonate membranes with 25nm nominal pores, were supplied from Poretics and used as received. Photographic paper was purchased from Ilford Galerie and used as received. Graphene oxide solution (5mg/ml) was obtained from Graphenea. N-Hydroxysuccinimide (NHS), 1-ethyl-3 (3-(dimethylamino)-propyl) carbodiimide (EDC), anti-human immunoglobulin G (produced in goat), human IgG (from serum), bovine serum albumin, chloridic acid, ethanalonammine (ETA), phosphate buffer saline (PBS) pH 7.4 tablets, potassium hexacianoferrate, chlorauric acid, sodium citrate tribasic, sodium chloride, and PTHLH antigen were purchased from Sigma Co, while PTHLH antibodies was purchased from Abytenk. Silver ink and grey colour dielectric were purchased from Sun Chemical Gwent Group. All the chemicals have been diluted in Milli-Q water (18MΩ cm^{-1}). All the electrochemical analyses were recorded using μAutolab II (Echo Chemie, The Netherlands) potentiostat/galvanostat connected to a PC and controlled by Autolab GPES 4.9007 software (General Purpose Electrochemical System). The Transmission Electron Microscopy (TEM) analysis was conducted using a JEM-2011 Jeol (Jeol Ltd., Japan). Scanning electron microscopy (SEM) images were acquired using a MAGELLAN 400L XHR, FEI Company, The Netherlands.

Au-NPs synthesis and antibody conjugation

Au NPs were synthesized following the Turkevich method [97]. Briefly, 50ml of 0.25 mM $AuHCl_4$ were heated up under vigorous stirring until boiling point. Then, 1.25 ml of 1% sodium citrate was quickly added to the boiling solution. During this process, the colour gradually changes from yellow to red and then to purple. The heater was switched off once an appropriate red tonality was observed. Finally, the solution was cooled down and stored at 4ºC. The as prepared Au NPs were conjugated with antibodies against Human IgG or PTHLH. This conjugation followed conditions that are detailed in the results section, because they were determined from the results obtained from the *Gold Aggregation Test* (GAT). The excess antibodies and BSA was removed by centrifugation. The solution was re-suspended with 2 mM Borate buffer pH 9.2

Fabrication of Reduced graphene oxide electrode and immunoassay

Graphene oxide was deposited on a photographic paper, slightly modifying the procedure of a previous work [98]. Briefly, a solution of 5 mg/ml graphene oxide was diluted in DI water and then filtered through a commercial polycarbonate membrane. After that, the membrane was contacted with a piece of photographic paper and GO was transferred from the membrane to the paper. The paper-based graphene oxide was reduced using a laser that was previously programmed to scribe a predefined shape. In this work, a circular working electrode of 3mm with coaxial reference and counter electrode was drawn down. External contacts and silver pseudo-

reference electrode were made using a silver ink, above the reduced GO (r-GO). This ink dries after 15 mins at 110°C. Then, the external contacts were insulated with a dielectric paste and dried at 70°C for 5 min. All these inks were deposited using a screen-printing machine. Morphology was analysed by scanning electron microscopy. Electrochemical measurements were carried out by an μAUTOLAB from -0.6 to +1 V vs. Ag with different scan rate, from 5mV/s to 500mV/s in 0.2M PBS, pH 7.4, with an electrochemical probe, such as potassium ferrocyanide. Electrochemical impedance spectroscopy was carried out in pure PBS at pH 7.4. To increase the affinity of the antibodies with the electrode, it was incubated with a solution of NHS and EDC in PBS pH 7.4. By this way, the surface of the working electrode was functionalized and anti-H-IgG or anti-PTHLH can easily bond to the electrode, via carbodiimide crosslinking. All the parameters of the incubation were optimized in terms of time and concentrations using CV, EIS or chronoamperometry. After immobilization with anti-Human IgG/PTHLH, the electrode surface was blocked, in order to avoid unspecific interactions. The working electrode was blocked with ETA. The bioassay was performed by an immune-sandwich using the conjugated Au-NPs and serial dilutions of H-IgG/PTHLH. All incubations were carried out by drop casting 6 μl of the solution, alternating with cleaning steps using PBS.

5.3 Results and discussion

Electrode characterization

Figure 5.2 shows the complete fabrication process.

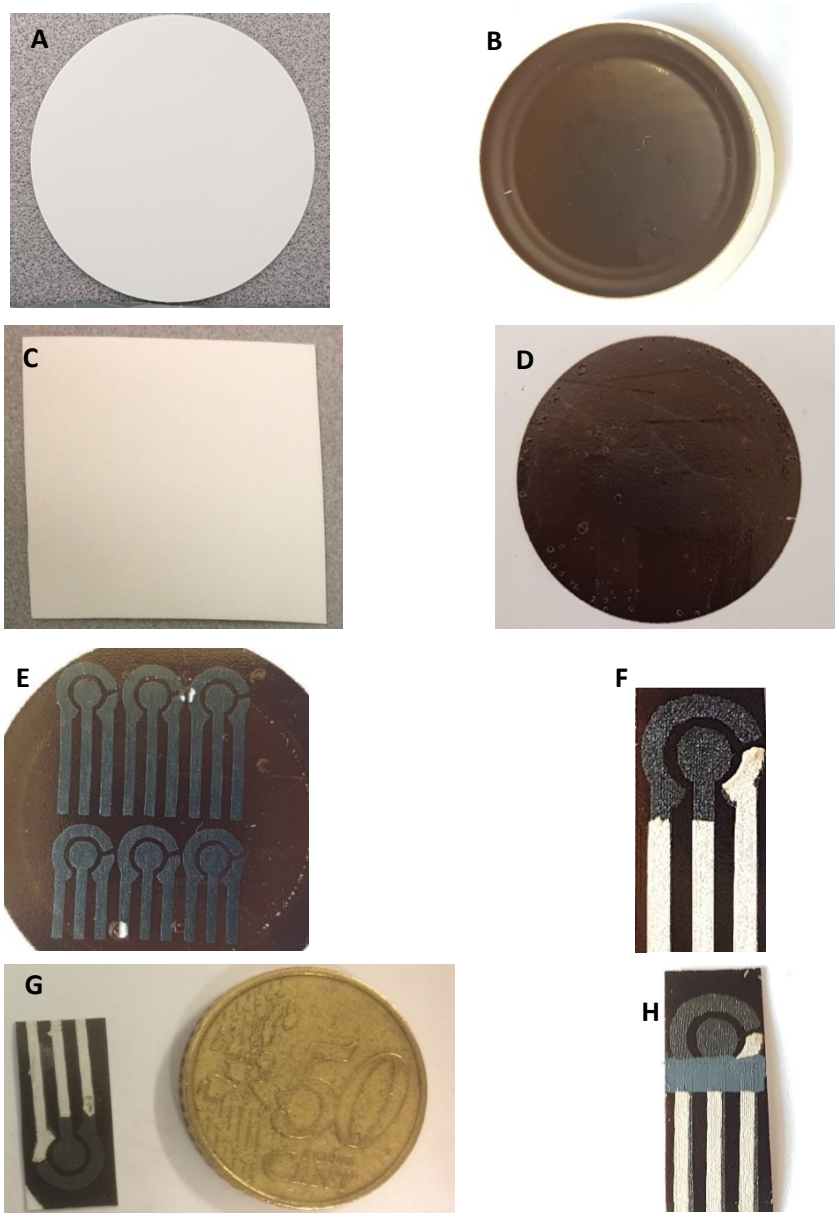

FIGURE 5.2 NITROCELLULOSE MEMBRANE BEFORE (A) AND AFTER (B) FILTERING WITH GO; PHOTOGRAPHIC PAPER BEFORE (C) AND AFTER (D) THE TRANSFER ; GO ON PAPER AFTER THE LASER SCRIBING (E-F); FINAL CONFIGURATION OF THE LSGO AFTER SCREEN-PRINTING THE SILVER INK (G) AND THE DIELECTRIC LAYER (H)

The GO solution was filtered through a nitrocellulose membrane (Figure 5.2A-B) and a uniform distribution of GO is observed. Transfer from the membrane, Spin coating and drop casting were used to deposit GO on the paper and the best results, in terms of simplicity, uniformity and reproducibility, were obtained by using the transfer from the membrane. Indeed, electrodes obtained through spin coating were not homogenous having a thicker layer in proximity of the centre of the paper (where the drop was dropped). By this way, the properties of the electrodes were not uniform, and the reproducibility would have diminished. On the other hand, drop casting is an easier technique that could enhance the mass production of the electrodes. Unfortunately, we found that the deposition based on this technique was of longer duration and required higher volume sample. Besides, while the transfer procedure did not require any control by the operator, the electrodes deposited by drop casting had to be checked before to pass to the next step because some parts of the photographic paper, sometimes, were lighter than others (that means a thinner GO layer). The GO was transferred from the membrane to the photographic paper (Figure 5.2C-D) and the reduction was made by the laser (Figure 5.2E-F). The electrode is shown in Figure 5.2G-H. After all these steps the electrode were very thin, small, and flexible as shown in Figure 5.3.

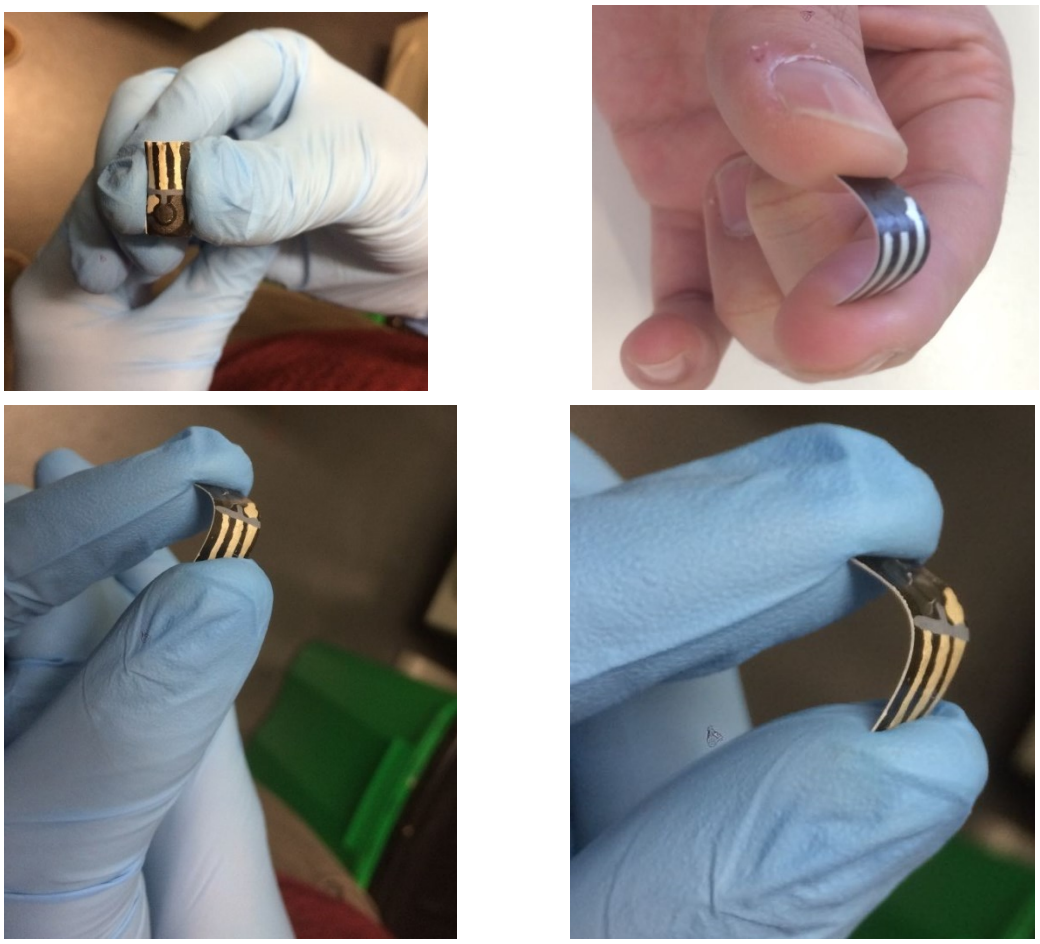

FIGURE 5.3 PICTURES SHOWING THE FLEXIBILITY OF THE PAPER BASED LASER SCRIBED DEVICE

The electrode features are highly affected by the properties of the graphene oxide layer, such as conductivity, porosity, and thickness. The main parameters to be considered to transfer the GO are the GO concentration and the filtering volume. Fixed the volume, the GO concentration was changed from 50µg/ml to 1000µg/ml and, different parameters have been checked, such as resistance, capacitance and electrochemical response in the presence of a probe. Each experiment was repeated five times and the resulting mean values are reported.

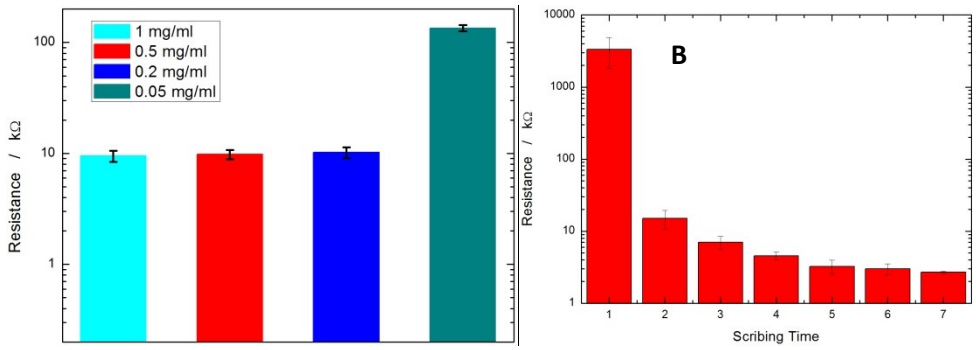

FIGURE 5.4 (A) EFFECT OF GO CONCENTRATION ON THE RESISTANCE OF LSGO ELECTRODE AND (B) EFFECT ON RESISTANCE OF LSGO ELECTRODE OF SCRIBING TIME

The resistance decreases increasing the GO concentration, reaching a plateau after 0.2 mg/ml (Figure 5.4A). This behaviour can be explained considering that the GO thickness that the laser is able to penetrate depends just on the speed, power and wavelength of the laser. Fixing these parameters, the reducible thickness is fixed and even if the GO thickness increases the sheet resistance will not decrease. The effect of the laser parameters, which are speed and number of scribes were also studied. The last one has a deep effect on the electrode resistance: the electrode after 1 scribe has a resistance in the MΩ range that drastically drops to kΩ range by scribing a second time, as showed in Figure 5.4B. As a compromise between electrode resistance and time consumption, the electrodes were scribed 3 times at the same speed. After evaluating different engraving speed, it can be concluded that it does not affect much the resistance, but it plays a role on the precision of the laser. Subsequently, the same electrodes were tested in a solution of 5mM $Fe^{2+/3+}$ and the signal amplitude increases with the GO concentration and become more invertible due to the smaller peak to peak distance. The electrode obtained with 0.5 mg/ml of GO has a better peak-to-peak separation and a lower peak intensity compared to that one with 0.2 mg/ml. These results indicate a better electrochemical behaviour by the thicker layer of GO despite the conductivity is the same. Surprisingly, moving from 0.5 to 1 mg/ml, the

peak-to-peak separation increases, therefore 0.5 mg/ml was chosen as an optimized concentration. The effect of direction of the laser scribe was checked as well. Indeed, the laser could scribe either vertically or horizontally: in the second case, the conductivity of the electrode was really poor, because the different line scribed by the laser (see Figure 5.5C) were hardly in touch.

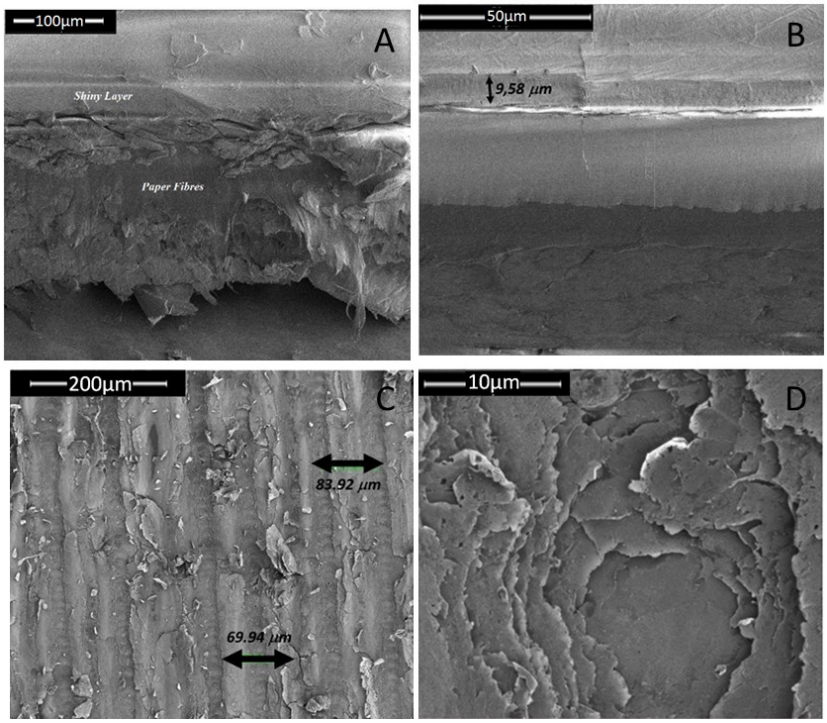

FIGURE 5.5 CROSS SECTION OF THE PHOTOGRAPHIC PAPER BEFORE (A) AND AFTER (B) GO DEPOSITION, TOP VIEW OF THE LASER SCRIBED GO AT LOW (C) AND HIGH (D) MAGNIFICATION

Five different samples were analysed and every following statement (in terms of porosity, GO thickness, and separation between lines) are based on the analysis of these samples Figures 5.5A, and B show the SEM cross-section images of the photographic paper before and after the GO deposition.. The bare paper is made of two distinct layers that are visible even at naked eyes

(Figure 5.5 A). On the top of the shiny layer, a thickness of about 10 µm ± 0.7 of GO is deposited (Figure5.5 B). After the laser scribing process (3 times), the electrode has an intrinsic porosity with an average distance between the laser lines of about 76 µm ± 6.2 (Figure5.5 C, and D).

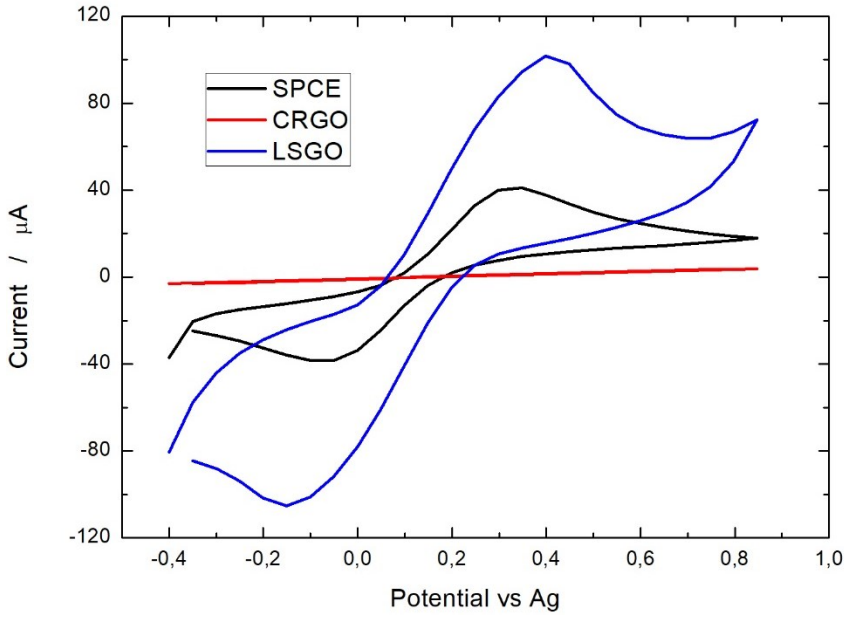

FIGURE 5.6 COMPARISON OF THE CV IN PRESENCE OF 5 MM $Fe^{2+/3+}$ USING LSGO (BLACK CURVE), SPCE (RED CURVE) AND CRGO (GREEN CURVE)

The effect of the high porosity can be seen in Figure 5.6. Here, 3 different electrodes were tested in a 5mM $Fe^{2+/3+}$solution: a Chemically Reduced Graphene Oxide (CRGO) electrode (red line), a Screen Printed Carbon Electrode (SPCE) (black line), and a LSGO (blue line). Both the SPCE and the CRGO were fabricated using a consolidated procedure. Despite the geometrical area of all these electrodes was the same (3mm diameter), the current signal of the LSGO electrode is more than twice compared to that one of SPCE. The CRGO electrode shows a small current signal, almost negligible compared to the LSGO. These results are due to the porosity of the electrode determining a higher surface area than an almost flat SPCE. Using

the Randles-Sevcik equation [99], an area of 2.12 cm^2 was calculated, which is 30 times higher than the geometrical one. This result agrees with the high porosity evidenced in Figures 5.5C, and D. The reproducibility of the sensing electrodes was tested (Figure 5.7), with a standard deviation lower than 5%. Furthermore, the effect of scan rate has been checked and a linear relation between the current peak and the square root of the scan rate was found. The peak-to-peak separation slightly increases with the scan rate suggesting that the $Fe^{2+/3+}$ reaction over this paper-based sensing electrode is semi-reversible.

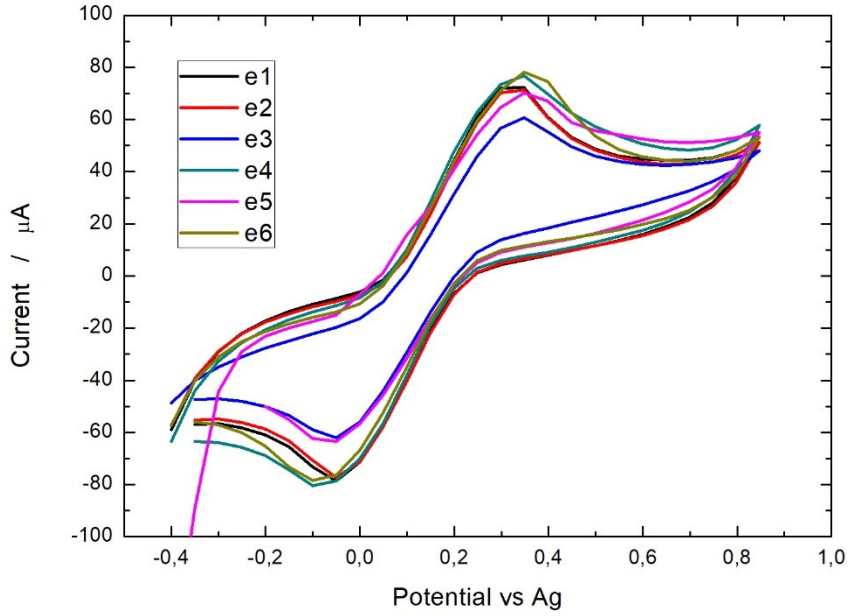

FIGURE 5.7 REPRODUCIBILITY OF 6 DIFFERENT LSGO ELECTRODES IN PRESENCE OF 5 MM $FE^{2+/3+}$

The main problem working with paper-based sensing electrodes is the disposability. Indeed, paper tends to absorb liquids, permanently modifying its structure, therefore these electrodes are generally used as disposable sensors. We choose to work with photographic paper because it has all the properties of paper, but it less absorbs liquids owing to the presence of the

shiny layer of Figure 5.5A This is confirmed by Figure 5.8, where CVs were carried out with the same electrode but in different days.

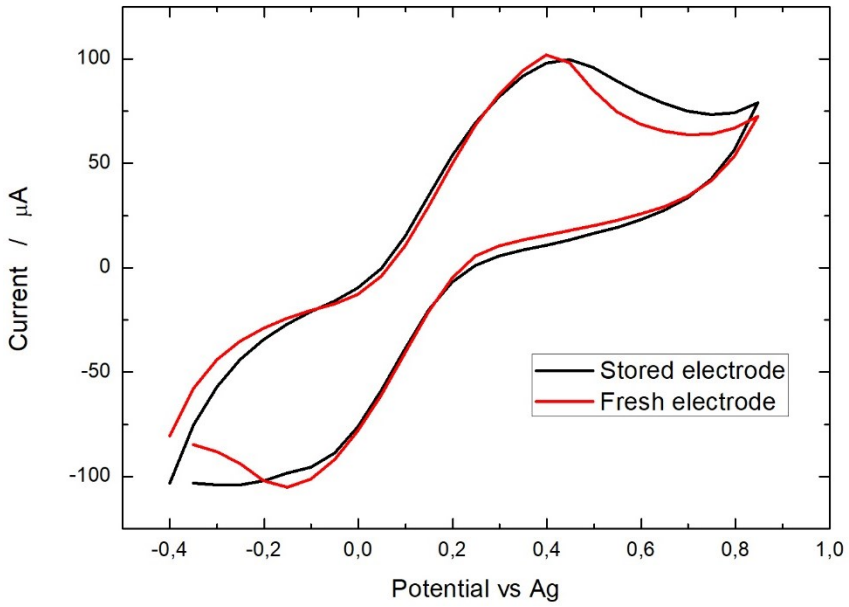

FIGURE 5.8 CV CARRIED OUT USING THE SAME LSGO ELECTRODE IN TWO DIFFERENT DAYS

The red CV of Figure 5.8 has been obtained with a fresh electrode, just after its preparation. Then, the liquid was removed by a micropipette and the electrode stored in air for 24h. After that time, fresh $Fe^{2+/3+}$ was dropped on the electrode and the black curve of Figure 5.8 was recorded. The curve is slightly modified, since the peak-to-peak separation was increased, but it can be considered a good result because the electrode maintained almost all its electro-activity. Therefore, we can assume that our paper-based sensing electrodes can be used more than once.

Au-NPs characterization and conjugation with antibodies

Figure 5.9 show a TEM images of Au-NPs where is possible to see that are monodisperse and spherically shaped.

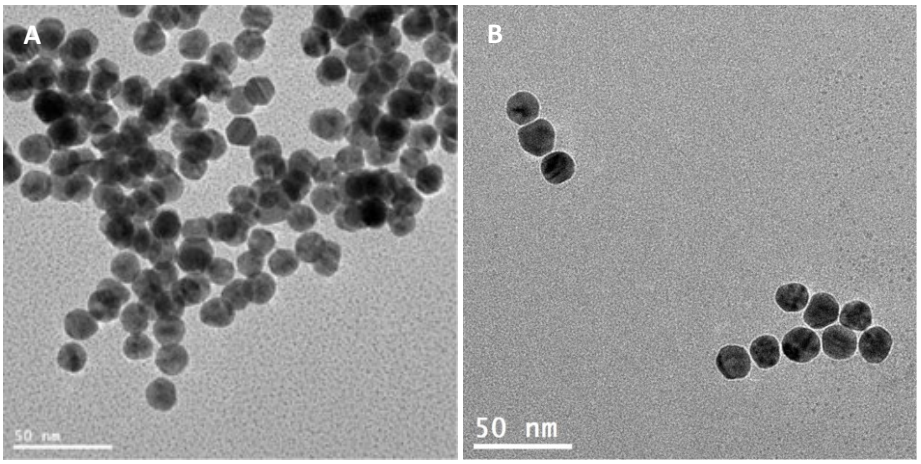

FIGURE 5.9 TEM IMAGES OF 20NM AU-NPS

In order to check the the Au NPs size and the conjugation of the NPs with the antibodies, a Gold Aggregation Test (GAT) was performed. This test was carried out using anti-human IgG, instead of anti-PTHLH, due to the much lower cost of this antibody. Briefly, 150 µl of Au NPs were mixed with 10 µl of antibodies at different concentration and shaked for 20 min at 4°C. Then, 20 µl of 10% NaCl were added and shaked again for 20 min. If the surface of the Au NPs is not covered with antibodies, aggregation occurs due to the presence of NaCl and therefore, as the concentration of antibodies increases, the emission spectrum shifts towards red. When the spectrum stops to shift, the NPs are fully covered by antibodies. Furthemore, the peak position can be releated to the Au NPs size when no NaCl is added [100-101]. Figure 5.10 shows the GAT of Au NPs and the results are summarised in Table 5.3.

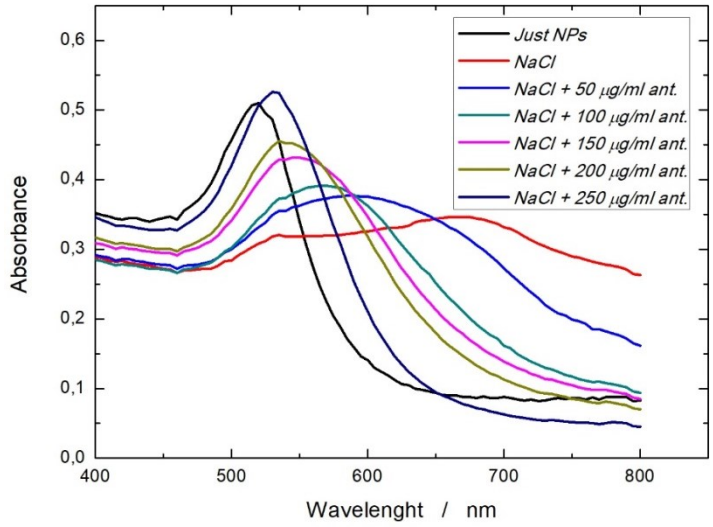

FIGURE 5.10 GOLD AGGREGATION TEST

The peak position of NPs is about 525nm and it stops to shift when 250µg/ml of antibodies were added (Figure 5.10). From the literature, the peak at 525 nm is releated to NPs with size of about 20 nm [100-101].

TABLE 5.3 RESULTS GAT OF FIGURE 5.10

	Peak Position
Au NPs (no NaCl)	*525 nm*
Au NPs + 50 µg /ml	*585 nm*
Au NPs + 100 µg /ml	*565 nm*
Au NPs + 150 µg /ml	*555 nm*
Au NPs + 200 µg /ml	*535 nm*
Au NPs + 250 µg /ml	*530 nm*

In order to use the conjugated Au NPs as tags for the immunoassay, the following procedure has been followed: 1.5 ml of NPs were mixed with 100µl of 250 µg/ml antibodies and shaked for 20 mins at 4°C at 650 RPM. Then, 100µl of 100 µg/ml BSA were added as blocking agent, and shaked in the same conditions. Finally, the NPs were centrifuged at 14000 rpm for 30 minand then were resuspended in a borate buffer at pH 9.2. The same amount of PTHLH antibodies was used to conjugate the NPs.

Application as immunoassay: optimization of the immunoassay

The first attempt to detect H-IgG was carried out using random parameters for all the incubation steps and the result is shown in Figure 5.11.

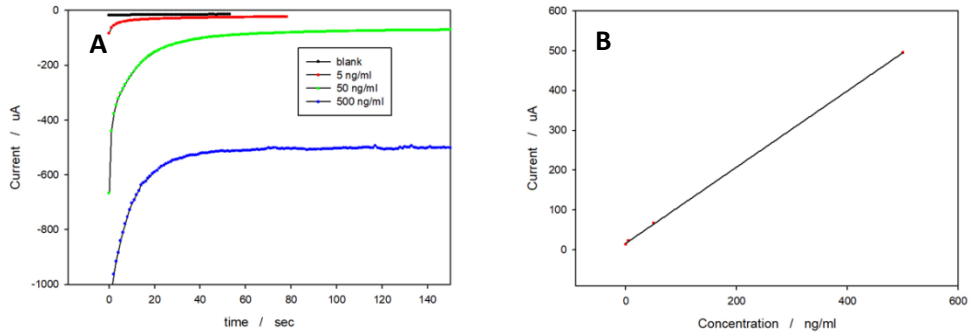

FIGURE 5.11 (A) HER OVER LSGO WITH DIFFERENT AMOUNT OF HUMAN IGG USING NOT OPTIMIZED PARAMETERS AND (B) CORRESPONDING CALIBRATION LINE

It can be observed that the system is able to detect Human IgG down to 5 ng/ml. However, the reproducibility was very scarce with a standard deviation higher than 200% (not shown). We think that this problem was due to the previous incubation steps that were not optimized but were selected according to some papers in the literature [93-102]. In order to increase the reproducibility, all the parameters of the incubation steps were optimized. The first step concerns the modification of the LSGO electrode with NHS and EDC, to create amino groups on the platform and facilitate covalent bond of the antibodies to the electrode [103]. After incubation with antibodies, the cell impedance should increase because antibodies are not conductive. To check the effect of the different incubation steps, EIS was carried out and the Bode Plot has been used to discriminate the best conditions. The higher the

impedance, the higher is supposed to be the density of antibodies attached on the electrode. We found that incubation 30 min long with 500mM NHS and 50mM EDC determines the highest increase in the total impedance. Using the same approach, the incubation with antibodies was optimized. The electrode was incubated with different amount of antibodies, for different time. After 30 min of incubation with optimized amount of NHS and EDC, EIS was performed. The surface modification with antibodies increases the electrode impedance that can be measured using EIS (Figure 5.12 A, B). The experiments were carried out using three different electrodes for each time and concentration. In Figure 5.12B the mean value is plotted with the corresponding standard deviation.

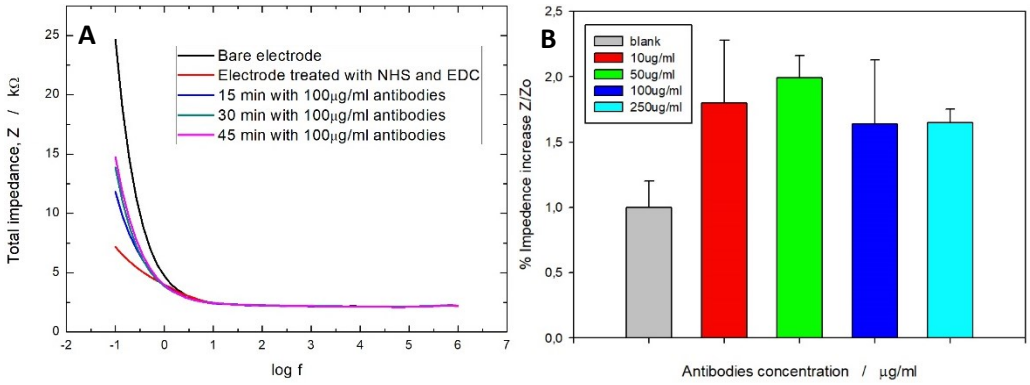

FIGURE 5.12 (A) EFFECT OF INCUBATION TIME OF 100 µG/ML OF ANTIBODIES ON THE TOTAL IMPEDANCE OF THE CELL AFTER INCUBATION WITH NHS AND EDC AND (B) EFFECT OF ANTIBODIES CONCENTRATION AFTER 30 MIN OF INCUBATION

Figure 5.12A and B show the cell impedance when H-IgG antibodies are incubated (after the incubation with the optimized amount of NHS and EDC). Figure 5.12B shows the impedance calculated as the ratio between the impedance after the incubation with antibodies (Z) and the impedance after incubation just with NHS and EDC (Z_0). In Figure 5.12 can be observed that 50µg/ml of antibodies gives the best performance both in terms of signal and

error. In order to detect proteins, like Human IgG, it is important that the signal comes just from the sandwiches avoiding that unspecific bonding of the gold tags with electrodes are read. In order to check the efficiency of the blocking step, CV in the presence of $Fe^{2+/3+}$ was performed after incubation with ETA (Figure 5.13).

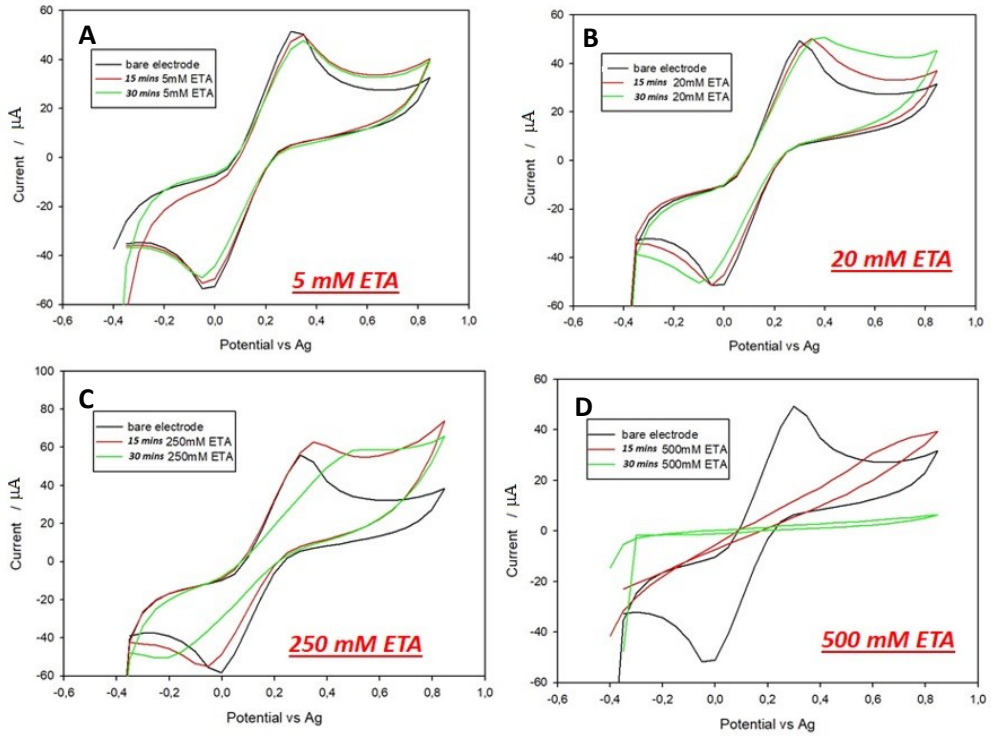

FIGURE 5.13 EFFECT OF BLOCKING TIME USING (A) 5 MM, (B) 20 MM, (C) 250 MM AND (D) 500 MM ETA

Both 15 and 30 mins of incubation with 5 mM of ETA are not able to block the surface that remains electroactive without any significant modification in peak position nor peak separation (Figure 5.13A). However, when the ETA concentration increases up to 20 mM, 30 min of incubation start to modify the electrode that became more irreversible (Figure 5.13B). When 250 mM ETA was tested, the electrode starts to be blocked after 15 min and becomes much

more irreversible after 30 min of incubation (Figure 5.13C). Instead, 500mM ETA almost totally block the electrode already after 15 min while a peak-free CV appear after 30 min of blocking (Figure 5.13D). Considering that the electrode still must be conductive, we select to incubate with 500 mM for 15 mins.

The effect of the incubation time with Au NPs has been investigated and the result is shown in Figure 5.14.

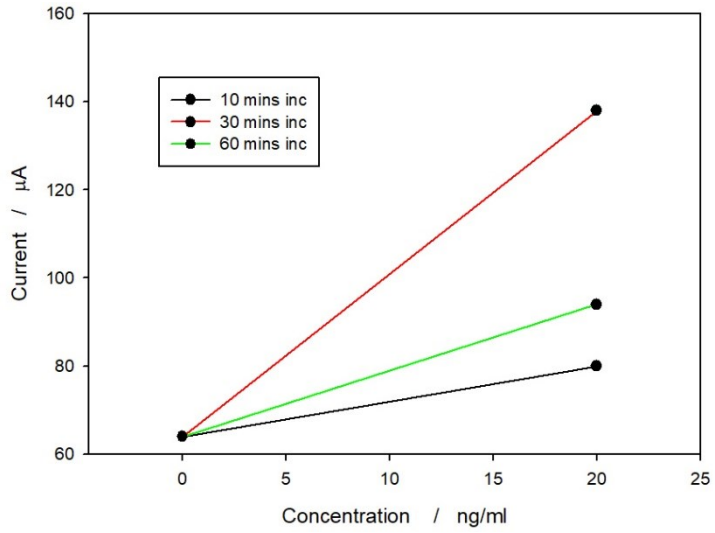

FIGURE 5.14 EFFECT OF INCUBATION TIME WITH AU-NPS AFTER INCUBATION WITH ALL THE OPTIMIZED PARAMETERS ON THE HER WITH 20 NG/ML OF H-IGG

The electrode was incubated with NHS, EDC, antibodies, and ETA using the optimized parameters. Then, 20 ng/ml of Human IgG were incubated for 15 min and pre-conjugated Au NPs were dropped on the electrode for different times. As it is possible to observe, the sensitivity increases when the incubation time with Au NPs increases from 10 to 30 min but it decrease when incubating for 1h. This behaviour can be explained by the Hooke effect, described below. According to this result, we decided to incubate with Au NPs for 30 min.

Electrochemical measurements on the immunoassay, calibration lines

To produce hydrogen, a cathodic potential has to be applied. pH and applied potential are the main parameters that have to be optimized. Figure 5.15 shows a Linear Sweep Voltammetry using LSGO and SPCE in 0.5 M HCl. This figure shows the CV of one LSGO and one SPCE but the same behaviour has been found with several other electrodes.

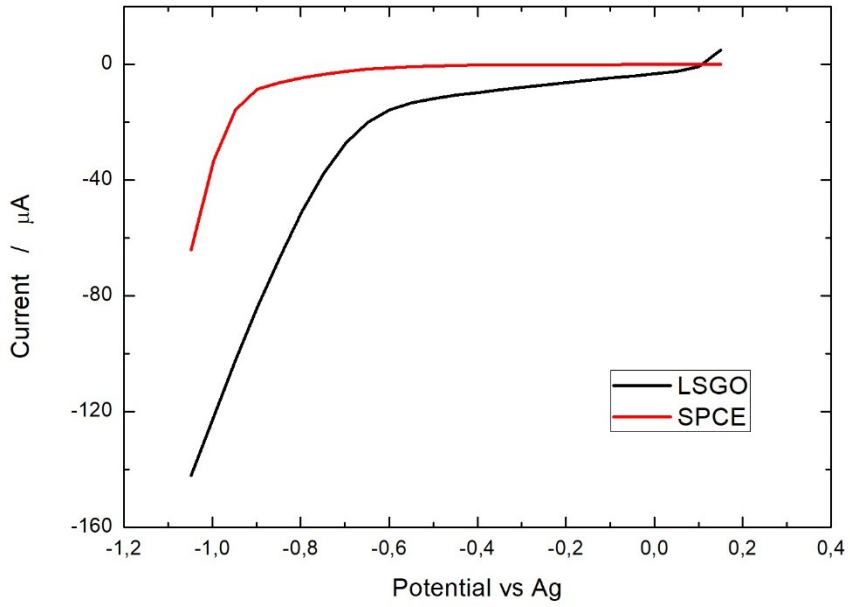

FIGURE 5.15 LSV CARRIED OUT IN 0.5 M HCL USING SPCE (RED LINE) AND LSGO (BLACK LINE)

HER starts at -0.6V vs Ag on the LSGO and at -0.8V on the SPCE, and occurs with lower overpotential on the LSGO electrode. This result shows that it is possible to have better performances with paper based LSGO rather than a bare SPCEs. This behaviour has been confirmed also by only addition on the electrode of different amounts of Au NPs, without any treatment with antibodies, and applying a fixed cathodic potential of -1V (Figure not shown).

The results show that, using both LSGO and SPCE, the higher is the concentration of NPs the higher is the current, so confirming that Au NPs are electroactive for hydrogen evolution. Besides, it confirmed that LSGO sensing electrodes are more performing than SPCE ones, because a higher current was recorded in the presence of the same NPs concentration.

In order to find the best potential to be applied for H_2 evolution on LSGO sensing electrode, different experiments with 20ng/ml of Human IgG were conducted, applying different potentials to catalyse hydrogen reaction.

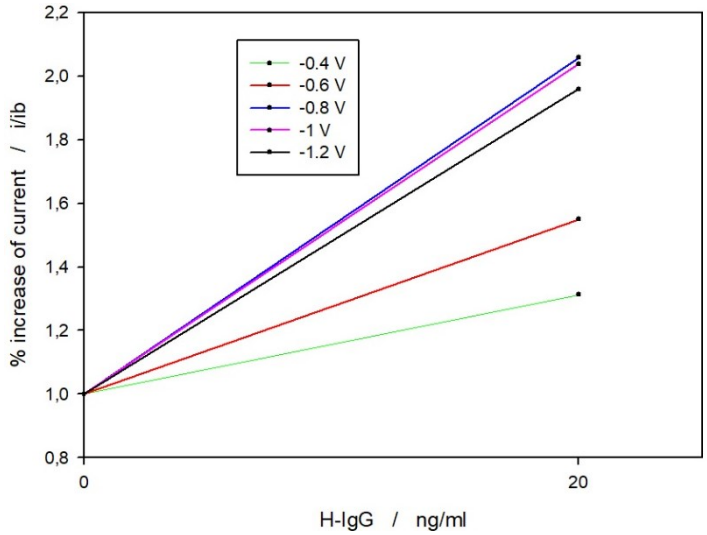

FIGURE 5.16 EFFECT OF THE APPLIED POTENTIAL ON THE DETECTION OF 20 NG/ML OF HUMAN IGG

TABLE 5.4 EFFECT OF THE APPLIED POTENTIAL ON THE DETECTION OF 20 NG/ML OF HUMAN IGG OF FIGURE 5.19

Applied Potential (V vs Ag)	*Blank Current (µA)*	*20 ng/ml (µA)*	*Sensitivity (µA ng $^{-1}$ ml)*	*Standard Deviation*
-0.4	*11.52*	*15.13*	*1.31*	*10 %*
-0.6	*12.77*	*19.8*	*1.55*	*31%*
-0.8	*27.32*	*56.25*	***2.05***	*53%*
-1	*60.9*	*124.3*	***2.03***	*7.5%*
-1.2	*79.1*	*155*	***1.95***	*8.3%*

Table 5.4 and Figure 5.16 show the results of these experiments that agree with Figure 5.15 (black curve). Indeed, the slope of the LSV curve of LSGO electrode of Figure 5.15 increases moving from -0.4 V to -0.7V vs. Ag and then it is constant from -0.8 V until -1.1 V vs Ag. So, it is reasonable to think

that current for HER has to follow the same behaviour. The results of Figure 5.16, summarised in Table 5.4, confirmed that sensitivity (and so the current) reached a plateau of about 2 μA ng^{-1} ml applying a potential higher than -0.8V. Anyway, we choose to work with an applied potential of -1V because it provided the best reproducibility. We also checked the effect of pH (in terms of HCl concentration), and we found that its effect is negligible moving from 0.5 to 2 M HCl (not shown).

The experiment of Figure 5.17A was carried out with the following procedure:

1. Incubation with NHS and EDC;
2. Incubation with NHS, EDC and antibodies;
3. Blocking with ETA;
4. Incubation with PBS pH 7.4 ***without H-IgG***;
5. Incubation with pre-conjugated NPs (20nm);
6. Chronoamperometry at -1 V in 0.5 M HCl.

In this way, no NPs are supposed to be into the electrode.

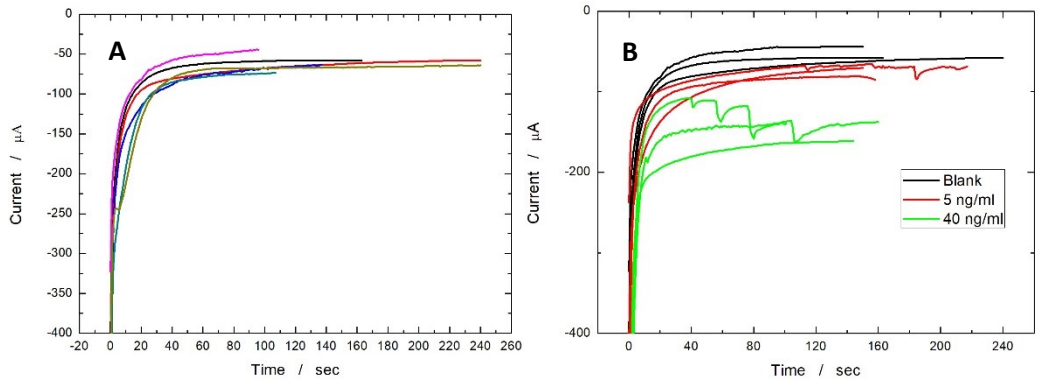

FIGURE 5.17 A) SIX DIFFERENT BLANKS, B) TRIPLICATE OF BLANKS, 5 NG/ML, 40 NG/ML OF H-IGG

Figure 5.17A clearly shows that the electrode is reproducible, with a standard deviation of about 8%. The curves of Figure 5.17B has been obtained following the same procedure of Figure 5.17A but with addition of different

amount of H-IgG into PBS. Figure 5.17B shows that current increases with Human IgG concentration, confirming that the sandwiches are on the surface of the sensing electrode. Sometimes, a sudden drop in the current was recorded as shown by one of the three green lines of Figure 5.17B. We think that this is due to hydrogen bubbles that accumulate over time on the electrode, shielding the surface. When the bubbles become big enough, they detach from the electrode so that the exposed area increases with the current. Furthermore, this result confirms that the lack in reproducibility discussed before (Figure 5.11) was due to the irreproducibility of the incubation steps. Indeed, after the optimization process, the reproducibility was greatly improved. Fig 5.18 A shows that the current increases with the Human IgG concentration.

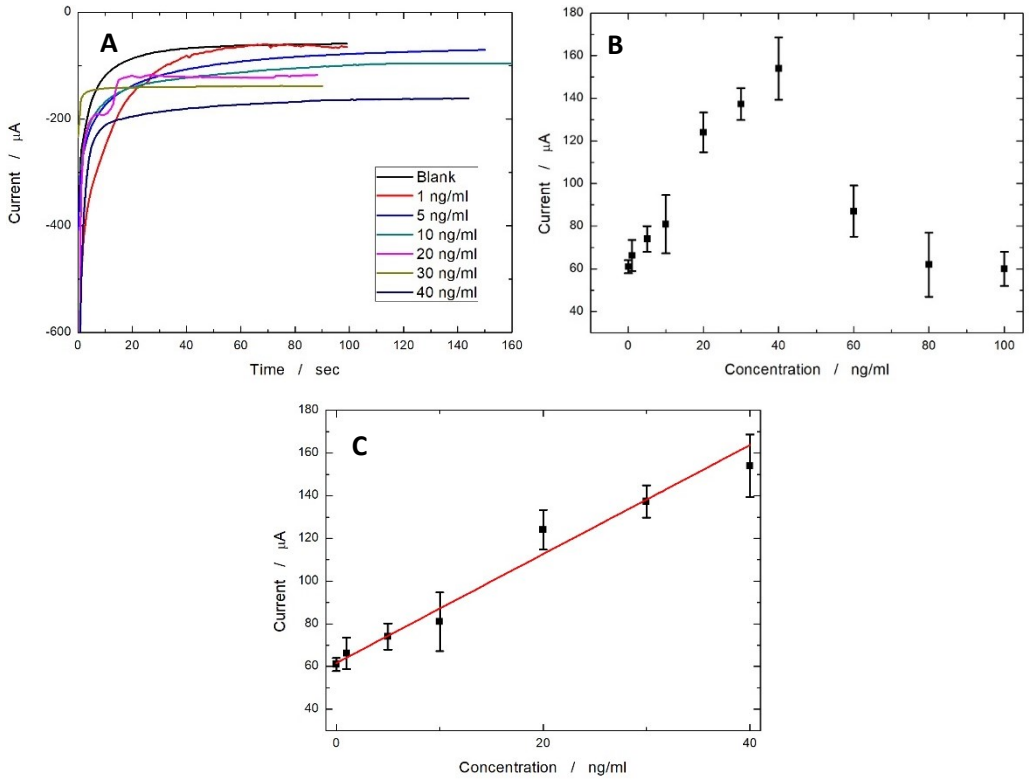

FIGURE 5.18 A) EFFECT OF INCREASING CONCENTRATION OF H-IGG AND (B) CORRESPONDING CALIBRATION LINE; C) CALIBRATION CURVE FROM 0 TO 100 NG/ML OF H-IGG

The corresponding calibration line is shown in Figure 5.18 B. We found a linear range from 1 to 40 ng/ml matched by the equation 2.42*C (ng/ml)+62.92, and a LOD of 3.78 ng/ml. At analyte concentrations higher than 40ng/ml, the current starts to decrease (see Figure 5.18C), due to an overcrowding effect, without reaching a plateau, according to the Hook law [104]. This behaviour is quite common in working with immunoassay, as confirmed by the literature [105-106-107]. This behaviour leads to a difficulty in the result processing because two different concentrations have the same current value. In order to overcome this problem, a secondary analysis has to be carried out. Indeed, the current will change differently depending on the Human IgG concentration: it will increase when the concentration is on the left side of the peak (when it is lower than 40 ng/ml), while it decreases if the concentration is on the right. In this way, it is possible to discriminate between the two different concentrations.

To decrease the LOD, we developed a new way to produce Au NPs, and we followed a slightly different procedure for the incubation. The results are shown in Figure 5.19. For the sake of clarity, the NPs prepared according the new procedure will be called Au NPs2.

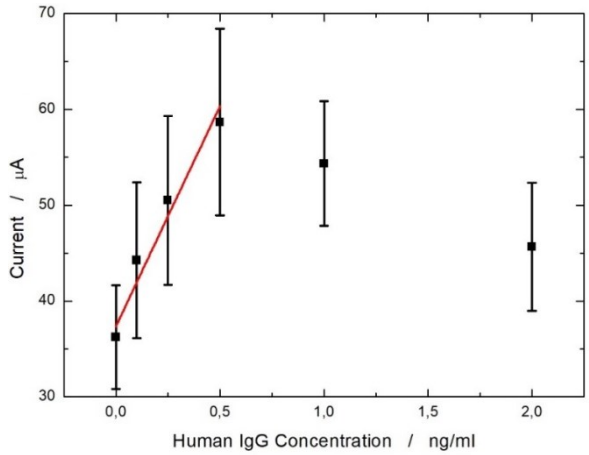

FIGURE 5.19 CALIBRATION CURVE FROM 0.1 TO 2 NG/ML OF H-IGG USING AU-NPS2

Figure 5.19 shows the calibration line obtained with Au-NPs2. The LOD shifted towards the pg/ml range, with a linear range from 100 to 500 pg/ml and a sensitivity of 0.43 μA/(pg/ml) was determined. Unfortunately, the standard deviation is higher in comparison with the calibration line of Figure 5.18B. We think that this problem could be due to:

- Not efficient incubation with these new NPs;
- Not efficient Au-NPs synthesis.

Anyway, these prelaminar results demonstrate that NPs play a key role in this technique and that it is possible to decrease the LOD optimizing either the gold nanoparticles synthesis or incubation steps.

PTHLH detection

The same incubation parameters, used for Human IgG, were applied to detect PTHLH. Indeed, both anti-PTHLH and PTHLH antigen are highly expensive chemicals and an optimization process would have required a too high amount of reagents. For the same reasons, just the Au-NPs1 were tested for PTHLH detection. Indeed, nevertheless the scarcer electrochemical behaviour of these NPs, we found a better reproducibility during both NPs synthesis and Human IgG detection.

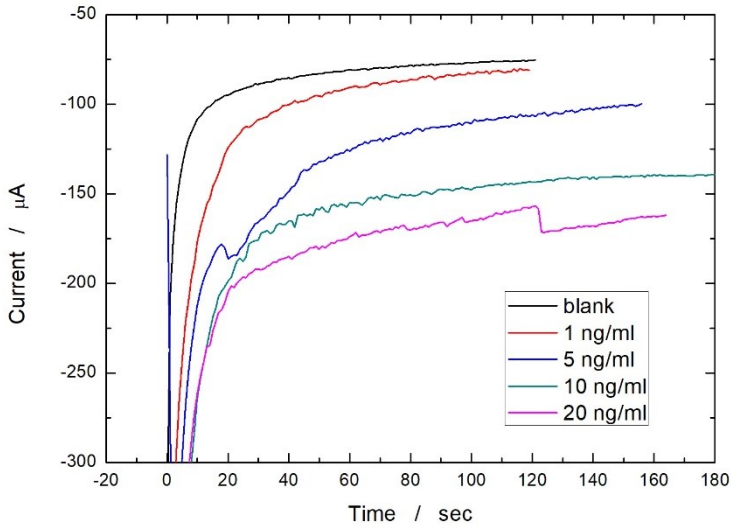

FIGURE 5.20 EFFECT OF INCREASING CONCENTRATION OF PTHLH USING AU-NPS1

Figure 5.20 shows the hydrogen evolution reaction on the LSGO with different amount of PTHLH antigen, after the conjugation with PTHLH antibodies and conjugated Au NPs. Sometimes, here again, the current shows some steps due to the presence of bubbles on the electrode surface. Anyway, a good sensitivity was found, and the current linearly increases with concentration from 1 to 30 $ngml^{-1}$ of PTHLH, as shown in Figure 5.21.

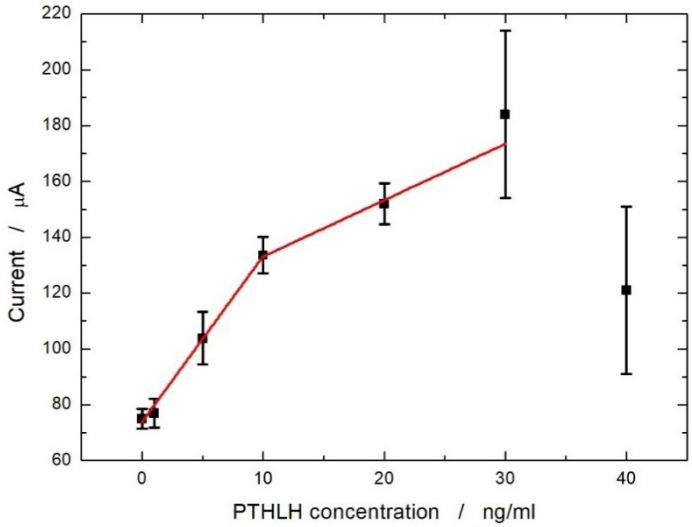

FIGURE 5.21 CALIBRATION CURVE FROM 0 TO 40 NG/ML OF PTHLG

Two different sensitivities were found: the first one of about 5.9 μA/(ng ml) from 1 to 10 ng/ml and a second one of about 2 μA/(ng ml) from 10 to 30 ng/ml. The regression lines are:

$i = 5.93*C+73.8$ with an R^2 of 0.991

$i = 2.02*C+112.89$ with an R^2 of 0.94

Here, the 'Hook effect' appears but at slightly lower concentration (30 ng/ml instead of 40 ng/ml of Human IgG). Furthermore, we found that the standard error of the electrode is less than 10% when PTHLH concentration is lower than 30 ng/ml (the 'Hook limit'), while it drastically increases when this limit is approached.

Despite the LOD is not low enough to detect PTHLH in a real sample (a useful linear range should be from 0.1/1 to 10/100 pg/ml), the result is satisfying because shows that i) Human IgG can be used as a model, (ii) PTHLH can be detected using electrochemical techniques, and (iii) it should be possible to decrease the LOD of the electrode in the pg/ml range by optimizing the PTHLH incubations and NPs synthesis.

In a previous work, lateral flows strips were used to detect both Human IgG [108] and PTHLH [109] using gold nanoparticles as marks. Using this new LSGO sensing electrode for detecting Human IgG, we decreased the LOD of about 20 times (the linear range started at 50 ng/ml using lateral flow), and the sensitivity is almost 500 times higher. The linear range in detecting PTHLH by using lateral flow started at 5 ng/ml, that is not far from that one obtained in this work. Anyway, it is important to highlight that lateral flow, being an optical method, suffers of interference due to the matrix of the real samples, and, moreover, we are quite confident that the LOD of Figure 5.21

can be decreased of at least 1 order of magnitude by optimizing the synthesis of the Au NPs2.

Comparison with bibliography

Table 5.5 shows some results concerning with the electrochemical detection of Human IgG, obtained in the last 5 years using different immunoassay configurations.

TABLE 5.5 COMPARISON OF DIFFERENT WORKS, IN THE LAST 5 YEARS, FOR ELECTROCHEMICAL DETECTION OF H-IGG

Electrode	*Immunoassay configuration*	*LOD ng/ml*	*Ref*
Ag-NWs – ZnO nanostr.	3	0.01	[110]
SPCE-GO	2	2	[76]
CuS-NWs	2	10^{-4}	[77]
SPCE-CdS	3	0.01	[61]
SPCE-CdS/CuS	3	0.01	[78]
SPCE-poly(2-aminobenzylamine)	2	0.15	[111]
SPCE-AP	3	10	[66]
LSGO-AuNPs	3	0.1	This work

Table clearly shows that our results agree very well with the average results of the literature.

It is not possible to make the same table for PTHLH detection by electrochemical methods because not many papers are published. As the best of my knowledge, all these works were already cited in Table 5.2 where it is possible to see that our results agree with the literature, mostly if we consider that the LOD can be decreased improving the Au-NPs size and the incubation steps.

5.4 Conclusions

A new, novel, cheap and easy way to produce paper based Laser Scribed Electrodes has been found. The process does not require any particular chemical and it is possible to obtain at least 6 electrodes, or even 8/10 optimizing the use of a commercial polycarbonate membrane. The morphological and electrochemical characterizations of the sensing electrode showed that it is highly porous and has better electrochemical properties than commercial SPCEs and 'home made' CRGO. We showed that the optimization of the deposition of the immunoassay plays a crucial role in improving the reproducibility of the technique. The optimization was carried out in a new and powerful way using just electrochemical techniques. Human IgG and PTHLH were detected achieving low Limit of Detection with good sensitivity. The NPs synthesis has a key role in this process, being able to decrease the LOD by 1 order of magnitude. This paper based sensing electrode opens new possibilities for electrochemical sensors for both clinical and environmental applications.

References

1 L. H. Gam, Breast cancer and protein biomarkers, World Journ. Exp. Med., 2012, 5, 86-91

2 S.M. Kang, H.J. Sung, J.M. Ahn, J.Y. Park, S.Y. Lee, C.S. Park, J.Y. Cho, The Haptoglobin β chain as a supportive biomarker for human lung cancers, Mol. Biosyst., 2011, 4, 1167-1175

3 C. Nowak, J. Sundstrom, S. Gustafsson, V. Giedraitis, L. Lind, E. Ingelsson, T. Fall, Protein Biomarkers for Insulin Resistance and Type 2 Diabetes Risk in Two Large Community Cohorts, Diabetes, 2016, 65, 276-284

4 R. M. Lequin, Enzyme Immunoassay (EIA)/Enzyme-Linked Immunosorbent Assay (ELISA), Clinic. Chem, 2005, 51, 2415-2418

5 E. Mylonakis, M. Paliou, M. Lally, T.P. Flanigan, J.. Rich, Laboratory testing for infection with the human immunodeficiency virus: established and novel approaches, Am. J. Med., 2000, 109, 568-576

6 P. Shi, S.J. Wong, Serologic diagnosis of West Nile virus infection, Expert Review of Molecular Diagnostics, 2003, 6, 733-741

7 F. Ricci, G. Adornetto, G. Palleschi, A review of experimental aspects of electrochemical immunosensors, Electrochim. Acta, 2012, 84, 74-83

8 M. C. Erlandsson, C. A. Jonsson, U. Islander, C. Ohlsson, H. Carlsten, Oestrogen receptor specificity in oestradiol‐mediated effects on B lymphopoiesis and immunoglobulin production in male mice, Immunology, 2003, 108, 346-351

9 S. Pan, R. Aebersold, R. Chen, J. Rush, D.R. Goodlett, M.W. McIntosh, J. Zhang, T.A. Brentnall, Mass spectrometry based targeted protein quantification: methods and applications, J. Proteome. Res., 2009, 2, 787-797

10 F. Baymann, D.A. Moss, W. Mantele, An electrochemical assay for the characterization of redox proteins from biological electron transfer chains, Anal. Biochem., 1991, 199, 269-274

11 J. Newman, A.P.F. Turner, Home blood glucose biosensors: a commercial perspective., Biosens. Bioelectron., 2005, 20, 2435–2453

12 M. Vestergaard, K. Kerman, M. Saito, N. Nagatani, Y. Takamura, E. Tamiya, A Rapid Label-Free Electrochemical Detection and Kinetic Study of Alzheimer's Amyloid Beta Aggregation, J. Am. Chem. Soc., 2005, 127, 11892–11893

13 J. Halliwell, A.C. Savage, N. Buckley, C. Gwenin, Electrochemical impedance spectroscopy biosensor for detection of active botulinum neurotoxin, Sensing BioSens. Res. 2014, 2, 12-15

14 K. Charoenkitamorn, P.T. Tue, M. Chikae, O. Chailapakul, Y. Takamura, Gold Nanoparticle‐labeled Electrochemical Immunoassay Using Open Circuit Potential for Human Chorionic Gonadotropin Detection, Electroanalysis 2018, 30, 1774 –1780

15 D. Tang, B. Su, J. Tang, J. Ren, G. Chen, Nanoparticle-Based Sandwich Electrochemical Immunoassay for Carbohydrate Antigen 125 with Signal Enhancement Using Enzyme-Coated Nanometer-Sized Enzyme-Doped Silica Beads, Anal. Chem., 2010, 4, 1527-1534

16 D-Q‐ Tang, D.J. Zhang, D.Y. Tang, H. Ai, One‐Step Electrochemical Immunoassay for Carcinoembryonic Antigen in Human via Back‐Filling Immobilization of Gold Nanoparticles on DNA‐Modified Gold Electrode, Electroanal., 2006, 18, 2194-2201

17 I. Kirsch, Electrochemical Immunoassays Monika J. Green, Philosophical Transactions of the Royal Society of London. Series B, Biological Science, Philos. Trans. R. Soc. Lond. B Biol. Sci., 2011, 366, 1781-1782
18 M. Aydin, E.B. Aydin, M.K. Sezginturk, A disposable immunosensor using ITO based electrode modified by a star-shaped polymer for analysis of tumor suppressor protein p53 in human serum, Biosens. Bioelectr., 2008, 107, 1-9
19 M.A. Tabrizi, Chapter 9 – The Electrochemical Aptasensors for the Determination of Tumor Markers, Graphene Bioelectr., 2018, 193-218
20 B. Patella, C. Sunseri, R. Inguanta, Nanostructured Based Electrochemical Sensors, Journal of nanoscience and nanotechnology, 2018, 18, 1-12
21 B. Patella, S. Piazza, C. Sunseri, R. Inguanta, NiO Thin Film for Mercury Detection in Water by Square Wave Anodic Stripping Voltammetry, Chemical Engineering Transaction, 2017,60,1-6
22 K.S. Novoselov, A.K. Geim, S.V. Morozov, D. Jiang, Y. Zhang, S.V. Dubonos, I. V. Grigorieva, A. A. Firsov., Electric field effect in atomically thin carbon films, Science, 2004, 306, 666-669
23 C. Petridis, D. Konios, M. M. Stylianakis, G. Kakavelakis, M. Sygletou, K. Savva, P. Tzourmpakis, M. Krassas, N. Vaenas, E. Stratakis, E. Kymakis, Solution processed reduced graphene oxide electrodes for organic photovoltaics, Nanoscale Horiz., 2016, 1, 375
24 A. Bonanni, M. Pumera, Graphene Platform for Hairpin-DNA-Based Impedimetric Genosensing, ACS Nano, 2011, 5, 2356
25 F. Xu, Y. Suna, Y. Zhang, Y. Shi, Z. Wen, Z. Li, Graphene–Pt nanocomposite for nonenzymatic detection of hydrogen peroxide with enhanced sensitivity, Electrochemistry Communications, 2011, 13, 1131-1134
26 N. Mohanty, V. Berry, Graphene-based single-bacterium resolution biodevice and DNA transistor: interfacing graphene derivatives with nanoscale and microscale biocomponents., Nano Lett, 2008, 8, 4469
27 E. Pérez-Ramírez, M. de la Luz-Asunción, A. L. Martínez-Hernández, C. Velasco-Santos, Graphene Materials to Remove Organic Pollutants and Heavy Metals from Water: Photocatalysis and Adsorption, Semiconductor Photocatalysis - Materials, Mechanisms and Applications, 2016
28 C.Fenzl, P. Nayak, T. Hirsch, O.S. Wolfbeis, H.N. Alsfareef, A.J. Baeumner, Laser-Scribed Graphene Electrodes for Aptamer-Based Biosensing, ACS Sens. 2017, 5, 616-620
29 D. Du, S. Guo, L. Tang, Y. Ning, Q. Yao, G.J. Zhang, Graphene-modified electrode for DNA detection via PNA–DNA hybridization, Sens. Act. B., 2013, 186, 563-570
30 R.Nurzulaikhaa, H. N. Limbc, I. Harrisona, S. S.Lima, A. Pandikumard, N. M. Huangd, S. P. Limd, G.S.H.Thiend, N.Yusoffd, I. Ibrahim ,Graphene/SnO2 nanocomposite-modified electrode for electrochemical detection of dopamine, Sensing and Bio-Sensing Research, 2015, 5, 42-49
31 Z. Wang, J. Yang, L. Gui , Development of a Graphene-Based Aptamer Sensor for Electrochemical Detection of Serum ECP Levels, Int. J. Electrochem. Sci., 2017, 12, 9502 – 9511
32 C. Berger, Z. Song, X. Li, X. Wu, N. Brown, C. Naud, D. Mayou, T. Li, J. Hass, A. N. Marchenkov, E.H. Conrad, P. N. First, W.A. De Heer, Electronic confinement and coherence in patterned epitaxial graphene, Science, 312, 2006, 1191-11196
33 M. Eizenberg, J.M. Blakely, Carbon monolayer phase condensation on Ni(111), Surf. Science, 1979, 82, 228-263
34 S. Pei, H.M. Cheng, The reduction of graphene oxide., Carbon, 2012, 50, 3210-3228
35 Z.S. Wu, W. Ren, L. Gao, B. Liu, C. Jiang, H. M. Cheng, Synthesis of high-quality graphene with a pre-determined number of layers, Carbon, 2009, 47, 493–499
36 D. R. Dreyer, S. Murali, Y. Zhu, R. S. Ruoff, C. W. Bielawsk, Reduction of graphite oxide using alcohols, J. Mater. Chem., 2011, 21, 3443-3447

37S. Stankovich, D.A. Dikin, G.H.B. Dommett, K.M. Kohlhaas, E.J. Zimney, E.A. Stach, R.D. Piner, S.T. Nguyen, R.S. Ruoff, Graphene-based composite materials, Nature,2006, 442, 282–286

38 S. Stankovich, D.A. Dikin, R.D. Piner, K.A. Kohlhaas, A.Kleinhammes, Y. Jia, Y. Wu, S.T. Nguyen, R.S. Ruoff, Synthesis of graphene-based nanosheets via chemical reduction of exfoliated graphite oxide, Carbon, 2007, 7, 1558-1565

39 M. J. Fernández-Merino, L. Guardia, J. I. Paredes, S. Villar-Rodil, P. Solís-Fernández, A. Martínez-Alonso, J. M. D. Tascón, Vitamin C is an ideal substitute for hydrazine in the reduction of graphene oxide suspensions, The Journal of Physical Chemistry C, 2010, 114, 6426-6432

40 G.K. Ramesha, S. Sampath, Electrochemical reduction of oriented graphene oxide films: an in situ raman spectroelectrochemical study, The Journal of Physical Chemistry C, 2009, 19, 7985-7989

41 Y.L. Zhang, L. Guo, H. Xia, Q.D. Chen, J. Feng, H.B. Sun, Photo reduction of graphene oxides: methods, properties, and applications, Adv. Opt. Mat, 2014, 1, 10-28

42 S. Y. Kang, C. C. Evans, S. Shukla, O. Reshef, E. Mazur, Patterning and reduction of graphene oxide using femtosecond-laser irradiation, Optics & Laser Technology, 2018, 103, 340-345

43 M. F. El-Kady, V. Strong, S. Dubin, R. B. Kaner, Laser Scribing of High-Performance and Flexible Graphene-Based Electrochemical Capacitors, Science, 2012, 335, 1326-133

44 V.Strong, S. Dubin, M.F. El-Kady, A. Lech, Y. Wang, B.H. Weiller, R.B. Kaner, Patterning and Electronic Tuning of Laser Scribed Graphene for Flexible All-Carbon Devices, ACS Nano., 2012, 6, 1395-1403

45 H. Tian, Y. Shu, Y.L. Cui, W.T. Mi, Y. Yang, D. Xie, T.L. Ren, Scalable fabrication of high-performance and flexible graphene strain sensors, Nanoscale., 2014, 2, 699-705

46 K. Griffiths, C. Dale, J. Hedley, M. D. Kowal, R. B. Kanerc, N. Keegan, Laser-scribed graphene presents an opportunity to print a new generation of disposable electrochemical sensors, Nanoscale, 2014, 22, 13613-13622

47 B. Yao, J. Zhang, T. Kou, Y. Song, T. Liu ,Y. Li, Paper-Based Electrodes for Flexible Energy Storage Devices, Adv. Mat., 2017, 4, 1700107

48 A. Vasilescu, G. Nunes, A. Hayat, U. Latif, J.L. Marty, Electrochemical Affinity Biosensors Based on Disposable Screen-Printed Electrodes for Detection of Food Allergens, Sensors, 2016, 16, 1863-1893

49 K. Islam, S. Damiati, A. Suhail, G. Pan, Development of a Label-Free Immunosensor for Clusterin Detection as an Alzheimer's Biomarker, Sensors, 18, 2018, 308

50 Z. Taleat, A. Khoshroo, M. Mazloum-Ardakani, Screen-printed electrodes for biosensing: a review (2008–2013), Microchimica Acta, 2014, 181, 865-891

51 K.C. Honeychurch, J.P. Hart, Screen-printed electrochemical sensors for monitoring metal pollutants,. TrAC Trends Anal Chem, 2003, 22, 456–469

52 A. Das, M.V. Sangaranarayanan, Electroanalytical Sensor Based on Unmodified Screen-Printed Carbon Electrode for theDetermination of Levo- Thyroxine, Electroanal., 2014, 27, 360-367

53 U. Jarocka, R. Sawicka, A. Gora-Sochacka, A. Sirko, W. Zagorski-Ostoja, J. Radecki, H. Radecka, Electrochemical immunosensor for detection of antibodies against influenza A virus H5N1 in hen serum, Biosens. Bioelectron., 2014, 55, 301-306

54 O. Parkash, C.Y. Yean, R.H. Shueb, Screen Printed Carbon Electrode Based Electrochemical Immunosensor for the Detection of Dengue NS1 Antigen, Diagnostic, 2014, 4, 165-180

55 https://www.abcam.com/human-chorionic-gonadotropin-beta-elisa-kit-ab108638.html

*56*https://www.biocompare.com/pfu/110627/soids/351074/ELISA_Kit/Prostate_Specific_Antigen

57 T. Vural, Y.T. Yaman, S. OZturk, S. Abaci, E.B. Denkbas, Electrochemical immunoassay for detection of prostate specific antigen based on peptide nanotube-gold nanoparticle-polyaniline immobilized pencil graphite electrode, J. Colloid. Interf. Sci., 2018, 510, 318-326

58 https://www.abcam.com/human-amyloid-beta-1-40-elisa-kit-ab193692.html

59 Y. Xing, X.Z. Feng, L. Zhang, J. Hou, G.C. Han, Z. Chen, A sensitive and selective electrochemical biosensor for the determination of beta-amyloid oligomer by inhibiting the peptide-triggered in situ assembly of silver nanoparticles, Int. J. Nanomed., 2017, 12, 3171-3179

60 https://www.lsbio.com/elisakits/human-igg-elisa-kit-clia-ls-f29203/29203

61 Z. Chen, M. Lu, Novel electrochemical immunoassay for human IgG1 using metal sulfide quantum dot-doped bovine serum albumin microspheres on antibody-functionalized magnetic beads, Anal. Chim. Acta, 2017, 979, 24-30

62 C.K. Tang, A. Vaze, J.F. Rusling, Paper-based electrochemical immunoassay for rapid, inexpensive cancer biomarker protein detection, Anal. Meth., 2014, 6, 8878-8881

*63https://www.antibodiesonline.com/kit/6227482/Aldo*Keto+Reductase+Family+7,+Member+A3+Aflatoxin+Aldehyde+Reductase+AKR7A3+ELISA+Kit/

64 Z. Kong, H. Wang, L. Zou, J. Zhenguo, Enhancement of aflatoxin B1 detection using electrochemical immunoassay method and 2-aminoethanethiol, Mat. Res. Express, 2018, 5, 066414

65 https://www.creative-diagnostics.com/Atrazine-EIA-Kit-122341-467.htm

66 E. Zacco, R. Galve, J. Adrian, M.P. Marco, M.I. Pividori, S. Alegre, Novel Electrochemical Immunoassay for the detection of toxic compounds in food and environment sample, Ibersensor, 2016,

*67*https://www.lsbio.com/elisakits/human-thyrotropin-tsh-elisa-kit-sandwich-elisa-ls-f5123/5123

68 https://www.sciencedirect.com/science/article/pii/0022175994903093

69 A.H. Loo, A. Bonanni, A. Ambrosi, H.L. Poh, M. Pumera, Impedimetric immunoglobulin G immunosensor based on chemically modified graphenes, Nanoscale, 2012, 4, 921-925

70 K.S. Anderson, S. Sibani, G. Wallstrom, J. Qiu, E.A. Mendoza, J. Raphael, E. Hainsworth, W.R. Montor, J. Wong, J.G. Park, N. Lokko, T. Logvinenko, N. Ramachandran, A.K. Godwin, J. Marks, P. Engstrom, J. Labaer, Protein microarray signature of autoantibody biomarkers for the early detection of breast cancer., J Proteome Res., 2011, 10, 85-96

71M.M. Reddy, R. Wilson, J. Wilson, S. Connell, A. Gocke, L. Hynan, D. German, T. Kodadek, Identification of candidate IgG biomarkers for Alzheimer's disease via combinatorial library screening, Cell., 2011, 144 132-142

72 J.D. Lewis, T he utility of biomarkers in the diagnosis and therapy of inflammatory bowel disease, Gastroenterology, 2011, 140, 1817-1826

73 M. Boes, T. Schmidt, K. Linkermann, B.C. Beaudette, A. Marshak-Rothstein, J. Chen, Accelerated development of IgG autoantibodies and autoimmune disease in the absence of secreted IgM, Chen. Proc. Natl. Acad. Sci.U.S.A., 2000, 97, 1184-1189

*74*https://www.lsbio.com/products/elisakits?q=Human+IgG&adid=7601&gclid=EAIaIQobChMI9522msah3QIVcSjTCh2RNQHsEAAYASAAEgIV1fD_BwE

75 L.P. Qiu, C.C. Wang, P. Hu, Z.S. Wu, G.L. Shen, R.Q. Yu, A label-free electrochemical immunoassay for IgG detection based on the electron transfer, Talanta, 2010, 83, 42-47
76 W. Jumpathong, J. Jakmunee, K. Ounnunkad, A Sensitive and Disposable Graphene Oxide Electrochemical Immunosensor for Label-free Detection of Human Immunoglobulin G, Anal. Sci., 2016, 32, 323-328
77 N. Wang, C. Gao, Y. Han, X. Huang, Y. Xu, X. Cao, Detection of human immunoglobulin G by label-free electrochemical immunoassay modified with ultralong CuS nanowires, Journ. Mat. Chem. B, 2015, 3, 3254-3259
78 D. Tang, J. Ren, M. Lu, Multiplexed electrochemical immunoassay for two immunoglobulin proteins based on Cd and Cu nanocrystals, Analyst, 2017,142, 4794-4800
79 I.C. Prado, M.E.T.A. Chino, A.L. Dos Santos, A.L.A. Souza, L.G. Pinho, E.R.S. Lemos, S.G. De Simone, Development of an electrochemical immunosensor for the diagnostic testing of spotted fever using synthetic peptides, Biosens Bioelectron. 2018, 100, 115-121
80 J.P. Vilardaga, G. Romero, P.A. Friedman, T.J. Gardella, Molecular basis of parathyroid hormone receptor signaling and trafficking: a family B GPCR paradigm, Cell. Mol. Life. Life. Sci., 2011, 68, 1-13
81 L.K. McCauley, T.J. Martin, Twenty-five years of PTHrP progress: from cancer hormone to multifunctional cytokine, J. Bone Miner. Res., 2012, 27, 1231-1239.
82 C. Zeng, X. Guo, W. Zheng et al., Identification of independent association signals and putative functional variants for breast cancer risk through fine-scale mapping of the 12p11 locus, Breast Cancer Res., 2016, 18, 64
83 C. Xu, Z. Wang, R. Cui, H. He, X. Lin, Y. Shen, H. Zhang, Co-expression of parathyroid hormone related protein and TGF-beta in breast cancer predicts poor survival outcome, BMC Cancer., 2015, 15, 925-935
84 E. Song, H. Hu, Translational Research in Breast Cancer, 2017
85 M. Yao, T. Murakami, K. Shioi, N. Mizuno, H. Ito, K. Kondo, H. Hasumi, F. Sano, K. Makiyama, N. Nakaigawa, T. Kishida, T. Nagashima, S. Yamanaka, T. Kubota, Tumor signatures of PTHLH overexpression, high serum calcium, and poor prognosis were observed exclusively in clear cell but not non clear cell renal carcinomas, Cancer Med., 2014, 3, 845-854
86 Z. Lu, X. Wu, X. Wu, W. Cao, Z. Shen, L. Wang, F. Xie, J. Zhang, T. Ji, M. Yan, W. Chen, Parathyroid hormone-related protein serves as a prognostic indicator in oral squamous cell carcinoma, J. Exp. Clin. Cancer Res., 2014, 100-113
87 W-M Chang, Y.F. Lin, C.Y. Su, H.Y. Peng, Y.C. Chang, J.R. Hsiao, C.L. Chen, J.Y. Chang, Y.S. Shieh, M. Hsiao, S.G. Shiah, Parathyroid Hormone-Like Hormone is a Poor Prognosis Marker of Head and Neck Cancer and Promotes Cell Growth via RUNX2 Regulation, Scientific Reports, 2017, 7, 1-13
88 https://www.fn-test.com/elisa/human/human-pthlhparathyroid-hormone-related-protein/

89 N.U. Truong, M.D. deB Edwardes, V. Papavasiliou, D. Goltman, R. Kremer, Parathyroid hormone-related peptide and survival of patients with cancer and hypercalcemia, Am. J. Med., 2003, 115, 115-121
90 W.D Fraser, J. Robinson, R. Lawton, B. Durham, S.J. Gallacher, I.T. Boyle, G.H. Beastall, F.C. Logue, Clinical and laboratory studies of a new immunoradiometric assay of parathyroid hormone-related protein, Clin. Chem., 1993, 39, 414-419.
91 M.R. Pandian, C.G. Morgan, E- Carlton, G.V. Segre, Modified immunoradiometric assay of parathyroid hormone-related protein: clinical application in the differential diagnosis of hypercalcemia, Clin. Chem., 1992, 38, 282-288
92 H.U. Kim, H.Y. Kim, A. Kulkarni, C. Ahn, Y. Jin, Y. Kim, K.N. Lee, M.H. Lee, T. Kim, A sensitive electrochemical sensor for in vitro detection of parathyroid hormone based on a MoS2-graphene composite, Sci. Rep., 2016, 6, 34587-34596
93 A. de la Escosura.Muniz, M. Espinoza-Castaneda, A. Chamorro-Garcia, C.J. Rodriguez-Hernandez, C. de Torres, A. Merkoci, In situ monitoring of PTHLH secretion in neuroblastoma cells cultured onto nanoporous membranes, Biosens. Bioelectron., 2018, 107, 62-68
94 H.M. Ozcan, M.K. Sezginturk, Detection of parathyroid hormone using an electrochemical impedance biosensor based on PAMAM dendrimers, Biotechnol. Prog., 2015, 31, 815-822
95 H.Y. Kim, S. Sato, S. Takenaka, M.H. Lee, Membrane-Based Microwave-Mediated Electrochemical Immunoassay for the In Vitro, Highly Sensitive Detection of Osteoporosis-Related Biomarkers, Sensors, 2018, 18, 2933-2944
96 S.C. Simsek, M.N.S. Karaboga, M.K. Sezginturk, A new immobilization procedure for development of an electrochemical immunosensor for parathyroid hormone detection based on gold electrodes modified with 6-mercaptohexanol and silane, Talanta, 2015, 144, 210-218
97 J. Kimling, M. Maier, B. Okenve, V. Kotaidis, H. Ballot, A. Plench, Turkevich Method for Gold Nanoparticle Synthesis Revisited, J Phys Chem B., 2006, 110, 15700-15707.
98 L. Baptista-Pires, C.C. Mayorga-Martínez, M. Medina-Sánchez, H. Montón, A. Merkoçi, Water Activated Graphene Oxide Transfer Using Wax Printed Membranes for Fast Patterning of a Touch Sensitive Device, ACS Nano., 2016, 10, 853-860
99 A.J.. Bard, L.R. Faulkner, Electrochemical methods fundamentals and applications, 2002, Chapter 6
*100*https://www.sigmaaldrich.com/technical-documents/articles/materials science/nanomaterials/gold-nanoparticles.html
101 Y.Q. He, S.P. Liu, L. Kong, Z.F. Liu, A study on the sizes and concentrations of gold nanoparticles by spectra of absorption, resonance Rayleigh scattering and resonance non-linear scattering, Spectrochim. Acta A: Molec. Biomolec. Spectrosc., 2005, 61, 2861-2866
102 A. Huang, W. Li, S. Shi, T. Yao Quantitative Fluorescence Quenching on Antibody-conjugated Graphene Oxide as a Platform for Protein Sensing, Scient. Rep., 2017, 7, 40772-40779
103 S.K. Vashist , Comparison of 1-Ethyl-3-(3-Dimethylaminopropyl) Carbodiimide Based Strategies to Crosslink Antibodies on Amine-Functionalized Platforms for Immunodiagnostic Applications, Diagnostics, 2012, 2, 23-33
104 M. G. Acker, D. S. Auld, Considerations for the design and reporting of enzyme assays in high-throughput screening applications, Perspectives in Science, 2014, 1, 56-57
105 S. Dodig, Interferences in quantitative immunochemical methods, Biochemia Medica, 2009, 19, 50-62
106 M. Pedrero, F. J. M. de Villena, C. Muñoz-San Martín, S. Campuzano, M. Garranzo-Asensio, R, Barderas, J. M. Pingarrón, Disposable Amperometric Immunosensor for the Determination of Human P53 Protein in Cell Lysates Using Magnetic Micro-Carriers, Biosensors, 2016, 6, 56-70

107 S. F. Amarasiri, J. R. Sportsman, G. S. Wilson, Studies of the low dose 'hook' effect in a competitive homogeneous immunoassay, Journal of Immunological Methods,1992, 151, 27-46
108 L. Rivas, M. Medina-Sanchez, A. de la Escosura-Muniz, A. Merkoci, Improving sensitivity of gold nanoparticle-based lateral flow assays by using wax-printed pillars as delay barriers of microfluidics, Lab. Chip., 2014, 14, 4406-4414
109 A. Chamorro-Garcia, A. de la Escosura-Muniz, M. Espinosa-Castaneda, C.J. Rodriguez-Hernarndez, C. de Torres, A. Merkoci, Detection of parathyroid hormone-like hormone in cancer cell cultures by gold nanoparticle-based lateral flow immunoassays, Nanomedicine, 2016, 12, 53-61
110 X. Cao, S. Liu, Q. Feng, N. Wang, Silver nanowire-based electrochemical immunoassay for sensing immunoglobulin G with signal amplification using strawberry-like ZnO nanostructures as labels, Biosens. Bioelectron., 2013, 49, 256-262
111 T. Putnin, W. Jumpathong, R. Laocharoensuk, J. Jakmunee, K. Ounnunkad, A sensitive electrochemical immunosensor based on poly(2-aminobenzylamine) film modified screen-printed carbon electrode for label-free detection of human immunoglobulin G, Artif. Cells Nanomed. Biotechnol., 2018, 46, 1042-1051

6 Conclusions and outlook

General Conclusions

In this doctoral thesis, the research work on the development of different nanostructured sensors for clinical and environmental applications was presented. The results obtained in this thesis showed that electrochemical sensors can be used in many fields, significantly improving the performances of the current analytical techniques that are often expensive, laborious, bulky and not portable.

The research activity was focused on the preparation of electrodes, using different techniques with the aim to obtain electrodes with different morphology, from NWs and NTs to NPs, from thin films to micro bands. Different electrochemical techniques were presented both to characterize and to test the electrodes. In the case of sensors made of nanostructures, the influence of the nanostructures size was showed and discussed. It was seen that electrodes with smaller nanostructures show better performances for sensing.

The first investigated sensor (described in Chapter 3) was concerned the detection of hydrogen peroxide using Pd or Cu nanostructures. It has been showed the effect of the nanostructures height and active material nature on the selectivity, LOD and stability. These types of sensors were also used to detect hydrogen peroxide for monitoring oxidative stress in living cells. This is still an ongoing work, but preliminary results showed that this technique can be used in this field.

In Chapter 4, two different sensors for heavy metals were described. Mercury, lead and copper were detected reaching low limit of detection, always lower than that one settled by the Environmental Protection Agency. The electrodes were able to detect metals also in real samples, such as undrinkable water and

river water. Metals were detected at neutral pH, using interdigitated gold microbands, exploiting a new and innovative technique able to modify the pH close to the electrode surface. This technique highly increases the palatability of electrochemical sensors for heavy metals detection in water.

The last sensor (described in Chapter 5) concerns the development of an electrochemical immunosensor for Human IgG and PTHLH using an innovative electrode. In fact, for the first time a paper-based electrode, made of laser reduced graphene oxide, was efficiently developed. We have achieved a LOD close to the ones of commercial ELISA Kits.

Ongoing works

Currently, in our Lab (Applied Physical Chemistry, DIID, University of Palermo) we are working to develop other two different sensors:

- An electrode made of electrochemically reduced graphene oxide and Au-NPs. These two compounds were deposited simultaneously into an Indium Tin Oxide substrate. The electrode has been fully characterized and we are using it to detect dopamine in blood. Dopamine is an important neurotransmitter that can be used for an early diagnosis of Alzheimer Disease. We reached low LOD (0.1 nM) with high sensitivity, reproducibility, and selectivity. This work will be submitted soon for publication. Furthermore, we like to improve the novelty of the work by using this electrode to detect, simultaneously, dopamine and other biomarkers for Alzheimer disease;
- We have patented a new and innovative way to produce silver-based electrodes from wasted CD-ROM. The patent has been accepted by the Italian Society of Patents, but it is not available yet. This technique allows us to produce reproducible electrodes and, moreover, to recover

an important and expensive material like polycarbonate. We used the Ag-based electrode to detect simultaneously Zn, Cd and Pb, and the preliminary results showed excellent features with LOD of about 1 ppb. Also this work will be submitted soon for publication.

7 List of publications, conferences and internships

7.1 Papers

1. C. Sunseri, C. Cocchiara, F. Ganci, A. Moncada, R.O. Oliveri, ***B. Patella****, S. Piazza, R. Inguanta, "Nanostructured Electrochemical Devices for Sensing, Energy Conversion and Storage", Chemical Engineering Transactions 47 (2016) 43-48.*

2. ***B. Patella****, R. Inguanta, S. Piazza, C. Sunseri, "Nanowire Ordered Arrays for Electrochemical Sensing of H2O2", Chemical Engineering Transactions 47 (2016) 19-24.*

3. ***B. Patella****, R. Inguanta, S. Piazza, C. Sunseri, "A Nanostructured sensor of hydrogen peroxide", Sensors and Actuators B: Chemical 245C (2017) 44-54.*

4. ***B. Patella****, S. Piazza, C. Sunseri, R. Inguanta, "NiO thin film for mercury detection in water by square wave anodic stripping voltammetry", Chemical Engineering Transactions, 60 (2017) 1-6.*

5. ***B. Patella****, C. Sunseri, R. Inguanta, "Nanostructured Based Electrochemical Sensors" Accepted for publication Journal of Nanoscienece and Nanotechnology.*

6. ***B. Patella****, C. Sunseri, C. Cocchiara, R. Inguanta, An innovative way to procude silver based electrode from wasted CDs and its application for heavy metal detection, Sensors and Actuators B, Under Submission*

7. ***B. Patella****, A. Sortino, C. Sunseri, R. Inguanta, ITO-rGO decorated with metal NPs for electrochemical detection of dopamine with negligible interference from uric and ascorbic acid in synthetic urine, Biosensors and Bioelectronics, Under Submission*

8. ***B. Patella****, R. Alvarez, A. Sena, A. Merkoci, Paper based Laser Scribed Graphene oxide electrodes as alternative electrochemical biosensors for Human IgG Detection, Advanced materials, Under Submission*

9. ***B. Patella****, Benjamin O'Sullivan, Robert Daly, Pierre Lovera, Rosalinda Inguanta, Alan O'Riordan, Reagent-free simultaneous detection of multiple metal contaminants in water using localised pH control, Journal of American chemical society, Under Submission*

7.2 Patent

1. R. Inguanta, C. Cocchiara, ***B. Patella****, G. Aiello, C. Sunseri, Metodo Per La Realizzazione Di Sensori Elettrochimici Con Materiali Recuperati Da Dispositivi Di Memorizzazione Di Scarto E Sensore Elettrochimico Ottenibile Con Tale Metodo, Italian Patent 102017000121268 del 25/10/2017*

7.3 Conferences

1. R. Inguanta, C. Cocchiara, F. Ganci, A. Moncada, ***B. Patella****, S. Piazza, C. Sunseri, S. Lombardo, Nanostructured materials for sensing, energy conversion and storage, X INSTM CONFERENCE, Favignana (TP), 28th June – 1st July 2015*

2. C. Sunseri, C. Cocchiara, F. Ganci, A. Moncada, R.O. Oliveri, ***B. Patella****, S. Piazza, R. Inguanta, "Nanostructured Electrochemical Devices for Sensing, Energy Conversion and Storage", NINE International Conference on Nanotechnology Based Innovative Applications for the Environment, 20-23 March 2016, Rome, Italy.*

3. ***B. Patella****, R. Inguanta, S. Piazza, C. Sunseri, "Nanowire Ordered Arrays for Electrochemical Sensing of H2O2", NINE International Conference on Nanotechnology Based Innovative Applications for the Environment, 20-23 March 2016, Rome, Italy.*

4. S. Piazza, ***B. Patella****, R. Inguanta, C. Sunseri, Pd-NWs ordered arrays for electrochemical sensing of H2O2, 67th Annual Meeting of the International Society of Electrochemistry, Electrochemistry, 21-26 August, 2016, Hague, Netherlands*

5. ***B. Patella****, S. Piazza, C. Sunseri, R. Inguanta, "NiO thin film for mercury detection in water by square wave anodic stripping voltammetry" 2nd International Conference On Nanotechnology Based Innovative Applications For The Environment, 24-27 September 2017, Rome, Italy*

6. R. Inguanta, C. Cocchiara, F. Ganci, M. G. Insinga, ***B. Patella****, S. Piazza, L. Oliveri, C. Sunseri, S. Lombardo, From sensors to electrochemical energy conversion and storage with nanostructured materials, NanoInnovation Conference & Exhibition, 26-29 September 2017 Rome Italy*

*7. R. Inguanta, **B. Patella**, S. Piazza, C. Sunseri, Electrochemical H2O2 sensors Based on Pd and Cu Nanostructures, 4° Convegno Nazionale Sensori, Catania, 21-23 Febbraio 2018.*

*8. R. Inguanta, **B. Patella,** S. Piazza, C. Sunseri, Thin Film Sensors for Mercury Ions Detection by Suare Wave Anodic Strippind Voltammetry, 4° Convegno Nazionale Sensori, Catania, 21-23 Febbraio 2018.*

*9. **B. Patella**, R. Inguanta, C. Sunseri, S. Piazza, NiO@Ni core shell for electrochemical detection of Hg ions, 69th Annual Meeting of the International Society of Electrochemistry, Electrochemistry, 2-7 September, 2018, Bologna, Italy*

7.4 Internships

1. Tyndall National Institute, Cork, Ireland, from 28/01/2017 to 1/08/2017, under supervision of Prof. Alan O'Riordan

2. Catalan Institute of Nanoscience and Nanotechnology, Barcelona, Spain, from 1/10/2017 to 31/03/2018, under supervision of Prof. Arben Merkoci

8 Acknowledgments

Doctoral work was certainly the most challenging moment of my, so far, short career. I had to put myself at stake, trying to fully understand not only the chemistry and engineering behind the phenomena discussed in the thesis, but also myself and my abilities. I dedicate this training process to myself, but also and above all to those people who have been close to me during these three years

Among them, the first ones are certainly my family, my *parents*, my *sisters* and my *nephews* and *nieces* who have supported and helped me for these 3 years of doctorate, always giving me the moral support that I needed, even in the most difficult moments.

I sincerely thank *Prof. Rosalinda Inguanta* and *Prof. Carmelo Sunseri* for giving me the opportunity to get in touch with this beautiful and difficult world, which is research. In addition, I thank them for giving me some of their knowledge on electrochemistry and for having scientifically formed me, as well as for the possibility to travel so much during these 3 years.

I want to thank my tutors during my internships, *Prof. Arben Merkoci*, *Prof. Alan O'Riordan* e *Dott. Pierre Lovera*. Thank you for dedicating your time and resources to me.

I would also like to express my immense gratitude to my work colleagues, from the oldest, *Dott. Cristina Cocchiara* and *Ing Isabella Mendolia*, to the newest, *Dott. Fabrizio Ganci*, *Ing. Pasquale Torchia*, *Ing. Giovanni Abbruzzo*, *Ing. Davide Alfieri*, *Ing. Andrea Bocchino*, *Dott. Giovanni Barone*, *Ing. Andrea Urru*, *Dott. Alexander Muller, Dott. Amadeo Sena*, *Dott.ssa Anna Testolin*, that, during this time, never stopped encouraging me and showing their esteem. I would like to thank the entire research group of the Applied Physical Chemistry,

Ing. Maria Grazia Insinga, *Ing. Claudio Zanca*, *Dott. Luigi Oliveri*, *Dott. Alessandra Moncada*, *Ing. Giuseppe Blanda* and *Ing. Giuseppe Greco*. Thank for the help in the lab and for the wonderful lunch breaks spent together.

Finally, I want to thank the person who most of all helped me, albeit for a short time, in my training as a researcher, and to whom I dedicate this doctoral thesis, *Prof. Salvatore Piazza*. I would have liked to share with you this goal, to which, probably, you would have commented by saying 'Nanfaruso, a si capiu nenti!. Thanks for all the breakfasts together, always seasoned with laughs, and thank you for having gave me this great opportunity.